REVIEWS OF MODERN PHYSICS, VOLUME 97, APRIL–JUNE 2025

Quantum physics of stars

M. Wiescher*

Department of Physics and Astronomy and the Joint Institute for Nuclear Astrophysics, University of Notre Dame, Notre Dame, Indiana 46556, USA

C. A. Bertulani

Department of Physics and Astronomy, East Texas A&M University, Commerce, Texas 75429, USA and Institut für Kernphysik, Technische Universität Darmstadt, Schlossgartenstraße 2, 64298 Darmstadt, Germany

C. R. Brune

Department of Physics and Astronomy and Institute of Nuclear and Particle Physics, Ohio University, Athens, Ohio 45701, USA

R. J. deBoer

Department of Physics and Astronomy and Joint Institute for Nuclear Astrophysics, University of Notre Dame, Notre Dame, Indiana 46556, USA

A. Diaz-Torres

Department of Physics, University of Surrey, Guildford GU2 7XH, United Kingdom

L. R. Gasques

Universidade de São Paulo, Instituto de Fisica, Rua do Matão, 1371, 05508-090 São Paulo, São Paulo, Brazil, Dipartimento di Matematica e Fisica, Università della Campania "L. Vanvitelli," Viale Lincoln 5, Caserta, Italy, and Istituto Nazionale di Fisica Nucleare, Sezione di Napoli, Via Cinthia snc, Napoli, Italy

K. Langanke

GSI Helmholtzzentrum für Schwerionenforschung, Planckstraße 1, 64291 Darmstadt, Germany and Institut für Kernphysik (Theoriezentrum), Fachbereich Physik, Technische Universität Darmstadt, Schlossgartenstraße 2, 64298 Darmstadt, Germany

P. Navrátil

TRIUMF, 4004 Wesbrook Mall, Vancouver, British Columbia V6T 2A3, Canada

W. Nazarewicz

Facility for Rare Isotope Beams and Department of Physics and Astronomy, Michigan State University, East Lansing, Michigan 48824, USA

J. Okołowicz

Institute of Nuclear Physics, Polish Academy of Sciences, Radzikowskiego 152, PL-31342 Kraków, Poland

D. R. Phillips

Department of Physics and Astronomy and Institute of Nuclear and Particle Physics, Ohio University, Athens, Ohio 45701, USA and Department of Physics, Chalmers University of Technology, SE-41296 Göteborg, Sweden

M. Płoszajczak

Grand Accélérateur National d'Ions Lourds (GANIL), CEA/DSM—CNRS/IN2P3, BP 55027, F-14076 Caen Cedex, France

S. Quaglioni

Lawrence Livermore National Laboratory, P.O. Box 808, L-414, Livermore, California 94551, USA

A. Tumino

Dipartimento di Ingegneria e Architettura, Università degli Studi di Enna "Kore", Cittadella Universitaria, 94100 Enna, Italy and INFN-Laboratori Nazionali del Sud, Via Santa Sofia 62, 95123 Catania, Italy

(published 27 May 2025)

Stars are slowly developing objects; the lifetimes of the different burning phases are determined by the strength of nuclear reactions, which in turn are defined by the quantum structure of the associated nuclei at the threshold and the respective reaction mechanisms. Stars, from the nuclear physics perspective, are cold environments where only a few of the key nuclear reactions have been measured at the actual stellar plasma temperatures. This is also the case for more dynamic astrophysical phenomena from the big bang to stellar explosions. Most of the nuclear reaction rates are therefore based on theoretical extrapolations. A number of discrepancies between these predictions and the associated stellar signatures have been observed, and many may be due to low-energy or near-threshold quantum effects. These effects need to be understood in order to reliably model nuclear reaction processes, not only for stars but also for low-temperature plasma environments such as controlled magnetic or inertial confinement fusion systems, which operate in similar temperature regimes. This review summarizes the various theoretical techniques presently used for deriving reaction rates and discusses possible quantum effects that may impact the reaction cross section near the reaction threshold. These resemble enhanced single-particle and cluster structures near threshold and associated interference effects. New experimental techniques such as deep-underground accelerators or the study of transfer reactions to mimic the quantum-mechanical transition strength, the so-called Trojan horse method, provide ways to directly or indirectly probe the reaction features that determine the reaction rates at stellar energies. This is demonstrated on a number of key nuclear reactions for different nucleosynthesis environments. Finally, current inconsistencies between experimental predictions and observations are discussed.

DOI: 10.1103/RevModPhys.97.025003

CONTENTS

*Contact author: mwiesche@nd.edu

I. INTRODUCTION

Nuclear astrophysics emerged as a field with a short but impactful paper by the young Russian physicist George Gamow, who was doing research in Göttingen, Germany. The paper, entitled "Zur Quantentheorie des Atomkerns [On the quantum theory of the atomic nucleus]" (Gamow, 1928), was primarily concerned with the tunneling probability of charged particles through the Coulomb barrier of the nucleus. While the paper was primarily concerned with the theoretical description of the α decay, it immediately became obvious that the formalism could also be applied to capture reactions involving charged particles. This enabled estimating nuclear reaction cross sections and reaction rates that determine the energy generation in stars during the various evolutionary stages, from hydrogen burning in the Sun to the final burning stage of massive stars. It became clear that these microscopic reaction processes, which depend on the nuclear structure of the reaction components and the quantum-mechanical transition probability, are key elements for providing reliable stellar models. The network of nuclear reactions feeding the different stellar burning phases can be summarized in the spirit of Gamow's paper as the quantum physics of stars. But stars are cold, and the typical energy range for nuclear fusion processes corresponds to a narrow energy window near the particle threshold, the Gamow window. Because of the Coulomb barrier, this energy range has been inaccessible experimentally, and the presence of unbound quantum states has made reliable calculations difficult. The aim of this review is to provide a deeper understanding of the quantum effects that govern nuclear reactions at near-threshold energies.

Thresholds correspond to boundaries between different phases of a collective system composed of multiple statistical entities. Threshold effects are features that have been observed in a wide range of such systems undergoing a sudden transition, a sudden change in the physical properties of the system, often expressed as a function of energy. It is a well-known phenomenon that indicates that something different or new has occurred, which prompts a rapid change in a system's collective behavior. Threshold effects occur in all sorts of collective systems (Kalai and Safra, 2006; Washington-Allen and Salo, 2007; Rothman, 2017), ranging from plant genetics (Reyment, 1982) to the so-called phenotypic threshold effect (Rossignol *et al.*, 2003), where changes in a specific genetic mutation rate can suddenly lead to a dramatic genetic change. These effects involve questions of ecological balance and their role in land management and restoration efforts (Bestelmeyer, 2006), as well as in thermoregulation of biological systems, where physiological mechanisms in producing or dissipating heat are initiated when certain external temperature limits are reached (Taylor *et al.*, 2019). Another example is the threshold fragmentation instability of large clusters in open aggregating systems that do not conserve mass (Berrones-Santos *et al.*, 2022). Such situations may happen in various socioeconomic systems, the self-organized criticality models of $1/f$ noise (Bak, Tang, and Wiesenfeld, 1987; Marković and Gros, 2014) and earthquake fractures (Lomnitz-Adler, 1993). Threshold effects are also a well-known phenomenon in medicine, where a critical limit in the quiet development of a disease is being crossed, resulting in a rapid change in health (Keim-Malpass *et al.*, 2020). Threshold effects even dictate the rules of financial systems when, after a long period of confidence in an apparently safe development or investment (bubble), consumer confidence disappears overnight and a financial crash occurs, as modeled by Minea and Villieu (2009). The investigation of such threshold effects is therefore of great interest for the predictability of dynamic behavior patterns into the range of the unknown.

Threshold effects occur in collective quantum systems: in atoms and nuclei and for elementary-particle collisions. Threshold effects in such systems reflect the change that manifests itself in the appearance of a new channel when a critical energy is reached that corresponds to the possibility that a previously unrealizable final state is produced in a reaction process. In atomic physics this is called the ionization process: above a certain energy, an electron or electrons are released from their Coulomb binding to the nucleus. In nuclear physics the analog of the ionization process is the breakup process of weakly bound nuclei, where the reaction pattern changes from elastic scattering to the emergence of new inelastic reaction channels (Wigner, 1948). In particle physics new elementary particles that were not present in the initial state can be produced above a certain critical energy corresponding to the difference in rest masses between the newly accessible final state and the initial state (Fonda and Ghirardi, 1964).

Threshold effects are often a direct result of conservation of flux since they appear at a branching point of the reaction flux. With the sudden opening of a new channel, a redistribution of the flux in other open channels appears, causing a modification or cusp in the reaction cross sections for the other reaction channels. The shape of the cusp strongly depends on the orbital-angular-momentum transfer in the reaction process. The investigation of the onset and the impact of threshold effects has therefore always been a long-standing goal in the study of reaction processes between particle systems to explore the regulatory pattern of the reaction system.

This question has been of particular interest in nuclear astrophysics, a field that is concerned with the synthesis of new elements in very-low-energy stellar plasma environments, since stellar temperatures correspond to energies close to reaction thresholds. Nuclear thresholds associated with the binding energy of the compound nucleus or the Q value of the reaction determine the opening of new reaction channels, and threshold effects influence the strength or the probability for a reaction to occur. A detailed investigation of these threshold effects through experimental and theoretical means is critical for the understanding of the nuclear reaction patterns at stellar energies in order to be able to make reliable predictions regarding the associated synthesis of the elements. This interest is not limited to stars, as it extends to the understanding of reaction or fusion processes in anthropogenic plasmas, which reach near-stellar energies and offer a new pathway to directly study stellar reaction processes (Gatu Johnson *et al.*, 2017).

Charged-particle nuclear reactions at very low energies are defined primarily by the Coulomb barrier, where Gamow was the first to calculate the quantum-mechanical tunneling probability (Gamow, 1928; Gurney and Condon, 1928). This effort led to a first estimate of reaction rates based on assumptions regarding the level structure in the associated nuclei (Gamow and Teller, 1938). In the following decades, the inclusion of orbital-angular-momentum considerations and the improved mathematical treatment that introduced the so-called Coulomb functions—the scattering solutions of the Schrödinger equation in the presence of the Coulomb potential—represented an important first step. The regular and irregular Coulomb functions (Bloch *et al.*, 1951) $F_\ell(\rho,\eta)$ and $G_\ell(\rho,\eta)$ enable calculations of the energy-dependent probability for charged-particle nuclear reactions to tunnel through the Coulomb and orbital-momentum barriers between two interacting charged particles. This Coulomb penetrability is expressed in terms of the Coulomb functions by (Lane and Thomas, 1958)

$$P_\ell = \frac{\rho}{F_\ell^2(\rho,\eta)+G_\ell^2(\rho,\eta)}. \tag{1}$$

The two parameters are $\rho = kr$, the dimensionless radius, and the Sommerfeld parameter $\eta = (Z_1Z_2e^2\mu)/(\hbar^2 k)$, with k the wave number; $r = r_0(A_1^{1/3}+A_2^{1/3})$ the interaction radius, where r_0 ranges from 1.2 to 1.4 fm and A_1 and A_2 are the mass numbers of the two interacting nuclei; Z_1 and Z_2 the electrical charge numbers of the interacting particles; and e the elementary charge. The parameter μ represents the reduced mass of the reaction system, which is typically calculated using the atomic masses of the interacting nuclei.

Besides the Coulomb barrier, the nuclear reaction cross section is determined by the quantum-mechanical probability for converting the initial system of two independent particles into a final nucleus through a direct reaction mechanism or into a final system of two particles or a photon and a recoil particle through a compound reaction mechanism. The compound state is an intermediary, highly excited, quantum configuration above the particle threshold that can either break up into different reaction channels or decay by γ-ray emission to the ground state, as visualized in Fig. 1.

The probability of the formation of such a compound state corresponds to its nuclear structure configuration as a single-particle or cluster state and can be observed as a single resonance in a nuclear reaction experiment. The center-of-mass energy $E = E_x - Q$, where E_x is the excitation energy of the unbound state in the compound system and Q is the Q value corresponding to the energy release in the reaction. The wave functions of the ground and excited states of the compound nucleus are characterized by different quantum configurations that can be described, for example, in terms of the shell-model or cluster-model theory; single-particle configurations resemble a single-particle wave function coupled to a core nucleus, while an α-cluster configuration can be described in similar terms. All of these components are usually present, but in varying strengths, which can be expressed in terms of spectroscopic factors (SFs) or asymptotic normalization coefficients (ANCs) as a signature for the level configuration (Mukhamedzhanov, Gagliardi, and

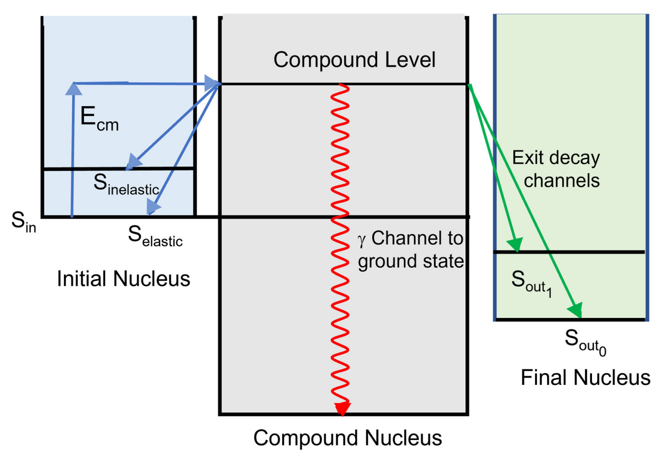

FIG. 1. Schematic drawing of the compound concept. In a first step the compound resonance (or resonances) is populated by capturing a particle with a center-of-mass energy E on the initial nucleus (blue lines). It then either decays back to the ground state as elastic scattering or to an excited state of the initial nucleus as inelastic scattering or decays into a different energetically open particle channel populating the ground state or excited states of a final nucleus (green lines). The third decay option is by γ-ray emission directly or by γ-ray cascades to the ground state of the compound nucleus (red line).

Tribble, 2001; Tribble et al., 2014). These quantities correspond to the transition strength with which these states can be populated, as discussed in Secs. II.D.5 and II.D.6; they can be determined experimentally through the study of transfer or radiative capture reactions, as discussed in terms of an R-matrix analysis in Sec. III.

Bound states can be populated by direct reaction mechanisms, depending on the transition probability, while unbound states appear as resonances in a nuclear reaction whose strengths are proportional to the transition strengths in the entrance and the exit channel of the compound system. Low-energy fusion reactions between light systems ($A \leq 4$) are typically dominated by nonresonant direct reaction mechanisms, while reactions between light nuclei ($6 \leq A \leq 24$) are characterized by single resonances and additional nonresonant components. The nonresonant transitions are traditionally described in terms of potential models, as summarized by Bethe (1937), while resonances are expressed in terms of Breit-Wigner peaks (Breit and Wigner, 1936), which developed into a more general R-matrix theory describing the interplay of resonant and nonresonant components, which are crucial for an extrapolation to the threshold (Lane and Thomas, 1958). At higher excitation energies and also for higher mass nuclei, multiple quantum configurations in the compound nucleus translate into a high-level density with a multitude of overlapping resonances contributing to the reaction rate (Hauser and Feshbach, 1952). The cross section is typically calculated in the framework of a statistical model relying on averaged parameters for the associated transition probabilities or strength functions. The basis for all of these model approaches was developed for the analysis of neutron capture reactions in the 1930s and 1940s but quickly expanded into the realm of charged-particle interactions, as described in an essay by Wigner (1995). These theories still provide the theoretical foundation for reaction theory and for the treatment of nuclear reactions in stars (Thompson and Nunes, 2009; Bertulani and Danielewicz, 2021). However, inherent to these theories are assumptions about the nature of the wave functions and the reaction mechanisms, which may affect the traditional technique of extrapolating from experimental data to stellar reaction rates.

These questions are important for low-energy nuclear reactions involving nuclei near stability and become even more important when one moves toward the regimes of open-quantum systems of highly neutron-rich or proton-rich nuclei. In the latter case, α clusterization plays an important role for capture rates in the αp process and in the end point of the rp process (Wiescher and Ahn, 2017).

Nuclear states near drip lines or above the lowest particle-emission threshold in stable nuclei cannot be described in a closed-quantum-system framework such as the nuclear shell model. Their properties are profoundly affected by the "environment," i.e., the many-body continuum representing scattering and decay channels. The states of open-quantum systems belong to a multidimensional network of states in neighboring nuclei, which are connected by virtual excitations, particle decays, and/or captures. Interaction via the continuum may lead to the formation of a near-threshold collective eigenstate of an open-quantum system that couples strongly to the nearby decay channels and carries many of its characteristics. This eigenstate, which has a pronounced single-particle or cluster structure, is responsible for the increased probability of single-particle or cluster capture or emission close to the decay threshold in many light nuclei. Notable examples are the α clustering in the Hoyle state of ^{12}C (Freer and Fynbo, 2014; Otsuka et al., 2022); ^{3}He clustering in the $7/2^-_1$ excited state of ^{7}Be (Vorabbi et al., 2019); the interference of multiple α-cluster states at the α threshold in ^{16}O that determine the low-energy cross section of the $^{12}C(\alpha,\gamma)^{16}O$ reaction (deBoer et al., 2017); the $1n$- and $2n$-halo configurations in the ground states of ^{11}Be and ^{11}Li, respectively (Varga, Suzuki, and Lovas, 2002); $2n$ radioactivity in ^{26}O (Kohley et al., 2013); the $5/2^+$ resonance near the $[^{10}B + n]$ threshold, which is key for the absorption of thermal neutrons, as discussed in Sec. II.E.4; and the experimental confirmation of the three-triton structure in ^{9}Li (Ma et al., 2021). This list can be extended to many similar examples for capture and reaction processes involving light nuclei (Freer et al., 2018) and may even play a significant role in the onset of a light r process (Görres et al., 1995; Bartlett et al., 2006).

The appearance of correlated (cluster) states close to open channels is a generic emergent phenomenon in open-quantum systems, fairly independent of the details of the interaction, that is related to the collective rearrangement of shell-model wave functions due to the coupling via the continuum. The richness of nuclear forces and the existence of nucleons in four distinct states—proton, neutron, spin-up, and spin-down states—make studies of the atomic nucleus in the low-energy continuum interesting. Near-threshold states and their properties are still *terra incognita* in nuclear physics. The resonances in the low-energy continuum, which carry an imprint of a nearby decay channel, play a crucial role not only in rare nuclear decays and exotic nuclear states but also for the question of the origin of the elements in the Universe produced in quiescent or explosive nucleosynthesis environments. Their importance can be direct, as this knowledge is necessary for the extrapolation of the reaction cross section, and also indirect because they provide evidence of the phenomenon of threshold states emerging from the coupling to the continuum.

In addition to these quantum effects on the nuclear potential level, the interaction of very-low-energy charged particles with the electrons usually occurs in the astrophysical environment or in the target-projectile combination in accelerator-based laboratory experiments needs to be considered. These interactions lead to screening effects in charged-particle fusion reactions, making them especially significant for nuclear astrophysics. They are threshold effects in the sense that they lower the reaction thresholds and, in particular cases, can shift nuclear resonances effectively across the particle threshold, thereby transforming them into bound states. As the atomic environments in stellar plasmas and laboratories differ markedly, the associated screening mechanisms require distinct approaches. In a few cases, the screening effect has been assessed in accelerator experiments but is found to deviate noticeably from theoretical expectations (Aliotta and Langanke, 2022). This deviation has to be resolved if the data are to be used in astrophysical applications. This is particularly relevant to solar models, where experimenters have succeeded in measuring some relevant cross sections at the energies corresponding to solar nucleosynthesis temperatures, such as for pp-chain reactions (Adelberger *et al.*, 2011), thus requiring the separation of screening enhancement from the data necessary in order to make them useful for reliable astrophysical applications. However, screening in plasmas within stars is not yet within experimental reach in nuclear laboratories, which require advanced theoretical investigations that are nearly independent of experimental validation, although some efforts to reproduce plasma conditions in the laboratory to study the screening effect have been undertaken (Gatu Johnson *et al.*, 2023). Evidently, more systematic and coordinated experimental efforts are necessary. Some theoretical explanations have attributed large screening potentials to clusterization effects in nuclear reactions, particularly those involving light nuclei (Spitaleri *et al.*, 2016).

In the framework of these considerations, we present the quantum physics phenomena that may cause effects within the energy range near the threshold, such as the emergence of broad single-particle or cluster structures near the particle threshold, as well as the associated interference patterns with direct capture, the tails of subthreshold states, or higher energy broad resonances. In Sec. II we first provide an overview of the different reaction models presently being used in low-energy nuclear physics. For modeling nonresonant processes between light nuclei, we focus first in Sec. II.A on *ab initio* reaction theory and then in Sec. II.B on applications of effective field theory. In Sec. II.C we first present the concept of open-quantum systems that emerge at the threshold, introducing unbound states as quantum configurations. This is followed in Sec. II.D by a discussion of how the configuration of these unbound states is influenced by the coupling of wave functions to the continuum, leading to the formation of pronounced cusps or near-threshold compound states, which are modeled in terms of the shell model embedded in the continuum (SMEC). This section also discusses a number of theoretical features that characterize these levels in appearance and strength through traditional parameters such as the SFs or ANCs. Section II.E demonstrates the SMEC approach in predicting the emergence of near-threshold resonance features on a number of recently analyzed light-ion-reaction samples near and beyond the line of stability.

Section III focuses on *R*-matrix theory, a more phenomenological reaction model that, however, has expanded in recent years into a multichannel formalism, which has considerably enhanced the predictive power of the approach. This approach has also recently benefited from new Bayesian uncertainty analysis methods that can be used to better characterize the uncertainty in cross-section extrapolations, as described in Sec. III.A. *R*-matrix theory is used here to demonstrate and visualize the aforementioned threshold features. It is used for extrapolating not only directly obtained cross-section data but also data obtained via the Trojan horse method (THM), which represents an indirect approach for exploring the resonance structure near the threshold in a complementary manner. The *R*-matrix section is therefore followed by Sec. III.B, in which the idea and procedure of the THM approach as well as the conversion of the transfer data into direct reaction data via *R*-matrix are presented.

These sections, which review the different aspects of nuclear reaction theory, are followed by Sec. IV, where we introduce the methods of converting experimentally obtained and extrapolated reaction cross sections into resonant and nonresonant reaction-rate contributions. These methods and their specific nomenclature were developed in the 1930s and 1940s and have been enshrined in multiple tabulations of thousands of reaction rates over the following decades. Modern calculations need to be adapted to ensure the continuance of the field and the accumulated data. As part of Sec. IV, we therefore summarize the methods and parameters traditionally used for determining the critical reaction components and energy regions for different stellar and anthropogenic plasma burning environments.

Section V shows specific examples of nuclear reactions in anthropogenic plasma burning as well as in stellar hydrogen, helium, and carbon burning environments. All of these represent complex reaction sequences; many of the associated reactions have been experimentally studied at higher laboratory energies, with the reaction rates relying on the application of theory for extrapolating the data toward the stellar energy range. For light-ion fusion processes, these calculations are based on effective field theory (EFT) and *ab initio* techniques, while for reactions involving higher mass compound nuclei exhibiting resonance features, the calculations are based on the aforementioned multilevel, multichannel *R*-matrix techniques. Section not only presents the low-energy features that have been observed but also discusses the uncertainties in the interpretation. For each of the different burning environments, a number of examples are presented that exhibit pronounced single-particle as well as cluster configuration features that can be considered near-threshold quantum wave coupling effects.

This is followed by Sec. VI, which addresses electron screening. Electron screening is due to the change of the deflective Coulomb barrier between two positively charged particles owing to the influence of the atomic electron shell or the surrounding electron cloud. This is a low-energy effect that seemingly causes an enhancement of the experimental cross-section data. Despite several reviews and discussion of the phenomenon, no satisfying theoretical treatments have been developed, and the screening corrections rely largely on reaction-dependent phenomenological considerations. Since screening can mimic threshold effects, it is important to discuss their impact in this context.

In Sec. VII, the final section before our conclusions are drawn in Sec. VIII, we present some observational evidence for deviations between the accelerator-based resonance studies and reaction rates derived from observed abundance features. There are only a few examples and they suffer from uncertainties in the stellar modeling techniques, but they provide some evidence that a closer look at these features is justified.

II. LOW-ENERGY REACTION MODELS

In the following sections, we provide an overview on developments in nuclear reaction theory that have been used to determine low-energy cross sections for bare nuclei and the corresponding nuclear reaction rates. The low-energy cross-section data have to be modified by the screening corrections associated with the specific stellar or experimental environment, as discussed in Sec. VI. Traditionally, experimental cross-section data used for nuclear astrophysics modeling have been described via phenomenological techniques that account for resonance contributions using single-level Breit-Wigner functions, plus possible nonresonant reaction components such as direct capture and high-energy resonance tail components, as more or less independent terms while ignoring possible interference effects. Extrapolation into the low-energy range primarily relied on fitting the low-energy slope of the S factor derived from data with linear or polynomial functions (Fowler, Caughlan, and Zimmerman, 1967, 1975). For nuclear reactions with heavier nuclei, the statistical Hauser-Feshbach model was typically utilized, with the prediction depending on the assumptions of high-level density as well as particle and γ-ray strength functions, which were derived by matching the predicted cross sections to the experimental data at higher energies (Holmes *et al.*, 1976; Thielemann, Arnould, and Truran, 1986; Rauscher and Thielemann, 2000; Rauscher, 2011; Koning and Rochman, 2012; Beard *et al.*, 2014). Many of the reaction rates obtained in this way are still used in modern rate libraries (Cyburt *et al.*, 2010). Several attempts have been made to use statistical assumptions to reach more reliable predictions at low energies (Sallaska *et al.*, 2013). However, reactions between light nuclei—as we consider them in this review—are characterized by specific enhanced single-particle or cluster structure configurations, which cannot be described in the framework of generalized statistical models.

Alternative methods have been developed based on the observation that, for astrophysically important reactions, the relevant bound and scattering states can be described by a common fragmentation into cluster states. In different degrees of sophistication, the models have in common that they attempt to describe nuclear bound states, scattering states, and resonances within the same unified framework. However, for astrophysical applications, some fine-tuning is needed in order to guarantee the reproduction of the energies of relevant states and thresholds. In the simplest realization, the nuclear states are approximated by two structureless fragments, with the dynamics stemming from a potential describing the relative motion. Such potential models have been applied to reactions that are important for solar burning (Christy and Duck, 1961; Tombrello and Parker, 1963; Bertulani, 1996). These models were then extended to describing the nuclear bound and scattering states using antisymmetrized many-body wave functions where the internal structure of the states was approximated by cluster structures. These microscopic cluster models exist in different realizations such as the resonating-group method (Tang, LeMere, and Thompsom, 1978; Descouvemont and Baye, 2010; Lashko, Vasilevsky, and Zhaba, 2024), the generator coordinate method (Langanke and Friedrich, 1986), the microscopic potential model (Langanke, 1994), the time-dependent cluster theory (Caurier, Grammaticos, and Sami, 1982; Drożdż, Okołowicz, and Płoszajczak, 1982; Bauhoff *et al.*, 1985), and the fermionic molecular dynamics model (Feldmeier, 1990; Kanada-En'yo, Kimura, and Ono, 2012). Usually, the models incorporate some empirical nucleon-nucleon (NN) interactions, while fermionic molecular dynamics attempt to use realistic NN interactions (Neff and Feldmeier, 2003; Kanada-En'yo, Kimura, and Ono, 2012). The microscopic cluster models were often successfully applied to nuclear structure problems, with the Hoyle state being the most prominent example (Tohsaki *et al.*, 2001; Chernykh *et al.*, 2007; Kanada-En'yo, 2007; Suzuki *et al.*, 2008; Neff and Feldmeier, 2009). [For *ab initio* studies, see Epelbaum *et al.* (2011), Lovato *et al.* (2016), and S. Shen *et al.* (2023).]

Astrophysical applications span over many light-particle reactions, with particular attention paid to the $^{3}\mathrm{He}(\alpha,\gamma)^{7}\mathrm{Be}$ (Liu, Kanada, and Tang, 1981; Kajino and Arima, 1984; Langanke, 1986; Altmeyer *et al.*, 1988; Wachter, Mertelmeier, and Hofmann, 1988; Csótó and Langanke, 2000; Kievsky *et al.*, 2008; Neff, 2011) and $^{7}\mathrm{Be}(p,\gamma)^{8}\mathrm{B}$ reactions (Descouvemont and Baye, 1988; Kolbe, Langanke, and Assenbaum, 1988; Johnson *et al.*, 1992; Csótó *et al.*, 1995; Csótó and Langanke, 1998; Descouvemont, 2004; Fossez *et al.*, 2015), which are both crucial for the production of high-energy solar neutrinos, and to the $^{12}\mathrm{C}(\alpha,\gamma)^{16}\mathrm{O}$ reaction (Descouvemont, Baye, and Heenen, 1984; Funck, Langanke, and Weiguny, 1985; Langanke and Koonin, 1985; Descouvemont and Baye, 1987; Drotleff *et al.*, 1993; Angulo and Descouvemont, 2000; Dufour and Descouvemont, 2008; Katsuma, 2008; deBoer *et al.*, 2017; Suzuki, 2021, 2023), with its importance for stellar helium burning. In addition, early attempts were made to study transfer reactions of medium-mass nuclei within the microscopic cluster model (Langanke, Stademann, and Weiguny, 1983) and, more recently, in the framework of the Gamow shell model (Mercenne *et al.*, 2023).

In the following sections, we review the important theoretical developments that focus on the calculation of nonresonant and resonant features in low-energy reaction cross sections, in particular, the emergence of near-threshold resonance phenomena. *Ab initio* methods, i.e., systematically improvable many-body approaches based on internucleon interactions and nucleonic degrees of freedom (Hergert, 2020; Ekström *et al.*, 2023), have seen dramatic progress over the past decade. They can now reach heavy nuclei (Hu *et al.*, 2022) and nuclear reactions (Navrátil and Quaglioni, 2020). Section II.A reviews the progress of *ab initio* nuclear reaction calculations in the context of astrophysical application. The EFT formulation of nuclear interactions is an alternative approach for nuclear cross-section calculations (Bedaque and van Kolck, 2002; Bertulani, Hammer, and van Kolck, 2002; Epelbaum, Hammer, and Meißner, 2009). Outlined in Sec. II.B, it offers a model-independent framework to extrapolate the reactions between light nuclei into the lower energy range. Resonances and cross sections can be described quantitatively using a real- and complex-energy shell model, a configuration-interaction approach; see Sec. II.C. This approach provides a straightforward explanation for the appearance of threshold states. In its most advanced no-core coupled-channel applications (Fernandez et al., 2023; Michel, Nazarewicz, and Płoszajczak, 2023), this method is capable of describing unbound configurations involving reaction channels with different mass or charge partitions.

Considerable improvement has also been made in developing new phenomenological as well as microscopic techniques in the calculation of nuclear cross sections for light particles. For phenomenological techniques the wider usage of the multichannel, multilevel R-matrix approach (Azuma et al., 2010) expanded the range of data that could be utilized to produce a more reliable cross-section calculation by parallel fitting the data of numerous reaction and decay channels. In Secs. II.A–II.E, we provide a summary of all these model techniques and the way that they can be utilized toward a reliable treatment of the reaction mechanism at very low energies that are inaccessible to experiments.

A. *Ab initio* reaction theory: Progress and status

Understanding the structure and the dynamics of atomic nuclei as systems of protons and neutrons interacting through the strong, electromagnetic, and weak forces is one of the major goals of nuclear physics. The reason why this goal has yet to be accomplished lies in the complex nature of the strong nuclear force emerging from the underlying theory of quantum chromodynamics (QCD) and in the challenging character of the quantum many-body problem for nucleons interacting via this force. At low energies relevant to nuclear physics, QCD is nonperturbative and difficult to solve. The relevant degrees of freedom for nuclei are nucleons, i.e., protons and neutrons, that are not fundamental particles but rather complex aggregations made up of quarks and gluons. The strong interactions among nucleons can be viewed as effective interactions emerging nonperturbatively from QCD. At present, our knowledge of NN interactions is limited to models. The most advanced and most fundamental of these models rely on a low-energy EFT of QCD, chiral EFT (Weinberg, 1991). This theory is built on the symmetries of QCD, including the approximate chiral symmetry. Chiral EFT involves unknown parameters, low-energy constants that in principle can be calculated within QCD but currently are fitted to experimental data. Chiral EFT naturally predicts higher-body forces, in particular, a three-nucleon (3N) interaction that is known to play an important role in nuclear structure and dynamics.

Ab initio calculations in nuclear physics use nucleons as the relevant degrees of freedom and also realistic internucleon forces (Hergert, 2020; Ekström et al., 2023). These forces are often the chiral EFT interactions that accurately describe the two-nucleon system and three-nucleon bound states. The forces are also calibrated to selected proton-deuteron scattering data and aim to predict the properties of atomic nuclei. Solving the *ab initio* nuclear many-body problem is a challenging task. The high-level strategy is to solve the nonrelativistic many-nucleon Schrödinger equation with internucleon interactions as the only input. This approach is more straightforward for well-bound nuclear states where one can apply numerous bound-state techniques. A realistic description of weakly bound and unbound states requires a proper treatment of continuum effects. For example, light nuclei are characterized by clustering and low-lying breakup thresholds; hence, applications of methods including the continuum are essential.

For the description of dynamics with the continuum, there are several successful exact methods for few-body systems with $A \leq 4$, for example, the Faddeev (Witała et al., 2001), Faddeev-Yakubovsky (Lazauskas and Carbonell, 2004), Alt-Grassberger and Sandhas (Deltuva and Fonseca, 2007), and hyperspherical harmonics methods (Kievsky et al., 2008). For $A > 4$ nuclei, the description of nuclear resonance properties, scattering, and reactions involves new approaches. Quantum Monte Carlo (Nollett et al., 2007; Lynn et al., 2016) and Faddeev-Yakubovsky methods (Lazauskas, 2018) are applied to calculate n-^{4}He scattering, nuclear lattice EFT calculations are applied to the ^{4}He-^{4}He scattering (Elhatisari et al., 2015), and the description of p-^{40}Ca scattering can be done within the coupled cluster method in the Berggren basis (Hagen and Michel, 2012). Powerful methods based on the no-core shell model (NCSM) (Navrátil, Vary, and Barrett, 2000a, 2000b; Barrett, Navrátil, and Vary, 2013), the no-core shell model with resonating-group method (NCSM RGM) (Quaglioni and Navrátil, 2009), and the no-core shell model with continuum (NCSMC) (Baroni, Navrátil, and Quaglioni, 2013a, 2013b; Navrátil et al., 2016) exist; they are later discussed in more detail. We also note that another NCSM-based method, the symmetry-adapted NCSM approach (Dytrych et al., 2020), has been applied to studying α clustering and can extend to a description of scattering (Launey, Mercenne, and Dytrych, 2021). Finally, the *ab initio* Gamow NCSM (Papadimitriou et al., 2013; Fossez et al., 2017; Li et al., 2021; Fernandez et al., 2023; Michel, Nazarewicz, and Płoszajczak, 2023), which is capable of describing nuclear resonances and near-threshold features, is also highlighted in this review.

The NCSMC is a unified framework for the treatment of both bound and unbound states in light nuclei. Using chiral NN and 3N interactions as the only input, the method is capable of predicting the structure and dynamics of light nuclei and, by comparing them to experimental data, test the quality of chiral nuclear forces. Describing a reaction (such as the scattering of protons from ^{7}Be) requires one to address both the correlated short-range behavior occurring when the reactants (proton and ^{7}Be) are close together, forming a composite nucleus (^{8}B), and the clustered long-range behavior occurring when the reactants are far apart. The NCSMC accomplishes this by adopting a generalized cluster expansion for the wave function of the reacting system, which, in the ^{8}B example, is given by

$$|\Psi^{J^\pi}_{^8\mathrm{B}}\rangle = \sum_\lambda c_\lambda^{J^\pi} |^8\mathrm{B}\lambda J^\pi\rangle + \sum_\nu \int dr\, r^2 \frac{\gamma_\nu^{J^\pi}(r)}{r} \hat{\mathcal{A}}_\nu |\Phi^{J^\pi}_{\nu r}\rangle. \qquad (2)$$

In the first term of Eq. (2), which consists of an expansion over (square-integrable) eigenstates of the composite system (^{8}B) obtained within the NCSM many-body harmonic oscillator basis with index λ, all A nucleons are treated on the same footing. In the second term of Eq. (2), which corresponds to a resonating-group method (Tang, LeMere, and Thompsom, 1978) expansion over (continuous) antisymmetrized channels, the wave function is factorized into products of cluster components (^{7}Be and p) and their relative motion, with proper bound-state or scattering boundary conditions,

$$|\Phi^{J^\pi}_{\nu r}\rangle = [(|^7\mathrm{Be}\alpha I^{\pi_t}\rangle|p\tfrac{1}{2}^+\rangle)^{(s)}Y_\ell(\hat{r}_{7,1})]^{(J^\pi)} \times \frac{\delta(r-r_{7,1})}{rr_{7,1}}, \quad (3)$$

where $|^7\mathrm{Be}\alpha I^{\pi_t}\rangle$ and $|p(1/2)^+\rangle$ are the eigenstates of the target (^{7}Be) and the projectile (proton), respectively. The vector $\boldsymbol{r}_{7,1}$ is the separation between the centers of mass of ^{7}Be and p, and the index ν labels the remaining quantum numbers. The discreet expansion coefficients $c^{J^\pi}_\lambda$ and the continuous relative-motion amplitudes $\gamma^{J^\pi}_\nu(r)$ are obtained as a solution to the generalized eigenvalue problem derived by representing the Schrödinger equation in the model space of Eq. (2). The cluster eigenstates (for example, ^{7}Be and p) are obtained within the NCSM, with the same Hamiltonian used to describe the entire system. In general, the sum over ν also includes excited states of clusters, as well as different cluster partitions.

The NCSMC approach has been applied to cross sections and rate calculations of several nuclear reactions relevant to astrophysics (Navrátil, Bertulani, and Caurier, 2006a; Navrátil and Quaglioni, 2020). The $^3\mathrm{H}(d,n)^4\mathrm{He}$ and $^3\mathrm{He}(d,p)^4\mathrm{He}$ reactions are leading processes in the primordial formation of the light elements (mass number $A \le 7$), affecting the predictions of big bang nucleosynthesis (BBN) for light-nucleus abundances (Serpico *et al.*, 2004). With its low activation energy and high yield, $^3\mathrm{H}(d,n)^4\mathrm{He}$ is the easiest reaction to achieve on Earth and is pursued by research facilities directed toward developing fusion power (Chadwick, Paris, and Haines, 2023). An advanced NCSMC investigation of the deuteron-triton (dt) fusion was presented by Hupin, Quaglioni, and Navrátil (2019). These calculations include both the $^4\mathrm{He} + n$ and the $^3\mathrm{H} + d$ (or $^3\mathrm{He} + d$) mass partitions in the cluster part of the NCSMC trial wave function given in Eqs. (2) and (3). While the main focus was on the calculation of observables for the polarized d and t nuclei that have not yet been measured, phase shifts, cross sections, and results for the mirror $^3\mathrm{He}(d,p)^4\mathrm{He}$ system were presented. Further details on these calculations are given in Sec. V.A.1.

An important input in modeling the solar-neutrino flux are the rates of the $^3\mathrm{He}(\alpha,\gamma)^7\mathrm{Be}$ and the $^7\mathrm{Be}(p,\gamma)^8\mathrm{B}$ radiative capture reactions (Navrátil, Bertulani, and Caurier, 2006a; Adelberger *et al.*, 2011). The $^7\mathrm{Be}(p,\gamma)^8\mathrm{B}$ reaction constitutes the final step of the nucleosynthetic chain leading to ^{8}B. *Ab initio* calculations of the $^7\mathrm{Be}(p,\gamma)^8\mathrm{B}$ reaction have been performed within the NCSMC formalism using a set of chiral NN and 3N interactions (Kravvaris *et al.*, 2023). The calculated S factor obtained with the most advanced interaction matches well with the direct measurement data (Junghans *et al.*, 2003) starting with the 1^+ resonance at $\approx$0.6 MeV in the energy range up to 2.5 MeV. At low energies below the 1^+ resonance, the predictions are slightly below the experiment results. Overall, the NCSMC calculations (Kravvaris *et al.*, 2023) are consistent with the latest recommended S-factor value at zero energy. Moreover, the theoretical uncertainty is reduced by more than a factor of 5. A more detailed description of these calculations is presented in Sec. V.A.4.

The $^3\mathrm{He}(\alpha,\gamma)^7\mathrm{Be}$ radiative capture plays an important role for both BBN and the solar pp chain (Adelberger *et al.*, 2011; Tribble *et al.*, 2014; Bertulani and Kajino, 2016). NCSMC calculations of ^{3}He-^{4}He and ^{3}H-^{3}He scattering are carried out starting with an NN and, more recently, also a 3N interaction. The properties of the low-lying resonances as well as those of the two bound states of ^{7}Be and ^{7}Li are reproduced well. With the scattering and bound-state wave functions obtained, the astrophysical S factor for the $^3\mathrm{He}(\alpha,\gamma)^7\mathrm{Be}$ solar-fusion cross section has been computed, as well as that of its mirror reaction $^3\mathrm{H}(\alpha,\gamma)^7\mathrm{Li}$ (Dohet-Eraly *et al.*, 2016; Atkinson *et al.*, 2025). At very low energies, the $^3\mathrm{He}(\alpha,\gamma)^7\mathrm{Be}$ S factor is in a good agreement with the measurements taken at the underground LUNA facility. This reaction is discussed further in Sec. V.A.3.

The production of ^{6}Li in BBN is dominated by $^4\mathrm{He}(d,\gamma)^6\mathrm{Li}$ radiative capture. The cross section at the relevant energies from 30 to 400 keV is poorly known, as direct measurements are hindered by the Coulomb repulsion between the ^{4}He and d nuclei. Moreover, indirect estimates relating the capture rate with the disintegration of ^{6}Li in the Coulomb field of a heavy target are hampered by the limited ability to cleanly separate the nuclear and electromagnetic contributions to the breakup cross section. Accurate theoretical predictions are therefore needed to guide the extrapolation of the existing direct measurements to the entire BBN range of energies. *Ab initio* NCSMC calculations have been performed for the $^4\mathrm{He}(d,\gamma)^6\mathrm{Li}$ reaction (Hebborn *et al.*, 2022). Contrary to previous studies, the $E1$ transitions are found to be negligible, and an enhancement of the capture below 100 keV comes from the previously neglected $M1$ transitions. The uncertainty in the predicted thermonuclear reaction rates is reduced by a factor of $\approx$7 compared to previous evaluations (Xu *et al.*, 2013). Further details can be found in Sec. V.A.2.

B. Ideas from effective field theory

EFT is based on the factorization of short-distance and long-distance physics. EFT methods were introduced in nuclear physics by Weinberg (1990, 1991, 1992). EFTs are formulated in terms of efficient degrees of freedom for the problem and so as to respect relevant symmetries. In this regard they are no different from any other quantum-mechanical model. Their point of difference lies in their inclusion of all relevant operators that both could govern the interaction and are consistent with the symmetries. This would produce an intractable problem, save that in an EFT one also identifies a set of short-distance, high-momentum scales and a set of long-distance, low-momentum scales. The operators are then organized in powers of the dimensionless ratio of these scales, and thus operators that carry higher powers of this ratio are less important. This in turn leads to expressions for the quantum-mechanical scattering amplitude—and ultimately for observables—in which less important effects occur at higher orders of the EFT expansion: a so-called power counting in which quantum-mechanical mechanisms are classified according to their impact on the amplitude.

EFTs are well suited for describing threshold physics. The reactions discussed in this review can be treated using effective two-body models, where the degrees of freedom are the particles in the entrance and exit channels. The EFT expansion systematizes these models. If clusterization within the participating nuclei is significant, the EFT can be formulated in terms of the degrees of freedom representing those clusters, thereby transforming the threshold dynamics description into a few-body problem.

The intellectual precursor of EFT relevant to the threshold physics discussed in this review is the few-body cluster-model calculations popular in the 1970s. However, this EFT, referred to as halo EFT or cluster EFT, organizes and updates those models. It organizes them by arranging mechanisms into a hierarchy based on power counting and updates them by ensuring that all mechanisms occurring at a given power-counting order are considered in the EFT calculation. Threshold physics calculations using halo or cluster EFT incorporate three-body forces and two-body currents that were rarely taken into account in cluster models.

An example of the early application of EFT to strong interactions at threshold is the case of the s-wave scattering of two particles, without Coulomb interactions, in the situation where there was a real or virtual bound state near the scattering threshold. The low-momentum scales in this problem are k and the characteristic momentum of the bound state is $1/a_0$. The high-momentum scale is set by the range of the interaction, which is of the order of the effective range r_0. The EFT is thus a dual expansion in the small parameters r_0/a_0 and r_0k. If we define $Q = r_0k$, then Weinberg (1991), Kaplan, Savage, and Wise (1998a, 1998b), Birse (1999), and van Kolck (1999) showed that the s-wave scattering amplitude in this EFT takes the form

$$f_{\mathrm{EFT}}(k) \propto \frac{1}{1/a_0 + ik}[1 + c_1(ka_0)Q + c_2(ka_0)Q^2 + \cdots]. \tag{4}$$

The functions c_n have nonanalytic dependence on the ratio of the light scales ka_0 but remain O(1) provided that $kr_0 \ll 1$. While we have written out Eq. (4) for the case of the s-wave scattering amplitude, an analogous formula applies for all low-energy processes involving s-wave interactions in the two-body system. The bound-state form factor, the radiative capture amplitude, Compton scattering from the bound state, etc., all have an expansion of the form of Eq. (4), as demonstrated for the NN system by Chen, Rupak, and Savage (1999). In that context the EFT is called pionless EFT.

Bertulani, Hammer, and van Kolck (2002) and Hammer and Phillips (2011) successfully applied the same methodology to ^{4}He-neutron scattering and the low-energy properties of ^{11}Be, respectively, thus extending "pionless EFT" to "halo EFT" (Bertulani, Hammer, and van Kolck, 2002). For a thorough review of halo EFT, see Hammer, Ji, and Phillips (2017).

The fact that the expansion of Eq. (4) has an identified small parameter makes it possible to assess the impact of the terms omitted from the description of the observables. Being able to compute beyond the leading order is thus a crucial piece of the EFT's phenomenological applicability. The next-to-leading-order (NLO) piece of this expansion (the piece $\propto c_1Q$) is due to the effective range r_0, which is introduced into the amplitude at NLO. At next-to-next-to-next-to-leading order (N^{3}LO) $[O(Q^3)]$, the shape parameter P_0 (which is assumed to scale $\approx r_0^3$) appears in the EFT expansion.

Recently, the Coulomb-free $^1S_0$ p-p scattering length has been determined by analyzing the cross section of the quasi-free $p + d \to p + p + n$ reaction at center-of-mass energies below 1 MeV. Without a Coulomb interaction, a model based on an EFT description in the universal window was developed to interpret the results (Tumino et al., 2023).

The impact of p waves on the scattering amplitude is also N^{3}LO unless there is a low-lying resonance or bound state in the p waves. The power counting for p waves in the presence of an additional low-energy scale associated with p-wave physics was worked out by Bertulani, Hammer, and van Kolck (2002) and Bedaque, Hammer, and van Kolck (2003). As with the s waves, the result can be understood in terms of an assignment of sizes to different p-wave effective-range parameters. The p-wave effective-range expansion is then systematically improved by the inclusion of additional orders in the EFT expansion parameter Q. This approach describes well, for example, the low-energy α-neutron (Bedaque, Hammer, and van Kolck, 2003), ^{10}Be-neutron (Hammer and Phillips, 2011), and ^{7}Li-neutron phase shifts (Rupak and Higa, 2011).

Charged-particle scattering in EFT has been implemented for proton-proton (Kong and Ravndal, 2000), α-α (Higa, Hammer, and van Kolck, 2008), and α-^{3}He scattering (Higa, Rupak, and Vaghani, 2018; Poudel and Phillips, 2022). For such problems the EFT reproduces the modified effective-range expansion of Bethe (1949), with a power counting that once again corresponds to particular choices for the size of the different effective-range parameters. The organization of the scattering amplitude in powers of a small expansion parameter is complicated in this case by the presence of an additional low-momentum scale associated with the Coulomb potential, $k/\eta \equiv k_C$, where η is the Sommerfeld parameter. The nonanalytic dependence of the inverse scattering amplitude on energy is then markedly more complicated than in the chargeless case, which means that more thought must be put into the organization of the EFT for situations where $\eta \approx 1$. Nevertheless, Higa, Hammer, and van Kolck (2008) and Poudel and Phillips (2022) both achieved systematic improvement in their description of charged-particle scattering data order by order in the EFT because they organized the modified effective-range expansion in s and p waves according to the size of the different effective-range parameters that occur. EFT applied to these problems can be thought of as reorganized effective-range theory, or effective-range theory with built-in uncertainty quantification.

Because the EFT by its construction reproduces the asymptotic behavior of scattering amplitudes and wave functions, calculating the external capture contribution to capture reactions is straightforward. The EFT then corrects this contribution through short-distance operators, which represent, for example, the contribution to the low-energy ^{7}Li(n,γ) capture amplitude from interparticle distances smaller than the range of the neutron-^{7}Li force. This is how the EFT incorporates "interior" contributions into its description of capture reactions. For weakly bound systems, this contribution is parametrically small. Because it occurs at short distances, it also cannot generate rapid energy dependence, so an expansion in powers of the photon energy is an expansion in ωr_0; i.e., it is organized similarly to the multipole expansion. This approach has been successfully applied to Coulomb dissociation on ^{11}Be (Hammer and Phillips, 2011; Capel, Phillips, and Hammer, 2018), ^{15}C (Rupak, Fernando, and Vaghani, 2012; Moschini, Yang, and Capel, 2019), and ^{19}C (Acharya and Phillips, 2013; Capel *et al.*, 2023), as well as to the radiative capture reactions $^7\mathrm{Li}(n,\gamma)$, and $^7\mathrm{Be}(p,\gamma)$ mentioned previously and $^3\mathrm{He}(\alpha,\gamma)$ (Higa, Rupak, and Vaghani, 2018; Zhang, Nollett, and Phillips, 2020).

As the collision energy is lowered toward the threshold for elastic scattering and capture reactions, the electromagnetic interaction plays a larger and larger role in the dynamics of charged-particle collisions. Incorporating the Coulomb interaction between the charged particles in the EFT is straightforward, as explained. Corrections to the electromagnetic force that go beyond the pointlike Coulomb field are a natural candidate for EFT calculations since the EFT expansion is akin to the multipole expansion. EFT can therefore easily incorporate the effect of the finite size of nuclei on the electromagnetic potential. The nuclear electric radius determines the coefficient of a higher-order operator governing the coupling of Coulomb photons to the nucleus (Chen, Rupak, and Savage, 1999; Hammer and Phillips, 2011). A similar higher-order operator incorporates the finite polarizability of nuclei into the internuclear electromagnetic potential (Chen *et al.*, 1998).

In the near-threshold regime, other corrections to the internuclear electromagnetic potential may also be important. Higher-order quantum electrodynamics effects are suppressed by a factor $\alpha_{\mathrm{em}} \approx 1/137$ compared to the Coulomb potential. But, given the exponential sensitivity of the reaction cross section to the height of the Coulomb barrier, they may need to be considered in certain contexts. Kamionkowski and Bahcall (1994) evaluated the vacuum-polarization corrections to capture reaction rates in the pp chain and the CNO cycle semiclassically. In particular, their calculation suggests that the reaction rate for $^3\mathrm{He}(\alpha,\gamma)^7\mathrm{Be}$ at solar energies falls by 1.6% once the vacuum polarization is considered. This argument was reexamined in the context of BBN by Pitrou and Pospelov (2020); the data and calculations of this reaction in the solar-fusion regime are now of sufficient precision for solar fusion such that the vacuum-polarization effect should now also be assessed there.

Vacuum polarization is a long-studied and measurable effect for proton-proton scattering. Bergervoet *et al.* (1988) performed a phase-shift analysis of pp-scattering data below 30 MeV (laboratory) with and without vacuum polarization. They found that the total χ^2 decreased by $\approx$100 when vacuum polarization was included in the model, an effect of 10 standard deviations for the data available at that time. Magnetic-moment interactions can also play a role at low energies—especially at forward angles, where they produce zero crossings in spin observables (Hogan and Seyler, 1970; Stoks and de Swart, 1990).

C. Continuum space in open-quantum-system approaches

Resonances and scattering features are genuine properties of quantum systems describing preferential decays of unbound states. Experimentally, the resonances are seen in cross sections as sharp peaks and exhibit a nearly exponential decay pattern as a function of time. The standard quantum mechanics in Hilbert space does not allow for the description of state vectors with exponential growth and an exponential decay (Baz', Zel'dovich, and Perelomov, 1969). Such states are simply discarded as unphysical. The usual procedure to deal with resonance states is either to extract their line shapes from the real-energy continuum-level density or to join the bound-state solution in the interior region with an asymptotic solution at large distances.

The aforementioned difficulties have been resolved by extending Hilbert space to the so-called rigged Hilbert space (Gel'fand and Vilenkin, 1964; Maurin, 1968; Bohm, 1978; Ludwig, 1983a, 1983b; Bohm, Dollard, and Gadella, 1989; de la Madrid, 2005, 2012; Antoine, 2021). The rigged Hilbert space is the Hilbert space equipped with distribution theory. In that sense the rigged Hilbert space is not the replacement but rather the enlargement of the Hilbert space. In this formulation the resonant wave functions are given by Gamow states, i.e., the eigenvectors of a Hamiltonian with complex eigenvalues. Gamow states can describe both sharp peaks in the cross section and decays of metastable states. Moreover, the shell model for open-quantum systems, as described in the following, can be conveniently formulated in the rigged Hilbert space.

Open-quantum systems are studied in different branches of physics, including nuclear physics, atomic physics, nanoscience, and quantum optics. In spite of their specific features, these different open-quantum systems exhibit common generic properties. What is identified as a quantum environment of the system depends on the physics context. The environments in quantum cosmology (Halliwell, 1991), quantum biology (Brookes, 2017), or quantum information science (Bennett and Shor, 1998) not only differ from one another but also differ from the environment of scattering states relevant to nuclear physics reaction problems (Okołowicz, Płoszajczak, and Rotter, 2003; Okołowicz, Płoszajczak, and Nazarewicz, 2012; Okołowicz, Nazarewicz, and Płoszajczak, 2013). In the standard approach, the dynamics of the system is considered explicitly, whereas the dynamics of the environment is treated implicitly. In this case evolution of the system is described in terms of the reduced density obtained by taking a partial trace over the exact density of a combined system plus environment. Hence, the evolution of the combined system plus environment is unitary. The main interest in studies using reduced density matrices is the energy transfer to the environment (the quantum dissipation) and/or the loss of coherence of the considered state(s) (the quantum decoherence).

In nuclear physics one deals with well-defined individual quantum states whose wave functions and preferential decay modes are studied experimentally. Consequently, quantum dissipation or quantum decoherence are not subjects of principal interest. The emphasis in the nuclear case is on the conservation of unitarity at the transition from well-bound states (the closed-quantum systems) to weakly bound or unbound states (the open-quantum systems) while approaching the limit of nuclear stability with respect to the particle emission. This transient regime is of special interest in nuclear astrophysics, particularly for understanding the nucleosynthesis of elements.

The key features of an open-quantum system are the interference processes between the states of a system and its environment. These aspects can be traced back to two basic processes: level repulsion and level clustering (Magunov, Rotter, and Strakhova, 1999; Okołowicz, Płoszajczak, and Rotter, 2003). In closed-quantum systems, the interaction between discrete levels is real; therefore, discrete levels with the same quantum numbers repel each other. However, in open-quantum systems, the level interaction may be complex, so the resonance states can either repel or attract each other.

When the energy distance between resonances becomes smaller than their width, a peculiar collectivization phenomenon takes place, namely, the total coupling strength becomes concentrated in a few states, while the remaining majority of states decouple from the continuum of the decay channels. This phenomenon, referred to as resonance trapping (Kleinwachter and Rotter, 1985; Sokolov and Zelevinsky, 1988; Rotter, 1991; Persson, Müller, and Rotter, 1996; Drożdż *et al.*, 2000; Stöckmann *et al.*, 2002; Auerbach and Zelevinsky, 2011), is related to the level crossings in the complex-energy plane. By increasing the strength of the coupling between discrete states and the environment of decay channels, the widths of most of the states decrease, while a few states become broad and dissolve into the continuum.

Near the particle-emission threshold, another collective rearrangement phenomenon takes place in which the essential role is played by a single "aligned" eigenstate of the open-quantum-system Hamiltonian, which carries many characteristics of the nearby decay channel (Okołowicz, Płoszajczak, and Nazarewicz, 2012; Okołowicz, Nazarewicz, and Płoszajczak, 2013). This state is a superposition of shell-model eigenstates having the same quantum numbers. The aligned eigenstate captures most of the continuum-coupling strength and, above the decay threshold, exhausts most of the decay width.

The standard shell model describes a nucleus as a closed-quantum system with nucleons occupying bound localized levels isolated from scattering states and decay channels. This picture is physically correct for low-lying states of well-bound nuclei. However, near the lowest particle-emission threshold, continuum coupling becomes more and more important. Moreover, near the threshold, the configuration mixing involving continuum states can no longer be treated as a small perturbation (Dobaczewski *et al.*, 2007). In fact, in the particle-unbound regime, nuclear states in neighboring nuclei form a network of interconnected states, with the clusters of correlated states in different domains of excitation energy, angular momentum, and nucleon number.

The incompleteness of a shell-model description of the atomic nucleus was realized early on. For instance, the inadequacy of perturbation theory for describing resonances was pointed out by Fano (1961), while the relative displacement of states in mirror nuclei was explained by the change of boundary conditions due to Coulomb wave function distortion in the external region (Ehrman, 1951; Thomas, 1952). Therefore, it was obvious that a radical conceptual change was required to resolve numerous drawbacks and inconsistencies present in the traditional nuclear shell model.

1. Real-energy frameworks

First attempts to reconcile the shell model with reaction theory were made by replacing the paradigm of the closed-quantum system with the paradigm of a system interacting with its environment of scattering states and decay channels. Using the projection operator technique, the collision matrix of the optical model was expressed in terms of the matrix elements of the nuclear Hamiltonian (Feshbach, 1958, 1962). This promoted the adaptation of the shell-model approach toward the treatment of nuclear reactions (Brenig, 1959; Fano, 1961; Rodberg, 1961; MacDonald, 1964a, 1964b) and, on the other side, led to various formulations of the continuum shell model in Hilbert space (Mahaux and Weidenmüller, 1969; Philpott, 1977; Rotter, Barz, and Höhn, 1978; Okołowicz, Płoszajczak, and Rotter, 2003; Volya and Zelevinsky, 2006). A version of the continuum shell model, the SMEC (Bennaceur *et al.*, 1999, 2000; Rotureau, Okołowicz, and Płoszajczak, 2006), provides a unified description of the nuclear structure and of reactions with up to two nucleons in the scattering continuum using the Hamiltonian for a closed-quantum-system shell model. The proper framework for this formulation of continuum shell model is the non-Hermitian quantum mechanics, which is an important alternative to the standard Hermitian quantum mechanics (Okołowicz, Płoszajczak, and Rotter, 2003; Moiseyev, 2011).

In the SMEC approach, one divides the Fock space of an A-particle system into two subspaces: the subspace of a bound nucleus, which consists of square-integrable functions of the standard shell model, and the subspace of the scattering environment embedding the system, which consists of scattering states and decay channels. The combined system—which consists of a bound nucleus and the environment—remains closed and is described by the Hermitian Hamiltonian. The dynamics in the nucleus is given by the energy-dependent effective Hamiltonian, which includes couplings to the subspace of the environment. The SMEC effective Hamiltonian is Hermitian below the lowest reaction threshold, whereas above the first threshold, the non-Hermitian part describes irreversible decay from the system to the environment. The SMEC eigenstates are the linear combinations of closed-quantum-system eigenstates, i.e., the shell-model eigenstates. The continuum-induced mixing of shell-model eigenstates is particularly strong if many avoided crossings of SMEC eigenstates appear (Okołowicz, Płoszajczak, and Rotter, 2003; Okołowicz, Płoszajczak, and Nazarewicz, 2012; Okołowicz, Nazarewicz, and Płoszajczak, 2013). These crossings can be studied by calculating either energy trajectories of the double poles of the scattering matrix for the complex-extended SMEC Hamiltonian or the continuum-coupling correlation energy. The latter is the expectation value in a given SMEC eigenstate of the continuum-coupling term, i.e., the difference between the SMEC effective Hamiltonian and the shell-model Hamiltonian.

2. Complex-energy frameworks

Difficulties with the treatment of resonances in the Hilbert space formulation of quantum mechanics could be overcome in a rigged Hilbert space. Mathematical formulation of the rigged Hilbert space (Gel'fand and Vilenkin, 1964; Bohm, 1978; de la Madrid, 2005; Antoine, 2021) was facilitated by the necessity to accommodate the Dirac formalism of bras and kets in quantum mechanics (Ludwig, 1983a, 1983b). The rigged Hilbert space is a natural setting for Gamow states (Gamow, 1928; Siegert, 1939) and therefore provides a rigorous mathematical framework for extending the domain of quantum mechanics into time-asymmetric processes like decays or captures. An important change with respect to the standard Hilbert space formulation of quantum mechanics is that one can accommodate a more general completeness relation, the so-called Berggren completeness relation (Berggren, 1968, 1978, 1996; Maurin, 1968; Berggren and Lind, 1993; Lind, 1993), where the contribution of real-energy scattering states is substituted for by the resonant contribution and the background contribution of complex-energy scattering states. In this way the resonant spectrum of Gamow states is treated in the same way as the bound-state spectrum. In this approach the only difference between narrow resonances and bound states is purely quantitative, namely, resonances have nonzero decay widths, whereas the bound states have no decay width.

The configuration-interaction approach based on Gamow states, the so-called Gamow shell model (Id Betan *et al.*, 2002; Michel *et al.*, 2002; Michel *et al.*, 2003, 2009; Papadimitriou *et al.*, 2013; Michel and Płoszajczak, 2021), is a complex-energy generalization of the standard shell model in which the harmonic oscillator basis is replaced by the Berggren basis that includes bound states, resonant states, and complex-energy scattering states. The shell model in this formulation respects unitarity in all regimes of the binding energy and provides a comprehensive description of both the configuration interaction and the shell structure while removing inconsistencies and limitations present in the standard shell model. We emphasize that, as in the standard shell model and contrary to the SMEC, the Gamow shell model describes nucleus-plus-scattering space as an isolated quantum system. Hence, no interaction with the environment is necessary to describe the system decay. In addition, as in the standard shell model and in contrast to a real-energy continuum shell model like the SMEC, the Gamow-shell-model Hamiltonian is Hermitian even though the Gamow-shell-model Hamiltonian matrix is complex symmetric as in the SMEC. As demonstrated by Kruppa *et al.* (2014) and Masui *et al.* (2014), the Gamow shell model can be related to a complex scaling method (Myo and Katō, 2020).

To describe nuclear reactions, one has to express the Gamow shell model in the coupled-channel representation (GSM CC) (Jaganathen, Michel, and Płoszajczak, 2014; Fossez *et al.*, 2015; Mercenne, Michel, and Płoszajczak, 2019; Michel and Płoszajczak, 2021; Fernandez *et al.*, 2023; Mercenne *et al.*, 2023). In this representation the Gamow shell model unifies the nuclear structure and nuclear reactions because the same Hamiltonian and the same many-body approach describe both the discrete part of the energy spectrum and the reaction cross sections at low excitation energies. Different formulations of the Gamow shell model, interchangeably using either Slater determinant or coupled-channel representations and formulated either in Jacobi coordinates or in cluster orbital shell-model variables (Suzuki and Ikeda, 1988), allow for the study of the consequences of flux conservation (unitarity) at and around reaction thresholds.

D. Coupling to the continuum and the emergence of threshold states

As the incident energy increases and a new reaction channel opens, the reaction threshold becomes a bifurcation point for the particle flux. The reaction cross sections around the threshold energy exhibit resonancelike structures that arise due to the unitarity of the scattering matrix and the resulting flux conservation. The energy profile of these structures, or cusps, which should not be associated with actual nuclear states, markedly differ from the usual Breit-Wigner shapes characteristic of nuclear resonances. Together with resonances, these near-threshold irregularities can impact the astrophysical S factor.

Based on general principles (specifically, the asymptotic behavior of the scattering wave function), Wigner (1948) formulated the threshold law for the elastic and total cross sections, which explains the appearance and properties of near-threshold cusps. A more quantitative explanation of this phenomenon was later given in terms of R-matrix theory (Baz, 1957; Breit, 1957; Newton, 1958; Fonda, 1961; Meyerhof, 1963; Baz', Zel'dovich, and Perelomov, 1969; Lane, 1970), as discussed in Sec. III. In the case of reactions with neutral particles such as neutrons, the low-energy behavior of the partial cross section $\sigma(i \to j)$ leading from channel i to channel j takes a particularly simple form. For an endoergic reaction with the production of slow neutral particles,

$$\sigma(i \to j) \approx k_j^{2\ell_j+1} \approx E_j^{\ell_j+1/2}, \tag{5}$$

while for an exoergic reaction (for example, the absorption of slow neutrons by nuclei),

$$\sigma(i \to j) \approx k_i^{2\ell_i-1} \approx E_i^{\ell_i-1/2}. \tag{6}$$

The best-known example for the relation of Eq. (6) is the $1/v$ law for the absorption of slow neutrons. As one can see in Eqs. (5) and (6) the energy-momentum derivative of the cross section exhibits a discontinuity when the reaction threshold is passed, which results in a cusp. This effect is particularly pronounced for the low partial waves $\ell = 0$ and 1.

A Wigner cusp also appears in SFs when the energy of a many-body state crosses the particle-emission threshold. One-neutron SFs in the ground states of ^{6}He and ^{7}He are shown in Fig. 2. The Hamiltonian parameters are varied in such a way that the ground states of the ^{5}He nucleus (upper panel), and ^{6}He nucleus (lower panel) vary from bound to unbound continuously, thus simulating formation of a composite system at different excitation energies. The Wigner cusp originates uniquely from coupling to the

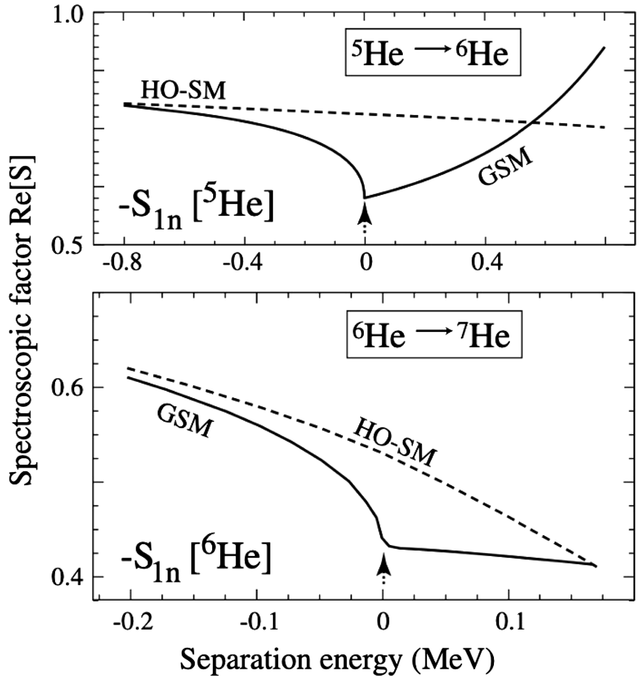

FIG. 2. Real part of the SF as a function of the (negative) one-neutron separation energy S_{1n}. Top panel: $\langle {}^6\mathrm{He(g.s.)}|[{}^5\mathrm{He(g.s.)} \otimes p_{3/2}]^{0^+}\rangle^2$. Bottom panel: $\langle {}^7\mathrm{He(g.s.)}|[{}^6\mathrm{He(g.s.)} \otimes p_{3/2}]^{0^+}\rangle^2$. The solid line represents Gamow-shell-model results, while the dotted line marks the standard shell-model approximation (HO-SM). The neutron-emission thresholds in ^{5}He (top panel) and ^{6}He (bottom panel) are indicated by arrows. Adapted from Michel, Nazarewicz, and Płoszajczak, 2007.

nonresonant continuum, as it disappears in standard shell-model calculations utilizing a basis of harmonic oscillator states; see Fig. 2. Note that in the complex-energy framework of the GSM, all quantities for resonances are normalized using the external complex scaling method and become complex. The real part, as explained by Berggren (1968), Michel and Płoszajczak (2021), and Myo and Katō (2020), is the average value, while the imaginary part can be related to the dispersion rate over time in the measurement and hence represents its statistical uncertainty. Figure 2 shows the real part of the calculated spectroscopic factors.

A Wigner cusp may appear in different reaction channels due to the channel-coupling phenomenon related to a flux redistribution. Indeed, owing to the flux conservation, the threshold anomaly present in an opening reaction channel can trigger the appearance of anomalies in other open channels with lower reaction thresholds. Ample experimental evidence exists for Wigner-type anomalies and channel-coupling effects in nuclear reactions (Adair, 1958; Almqvist, Bromley, and Kuehner, 1960; Wells, Tucker, and Meyerhof, 1963; Moore *et al.*, 1966; Hategan, 1973; Hodgson, 1976; Switkowski, Heggie, and Mann, 1978; Abramovich, Guzhovsky, and Lazarev, 1992; Starostin *et al.*, 2005; Batley *et al.*, 2006; Abramovich, 2015) and atomic processes (Wang, Chu, and Laughlin, 1994; Sadeghpour *et al.*, 2000; Bilodeau *et al.*, 2009; Caradonna *et al.*, 2012), as well as in condensed matter physics (Ishigami *et al.*, 2018).

The appearance of near-threshold resonances can be explained in terms of the increased density of levels that have large reduced widths (Inglis, 1962; Barker, 1964; Lane, 1970). For neutron channels this enhancement is largest for low barrier potentials, i.e., for low partial waves (Barker, 1964; Okołowicz, Płoszajczak, and Nazarewicz, 2012; Okołowicz, Nazarewicz, and Płoszajczak, 2013). The enhancement of the level density depends weakly on the nuclear mass, and hence near-threshold effects for neutron channels can be observed in both light and heavy nuclei.

For charged-particle channels, the enhancement of the level density depends both on the strength of the Coulomb interaction and on the angular momentum involved. The maximum of the enhancement factor is shifted above the threshold and decreases with increasing strength of the Coulomb interaction (Okołowicz, Płoszajczak, and Nazarewicz, 2012; Okołowicz, Nazarewicz, and Płoszajczak, 2013). Hence, the effect is strongest in the p- and sd-shell nuclei.

The continuum-level density $g_\ell(E)$ is proportional to the energy derivative of the scattering phase shift $\delta_\ell(E)$ (Beth and Uhlenbeck, 1937; Kruppa and Arai, 1999),

$$g_\ell(E) = \frac{2\ell + 1}{\pi}\frac{d\delta_\ell(E)}{dE}. \tag{7}$$

Equation (7) naturally connects the Wigner cusp phenomenon with the appearance of threshold resonances and antibound (or virtual) states (Ohanian and Ginsburg, 1974).

The threshold effects in nuclear reactions such as the Wigner cusp are manifestations of the quantum openness of the nuclear many-body system. In Secs. II.D.1–II.D.8, threshold physics is discussed within open-quantum-system frameworks, which allow for the coherent incorporation of the particle continuum into a many-body description.

1. Resonant states in the complex-momentum plane

The classification of resonant states (poles of the S matrix) in the complex-k plane is shown in Fig. 3. This classification applies to a general many-body case (Humblet and Rosenfeld, 1961), not only to the single-particle situation often discussed in the context of the Berggren ensemble.

The bound states lie on the positive imaginary-k axis. The decaying poles in the fourth quadrant, which lie close to the real-k axis and have a real energy $\mathrm{Re}(E) > 0$ and width $\Gamma = -2\,\mathrm{Im}(E) > 0$, can be interpreted as narrow resonances seen experimentally as narrow peaks in cross sections. The poles with $\mathrm{Re}(E) < 0$ and $\Gamma > 0$ located below the $-45°$ line can be associated with subthreshold resonant states (Mukhamedzhanov *et al.*, 2010); an example of such a state is the diproton (Kok, 1980). The antibound (or virtual) states with $\mathrm{Re}(E) < 0$ and $\Gamma = 0$ lie on the negative imaginary-k axis or on the second Riemann energy sheet (Ohanian and Ginsburg, 1974); a dineutron is believed to be such an antibound state (Babenko and Petrov, 2013). In this case the attractive interaction between the two neutrons is insufficient to produce a bound state, but the nearly bound nature is manifested by enhanced $n + n$ scattering just above threshold.

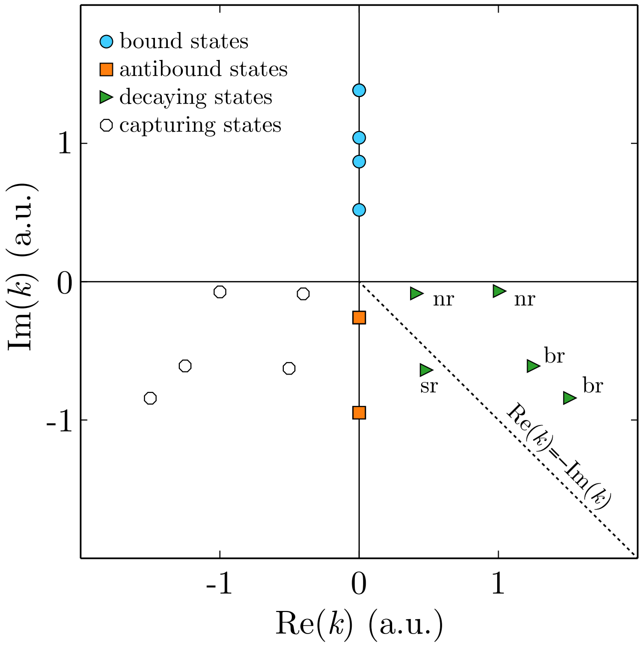

FIG. 3. Resonant states in the complex-k plane. The momentum is expressed in arbitrary units (a.u.). Bound, antibound, decaying, and capturing resonant states are marked, as are narrow resonances (nr), broad resonances (br), and subthreshold resonances (sr). The distribution of poles is symmetric with respect to the imaginary k axis because of time-reversal symmetry; thus, capturing states are presented as the time-reversed decaying states. The dashed $-45°$ line separates decaying resonant states from subthreshold poles.

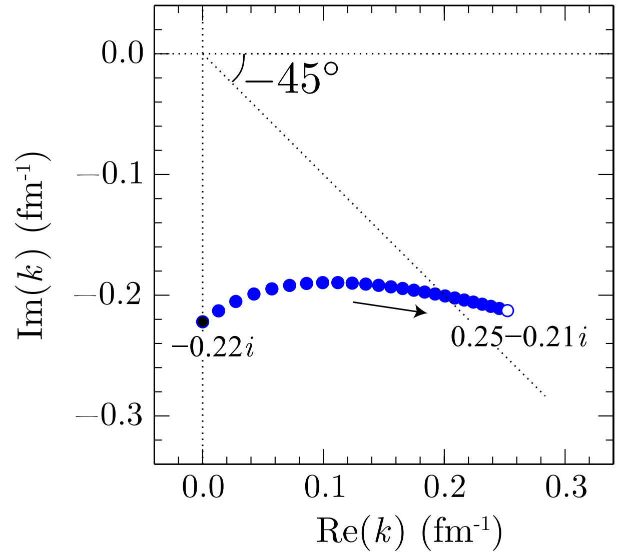

FIG. 4. The trajectories of the two threshold poles in the $\ell = 0$ channel of the Woods-Saxon and Coulomb potential in the complex-momentum plane as a function of the core charge $-Z_c e$. The trajectory begins at $Z_c = 0$ (black dot, $n + {}^9$Li) and ends at $Z_c = 6$ (open circle, $p + {}^9$C). Adapted from Wang et al., 2019.

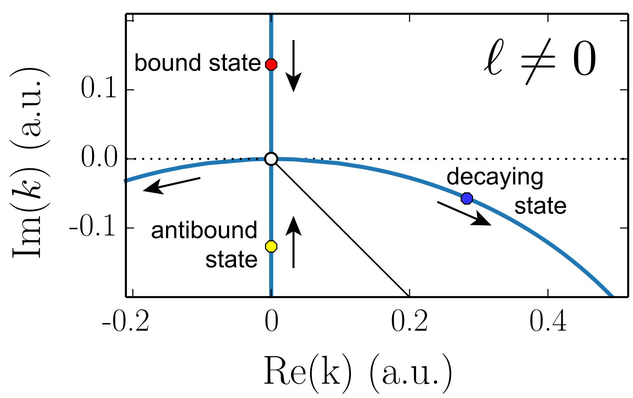

FIG. 5. The trajectory of the $\ell \neq 0$ resonant state in the complex-k plane as a function of the binding potential depth. The potential strength decreases along the direction indicated by the arrow. The positions of the bound and antibound states are marked. The momentum is in arbitrary units (a.u.).

The broad resonant states are located above the $-45°$ line and their widths are comparable with Re(E).

2. Bound-to-unbound transition

As the parameters of the Hamiltonian vary, resonant poles move in the complex-k plane. With the decreasing strength of the binding potential, the originally bound pole crosses the separation-energy threshold. What happens next depends on whether one is dealing with neutral or charged particles, and also on the associated orbital angular momentum (Domcke, 1981; Lovas et al., 2002; Mao, Fossez, and Nazarewicz, 2018; Wang et al., 2019).

After crossing the threshold, the s-wave-dominated bound state becomes an antibound pole (no Coulomb interaction) or a so-called subthreshold pole [Coulomb interaction is present for which the imaginary part of energy is larger than the real part (Kok, 1980; Mukhamedzhanov et al., 2010; Wang et al., 2019)]. To illustrate this, Fig. 4 shows the trajectory of the antibound state of ^{10}Li in the complex-k plane by gradually increasing the Coulomb interaction by way of changing the core charge $-Z_c e$ from zero ($n + {}^9$Li) to the full $p + {}^9$C value at $Z_c = 6$; see Wang et al. (2019) for details. At $Z_c = 0$ the antibound state of ^{10}Li is predicted. With increasing Z_c this pole goes through the region of subthreshold resonances and eventually becomes a threshold resonant state in ^{10}N at $Z_c = 6$.

For states with $\ell \neq 0$, the trajectory follows the generic pattern discussed by Domcke (1981) and Mao, Fossez, and Nazarewicz (2018) and illustrated in Fig. 5. As the binding decreases, the bound state with $\ell \neq 0$ and the shadow antibound pole meet at the threshold and produce an exceptional point. (Close to the threshold, the bound state and the shadow antibound state are located symmetrically to the origin.) As the binding interaction decreases further, two resonant poles—one decaying and one capturing [symmetric with respect to the Im(k) axis]—appear and move into the complex-k plane.

3. Existence of a nuclear state

Moving away from particle thresholds, either in isospin or excitation energy, the decay widths of nuclear states increase, eventually melting into the particle continuum as their lifetimes become comparable with the reaction and single-particle timescales below 10^{-22} s. Here the notion of the nuclear state becomes questionable, as the timescales are too short to generate the nuclear mean field (Thoennessen, 2004). In this regime the broad bumps in cross sections should be understood in terms of scattering features rather than well-defined resonances. For $A \approx 8$ the decay width at the boundary of the single-particle timescale is of order $\Gamma = 3.5$ MeV (Wang et al., 2019). Note that the level density or spectral function of Eq. (7) of scattering features is expected to deviate strongly from the Breit-Wigner shape that is characteristic of resonances. Such deviations, if present, imply a nonexponential character of quantum decay (Ramírez Jiménez and Kelkar, 2018; Wang et al., 2023; Volya and Zelevinsky, 2024).

There are numerous examples of scattering features. They include the dineutron (an antibound state manifested by enhanced $n + n$ scattering cross section just above threshold); the diproton (a subthreshold resonance); and a tetraneutron (Duer et al., 2022), which is a final-state effect (Deltuva, 2018; Higgins et al., 2020). The first excited state of ^{8}C and the ground states of ^{9}N and ^{9}He can also be understood as scattering features (Charity et al., 2023). The low-energy bumps in cross sections that are attributed to scattering features can significantly impact astrophysical S factors; hence, their recognition and identification are important.

4. Mirror nuclei

Threshold effects are particularly visible in pairs of mirror nuclei whose structure should be identical within the limit of isospin symmetry. In reality, differences between mirror partners are always present due to electromagnetic effects. In particular, the Coulomb force results in asymmetries between proton and neutron thresholds and the different asymptotic behavior of proton and neutron wave functions, both of which are manifested through the Thomas-Ehrman effect (Ehrman, 1951; Thomas, 1951a, 1952; Auerbach and Vinh Mau, 2000; Grigorenko et al., 2002; Michel, Nazarewicz, and Płoszajczak, 2010). A good illustration of the Thomas-Ehrman effect, shown in Fig. 4, is the difference between the ground-state poles of the mirror nuclei ^{10}Li and ^{10}N (Wang et al., 2019), which is analogous to the situation seen in the mirror pair of a dineutron and a diproton. The Thomas-Ehrman phenomenon is thus expected to impact the low-energy cross sections, SFs, and ANCs (Michel, Nazarewicz, and Płoszajczak, 2010; Okołowicz et al., 2012). In particular, single-particle ANCs exhibit generic behavior that is different for charged and neutral particles (Timofeyuk and Descouvemont, 2005; Timofeyuk, Johnson, and Mukhamedzhanov, 2006; Okołowicz et al., 2012; Brune, 2020). In the following we summarize the concepts of both the SFs and the ANCs as they are presently used in reaction cross-section estimates.

5. Spectroscopic factors

The reaction cross sections are often approximated by the product of the single-particle cross section derived from a one-body potential scattering model and the spectroscopic factor. For example, in terms of asymptotic normalization coefficients, the spectroscopic factor $\mathcal{S}_{s\ell}$ is (Macfarlane and French, 1960; Mukhamedzhanov, Gagliardi, and Tribble, 2001)

$$\mathcal{S}_{s\ell} = \frac{C_{s\ell}^2}{b_{s\ell}^2}, \tag{8}$$

where $C_{s\ell}$ is the experimentally measured ANC and $b_{s\ell}$ is the single-particle ANC calculated from a model. Usually, spectroscopic factors are calculated in the closed-quantum-system shell model. Consequently, the cross-section anomalies due to the proximity of decay thresholds are absent. Moreover, shell-model spectroscopic factors are often calculated in a restricted model space, and hence they contain a spurious basis dependence.

The near-threshold behavior of spectroscopic factors depends on the interference between resonant states and the nonresonant continuum. This behavior is therefore a direct consequence of unitarity near the particle-emission threshold. As spectroscopic factors monitor the occupancy of single-particle shells, their variation also reveals the modification of the NN interaction and NN correlations.

The Gamow-shell-model calculation of spectroscopic factors using a complete Berggren basis has demonstrated cusps identical to those known in the reaction cross sections (Michel, Nazarewicz, and Płoszajczak, 2007). They are particularly visible for neutron $\ell = 0$ and 1 waves, while their manifestation is less apparent in neutron waves with $\ell \geq 2$.

Variations of spectroscopic factors in the neighborhood of charged-particle decay thresholds are different from those near neutral-particle thresholds (Michel, Nazarewicz, and Płoszajczak, 2007). This difference has important consequences for the microscopic properties of nuclear states at the opposite extremes of nuclear stability, namely, at the neutron and proton drip lines.

Calculation of spectroscopic factors in open-quantum-system frameworks of the Gamow shell model and the SMEC allows for the investigation of their dependence on the separation energy. By comparing the calculated spectroscopic factors with those obtained in the closed-quantum-system shell model, the continuum effects on spectroscopic factors can be quantified. It was found that the value of the one-nucleon spectroscopic factor in well-bound states obtained in the open-quantum-system frameworks is significantly reduced compared to the traditional shell-model value (Wylie et al., 2021). This surprising behavior can be explained by the coupling to the nonresonant continuum space. If a well-bound minority species nucleon is removed from a well-bound orbit, then the daughter nucleus moves in the direction of the drip line. This leads to a significant change in configurations of majority species nucleons (weakly bound nucleons) that are impacted by continuum effects; thus, the spectroscopic factor is reduced. Hence, in the vicinity of the neutron (proton) drip line, protons (neutrons) are more strongly correlated. This effect has also been noted in dispersive optical-model studies (Dickhoff, 2010).

While conceptually the same, the use of spectroscopic factors has been largely replaced by the ANC due to its reduced model dependence (Mukhamedzhanov and Blokhintsev, 2022). The goal is to find a way to characterize the strengths of bound states in a manner analogous to the partial width for an unbound state. In this way the ANC provides a more accurate way of communicating the strength of a bound state across different theories, in particular, between the previously described potential models and R-matrix theory, as discussed later.

6. Asymptotic normalization coefficients

As discussed in Sec. II.D.5, spectroscopic factors characterize the single-particle or cluster structure of bound states. The main drawback of this method is that the spectroscopic factor is a heavily model-dependent quantity. This makes it challenging to compare spectroscopic factors that are derived using different model assumptions. The ANC is the bound-state analog to a partial width and is a model-independent quantity; see Mukhamedzhanov and Blokhintsev (2022) for a recent review. As described by Mukhamedzhanov and Tribble (1999), for example, the spectroscopic factor is related to the square of the ANC divided by the square of a single-particle ANC. The ANC is a model-independent quantity that can in principle be experimentally determined, while the single-particle ANC must be calculated from a specific model. In practice, the experimental determination of ANCs typically involves some model dependence, but it is reduced compared to the spectroscopic factor.

ANCs can be derived through the analysis of direct reaction data, where they are correlated to the cross section of direct capture transitions or directly to the strength of near-threshold resonances. They also play also an important role in the analysis of single-particle or cluster transfer reactions and the associated analysis of Trojan horse data. Note that both methods suffer from significant systematic uncertainties. Transfer reaction studies contain uncertainties not only from experimental measurements of the transfer cross sections but also pertaining to the distorted-wave-Born-approximation (DWBA) or coupled-channel models used. For example, many α-particle transfer studies employ the $(^6\mathrm{Li}, d)$ reaction; hence, the resulting ANC depends on the ANC of ^{6}Li. While this ANC was believed to be well established, recent *ab initio* calculations suggest that it should be 30% larger than the accepted value (Hebborn *et al.*, 2022), thus decreasing all ANCs that were determined relative to it by a similar amount. A difference of 30% is significant compared to the uncertainties of many ANCs, where some give uncertainties below 20% (Brune *et al.*, 1999; Avila *et al.*, 2015a). The uncertainties in the potential model parameters are often the limiting factor for the precision obtained. However, in cases where the kinematics are favorable, sub-Coulomb transfer reactions are possible (Brune *et al.*, 1999), thus significantly alleviating this dependence. In Sec. III.A.1 we discuss in more detail the use of the ANC in the framework of the THM approach and in R-matrix simulations.

7. Chameleon nature of near-threshold states

Observation of near-threshold irregularities in spectroscopic factors raise the following question: How does the proximity of the particle-emission threshold change the structure of nuclear states? In this context coupling to the nonresonant scattering continuum is essential for describing the energy dependence of reaction channel probabilities, overlap functions, and spectroscopic factors; i.e., this coupling is crucial to preserving the unitarity.

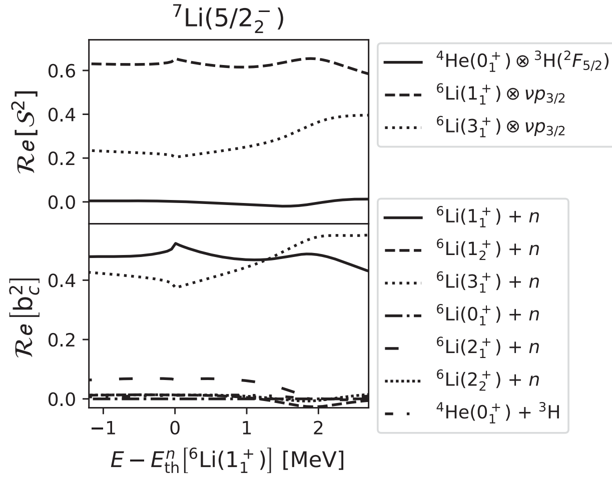

FIG. 6. Spectroscopic factors and reaction channel probabilities in the $5/2_2^-$ state of ^{7}Li are calculated in the GSM CC as a function of the distance with respect to the neutron-emission threshold $[^6\mathrm{Li}(1_1^+) \otimes n(\ell j)]^{J^\pi}$. Upper panel: the real part of the spectroscopic factors $\mathrm{Re}(\mathcal{S})$. Lower panel: the real part of the channel weights $\mathrm{Re}(b_c^2)$. The vertical dotted line shows the experimental position of the $5/2_2^-$ state. Adapted from Fernandez *et al.*, 2023.

Figure 6 illustrates the salient dependence of spectroscopic factors and channel probabilities in the $5/2_2^-$ resonance in ^{7}Li on the energy difference with respect to the lowest one-neutron decay threshold $[^6\mathrm{Li}(1_1^+) \otimes n(\ell j)]^{J^\pi}$ (Fernandez *et al.*, 2023). Only the largest neutron and tritium spectroscopic factors and channel probabilities are shown. The quantum numbers of a many-body projectile are customarily denoted by $^{2J_{\mathrm{int}}+1}(L)_{J_{\mathrm{P}}}$, where J_{int}, L, and J_{P} are the intrinsic spin of the projectile, its center-of-mass angular momentum, and the total angular momentum, respectively. These angular quantum numbers are denoted by ℓj when one deals with one-nucleon projectiles. In the case of the reaction channel involving tritium, $J_{\mathrm{int}} = 1/2$, $L = 3$, and $J_{\mathrm{P}} = 5/2$. In Fig. 6, we show only the real parts of the spectroscopic factors and the reaction channel probabilities.

The energy difference between the $5/2_2^-$ state and the neutron threshold is varied by changing the depth of the ^{4}He-core potential (Fernandez *et al.*, 2023). A Wigner cusp may be evident both in the probability of the reaction channel $[^6\mathrm{Li}(1_1^+) \otimes n(\ell j)]^{5/2^-}$ and in the real part of the spectroscopic factor. At higher energies below the opening of the next neutron channel $[^6\mathrm{Li}(3_1^+) \otimes n(\ell j)]^{J^\pi}$, the probability of this reaction channel starts to dominate the $5/2_2^-$ wave function.

This example demonstrates that the many-body state of the open quantum system (see Sec. I) mimics certain features of its environment regarding scattering states and reaction channels; i.e., the microscopic structure of the open-quantum-system eigenstate is not immutable. In this sense the alignment of a many-body state at the threshold of a decay channel (Okołowicz, Płoszajczak, and Nazarewicz, 2012, 2020; Okołowicz, Nazarewicz, and Płoszajczak, 2013; Okołowicz et al., 2018) is simply a specific manifestation of the generic chameleon nature of the nuclear open-quantum-system states.

8. Near-threshold clustering

What can be said about the properties of many-body states around the reaction threshold? Are they universal, independent of any particular realization of the Hamiltonian? The configuration mixing that involves discrete resonant states and a continuum of nonresonant scattering states is a source of numerous collective phenomena, such as resonance trapping (Kleinwachter and Rotter, 1985; Sokolov and Zelevinsky, 1988; Rotter, 1991; Persson, Müller, and Rotter, 1996; Drożdż et al., 2000; Stöckmann et al., 2002), the superradiance effect (Dicke, 1954; Auerbach and Zelevinsky, 2011), near-threshold clustering and correlations (Okołowicz, Płoszajczak, and Nazarewicz, 2012; Okołowicz, Nazarewicz, and Płoszajczak, 2013; Okołowicz et al., 2018; Fernandez et al., 2023), multichannel coupling effects in reaction cross sections (Baz, 1957; Newton, 1959; Hategan, 1973, 1978) and shell occupancies (Michel, Nazarewicz, and Płoszajczak, 2007), the modification of spectral fluctuations (Fyodorov and Khoruzhenko, 1999), and deviations from Porter-Thomas resonance width distributions (Drożdż et al., 2000; Koehler et al., 2010; Celardo et al., 2011).

The phenomenon of clustering near cluster emission thresholds does not find a coherent explanation within the standard shell-model framework, which neglects the continuum-coupling effects. As discussed, R-matrix theory predicts an increased density of levels with large reduced widths near thresholds (Barker, 1964). Ikeda, Takigawa, and Horiuchi (1968) noted that α-cluster states can be found near α-particle decay thresholds. The proposed scheme (known as the Ikeda diagram), which is shown in Fig. 7, was later extended into various nuclear molecular configurations in neutron-rich nuclei (von Oertzen, Freer, and Kanada-En'yo, 2006; von Oertzen and Milin, 2014).

Extensive SMEC studies (Okołowicz, Płoszajczak, and Nazarewicz, 2012; Okołowicz, Nazarewicz, and Płoszajczak, 2013) demonstrated that the low-energy coexistence of the clusterlike and shell-model-like configurations explained the origin of the Ikeda diagram and formulated its generalization: the coupling to a nearby particle-emission channel induces the correlations in the shell-model wave functions that are the imprint of this channel. The specific aspects of this generic phenomenon depend both on the energy and kind of various particle-emission thresholds and on the stability of correlated multiparticle systems in the final state after the decay.

A microscopic description of states close to the particle-emission threshold requires the unitary formulation of the transition across the reaction threshold between the two continuous phases of the scattering process. Proximity of the particle-emission threshold, which is the branching point of the particle flux, induces the collective mixing of shell-model states, in which an essential role is played by a single eigenstate of the open-quantum-system Hamiltonian, the so-called aligned eigenstate. The presence of cluster states near their corresponding cluster emission thresholds is a signature of a profound change in the near-threshold shell-model wave function and a direct manifestation of the continuum-coupling-induced correlations.

The domain of aligned states is not restricted to the large-density resonance region at high excitation energies; it can also correspond to a bound state at energies below the lowest decay threshold. For example, neutral-cluster configurations are expected to appear primarily below the threshold due to the rapid growth of the decay width with energy. Noteworthy examples of neutral clustering are one- and two-neutron halos in light nuclei.

E. Threshold-aligned resonant states

As discussed in Sec. II.D, near-threshold or threshold-aligned levels can be considered the rule rather than the exception in light-ion systems, as can be demonstrated as cluster configurations in multiple examples, a phenomenon that was visualized using the Ikeda diagram shown in Fig. 7 (Ikeda, Takigawa, and Horiuchi, 1968).

Note that a similar diagram can be generated to visualize other even-even nuclear systems, such as a diproton or a dineutron coupled to the displayed self-conjugate nuclei. Such configurations are of great importance for interpreting the underlying nuclear resonance structure of the αp process or the structure of α-induced neutron sources, respectively (Wiescher and Ahn, 2017). Near-threshold cluster configurations could play an important role, as later shown in one of our examples (Wiescher, deBoer, and Görres, 2023).

Figure 8 shows examples of threshold-aligned states near the proton and neutron thresholds in nuclei near self-conjugate systems. The numbers mark the respective neutron and proton separation energies in the compound system and identify the range in which resonance or subthreshold structures with enhanced proton or neutron strength is expected to emerge.

As such, they are important phenomena in low-energy reaction physics, particularly in nuclear astrophysics. Depending on their respective contributions, the near-threshold resonant states may substantially change the low-energy cross sections and reaction rates. The generic behavior of reaction cross sections for neutral and charged particles is given by the Wigner threshold law (Wigner, 1948). In this context it is important to consider the energy of the threshold-aligned state where the tail of the weakly bound state may significantly change the reaction rate.

The impact of such levels as resonances but also as subthreshold configurations may be significant since the reaction rate would be exponentially enhanced depending on the specific level parameters. In the following we discuss some examples of threshold-aligned states.

In the following we discuss a few selected examples of narrow resonances near the particle threshold that have a large impact at certain nucleosynthesis sites. The importance of such "fortuitously" placed resonances in nucleosynthesis is well known (Wiescher and Ahn, 2017; deBoer et al., 2020; Wiescher et al., 2021). The eminent example is the Hoyle state (Hoyle, 1954; Fick, 1978), the second 0^+ state in the vicinity of the ^{8}Be + α threshold, which γ decays into the ground state of ^{12}C and allows for the synthesis of ^{16}O through subsequent α-particle capture. However, studies of resonances and scattering features in exotic nuclei, for example, ^{9}N (Charity et al.,

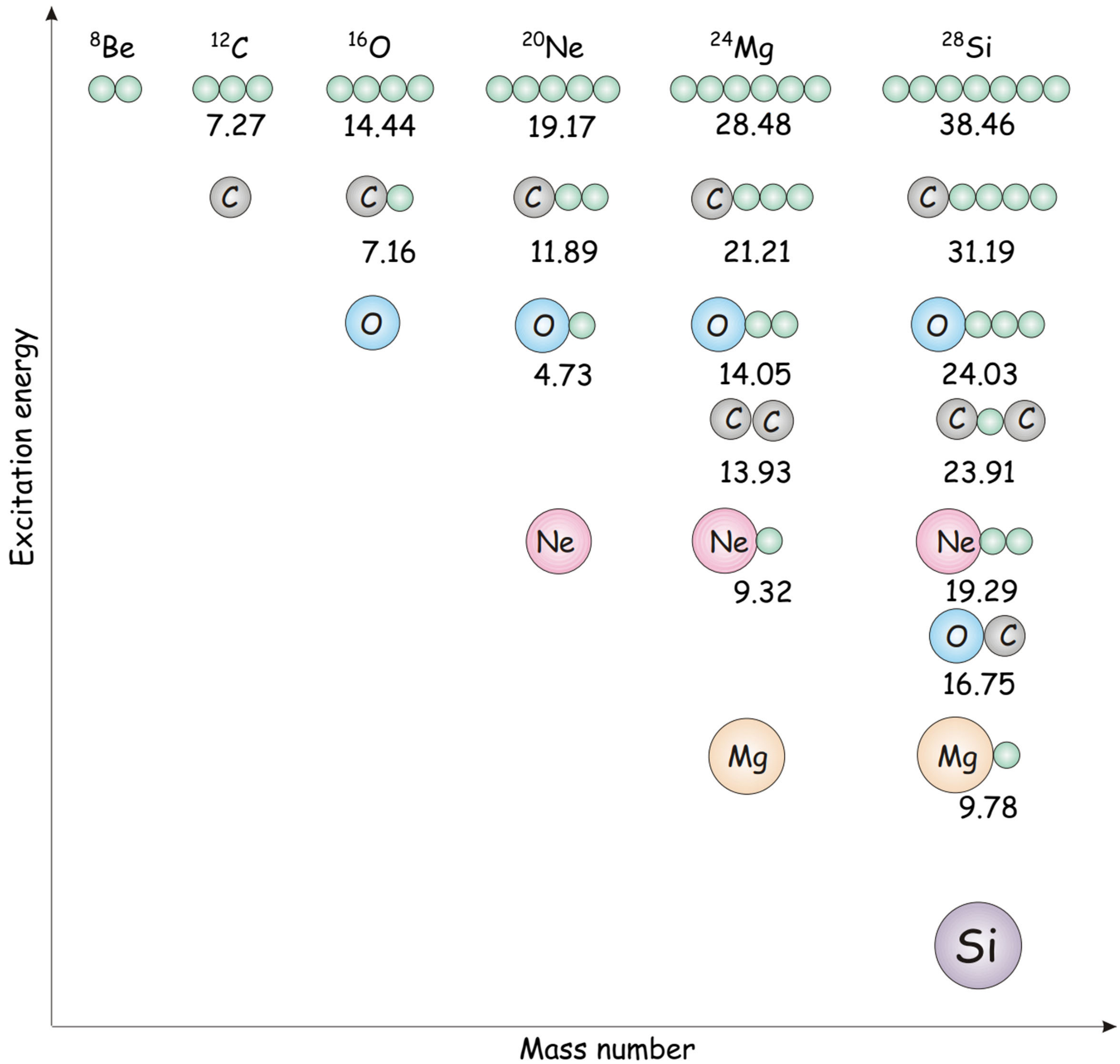

FIG. 7. The well-known Ikeda diagram visualizing ^{4}He and ^{12}C cluster configurations in self-conjugate nuclei. The configurations are labeled with their excitation energies for the specific configurations on display.

2023), ^{13}F (Charity et al., 2021), ^{15}F (de Grancey et al., 2016), ^{14}O (Charity et al., 2019), ^{11}Li (Okołowicz, Płoszajczak, and Nazarewicz, 2012), ^{11}B (Ayyad et al., 2019; Okołowicz, Płoszajczak, and Nazarewicz, 2020, 2022; Ayyad et al., 2022; Kolk et al., 2022; Lopez-Saavedra et al., 2022), ^{12}Be (J. Chen et al., 2021), ^{26}O (Kondo et al., 2016), and ^{28}O (Kondo et al., 2023), have generated considerable insight into the formation mechanism of threshold-aligned states and may play a role in explosive nucleosynthesis processes, such as the hot pp chains (Wiescher et al., 1989; Wiescher et al., 2021), the rp process (Schatz et al., 1998; Lau et al., 2018), and the νp process (Fröhlich et al., 2006; Pruet et al., 2006) on the neutron deficient side and the onset of the r process (Terasawa et al., 2001; Bartlett et al., 2006; Otsuki et al., 2006) on the neutron-rich side of the line of stability. We now discuss several cases where the near-threshold emergence of single-particle states could impact the reaction cross-section analysis at low energies.

1. $J^\pi = 2_1^-$ resonance in ^{6}Be

An interesting case is the $A = 6$ system; a $J^\pi = 2^-$ unbound state has been identified at 14.6 MeV in the ^{6}He nucleus and at 17.98 MeV in the ^{6}Li system (Blatt et al., 1968), but the mirror state has been elusive thus far in the ^{6}Be system. Coulomb and Thomas-Ehrman shift evaluations suggest that this state is close to the ^{3}He + ^{3}He threshold at 11.488 MeV. Despite several efforts (Fetisov and Kopysov, 1975; Bonetti et al., 1999), this level has not been found, possibly due to a large proton partial width. As it is near the threshold, this level may

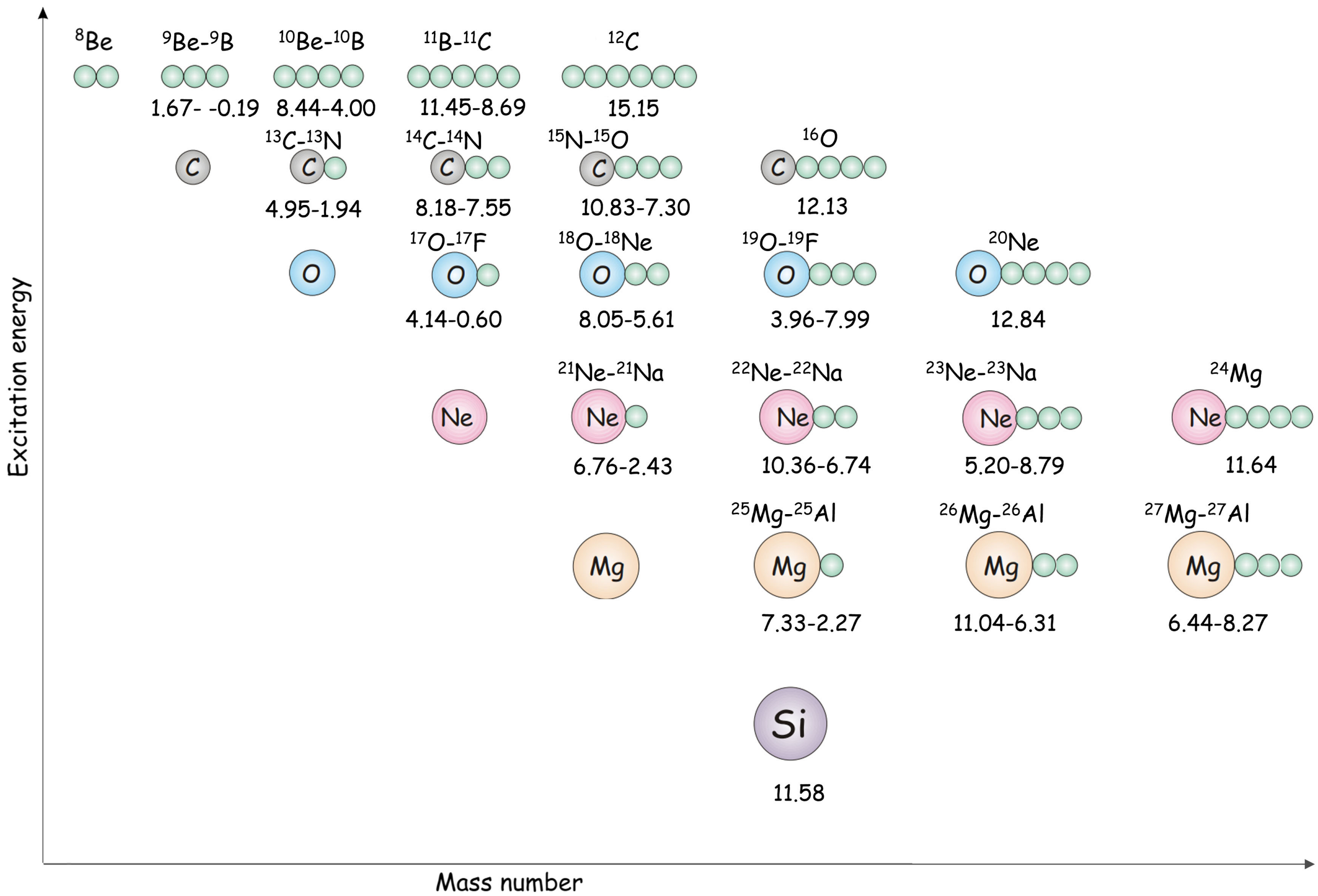

FIG. 8. Near-threshold states in nuclei near self-conjugate systems. The numbers mark the neutron and proton separation energies in the compound system and identify the range in which the large proton and neutron capture strength is expected to appear.

have a significant impact on the $^3\mathrm{He} + {}^3\mathrm{He}$ fusion cross section affecting the relative strength of the pp-I chain with respect to the pp-II chain in the hydrogen burning of the Sun (Fowler, 1972), which would also impact solar-neutrino production. Direct measurements at very low energies in underground accelerator studies did not show any direct evidence for a resonance (Junker *et al.*, 1998). The cross-section data exhibit an increase toward lower energies. This may suggest an underlying broad resonance contribution, but it has been explained as a consequence of electron screening, as discussed in more detail in Sec. VI.B). The large uncertainties in the data impede a reliable analysis (Adelberger *et al.*, 2011). In addition, indirect studies with transfer reactions have failed to provide information on such a state (Chae *et al.*, 2012). Furthermore, no indications have been provided by plasma fusion experiments probing $^3\mathrm{H} + {}^3\mathrm{He}$ (Zylstra *et al.*, 2016) or $^3\mathrm{He} + {}^3\mathrm{He}$ near the threshold regions in ^{6}Li and ^{6}Be (Zylstra *et al.*, 2017). These measurements are, however, inconclusive in terms of possible low-energy contributions due to plasma screening effects as discussed in Sec. VI.A.2. However, the agreement between the neutrino observations from the pp chains and the predictions based on neutrino oscillations suggest that the influence of such a resonance might be negligible on the low-energy cross section.

2. $J^\pi = 5/2^-_1$ resonance in ^{9}Li

The case of threshold-aligned resonance levels is also valid for neutron capture reactions (Fossez *et al.*, 2015). Cases like that have been identified in $^7\mathrm{Li}(n,\gamma)$ (Heil *et al.*, 1998), $^{17}\mathrm{C}(n,\alpha)$ (Schatz *et al.*, 1993; Oliva and Guardo, 2024), and other light-ion cases (Herndl *et al.*, 1999). We discuss two examples here involving neutron-rich compound systems such as ^{9}Li and ^{14}C.

Measurements of the $^8\mathrm{Li}(n,\gamma)^9\mathrm{Li}$ reaction cross section are extremely challenging. Owing to the short half-life of ^{8}Li, the experimental efforts to determine the neutron capture cross section have concentrated on indirect measurements. These included (i) the Coulomb dissociation of the ^{9}Li beam passing through the virtual photon field of a high-Z nucleus (Zecher *et al.*, 1998; Kobayashi *et al.*, 2003), (ii) the transfer reaction to obtain experimental spectroscopic factors that have then been used to calculate the neutron capture cross section in the potential model (Li *et al.*, 2005; Guimarães *et al.*, 2007), or (iii) the study of radiative capture cross sections in the mirror reaction: $^8\mathrm{B}(p,\gamma)^9\mathrm{C}$ (Mohr, 2003). Moreover, the experimental analysis should be able to investigate the role of low-energy resonance $J^\pi = 5/2^-_1$, which is only 234 keV above the neutron threshold.

Theoretical analysis has included the microscopic cluster model (Descouvemont, 1993b), the modified potential cluster model (Dubovichenko and Dzhazairov-Kakhramanov, 2016), or the potential model (Bertulani, 1999; Banerjee, Chatterjee, and Shyam, 2008). Recently, investigations of ^{8}Li$(n,\gamma)^9$Li reactions were reported in the NCSMC (McCracken *et al.*, 2021) and in the GSM CC (Dong *et al.*, 2022, 2023b).

In the GSM-CC studies, the near-threshold $5/2_1^-$ resonance, which contributes significantly to the $E1$ neutron capture cross section, is obtained 112 keV above the calculated threshold, and its width $\Gamma_{\rm th} = 112$ keV is close to the experimental value $\Gamma_{\rm exp} = 106$ keV. The calculated neutron spectroscopic factor $\langle ^9{\rm Li}(5/2_1^-)|[^8{\rm Li}_{\rm g.s.}(2_1^+) \otimes \nu_{\ell_j}]\rangle$ of the $J_1^\pi = 5/2^-$ equals 0.8, which agrees with the experimental value 0.93(20) obtained in the (d,p) reaction (Wuosmaa *et al.*, 2005). The large value of the spectroscopic factor underlines an important role of this resonance in the synthesis of ^{9}Li. Figure 9 compares direct and total neutron radiative capture cross sections calculated in the GSM CC. In the total neutron capture cross section, all relevant $E1$, $M1$, and $E2$ transitions in the capture to the $J^\pi = 3/2_1^-, 1/2_1^-, 5/2_1^-$ final states are added up. The experimental upper limits are listed in Fig. 9 (Zecher *et al.*, 1998). It is seen that the GSM-CC results are consistent with these upper limits, and the calculated rates of the neutron capture reaction ^{8}Li$(n,\gamma)^9$Li indicate the destruction of ^{8}Li in the early Universe and a reduction of the nucleosynthesis of heavier elements in the main chain of reactions: $^8{\rm Li}(\alpha,n)^{11}{\rm B}(n,\gamma)^{12}{\rm B}(\beta^+)^{12}{\rm C}\cdots$.

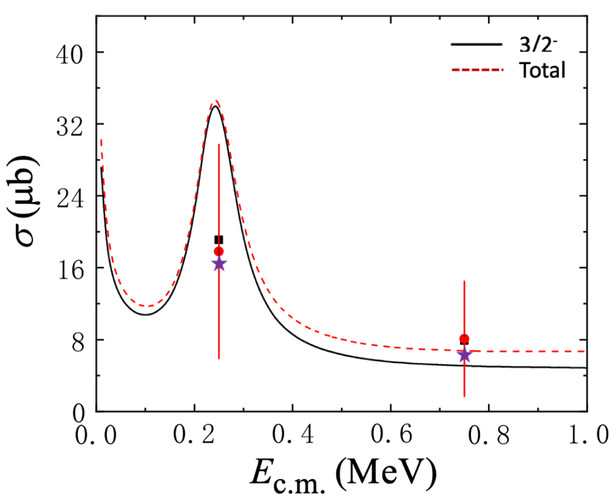

FIG. 9. Experimental (Zecher *et al.*, 1998) and GSM-CC (Dong *et al.*, 2022, 2023b) neutron radiative capture cross section of the reaction ^{8}Li$(n,\gamma)^9$Li are plotted as a function of the neutron projectile energy in the $n + {}^8$Li center-of-mass frame. The solid line shows the direct GSM-CC capture to the ground state $J^\pi = 3/2_1^-$ of ^{9}Li and the dashed red line exhibits the GSM-CC total neutron radiative capture cross section, which is a sum of contributions from the capture to $J^\pi = 3/2_1^-, 1/2_1^-$, and $5/2_1^-$ final states. The red points and black squares are the upper limits obtained in the Coulomb-dissociation experiment with Pb and U targets, respectively (Zecher *et al.*, 1998). The magenta stars depict the GSM-CC results. Experimental and GSM-CC cross sections at $\tilde{E}_n = 0.25$ MeV and 0.75 MeV correspond to average cross sections in the two decay energy bins: $E_n \in [0.0, 0.5]$ MeV and $E_n \in [0.5, 1.0]$ MeV. Adapted from Dong *et al.*, 2023b.

The GSM-CC model has been also applied to analyze the mirror radiative capture reaction cross section ^{8}B$(p,\gamma)^9$C (Dong *et al.*, 2023a, 2023c). The calculated astrophysical S factor at $E = 0$ agrees with the majority of experimental results, with the exception of those by Fukui, Ogata, and Yahiro (2015) that were extracted from the transfer reaction ^{8}B$(d,n)^9$C.

3. $J^\pi = 1/2_3^+$ resonance in ^{11}B

There has been considerable interest in the β^--delayed proton decay of the neutron-rich halo nucleus ^{11}Be. Experimentally, the strength of this decay mode turned out to be unexpectedly high; an explanation for this puzzling result was proposed by Riisager *et al.* (2014) as the possible presence of a narrow resonance in ^{11}B, slightly above the proton emission threshold in ^{11}B. Okołowicz, Płoszajczak, and Nazarewicz (2020) suggested that this resonance corresponds to a $1/2_3^+$ state in ^{11}B that carries a large imprint of the proton decay channel.

The collectivization of the $1/2_3^+$ state in ^{11}B, as predicted by the SMEC, is illustrated in Fig. 10, where it shows the real part of the continuum-coupling correlation energy $E_{\rm corr}$ as a function of the proton energy E_p. For the $1/2_3^+$ SMEC eigenstate, the four $1/2^+$ shell-model eigenstates are coupled in the $\ell = 0$ partial wave to the one-proton decay channel. The strongest collectivization is predicted to be $E_p^* \approx$ 142 keV, which is close to the experimental energy of the resonance.

The proton-emitting threshold state has been observed in two independent experiments, proton resonance scattering (Ayyad *et al.*, 2022) and $^{10}{\rm Be}(d,n) \to {}^{10}{\rm Be} + p$ reactions (Lopez-Saavedra *et al.*, 2022), which are in full agreement with the SMEC results (Okołowicz, Płoszajczak, and Nazarewicz, 2020, 2022). Okołowicz, Płoszajczak, and Nazarewicz (2022) argued that the controversy about the value of the branching ratio for $b_{\rm r}(\beta^-{\rm p})$ decay cannot be resolved if the $\beta^-\alpha$-decay branch is not considered as well. It was shown that the $b_{\rm r}(\beta^-\alpha)$ branching ratio (Refsgaard *et al.*,

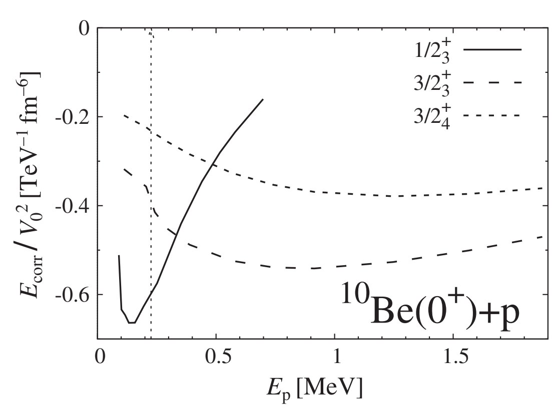

FIG. 10. The real part of the continuum-coupling correlation energy computed in the SMEC approach. The calculations consider the coupling to both the proton and neutron reaction channels. Zero energy corresponds to the proton decay threshold. The neutron decay threshold is marked with a thin vertical line. Adapted from Okołowicz, Płoszajczak, and Nazarewicz, 2020.

2019) and the width of the proton resonance $\Gamma_p(1/2_3^+)$ (Ayyad et al., 2019, 2022) can be consistently described. However, the branching ratio $b_r(\beta^- p)$ calculated in the SMEC disagrees with the reported experimental value (Ayyad et al., 2019). The disagreement with this experimental finding was reported by Riisager et al. (2020) and Sokołowska et al. (2024).

The astrophysical implications of such a threshold state have not yet been considered in detail, but enhanced proton capture on ^{10}Be through this resonance may cause an enhancement for the endothermic $^{10}\mathrm{Be}(p,n)^{10}\mathrm{B}$ reaction serving as an additional internal neutron source in the expanding neutrino-driven supernova shock front environment while impacting the abundance distribution during the reassembling of light nuclei (Terasawa et al., 2001). This aspect would deserve some modeling consideration with respect to the overall neutron budget in that environment.

4. $J^\pi = 5/2_6^+$ resonance in ^{11}B

^{10}B is the most important neutron absorber used in the control rods in nuclear reactors (Mughabghab, Divadeenam, and Holden, 1982). The key role in the neutron absorption process is played by the reaction $^{10}\mathrm{B}(n,\alpha)^7\mathrm{Li}$, where the near-threshold resonance $J^\pi = 5/2^+$ in ^{11}B at an excitation energy $E = 11.600(20)$ MeV plays a major role. The resonance is situated ~150 keV above the $^{10}\mathrm{B} + n$ reaction threshold. The reaction $^{10}\mathrm{B}(n,\gamma)^{11}\mathrm{B}$ controlled by the same $J^\pi = 5/2^+$ resonance is also interesting because ^{11}B is a part of the reaction chains of the inhomogeneous big bang models.

The $5/2^+$ resonance is known to decay by α and neutron emission. The large neutron capture cross section on the boron target at low bombarding energies suggests that this resonance has a large imprint of the $[^{10}\mathrm{B}(3_1^+) \otimes n(s_{1/2})^{5/2^+}]$ reaction channel on its wave function. The collectivization of the narrow near-threshold resonance $5/2^+$ due to the coupling of all $5/2^+$ shell-model eigenstates to the neutron decay threshold was studied in the SMEC (Okołowicz, Płoszajczak, and Nazarewicz, 2020). In this calculation state $5/2_6^+$ is found in the vicinity of the neutron decay threshold. It is coupled in an $\ell = 2$ partial wave to the $[^{10}\mathrm{B}(3_1^+) \otimes n(s_{1/2})]^{5/2^+}$]-decay channel.

Figure 11 shows the real part continuum-coupling correlation energy as a function of the neutron energy E_n for the $5/2_6^+$ state. The coupling to the one-neutron decay channel $[^{10}\mathrm{B}(3_1^+) \otimes n(s_{1/2})]^{5/2^+}]$ is almost 10 times stronger than is found for the $1/2_3^+$ eigenvalue; see Fig. 10. The minimum of the continuum-coupling correlation energy is predicted to be $E_n^* = 113$ keV, which is close to the experimental energy of the $5/2^+$ resonance.

5. $J^\pi = 5/2_2^+$ resonance in ^{11}C

^{11}C, the mirror nucleus of ^{11}B, plays an important role in boron-proton fusion reactor environments as a catalyzer for the $^{10}\mathrm{B}(p,\alpha)^7\mathrm{Be}$ reaction. By producing a long-lived isotope of ^{7}Be, this reaction poisons the aneutronic fusion process $^{11}\mathrm{B}(p,2\alpha)^4\mathrm{He}$ ($Q = 8.7$ MeV) (Wiescher et al., 2017; Magee et al., 2023), which by itself does not produce any long-lived radioactive products. The $^{10}\mathrm{B}(p,\alpha)^7\mathrm{Be}$ reaction may,

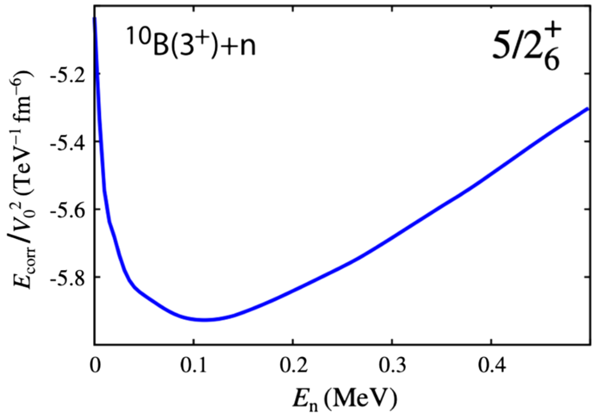

FIG. 11. The real part of the continuum-coupling correlation energy computed in the SMEC approach for the $5/2_6^+$ resonance is plotted as a function of the neutron energy E_n in the continuum. Zero energy corresponds to the neutron decay threshold. Adapted from Okołowicz, Płoszajczak, and Nazarewicz, 2020.

however, also play an important role in the hot pp chains (Wiescher et al., 1989) by back processing material branching across the mass $A = 8$ mass gap toward ^{7}Be (Kolk et al., 2022), while a weaker $^{10}\mathrm{B}(p,\gamma)^{11}\mathrm{C}$ provides a link to the carbon nitrogen mass range (Wiescher et al., 1983). In that role the reaction is important in first star nucleosynthesis patterns (Wiescher et al., 2021). There are potentially two near-threshold resonances that could play an important role in the two reaction branches, $^{10}\mathrm{B}(p,\alpha)^7\mathrm{Be}$ and $^{10}\mathrm{B}(p,\gamma)^{11}\mathrm{C}$. One of the resonances corresponds to a state of $J^\pi = 5/2_2^+$, which is merely 10 keV above the proton threshold (Angulo, Schulte et al., 1993; Wiescher et al., 2017), and the second one corresponds to a level with spin-parity of $J^\pi = 7/2_1^+$, which is bound by 35 keV with respect to the proton threshold. Both resonances are α emitters, but the strong coupling to the one-proton channel $[^{10}\mathrm{B}(3^+) \otimes \mathrm{p}(\ell_j)]^{J^+}$ changes their structure significantly, as found in the SMEC analysis (Okołowicz, Płoszajczak, and Nazarewicz, 2023, 2024). The $J^\pi = 7/2_1^+$ state couples strongly to the continuum in the $d_{5/2}$ wave, whereas the major continuum coupling of the $J^\pi = 5/2_2^+$ state is in the $s_{1/2}$ wave. Consequently, the spectroscopic factor $\mathcal{S}_{d5/2} = 0.38$ dominates in the $7/2^+$ state, whereas the $\mathcal{S}_{s1/2} = 0.33$ spectroscopic factor is most important in the $5/2_2^+$ state, and its value is close to the experimental spectroscopic factor reported in the direct capture reaction (Wiescher et al., 1983). The theoretical SMEC analysis and recent R-matrix calculations by Mukhamedzhanov (2023) showed that the $J^\pi = 7/2_1^+$ state does not have any significant influence on the low-energy cross section of the $^{10}\mathrm{B}(p,\alpha_0)^7\mathrm{Be}$ reaction.

The very-low-energy cross section of $\sigma(10\ \mathrm{keV}) \approx 1.38 \times 10^{-15}$ b (Mukhamedzhanov, 2023) of the $^{10}\mathrm{B}(p,\alpha)^7\mathrm{Be}$ reaction cannot be measured directly in accelerator-based measurements, but, owing to its large enhancement in cross section via the resonance that corresponds to the $J^\pi = 5/2_2^+$ state, Angulo, Engstler et al. (1993) was able to measure down to 17 keV. This resonance might be accessible at energies achieved by the National Ignition Facility (Hogan et al., 2001) or OMEGA EP (Guardalben et al., 2020), two laser-driven hot plasma facilities. The cross section for, and information about, the near-threshold resonances in ^{11}C are known from indirect THM measurements (Lamia et al., 2007; Spitaleri et al., 2014, 2017; Cvetinović et al., 2018) or from the phenomenological R-matrix analysis of the data obtained at higher energies (Wiescher et al., 2017; Kolk et al., 2022). It has been argued that the THM-based analysis is inconsistent and requires improved experimental data (Spitaleri et al., 2017; Wiescher et al., 2017).

6. $J^\pi = 2_2^+$ resonance in ^{14}C

An ideal case to experimentally test predictions concerning the collectivization of a near-threshold state is offered by ^{14}C. Here the near-threshold state is located at $E_x = 8318$ keV, i.e., 142 keV above the neutron-emission threshold, has $J^\pi = 2^+$ (it is the second excited 2^+ state in ^{14}C), and has a total width of 3.4 keV (von Oertzen et al., 2004). This resonance may enhance the neutron capture reaction $^{13}\mathrm{C}(n,\gamma)^{14}\mathrm{C}$ as potential neutron poison limiting the efficiency of the $^{13}\mathrm{C}(\alpha,n)^{16}\mathrm{O}$ neutron source in asymptotic giant branch (AGB) star intershell burning (Bisterzo et al., 2015).

Figure 12 shows the $B(E2)$ reduced transition probability calculated in the SMEC (Płoszajczak and Okołowicz, 2020) for the $E2$ transition from the first three 2^+ excitations to the ground 0_1^+ state as a function of the continuum-coupling strength V_0. For the transitions $2_n^+ \to 0_{\mathrm{gs}}^+$ ($n = 2$ and 3), a real part of the reduced transition probability is shown. The dotted vertical line in Fig. 12 shows the value of V_0 for which the experimental $B(E2)$ probability of the $2_1^+ \to 0_{\mathrm{gs}}^+$ transition is reproduced in the SMEC with the WBP interaction, where the acronym represents the p-sd Hamiltonian of Warburton and Brown (Yuan, 2017). For this value of V_0, the $B(E2)$ probability for the $2_2^+ \to 0_{\mathrm{gs}}^+$ is enhanced by a factor of ≈340 with respect to the SM value and is the largest of the considered $2_n^+ \to 0_{\mathrm{gs}}^+$ ($n = 1$, 2, and 3) transitions.

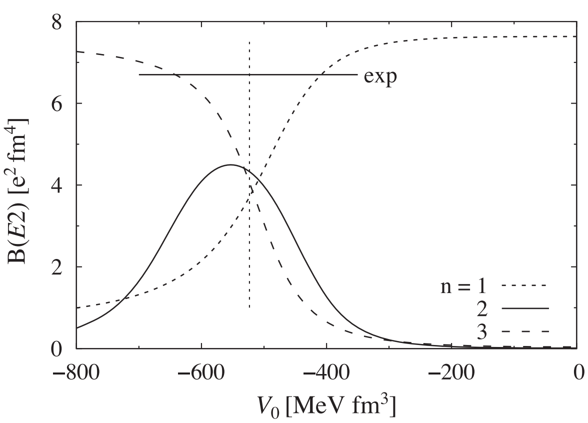

FIG. 12. $B(E2)$ probabilities in the SMEC for the $2_n^+ \to 0_{\mathrm{gs}}^+$ ($n = 1$, 2, and 3) transitions of ^{14}C as a function of the continuum-coupling constant. SM results correspond to $V_0 = 0$. The $B(E2)$ result reported by Raman et al. (1990) is shown as a straight horizontal line. Adapted from Płoszajczak and Okołowicz, 2020.

Previous studies of the $^{13}\mathrm{C}(n,\gamma)^{14}\mathrm{N}$ reaction have focused primarily on lower neutron energies (Shima et al., 1997) but also extend to the range of the threshold resonance (Raman et al., 1990) in order to investigate the role of this reaction as a neutron poison in s-process environments. It was, however, shown in accelerator mass spectrometry studies (Wallner et al., 2016) that the low-energy tail contribution of a d-wave resonance does not significantly impact the neutron flux for the s-process environment (Lugaro, Pignatari et al., 2023).

However, the $^{13}\mathrm{C}(n,\gamma)$ reaction may play a role in higher temperature environments such as those expected in early carbon enhanced metal-poor stars for the intermediate or i process (Denissenkov et al., 2017), where rapid convection is expected to transfer ^{13}N or its daughter ^{13}C rapidly into hot environments generating a higher neutron flux (Clarkson, Herwig, and Pignatari, 2018). At these conditions ^{13}C may be acting as a neutron poison. Earlier calculations by Herndl et al. (1999) suggested that the reaction rate is essentially determined by the 143 keV resonance at temperatures above $T \approx 3 \times 10^8$ K, where as the s- and p-wave direct capture contributions dominate at lower temperatures.

The reported experimental value of the total radiation width for this resonance is $\Gamma_\gamma(2_2^+) = 0.215^{+0.084}_{-0.035}$ eV (Raman et al., 1990). Thge SMEC, using the WBP interaction and V_0 adjusted to reproduce an experimental γ-emission lifetime of the particle-bound state 2_1^+, yields $\Gamma_\gamma(2_2^+) = 0.139^{+0.005}_{-0.011}$ eV. This width, which is measurable with Gammasphere (Corbari et al., 2023), could provide a rigorous test of the dependence of the transition probability $B(E2; 2_2^+ \to 0_{\mathrm{gs}}^+)$ on V_0 and hence could quantify the influence of the coupling to the decay channel on the γ-decay probability.

7. $J^\pi = 1/2_1^-$ resonance in ^{15}F

An impressive illustration of the generic alignment mechanism in near-threshold resonances was observed in the narrow near-threshold resonance $J^\pi = 1/2_1^-$ in ^{15}F. The ground state $J^\pi = 1/2_1^+$ of ^{15}F is one-proton unbound by ≈1.3 MeV and has been observed as a broad resonance with $\Gamma \approx 376$ keV. The first excited state at ≈2.8 MeV has $\Gamma \approx 300$ keV. The structure of the ground (first excited) state has been interpreted as mainly a proton orbiting with $\ell = 0$ ($\ell = 2$) around a $^{14}\mathrm{O}_{\mathrm{gs}}$ core (Fortune and Sherr, 2005). The second excited state $J^\pi = 1/2_1^-$ at ≈4.8 MeV above the ($^{14}\mathrm{O} + p$)-decay threshold has been observed to be a narrow resonance with $\Gamma \approx 36$ keV (de Grancey et al., 2016) even though it lies well above the Coulomb-plus-centrifugal barrier, and above the two-proton decay threshold.

The proximity of the two-proton decay channel is one reason for its narrow width. The coupling of the $1/2^-$ shell-model closed-quantum-system eigenstates to the $2p$-decay channel induces a collective rearrangement in the wave function of the lowest eigenstate that aligns with the ($^{13}\mathrm{N}_{\mathrm{g.s.}} + 2p$)-decay channel. The Gamow shell model predicts that the wave function of the $1/2_1^-$ resonance will be an almost pure wave function of two protons in $s_{1/2}$ resonant and nonresonant shells with a small spectroscopic factor $S_{\mathrm{SF}}^{(1/2^-)} = 0.0035$ to the ground state of ^{14}O (de Grancey et al., 2016). Hence, the one-proton decay is disfavored, and the available energy for the two-proton decay to the ground state of ^{13}N is only $Q_{2p} = 129$ keV, which leads to a width $\Gamma_{2p} \approx 4 \times 10^{-11}$ eV in the Wigner limit. Consequently, the proton decay of this resonance is strongly suppressed.

Slightly above the $1/2_1^-$ state, one finds two narrow resonances: a $5/2_1^-$ one at $\approx$5.9 MeV ($\Gamma = 3$ keV) and a $3/2_1^-$ resonance at $\approx$6.3 MeV ($\Gamma = 28$ keV) (Girard-Alcindor et al., 2022). Their structures differ from the $1/2_1^-$ state because of their proximity to the open inelastic channels, $[^{14}\mathrm{O}(1_1^-) \otimes (0d_{5/2})]^{3/2^-,5/2^-}$, and to the closed inelastic channels, $[^{14}\mathrm{O}(2_1^+) \otimes (0p_{1/2})]^{3/2^-,5/2^-}$, $[^{14}\mathrm{O}(3_1^-) \otimes (1s_{1/2})]^{5/2_1^-}$, and $[^{14}\mathrm{O}(2_1^-) \otimes (1s_{1/2})]^{3/2_1^-}$, which contribute significantly to the observed properties of these excitations.

III. CONSIDERATIONS FOR *R*-MATRIX APPLICATIONS

The impact of threshold resonance states discussed in Sec. II can be described in the framework of the phenomenological R-matrix theory. This is an approach for describing reaction cross sections that is frequently used for describing low-energy capture and fusion reactions for light nuclei (Wigner, 1946; Wigner and Eisenbud, 1947; Bloch, 1957; Lane and Thomas, 1958; Vogt, 1962; Konnecke, 1982; Kajino, Bertsch, and Barker, 1989; Barker and Kajino, 1991; Azuma et al., 2010; Descouvemont and Baye, 2010; deBoer et al., 2017). This approach takes into account interference effects between resonances, barrier penetration, and threshold effects such as subthreshold resonances and the effects of channel thresholds on cross sections. R-matrix theory also provides a natural explanation for the enhanced probability of finding an energy level near a channel threshold if the level couples strongly to that channel (Barker, 1964), as discussed from the open-quantum-system perspective in Sec. II.D.8. The usual implementation of R-matrix theory assumes that there is only a Coulomb potential beyond the channel radius, which lies near the nuclear surface. The wave function inside the channel radius is not modeled directly. Only its projections onto channels at the channel radii, the reduced-width amplitudes, appear in the calculations. For low-energy nuclear astrophysical reactions, R-matrix theory is used to extrapolate experimental data, obtained at higher energies, toward the Gamow range of stellar reactions. The choice of channel radius can have significant impacts on the quality of fits to both the data and the cross sections, especially for fits to elastic scattering data (deBoer et al., 2017).

In heavier nuclei the density of levels is much higher, and it becomes intractable to characterize levels on an individual basis. Instead, average cross sections can be modeled, an approach that is implemented in practice using Hauser-Feshbach theory (Hauser and Feshbach, 1952). The critical quantities when calculating fusion or capture cross sections in this framework are the transmission functions, which model the Coulomb and the angular-momentum barrier penetration as well as the coupling of particular channels to the compound nucleus. In practice, the transmission functions for nucleonic (i.e., nonphoton) channels are calculated from phenomenological Woods-Saxon optical potentials. Fusion cross sections far below the Coulomb barrier are highly sensitive to the imaginary part of the tail of this optical potential, i.e., to its behavior at radii well outside the nucleus (Mohr et al., 2020). Regardless of whether the Hauser-Feshbach picture of low-energy fusion reactions is correct, it highlights the important role that details of the interparticle potential can play in these problems and also casts some doubt on the use of simple Coulomb functions to calculate the penetration factor at the channel radius.

One way to assess the effect of the tail of the nuclear potential on barrier penetration would be to include this tail in the calculation of the penetration factors and other Coulomb quantities used in R-matrix calculations (Johnson, 1973; Koonin, Tombrello, and Fox, 1974; Langanke and Koonin, 1983, 1985). One effect of the tail of the nuclear potential is a renormalization of the reduced-width amplitudes due to a decrease in the penetration factor. The energy dependence of the barrier penetration factor is also modified, but the overall effect on cross-section extrapolations has never been quantified. In addition, the inclusion of the potential tail likely impacts the choice of channel radius. This approach also unifies the phenomenological treatment of nuclear states between R-matrix methods and single-particle plus spectroscopic factor descriptions, such as those used in transfer reactions (Brune, 2020).

In a situation that little is known about, we finally point out that the level structure near the reaction threshold immediately leads to a large source of uncertainty in any extrapolation. Unknown levels can lead to orders-of-magnitude differences in the cross section. Some examples of analyses that face this type of challenge were given by deBoer et al. (2021), Zhang et al. (2022), and Gula et al. (2023). Extreme cases are then used to estimate the uncertainty, with single-particle or full clusterization limits for the strength of hypothetical levels taken. In the R-matrix theory, a single-particle limit or full-cluster configuration can be approximated by taking a dimensionless reduced width equal to 1 (Kanada-En'yo, Suhara, and Taniguchi, 2014),

$$\theta^2 = \gamma^2/\gamma_W^2 \approx 1, \tag{9}$$

where γ^2 is the reduced width and γ_W^2 is the Wigner limit given by

$$\gamma_W^2 = 3\hbar^2/2\mu a_c^2, \tag{10}$$

with μ the reduced mass and a_c the channel radius. The spectroscopic factor $\mathcal{S}_{s\ell}$ and the dimensionless reduced width θ^2 are often seen as identical, but care must be taken so that a consistent choice of boundary conditions and channel radius are used for all calculations (Cooper, Galati, and Hornyak, 1974).

A. Input parameter and uncertainty analysis

A practical challenge in accurately quantifying the uncertainty and extrapolation in R-matrix fits has always been the propagation of all data uncertainties through the model. For the most part, past analyses have been concerned mainly with the experimental uncertainties in the reaction data itself because, in many cases, these uncertainties dominate. However, as reaction data became more precise, other sources of uncertainty became more significant, such as uncertainties in experimental resolution functions, masses, and bound-state level parameters. In most R-matrix fitting routines, the uncertainties of these parameters are not included in the χ^2 function. Bayesian parameter estimation (see Sec. III.A.2) has been shown to be a more consistent and more flexible approach.

1. The role of ANCs in R-matrix calculations

In R-matrix theory, the reduced-width amplitude of a bound state is related to the ANC ($C_{\lambda c}$) via

$$C_{\lambda c} = \frac{(2m_\alpha a_c)^{1/2}}{\hbar W_c(a_c)} \frac{\gamma_{\lambda c}}{[1 + \sum_{c'} \gamma^2_{\lambda c'} (dS_{c'}/dE)(E_\lambda)]^{1/2}}, \qquad (11)$$

where $W_c(a_c)$ is the exponentially decaying Whittaker function evaluated at the channel radius, while S_c is the shift function and E_λ is a level energy. This relation was first given by Thomas (1951b) and is discussed extensively by Mukhamedzhanov and Tribble (1999).

The ANC-based methods are powerful tools for extrapolating cross sections down to near-threshold energies when either a subthreshold state or radiative direct capture (or both) are present. Table I shows the ANCs obtained from several phenomenological R-matrix analyses in order to gauge the consistency between ANCs determined from transfer reaction data by way of nuclear reaction models, such as the distorted-wave Born approximation and the coupled-channel model, and those obtained from direct data, often coupled with a phenomenological R-matrix analysis. The ANC values agree within 20% percent, which is the typical uncertainty range associated with DWBA calculations due to model-dependent parameters.

Extractions of ANCs from R-matrix-based cross-section analyses of direct data have similar issues. Here the direct data are used to constrain the high-energy tail contribution from subthreshold states. Depending on the subthreshold state or radiative direct capture strength, the experimental data may be sensitive to its contribution to the cross section only over a limited energy range. This energy range may only be at the lowest energy of the direct data, where uncertainties are largest and poorly characterized. There are also significant model uncertainties. In the case of an R-matrix model, the largest uncertainties often come from background contributions, which model the low-energy tail contributions of higher energy resonances that are not explicitly mapped by the experimental data or that of a direct mechanism. Background contributions are often required to precisely reproduce off-resonance interference patterns, which usually corresponds to a specific J^π. However, in the case of extrapolation, especially when the extrapolation falls into an off-resonance region, background levels from additional J^π should be included. With the advent of Bayesian sampling routines, this has become more feasible. One way to lessen the uncertainty due to background levels is to make measurements over a wider energy range, but this comes at the cost of an increase in the complexity in the R-matrix analysis.

ANCs play a major role in the extrapolation of many proton-induced reactions, such as those of the pp chains and the CNO and NeNa cycles. ANCs are also important for α-particle-induced reactions such as $^{12}C(\alpha,\gamma)^{16}O$, $^{13}C(\alpha,n)^{16}O$, and $^{16}O(\alpha,\gamma)^{20}Ne$. As many of these reactions have now been studied using both transfer and direct reactions to constrain the ANCs of threshold levels, some measure of the consistency between the different methods can be gauged, as summarized in Table I for several reactions.

2. Data renormalization and Bayesian methods for R-matrix fits

A parallel analysis of multiple reaction channels probing the same excitation range in the compound nucleus is of considerable advantage for the R-matrix evaluations of nuclear reactions with light nuclei (Brown et al., 2018). Such a comparison is especially useful for checking experimental energy calibration and resolution consistency.

Accurate extrapolation to very low energies requires careful consideration of physical constants in the R-matrix

TABLE I. Comparison of an ANC selection determined both by transfer measurements and through R-matrix fits to low-energy data. When multiple intrinsic spin-angular-momentum channels (s, ℓ) are possible, they are indicated in the level energy column.

System	E_x (MeV)	J$^\pi$	Transfer reaction: ANC (fm$^{-1/2}$)	R matrix: ANC (fm$^{-1/2}$)
^{7}Be	0.0	$3/2^-$	$(^3He, d)$: 4.56(12) (Kiss et al., 2020)	$^3He(\alpha,\gamma)^7Be$: 4.0(1) (Odell et al., 2022)
	0.43	$1/2^-$	$(^3He, d)$: 3.59(7) (Kiss et al., 2020)	$^3He(\alpha,\gamma)^7Be$: 3.0(1) (Odell et al., 2022)
			$(^{10}B, ^9Be)$: 1.63(13) (Artemov et al., 2022)	
^{15}O	6.79	$3/2^+$	$(^3He, d)$: 4.6(5) (Bertone et al., 2002)	$^{14}N(p,\gamma)^{15}O$: 4.61–4.69 (Adelberger et al., 2011)
			$(^3He, d)$: 5.2(6) (Mukhamedzhanov et al., 2003)	
^{16}O	0.0	0^+	$(^6Li, d)$: 337(45) (Shen et al., 2020)	$^{12}C(\alpha,\gamma)^{16}O$: 709 (Sayre et al., 2012)
				58 (deBoer et al., 2017)
	6.92	2^+	$(^6Li, d)$: $1.02(13) \times 10^5$ (Shen et al., 2019)	1.59×10^5 (Sayre et al., 2012)
				1.55×10^5 (Shen et al., 2020)
^{17}O	6.36	$1/2^+$	$(^6Li, d)$: 1.90(18) (Avila et al., 2015b)	$^{13}C(\alpha,n)^{16}O$: 1.45(17) (Gao et al., 2022)
^{21}Na	0.0	$3/2^+$	$(^3He, d)$: 0.46(4) (Mukhamedzhanov et al., 2006)	$^{20}Ne(p,\gamma)^{21}Na$: 0.44(6) (Lyons et al., 2018)
	0.332	$5/2^+$	1.67(13) (Mukhamedzhanov et al., 2006)	1.6(3) (Lyons et al., 2018)
	2.452	$1/2^+$	$7.8(5) \times 10^{16}$ (Mukhamedzhanov et al., 2006)	$2.80(14) \times 10^{17}$ (Lyons et al., 2018)

calculations. It is often the case that masses are determined to a precision such that their uncertainties are negligibly small, but this is not always the case, especially when one deals with radioactive nuclei and reactions that populate excited states in the final nucleus. Further, there is an ambiguity regarding which masses should be used: atomic or nuclear. The differences in these masses can be significant. For example, the $^{16}O(p,\gamma)^{17}F$ reaction (Rolfs, 1973; Chow, Griffiths, and Hall, 1975; Morlock *et al.*, 1997), depending upon the mass used, leads to as much as a $\approx 3\%$ difference in the extrapolated S factor at zero energy. This is significant considering that a recent statistical analysis by Iliadis, Palanivelrajan, and de Souza (2022) found that the other primary uncertainties lead to only an approximately 4% uncertainty. This may be a limiting factor for the uncertainty of several reactions that has not yet been addressed in the literature.

With phenomenological models, much of the accuracy of the resulting extrapolation comes from an accurate comparison of the model with the experimental data. The complication arises because all experimental data are somewhat distorted by experimental resolution. In the best-case scenarios, the cross section changes slowly with energy and these effects are negligible compared to other experimental uncertainties. This is the case for reactions like $^{3}He(\alpha,\gamma)^{7}Be$, where the cross section is dominated by nonresonant reaction mechanisms. However, many reactions are dominated by resonances, where the cross section only varies slowly with energy in the tail's off-resonance regions, but these can vary rapidly over the resonance peaks and in interference regions. If the energy variation in the cross section is large compared to beam-energy loss through the experimental target, the experimental yield will be significantly distorted. These resolution effects can be either folded into the model or unfolded from the experimental data. Both methods have their advantages and disadvantages, and each carries associated uncertainties that typically have not propagated into the final reported uncertainties.

Extrapolation of experimental data into the unknown threshold regions not only requires the extraction of the reaction contributions from the available data; it also requires a reliable treatment of uncertainties, including their propagation to predicted quantities. There has been significant recent progress on this front thanks to the use of Bayesian techniques for R-matrix analysis and the extrapolation of reaction cross sections by Moscoso *et al.* (2021), Odell, Brune, and Phillips (2022), and Odell *et al.* (2022). These analyses demonstrate several advantages of a Bayesian approach to R-matrix parameter estimation and extrapolation. In the context of this review they are particularly important since they enable a crisp answer to the question of whether certain threshold features are consistent with (multichannel) reaction data at a given Bayesian credibility level.

Bayesian algorithms are not limited to assumptions about the shape of posterior parameter distributions (for example, the assumption of a Gaussian posterior for covariance matrix calculation). They therefore allow for a more detailed understanding of the uncertainties on all quantities in the fit. Using sampling to determine the posterior for R-matrix parameters, it is straightforward to observe which parameters are well determined and which are not whether there are multiple solutions for the fit of roughly equal probability.

We collectively denote the R-matrix parameters—together with any parameters associated with our model of experimental details: normalizations, energy shifts, etc.—as θ, and we denote the datasets under consideration as D. Our goal is to then compute the posterior probability distribution $p(\theta|D,I)$, where I denotes other information about the R-matrix fit and the experiment, for example, priors on the possible normalization uncertainty, the resonance content of the R-matrix model, and the channel radius. Bayes's theorem relates this posterior to the likelihood $\equiv p(D|\theta,I)$ and the prior $p(\theta|I)$ according to

$$p(\theta|D,I) = \frac{p(D|\theta,I)p(\theta|I)}{p(D|I)} \propto p(D|\theta,I)p(\theta|I), \qquad (12)$$

where we have used the fact that $p(D|I)$ is a constant with respect to θ and thus does not affect the parameter estimation.

Most Bayesian R-matrix analyses have used a standard likelihood,

$$p(D|\theta,I) \propto \exp[-\chi^2(\theta)/2], \qquad (13)$$

where $\chi^2(\theta)$ is the χ-squared value of the R-matrix fit at a particular parameter value θ to the data D. Typically, the experimental errors that appear in the χ^2 are assumed to be uncorrelated, but this assumption can be lifted. Broad priors are then adopted for the R-matrix parameters, although the Bayesian framework does make it easy to, for example, include positivity requirements on parameters or indicate a preference for reduced-width amplitudes that fall below the Wigner limit.

The posterior $p(\theta|D,I)$ is then straightforward to write, but in most cases it can be evaluated only by sampling. Markov chain Monte Carlo sampling is a standard tool for this.

The R-matrix extrapolation of data to threshold is then straightforward since the R-matrix model can be evaluated on the set of parameter samples $\{\theta_i\}$ produced by the sampling. The results of this procedure yield not only a mean value but also a 1σ interval and, if desired, information on whether or not the tails of the distribution are Gaussian.

Before closing this section, we point out that everything said here regarding R-matrix extrapolation of data down to threshold also applies to halo EFT extrapolations of reaction data to the threshold region. EFT expressions for cross sections and S factors, as discussed in Sec. II.B, contain parameters that must be estimated from data, and a Bayesian approach has been profitably applied in this context as well, as we see in regard to the reactions that we soon discuss.

B. Theory of the Trojan horse method

The THM is an indirect method whose theoretical background is rooted in the study of direct processes, specifically, in the investigation of quasifree reaction mechanisms (Typel and Baur, 2003; Tribble *et al.*, 2014). The THM is a means of determining the cross section of the binary process $A(x,b)B$ at astrophysical energies. This is achieved by measuring the Trojan horse reaction, which involves a two-body to three-body process (2 → 3 particles), namely, $a + A \rightarrow b + B + s$, under quasifree kinematics conditions. In this scenario the particle referred to as the Trojan horse, denoted as $a = (sx)$, possesses a dominant cluster structure. This process contributes to the cross section in a three-body phase space where the momentum transfer to the spectator nucleus (s) is minimal and is known as the quasifree kinematics regime. The transferred nucleus (x) is considered virtual, meaning its energy and momentum are not governed by the typical energy-momentum relation for a free particle. This characteristic gives the $A(x,b)B$ reaction a partially off-shell nature. The relative motion between A and a occurs at an energy higher than the Coulomb barrier, ensuring that the transfer of the nucleus x takes place within the nuclear field of A without being suppressed by Coulomb forces or affected by electron screening. However, the $A + x$ reaction occurs at a sub-Coulomb center-of-mass energy (E) due to the excess energy required for the breakup of the Trojan horse nucleus $a = (xs)$ (Mukhamedzhanov, Kadyrov, and Pang, 2020).

From energy and momentum conservation principles, one obtains

$$E = \frac{m_x}{m_x + m_A} E_A - \frac{p_s^2}{2\mu_{sF}} + \frac{\boldsymbol{p}_s \cdot \boldsymbol{p}_A}{m_x + m_A} - B_{xs}, \tag{14}$$

with m_i and $\boldsymbol{p}_i$ the mass and momentum of particle i, $\mu_{ij} = m_i m_j/(m_i + m_j)$ the reduced mass of particles i and j ($F = A + x = b + B$), and $F_{xs} = m_s + m_x - m_a$ the binding energy of clusters x and s inside a. E can vary within a range determined by the momentum of the spectator particle p_s and/or its emission angle. As for p_s, its values should not overcome the theoretical upper limit for the relative momentum p_{xs} between x and s (in the laboratory system $\boldsymbol{p}_{xs} = \boldsymbol{p}_x = -\boldsymbol{p}_s$) represented by the on-the-energy-shell bound-state wave number $\kappa_{xs} = \sqrt{2\mu_{xs} B_{xs}}$. In the plane wave impulse approximation, the three-body reaction can be factorized into two terms and given by

$$\frac{d^3\sigma}{d\Omega_B d\Omega_b dE_B} = (KF)|\phi(p_{xs})|^2 \left[\frac{d^2\sigma_{xA\rightarrow bB}}{dEd\Omega}\right]^{\mathrm{HOES}}, \tag{15}$$

which shows their close connection. In Eq. (15) KF is a kinematic factor containing the final-state phase-space factor and is a function of the masses, momenta, and angles of the outgoing particles (Tumino et al., 2021); $|\phi(p_{xs})|^2$ is the Fourier transform of the radial wave function for the $\chi(\mathbf{r}_{xs})$ intercluster motion whose functional dependence is fixed by the xs system properties; and $d^2\sigma_{xA\rightarrow bB}/dEd\Omega^{\mathrm{HOES}}$ is the half-off-energy-shell differential cross section for the binary $A(x,b)B$ reaction. The agreement between the shapes of the theoretical and experimental momentum distributions of particle s was taken as proof of the validity of the plane wave impulse approximation and, consequently, the factorization mentioned earlier. The THM has been applied to several reactions of astrophysical interest; see Tumino et al. (2018), Lamia et al. (2020), Pizzone et al. (2020), Hayakawa et al. (2021), and La Cognata et al. (2022). It is an extremely powerful method to explore the near-threshold regions without being handicapped by the Coulomb barrier. One limitation lies in the requirement to normalize the extracted cross sections to experimental data directly obtained, along with the challenges posed by the possible uncertainties linked to the theoretical conversion of the THM to binary cross sections. Recent endeavors have focused on improving and broadening the theoretical framework that connects these cross sections while also assessing the systematic uncertainties stemming from model dependencies. For an overview of advancements in the theoretical framework, see Tribble et al. (2014) and Tumino et al. (2021). In scenarios where broad resonances dominate reactions, the adapted R-matrix approach (La Cognata et al., 2015; Trippella and La Cognata, 2017) has been instrumental in addressing half-off-energy-shell and energy resolution effects within the well-established R-matrix framework. Noteworthy benefits include enabling a multichannel depiction of the reaction process [as exemplified in $^{12}C + ^{12}C$ fusion investigations, which were discussed by Tumino et al. (2018)] and incorporating a DWBA-based account of the quasifree process, potentially allowing for a normalization method that bypasses the necessity of direct data usage (La Cognata et al., 2010). For reactions that are primarily characterized by narrow resonances, a streamlined approach has been introduced to derive resonance strengths directly from the reaction cross section (La Cognata et al., 2022). Through a multiresonance normalization procedure and leveraging covariance in error propagation, systematic errors arising from normalization and theoretical aspects have been minimized to the percentage level.

IV. ASTROPHYSICAL AND ANTHROPOGENIC PLASMA ENVIRONMENTS

Low-energy reaction cross sections determine the reaction rates of nuclear processes in anthropogenic as well as stellar plasmas (Casey et al., 2017). Such plasma burning occurs at temperatures that could be considered cold in terms of nuclear physics energies. Nuclear reactions with charged particles at such temperatures are severely suppressed by the Coulomb barrier and the cross-section features need to be explored at the corresponding energy range. This energy range is near the threshold, depending on the temperature in the plasma environment, as discussed in Secs. IV.A–IV.C. For light compound nuclei, the level density near thresholds is still low, and for fusion reactions in these systems nonresonant contributions often dominate. This is the case for fusion reactions between light hydrogen isotopes such as $^2H + ^2H$ that are relevant to energy generation in fusion reactors. This is also the situation for fusion reactions that involve hydrogen and helium isotopes and are important in stellar hydrogen burning of low-mass stars like the Sun. For the $^2H + ^3H$ and helium fusion processes like $^3He + ^3He$ and $^3He + ^4He$, the situation becomes more complex because of the possibility of near-threshold resonance effects. The effective energy range for such nonresonant processes is typically described as the Gamow window or Gamow range and is discussed in Sec. IV.A.

A. The Gamow range nonresonant reaction processes

It has long been understood that the only possible interaction between charged particles in stellar matter or other hot plasma environments occurs for particles in the high-energy tail of the Maxwell-Boltzmann distribution (Atkinson and Houtermans, 1929; Gamow and Teller, 1938; Bethe, 1939). The penetrability formula of Eq. (1) implies that the energy of all the other particles in the distribution is small enough that their probability of tunneling through the Coulomb and orbital-angular-momentum barrier is vanishingly small. The energy range where the two probability distributions (the Maxwell-Boltzmann distribution and the penetrability for two charged particles of relative orbital momentum $\ell = 0$) overlap is called the Gamow window. This characterizes the bulk of the effective energy range that contributes to nonresonant nuclear reaction processes at stellarlike temperatures. Low-energy resonances can enhance the cross section, and hence the reaction probability, if the resonance strength is sufficiently large.

Quantitatively, the Gamow window approximately resembles a Gaussian with a center E_G and a width ΔE, both in mega-electron-volts, as shown in Fig. 13, given by

$$E_G = 0.122(Z_1^2 Z_2^2 \mu T_9^2)^{1/3}. \tag{16}$$

The width has traditionally been defined as the $1/e = 0.368$ of the Gauss distribution since that is the energy range where most reactions are expected to occur, as discussed by Gamow and Teller (1938) and Bethe (1937),

$$\Delta E = 0.236(Z_1^2 Z_2^2 \mu T_9^5)^{1/6}. \tag{17}$$

where Z_1 and Z_2 are the numbers of protons of the interacting particles, μ is the reduced mass, and T_9 is the stellar temperature in units of 10^9 K.

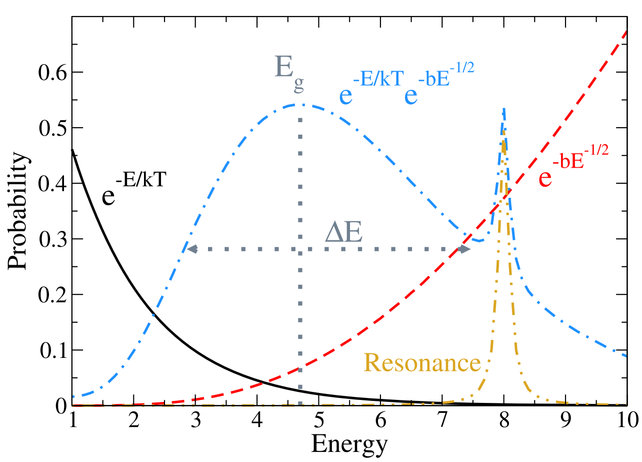

FIG. 13. The convolution of the Maxwell-Boltzmann and penetrability functions results in an approximately Gaussian distribution that is characterized by a Gamow peak energy (E_G) and width (ΔE). The Gamow peak energy is calculated under the assumption of a slowly varying cross section; thus, contributions from narrow resonances can be important even when outside of this estimated energy window.

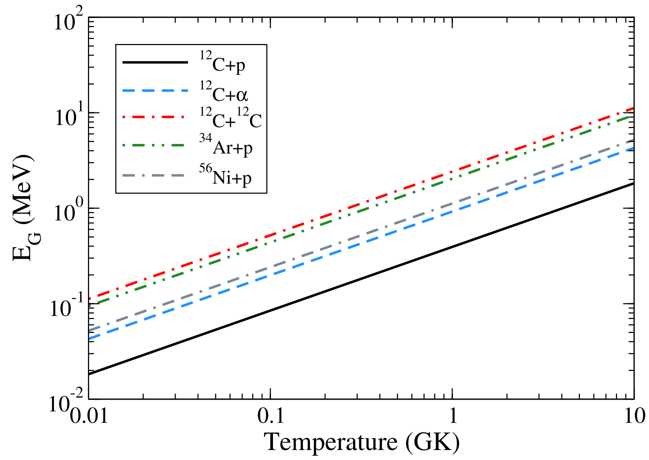

FIG. 14. The Gamow peak energy E_G, in MeV, shown as a function of temperature in GK. This is shown for several capture and fusion reactions involving ^{12}C. Also shown is the energy of the Gamow window for certain capture reactions of relevance in explosive environments at temperatures above 0.5 GK: α capture reactions on ^{34}Ar and proton capture reactions on ^{56}Ni. The cross section below these energies is needed to interpret the reaction rate.

This translates into very low energies for light-particle capture reactions where the cross section is characterized by a strong exponential decline due to the Coulomb barrier. Because of this steep decline, the cross section in most of these cases is not accessible to direct measurements. Figure 14 provides selected examples of typical Gamow peak energy values for certain reactions associated with the common temperatures for reaction rates in quiescent burning below ≈1.0 GK. It also shows the Gamow peak energies of reactions that are relevant to explosive burning in higher temperature environments. Toward higher temperatures nuclear reactions with low Q values are in statistical equilibrium with inverse reactions. Under these conditions the specific reaction rates become irrelevant since the nucleosynthesis evolution is determined primarily by the nuclear binding energies (Clifford and Tayler, 1965; Bodansky, Clayton, and Fowler, 1968; Thielemann and Arnett, 1985; Hix and Thielemann, 1996).

B. The astrophysical S factor

The astrophysical S factor, or simply the S factor, is an energy-dependent function that was introduced in its current form by Salpeter (1952). However, the concept goes back to Gamow and Teller (1938) and Bethe (1939) and his review in 1937—the "Bethe bible" (Bethe, 1937)—in which the role of the penetrability in low-energy charged-particle cross sections was summarized based on the penetrability estimates first presented by Gamow (1928). The expression

$$S(E) = E\sigma(E)e^{2\pi\eta} \tag{18}$$

introduces the S factor at energy E as a cross section approximately corrected for the asymptotic energy dependence of tunneling through the Coulomb barrier and its dependence of the de Broglie wavelength reflected by the energy term in the equation.

We point out that the S factor was simply an early way to facilitate a more reliable extrapolation of the cross section by approximating the dominant Coulomb barrier penetration factor of Eq. (1) in Eq. (18) at low energies via a simplified penetrability function for charged s-wave particles (orbital momentum $\ell = 0$) $e^{-2\pi\eta}$ (Bethe, 1937; Humblet, Fowler, and Zimmerman, 1987). The S factor was not thought to be a physical entity of deeper meaning, as often assumed or interpreted (Hwang *et al.*, 2023), that can be reparametrized by changing Coulomb or potential functions. By construction, the function $S(E)$ contains all the remaining information on the quantum-mechanical components of the transition strength between the initial and the final nuclear configuration, the interplay of the orbital momentum and Coulomb barrier for collisions where $\ell \neq 0$ and modifications to the Coulomb penetrability due to, for example, finite-size effects.

When written in terms of the S factor, the thermonuclear reaction rate for a pair of reacting nuclei jk becomes

$$N_A\langle\sigma \mathrm{v}\rangle_{j,k} = 7.83\times 10^9\left(\frac{Z_1Z_2}{\mu_{j,k}T_9^2}\right)^{1/3} \times S_{\mathrm{eff}}\exp\left(-4.2487\left[\frac{Z_1^2Z_2^2\mu_{j,k}}{T_9}\right]^{1/3}\right)\left[\frac{\mathrm{cm}^3}{\mathrm{s\,mol}}\right], \tag{19}$$

where S_{eff} is the effective S factor in MeV b within the Gamow range of the reaction, T_9 is the temperature in units of 10^9 K, and μ_{jk} is the reduced mass in atomic mass units. Equation (19) represents an approximate expression (derived using the saddle-point method) but is most accurate for low temperatures.

In the early Bethe paper (Bethe, 1937), the S factor was assumed to be a constant since the possibility of threshold effects or near-threshold resonances dramatically changing the quantum-mechanical transition strength had not yet been considered. But several factors could introduce an energy dependence to the S factor at extremely low energies—these include atomic effects as well as nuclear reaction features. Atomic effects are mainly the result of so-called electron screening, which corresponds to the effective reduction of the Coulomb barrier between two positively charged nuclei in the presence of free electron clouds in the stellar plasma or the atomic electron shells surrounding the target nuclei in experiments. Because the electrons reduce the deflecting Coulomb barrier, this effect translates into an increase in the S factor and therefore the reaction rate. The screening effect appears to be substantially more complex than previously thought, and its impact depends not only on the distribution of electrons surrounding the interacting nuclei but also on the specific shape and structure of the latter (Spitaleri *et al.*, 2016). These effects must be taken into consideration for a reliable extraction and extrapolation of the S factor from higher energy experimental data, as further discussed in Sec. VI.

The nonresonant reaction components are historically divided into two categories: tails of broad resonances and contributions based on direct reaction mechanisms. Traditionally, these nonresonant or broad resonant reaction components are described in terms of the $S(E)$ factor of Eq. (18). For nonresonant s-wave ($\ell = 0$) contributions the $S(E)$ factor varies only mildly with energy owing to deviations of the actual Coulomb penetrability from that of point-like charges and from contributions from nonzero orbital momenta and near-threshold phenomena. In earlier tabulations of astrophysical reaction rates, the low-energy dependence of the effective astrophysical $S(E)$ factor was expressed in terms of a Taylor series as

$$S(E) = S(0) + S'(0)E + \tfrac{1}{2}S''(0)E^2, \tag{20}$$

which was obtained via a polynomial fit to laboratory data at higher energies (Fowler, Caughlan, and Zimmerman, 1967, 1975). This approach, forced by computational limitations at the time, was not guided by physical models and introduced large uncertainties into many of the reaction rates still used today.

For heavy-ion fusion reactions, the semiclassical argument that motivates the relationship between the cross section and the S factor assumes a Coulomb interaction between point particles, while interacting nuclei actually have an extended size, which led to a revised definition of the S factor for fusion reactions by Trentalange *et al.* (1988). To maintain a constant value for the S factor, an additional correction term was used that takes the extension of the nucleus into account; this revised factor was labeled as $\tilde{S}(E)$ (Patterson, Winkler, and Zaidins, 1969). This dependence on extended nuclear size raises the following question: To what extent do the adopted Coulomb functions provide a reliable platform for the extrapolation of α- and heavier-ion-induced reactions in a stellar burning environments? This will be of particular importance at very low energies, where the Coulomb functions need to be calculated precisely, and even small disturbances may exponentially impact low-energy cross section and S-factor predictions.

Such disturbances at the extremely low energies of stellar burning may be associated with the choice of nuclear potential for theoretical extrapolations of the cross sections or S factors in the framework of a potential model such as distorted-wave Born approximation or a hybrid potential model and R-matrix approach traditionally based on a Woods-Saxon or square-well potential (Christy and Duck, 1961; Tombrello and Parker, 1963; Bertulani, 1996). While the choice of potential and potential parameters have only a limited impact on the cross-section predictions at higher energies achievable in laboratory experiments when one extrapolates to extremely low energies where the low cross sections inhibit direct reaction studies, the penetrability is affected by the extent of the parameters and diffuseness of the interior nuclear potential (Wiescher *et al.*, 1980).

Further uncertainty in the extrapolation of measured S factors into the unknown energy range of stellar burning may be due to the tailing of subthreshold states into the unbound region, causing direct interference between bound and unbound states or nonresonant direct reaction components affecting cross-section and S-factor predictions in the stellar energy range (Rolfs *et al.*, 1975; Lyons *et al.*, 2018; Liu *et al.*, 2020; Gula *et al.*, 2023). Other near-threshold effects influencing the very-low-energy reaction behavior may be due to a direct coupling of the wave functions of bound states with the continuum causing the formation of pronounced single-particle states as, for example, in the compound nucleus ^{19}F near the proton threshold (Lorenz-Wirzba *et al.*, 1979; Wiescher *et al.*, 1980) or cluster configurations at low energies near the α threshold (Okołowicz, Płoszajczak, and Nazarewicz, 2012; Okołowicz, Nazarewicz, and Płoszajczak, 2013; Fernandez *et al.*, 2023; Wiescher, deBoer, and Görres, 2023).

The incompressibility of nuclear matter has been suggested as the reason for a further reduction of heavy-ion fusion cross sections beyond the impact of the Coulomb barrier (Jiang *et al.*, 2006). This "hindrance" is generally modeled by introducing a correction to the nuclear potential (Michaud, 1973; Mişicu and Esbensen, 2006). Near-threshold resonance configurations may also be due to potential-driven effects since the emergence of structures may not be correlated with quantum-physical compound configurations but with dynamical processes associated with the fusion of two particles, as discussed in Sec. V.C.5 (Newton *et al.*, 2004; Diaz-Torres and Wiescher, 2018).

C. Resonance terms in cross section and reaction rate

Resonances are two-step reactions that are correlated to excited states in the compound nucleus. They frequently dominate the reaction rates for nuclear and radiative capture reactions in compound systems with increasing level densities. While resonances in reactions with low-Z partners are often broad and therefore difficult to distinguish from nonresonant contributions toward higher Z systems, the resonances become narrow due to the impact of the Coulomb barrier in the low-energy proton α or even heavy-ion entrance channels for a compound reaction. Broad resonance contributions to the reaction rate are typically treated in the framework of the S-factor approach, with the function described in Eq. (20) fitted to the S-factor data. For narrow resonances the reaction rate is derived by integrating over the corresponding Breit-Wigner function of the resonance, which yields the resonance strength

$$\omega\gamma = \frac{(2J+1)}{(2J_1+1)(2J_2+1)}\frac{\Gamma_{\rm in}\Gamma_{\rm out}}{\Gamma}, \tag{21}$$

where $\Gamma_{\rm in}$ and $\Gamma_{\rm out}$ are the production and decay widths, respectively, J is the total angular momentum of the resonance, J_1 and J_2 are the total angular momenta of the nuclei in the entrance channel, and Γ is the total width of the resonance. These quantities can be determined using indirect techniques (Iliadis *et al.*, 2001; Bertulani and Gade, 2010; Tribble *et al.*, 2014; Aumann and Bertulani, 2020), although the uncertainty in $\omega\gamma_i$ is more challenging to quantify since it depends on some theoretical assumptions.

For low-energy proton or α capture reactions in stellar hydrogen and helium burning, the corresponding resonance strengths are largely reduced by the Coulomb barrier and therefore determine the resonance strength. The branchings between different exit channels such as γ and particles are determined by their respective fraction of the total resonance width.

In this case of narrow resonances in a reaction j, k, the corresponding reaction rate can be approximated by Eq. (22), assuming that interference effects can be neglected:

$$N_A\langle\sigma v\rangle_{j,k} = 1.5394\times 10^{11}(\mu_{j,k}T_9)^{-3/2} \times \sum_i \omega\gamma_i \exp\left(\frac{-11.605E_{R_i}}{T_9}\right)\left[\frac{\rm cm^3}{\rm s\,mol}\right], \tag{22}$$

where μ is the reduced mass, T_9 is the temperature in units of 10^9 K, and $\omega\gamma_i$ and E_{R_i} are the strength and energy of the ith resonance (in mega-electron-volts), respectively. In this case only $\omega\gamma_i$ and E_{R_i} need to be determined for each resonance, with $\omega\gamma_i$ the resonance strength.

While near-threshold effects include resonant reaction contributions from the population of compound states due to the aforementioned coupling effects, they may also involve the contribution of subthreshold levels tailing into the unbound regions above the thresholds. In addition, these effects may affect the reaction rates through complex interference patterns that also may include interference with direct reaction contributions.

Pronounced single-particle and cluster configurations near the threshold due to the coupling of multiple wave functions are observed in multiple low-energy proton- and α-induced reactions. These studies have been performed in recent years based on various models. In Sec. V we highlight some important examples based on analyses using the previously introduced approaches: *ab initio*, EFT, and parametrization of data within the framework of R-matrix techniques. EFT and R-matrix analyses not only relies on fitting the existing datasets at higher energies but also takes into account the available nuclear structure information since this may provide complementary information about the existence and strength of reaction contributions near the threshold. The analyses nevertheless depend on the datasets, which should be consistent in order to provide a reliable uncertainty analysis of the cross-section extrapolation into the unknown energy range of astrophysical interest. All these effects may have a substantial impact on the reliable extrapolation of laboratory cross-section data.

Direct measurement of the impact of these quantum factors is extremely challenging because of the exponential decrease of the cross section toward the stellar energy range. Understanding these effects requires low-background measurements performed in deep-underground environments; a sufficient reduction in the natural cosmic ray background can be obtained there, making the detection of a statistically significant reaction signal possible.

As discussed in Sec. III.B, the direct approach of measuring low-energy cross sections and reaction features can be supplemented by indirect techniques (Baur, 1986; Baur, Bertulani, and Rebel, 1986; Tribble *et al.*, 2014) such as the THM. The combination of the two complementary methods provides a path toward a better understanding of the near-threshold phenomena, as demonstrated in Sec. V for a number of specific examples of key reactions for stellar nucleosynthesis.

V. SELECTED KEY REACTIONS IN NUCLEAR ASTROPHYSICS

In this section we discuss a number of astrophysically relevant reactions for hydrogen, helium, and carbon burning environments in which pronounced single-particle states, α clusters, and possibly even ^{12}C-cluster configurations may emerge through the coupling of bound-state wave functions to the continuum. The selected examples are of considerable importance for anthropogenic and stellar burning environments, with the experimental cross sections showing signatures of the threshold effects outlined and predicted previously in the review. These signatures will be characterized primarily by pronounced single-particle or cluster strength of near-threshold resonances since at very low energies large single-particle SFs or ANCs in the entrance channel determine the resonance strength. These SFs or ANCs should exceed the average values for resonance states at higher energies. The threshold states should have been observed directly or, alternatively, as tail contributions from subthreshold levels or through interference features in the low-energy cross sections.

A. Thermonuclear fusion reaction in stellar hydrogen burning

In the following we present some examples of reactions that play an important role in hydrogen burning environments. Our first example also includes a reaction that typically occurs in efforts to develop commercially viable power from nuclear fusion and also plays a role in high-density neutron-rich environments such as the big bang or the onset of the neutrino-driven wind model of a core collapse supernovae. These examples feature cases of low level density and small Q values, for which the cross section is dominated by direct capture components but influenced by neighboring cluster configurations, which may identify as threshold-aligned states. These cases are part of the pp chains, a reaction sequence that determines the energy production of the Sun (Adelberger *et al.*, 2011).

The later examples are associated with hydrogen burning through the CNO and NeNa cycles (José, Coc, and Hernanz, 1999; Wiescher *et al.*, 2010) in stellar cores or shells of more massive stars, in which basically all of the proton capture reactions have strong resonances with pronounced single-particle strength near the threshold. They may not have been labeled in the past as threshold-aligned resonance features, but the near-threshold location and the pronounced single-particle strengths identifies them as such. Cases of pronounced subthreshold configurations such as the $^{16}\mathrm{O}(p,\gamma)^{17}\mathrm{F}$ reaction can be associated with relatively low cross sections, which impact the cycle periods, energy generation, and the emerging abundance structure in the burning process.

1. Deuterium-tritium fusion

A principal example of thermonuclear fusion is the reaction $d + t \to \alpha + n + 17.6$ MeV. This reaction was first identified by Emil Konopinski as a much faster fusion process compared to $d + d$ fusion (Chadwick *et al.*, 2023; Paris and Chadwick, 2023, 2024) and became the driving reaction for thermonuclear weapons. Today, this reaction is central to research on fusion reactors; it was recently used to demonstrate a successful net energy gain at the National Ignition Facility (Abu-Shawareb *et al.*, 2022; Kritcher *et al.*, 2022; Zylstra *et al.*, 2022). Recent theoretical predictions suggest that the use of a high-intensity-laser field could lead to a reduction of the deflecting Coulomb field through screening enhancement and consequently to an increase in the low-energy cross section of the fusion process (Thomson, Moschini, and Diaz-Torres, 2024).

The cross section and S factor are characterized by a pronounced resonance at $E = 65$ keV above the dt threshold with a peak cross section of 4.88 b, as shown in Fig. 15. For comparison, the $n + {}^{239}\mathrm{Pu}$ fission cross section at the same energy is only 1.6 b. The large fusion cross section at $E = 65$ keV is due to the formation of a $J^\pi = 3/2^+$ resonance in the unbound ^{5}He nucleus at 16.84 MeV excitation energy, just above the dt fusion threshold at 16.792 MeV. This resonance clearly identifies as an example for a threshold-aligned state with a pronounced cluster configuration exhibited by its strength in the fusion cross section, as discussed later. It plays an important role in many astrophysical and anthropogenic applications.

dt fusion is a leading process in the primordial formation of the lightest elements (mass number $A \leq 7$) affecting the predictions of BBN models for light-nucleus abundances (Serpico *et al.*, 2004). Because of the enhancement from the $3/2^+$ ^{5}He resonance, dt fusion is responsible for the creation of 99% of primordial ^{4}He (Smith, Kawano, and Malaney, 1993). The remaining 1% comes from its mirror reaction, $^3\mathrm{He}(d,p)^4\mathrm{He}$ or d^3He, fusion (Smith, Kawano, and Malaney, 1993). This process also benefits from the isospin-mirror $3/2^+$ resonance but is suppressed with respect to dt because of the larger Coulomb repulsion between d and ^{3}He. Since this primordial helium became a source for the subsequent creation of carbon and other heavier elements, a substantial portion of our body owes its existence to dt fusion (Chadwick, Paris, and Haines, 2023).

The ^{5}He $3/2^+$ resonance was discovered by Bretscher and French (1949) during an investigation of dt fusion at low energies. The appearance of a resonance so close to the dt threshold and the strong cross-section enhancement it produced came as a surprise (Chadwick *et al.*, 2023). The cross section was subsequently expressed in terms of R-matrix theory, coupling the direct and resonant components of the reaction cross section (Bosch and Hale, 1992). Recent R-matrix analyses of this reaction have utilized Bayesian approaches to estimate uncertainties (de Souza *et al.*, 2019; Odell, Brune, and Phillips, 2022). Today, the structure of this enigmatic state and the complex five-nucleon dynamics underlying the dt and d^3He reactions can also be accurately described and explained by *ab initio* nuclear theory, starting with validated (realistic) interactions among the nucleons. Following pioneering calculations performed within thex‘ NCSM-RGM formalism using a realistic NN interaction (Navrátil and Quaglioni, 2012), a much more advanced NCSMC investigation of the dt fusion was presented by Hupin, Quaglioni, and Navrátil (2019). This work used NN and 3N interactions from chiral EFT and also gave results for the mirror $^3\mathrm{He}(d,p)^4\mathrm{He}$ system. The calculations there include both the $^4\mathrm{He} + n$ ($^4\mathrm{He} + p$) and $^3\mathrm{H} + d$ ($^3\mathrm{He} + d$) mass partitions in the cluster part of the NCSMC trial wave function given in Eqs. (2) and (3).

In Fig. 15(a) we compare the NCSMC computed astrophysical S factor with established measurements. The experimental peak at the center-of-mass energy $E = 49.7$ keV corresponds to the enhancement from the $3/2^+$ resonance of ^{5}He. The calculations underpredict the experiment by 15% (the dashed green line versus the red circles in Fig. 15(a)). This can be traced back to the overestimation of the $3/2^+$ resonance centroid by a few kilo-electron-volts. This is certainly within the expected accuracy of a chiral EFT interaction that is truncated at a finite order and fit to data of finite precision. To overcome this issue and arrive at an accurate evaluation of polarized dt reaction observables, a phenomenological correction of -5 keV was applied to the position of the resonance centroid. This resulted in noteworthy agreement with the experimental S factor over a wide range of energies (the blue line). A detailed explanation of how such a correction was obtained was provided in the method section of Hupin, Quaglioni, and Navrátil (2019). The discrepancies between the experimental S-factor data and the theoretical model predictions at very low energies have been interpreted as a consequence of electron screening (Langanke and Rolfs, 1989), which was not included in the analysis by Hupin, Quaglioni, and Navrátil (2019). Figure 15(b) presents the differential cross section in the center-of-mass frame at the scattering angle of $\theta = 0°$ over a range of energies up to the deuterium breakup threshold. The results (solid blue and dashed green lines) also match the evaluated differential cross section.

One infers from the diagonal phase shifts obtained within the NCSMC (Hupin, Quaglioni, and Navrátil, 2019) that the $3/2^+$ resonance is dominated by an s wave in the relative motion of the deuterium and tritium nuclei with their spins aligned ($1^+ + 1/2^+$). There is also a significant distortion in the d-wave diagonal phase shift in the $n + {}^4\mathrm{He}$ system, indicating that the resonance has a complex five-body nature.

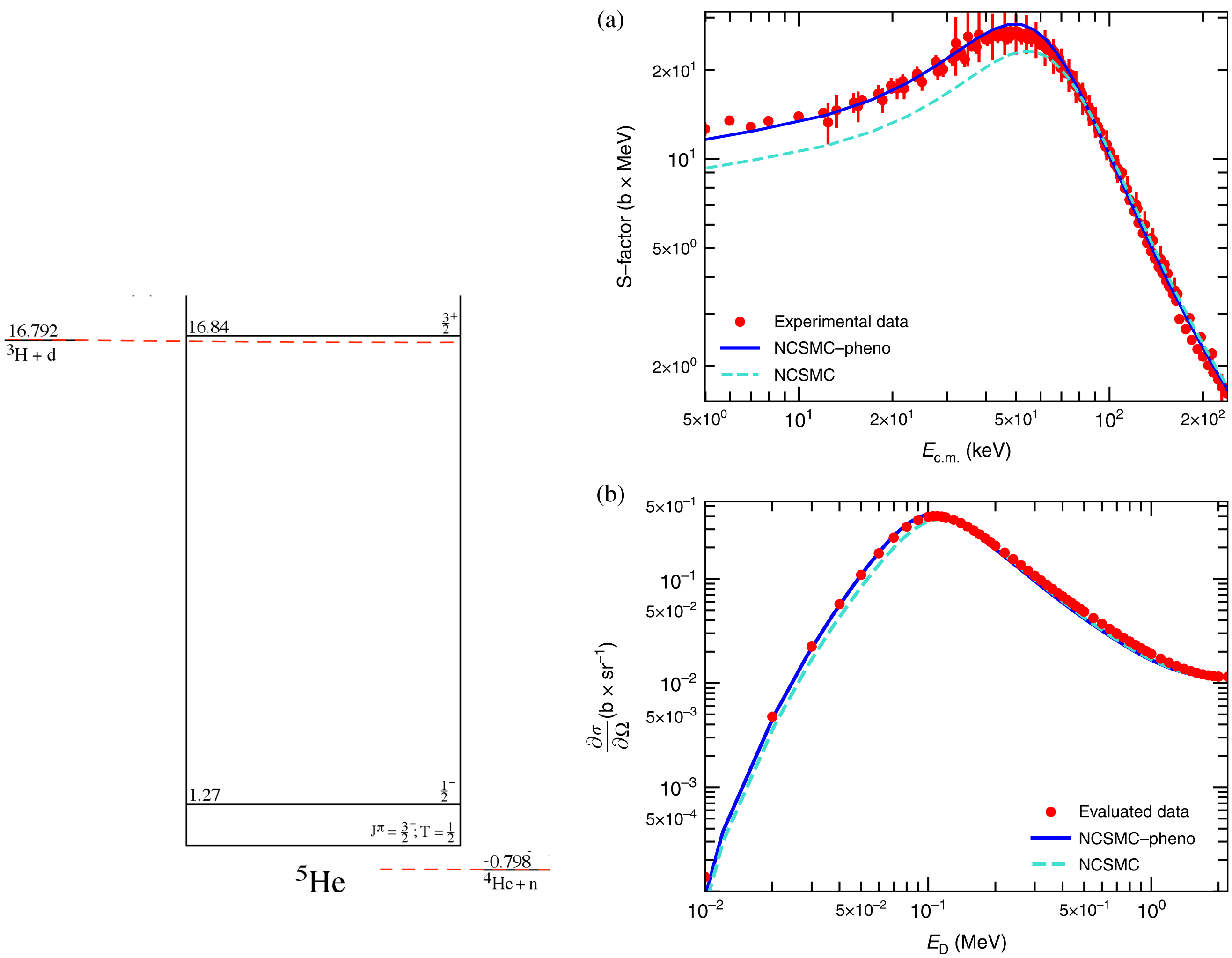

FIG. 15. Left panel: level diagram of ^{5}He. (a): Astrophysical S factor of the $^3\mathrm{H}(d,n)^4\mathrm{He}$ reaction as a function of the energy in the center-of-mass frame compared to the available experimental data. (b): Angular differential cross section as a function of the deuterium incident energy E_d at the center-of-mass scattering angle of $\theta = 0°$ compared to the evaluated data. NCSMC and NCSMC-pheno stand for the results of the calculations before and after a phenomenological correction of 5 keV to the position of the $3/2^+$ resonance. See Hupin, Quaglioni, and Navrátil (2019) for details.

The dt fusion reaction apparently proceeds from an s wave to a d wave in $n + {}^4\mathrm{He}$, implying the importance of the nuclear tensor force as well as the 3N force for the fusion process.

2. ${}^4\mathrm{He}(d,\gamma){}^6\mathrm{Li}$

The production of primordial ^{6}Li in the big bang is dominated by ${}^4\mathrm{He}(d,\gamma){}^6\mathrm{Li}$ radiative capture. The same reaction also plays a role in the first stars, where it is a part of the cycle ${}^4\mathrm{He}(d,\gamma){}^6\mathrm{Li}(\alpha,\gamma){}^{10}\mathrm{B}(\alpha,d){}^{12}\mathrm{C}$ (Wiescher *et al.*, 2021), which is expected to contribute to the formation of ^{12}C in this environment. The Q value for this reaction is low ($Q = 1.4743$ MeV), identifying ^{6}Li as a weakly bound d-α configuration, as suggested in the Ikeda diagram. The first excited state $J^\pi = 3^+$ in ^{6}Li at $E_x = 2.186$ MeV is the sole resonance in this energy range at $E = 0.712$ MeV. These features may play a role in the interpretation of the so-called Li problem.

Although the BBN predictions for the abundances of hydrogen and helium are in agreement with astrophysical observations, they fall short in the cases of lithium isotopes. The abundance of ^{7}Li is overpredicted by a factor of 2–4 compared to the observational data labeled as the Spite plateau (Spite and Spite, 1982), while that of ^{6}Li is underpredicted, but by 3 orders of magnitude (Fields, 2011). It has been argued that the origin of these discrepancies could be physics beyond the standard model or systematic uncertainties in inferring the primordial abundances from the composition of metal-poor stars (Asplund *et al.*, 2006; Cyburt *et al.*, 2016). But it is also possible that part of the discrepancy could be explained by inaccuracies in the nuclear reaction rates, which are the main inputs to the BBN reaction network. Present data suggest that the cross section below the resonance at $E = 0.712$ MeV in ${}^4\mathrm{He}(d,\gamma){}^6\mathrm{Li}$ is dictated by pronounced nonresonant direct capture and interfering tail contributions, but disagreements exist about the relative strength of these contributions.

To address this issue, *ab initio* NCSMC calculations of the ${}^4\mathrm{He}(d,\gamma){}^6\mathrm{Li}$ radiative capture reaction were performed recently using chiral NN and 3N interactions as input (Hebborn *et al.*, 2022). At BBN energies from 30 to 400 keV, the ${}^4\mathrm{He}(d,\gamma){}^6\mathrm{Li}$ reaction rate is poorly known. On the experimental side, there are large discrepancies between existing datasets based on direct and indirect techniques, as discussed in the following. Direct measurements are hindered by the Coulomb repulsion between the ^{4}He and d nuclei. Consequently, there are only two direct measurements in the BBN energy range, at 94 and 134 keV (Anders *et al.*, 2014). Indirect estimates relating the radiative capture rate to the disintegration of ^{6}Li in the Coulomb field of a heavy target overcome the low statistics but suffer from systematic uncertainties caused by the difficulty of cleanly separating the nuclear and electromagnetic contributions to the breakup cross section (Baur, Bertulani, and Rebel, 1986; Kiener *et al.*, 1991; Hammache *et al.*, 2010). Furthermore, in Coulomb-dissociation experiments, the $E2$ component is strongly enhanced compared to $E1$ relative to their roles in the capture reactions (Typel, Bläge, and Langanke, 1991; Kharbach and Descouvemont, 1998; Igamov and Yarmukhamedov, 2000). Thus, these experiments could not address the question of whether $E1$ transitions contribute to the capture cross sections at primordial energies as was speculated (Robertson *et al.*, 1981).

In contrast to previous studies, the NCSMC calculations of Hebborn *et al.* (2022) find $E1$ transitions to be negligible. They also find an enhancement of the radiative capture below 100 keV driven by previously neglected $M1$ transitions. The uncertainty in the predicted thermonuclear reaction rates is reduced by an average factor of 7 compared to the previous evaluation (Xu *et al.*, 2013). The calculated S factor is compared to experimental data in the top panel of Fig. 16. Once the 3N interaction is included in the Hamiltonian, the calculated S factor matches the data well at and between the 3^+ ($E = 0.71$ MeV) and 2^+ resonances ($E = 2.84$ MeV). At the lower relevant BBN energies, the NCSMC calculations agree with the direct measurements of the LUNA Collaboration (Anders *et al.*, 2014). However, the calculations are incompatible with the results inferred from breakup data (Kiener *et al.*, 1991), which have been shown to suffer from model dependence (Hammache *et al.*, 2010). The relative importance of the electromagnetic $E2$, $E1$, and $M1$ transitions varies with energy; see the bottom right panel of Fig. 16. It was found that the $E2$ transitions dominate the nonresonant and resonant capture, which is in line with previous theoretical works. Departing from those previous studies, a sizable $M1$ component was found that was not previously predicted. This $M1$ contribution arises from the internal dipole magnetic moments of the ^{6}Li and d nuclei, making a full microscopic description essential for an accurate calculation.

3. ${}^3\mathrm{He}(\alpha,\gamma){}^7\mathrm{Be}$

Another similar case is the classic example of the ${}^3\mathrm{He}(\alpha,\gamma){}^7\mathrm{Be}$ reaction. This remains intriguing because, despite considerable past experimental effort, there is still not a unique description of the entire low-energy cross-section range (Adelberger *et al.*, 1998, 2011). While more reliable data at low energies suggest an increase in S factor toward lower energies, the challenge is to develop a comprehensive interpretation of this observation. At higher energies the cross section is thought to be dominated by broad resonance structures tailing into a classic direct capture mechanism (Christy and Duck, 1961; Tombrello and Parker, 1963), but the physical origins of the underlying contributions to the slight increase at low energies remain an open question.

From the astrophysics point of view, this reaction is a key process in the pp chain since it controls the branching between the pp-I and pp-II chains. The strength of the reaction primarily influences the production of solar neutrinos from the ^{7}Be electron capture decay to ^{7}Li and the β decay of ^{8}B to ^{8}Be with subsequent two-α breakup. The reaction rate is directly correlated with the strength of the ${}^3\mathrm{He}(\alpha,\gamma){}^7\mathrm{Be}$ reaction cross section at solar core temperatures near 0.015 GK; the observed neutrino flux provides important insight into the solar interior but reliability depends on the extrapolation of the reaction cross section into the corresponding Gamow energy range.

High-precision solar-neutrino flux measurements sustained a steady interest in measurements of this reaction and repeated experimental studies (Parker and Kavanagh, 1963; Nagatani,

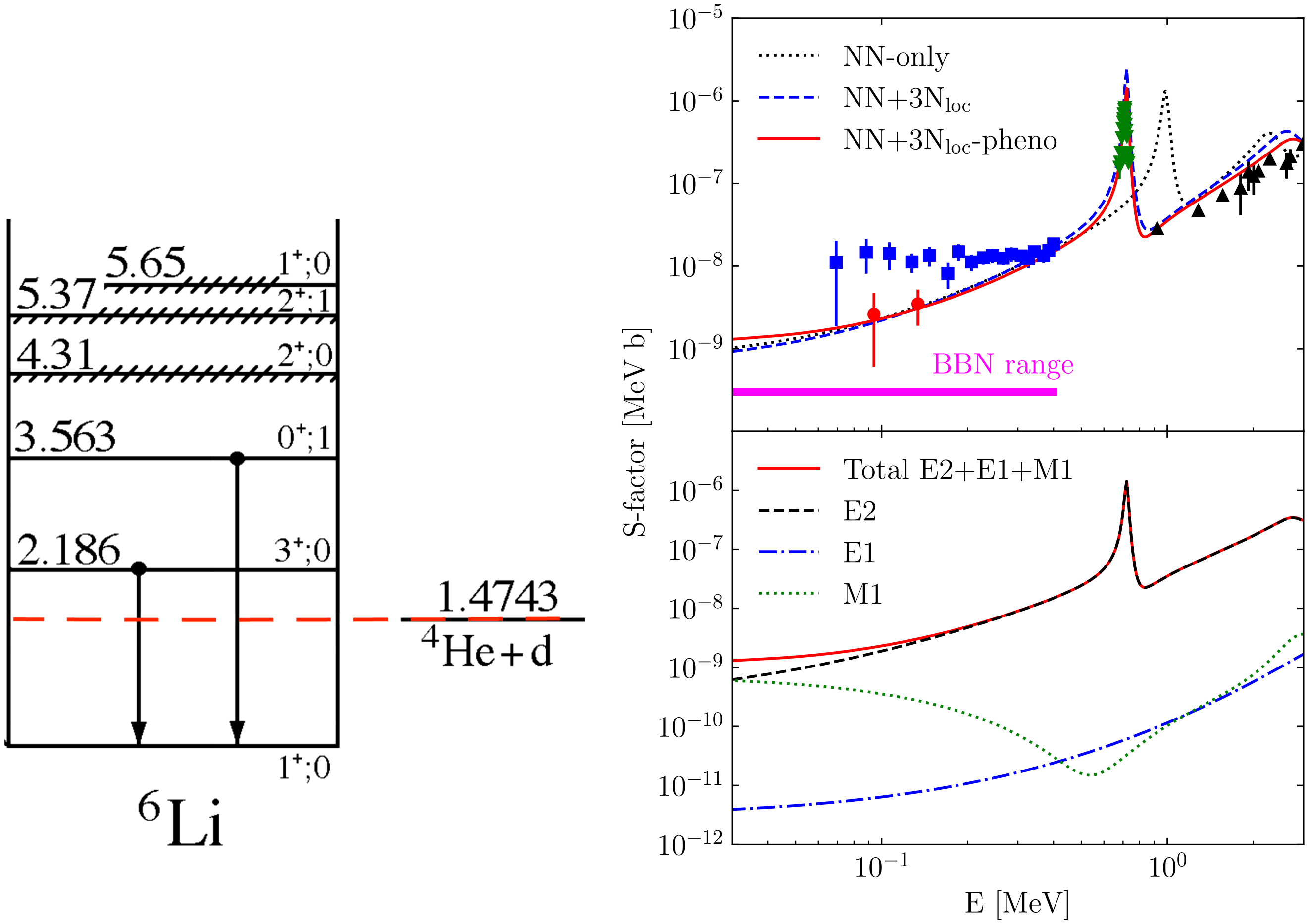

FIG. 16. Left panel: level diagram of ^{6}Li. Top right panel: predicted S factor for the $^4\mathrm{He}(d,\gamma)^6\mathrm{Li}$ reaction compared with data taken from Anders *et al.* (2014) (red circles), Kiener *et al.* (1991) (blue square), Mohr *et al.* (1994) (green down triangles) and Robertson *et al.* (1981) (black up triangles). The data marked as blue squares are based on Coulomb-dissociation measurements, while the other datasets are based on direct reaction studies. Calculations were obtained using the SRG-evolved N^{3}LO NN potential (NN only) (Entem and Machleidt, 2003) and $\mathrm{NN} + 3\mathrm{N}_{\mathrm{loc}}$ (Gazit, Quaglioni, and Navrátil, 2019) without ($\mathrm{NN} + 3\mathrm{N}_{\mathrm{loc}}$) and with ($\mathrm{NN} + 3\mathrm{N}_{\mathrm{loc}}$-pheno) the phenomenological energy adjustment. Bottom right panel: $E2$, $E1$, and $M1$ components of the predicted S factor for the $^4\mathrm{He}(d,\gamma)^6\mathrm{Li}$ reaction obtained with $\mathrm{NN} + 3\mathrm{N}_{\mathrm{loc}}$-pheno. Adapted from Hebborn *et al.*, 2022, where further details are given.

Dwarakanath, and Ashery, 1969; Kräwinkel *et al.*, 1982; Osborne *et al.*, 1982, 1984; Robertson *et al.*, 1983; Volk *et al.*, 1983; Alexander *et al.*, 1984; Hilgemeier *et al.*, 1988) throughout the 1970s and 1980s were finally able to resolve the data inconsistencies between measurements made via prompt γ-ray detection and those using the activation technique (Adelberger *et al.*, 2011). Over the past 25 years, continued independent and consistent measurements (Bemmerer *et al.*, 2006; Brown *et al.*, 2007; Confortola *et al.*, 2007; Gyürky *et al.*, 2007; Costantini *et al.*, 2008; di Leva *et al.*, 2009; Su *et al.*, 2010; Carmona-Gallardo *et al.*, 2012; Bordeanu *et al.*, 2013; Kontos *et al.*, 2013) have driven the uncertainty at solar energies down to $\approx 4\%$. Even so, with the unprecedented accuracy of modern solar-neutrino measurements, the uncertainty in this cross section is one of the dominant sources of uncertainty in this aspect of solar modeling (Adelberger *et al.*, 1998, 2011).

Because it populates a light system, the $^3\mathrm{He}(\alpha,\gamma)^7\mathrm{Be}$ reaction provides an excellent opportunity to compare different types of nuclear models, including *ab initio* (Neff, 2011; Dohet-Eraly *et al.*, 2016; Atkinson *et al.*, 2025), microscopic cluster models (Kim, Izumoto, and Nagatani, 1981; Kajino and Arima, 1984; Kajino, 1986; Langanke, 1986; Kajino, Toki, and Austin, 1987; Csótó and Langanke, 2000), variational Monte Carlo (Nollett, 2001), halo EFT (Premarathna and Rupak, 2020; Zhang, Nollett, and Phillips, 2020; Paneru *et al.*, 2024), potential models (Christy and Duck, 1961; Tombrello and Parker, 1963; Mohr *et al.*, 1993; Baye and Brainis, 2000; Dubovichenko, 2010; Tursunov, Turakulov, and Kadyrov, 2021), and R matrix (Descouvemont *et al.*, 2004; Kontos *et al.*, 2013; deBoer *et al.*, 2014; Paneru *et al.*, 2024). The application of these different methods provides additional insight into the model uncertainty associated with the extrapolation of the low-energy cross section. While the adopted values are usually based on fits using EFT or the R matrix, there is added confidence in these phenomenological descriptions because of their good agreement with *ab initio* calculations; see Sec. II.A.

However, from a phenomenological R-matrix perspective, understanding the different reaction mechanisms that make up

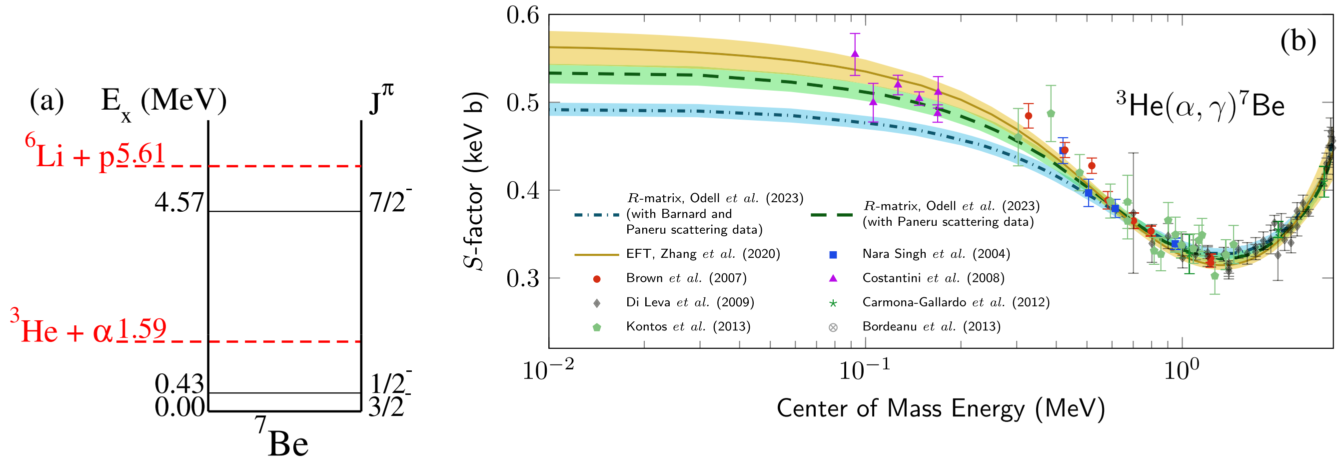

FIG. 17. (a) Level diagram of the ^{7}Be system at low energies. (b) Total radiative capture S-factor data for the ^{3}He$(\alpha,\gamma)^7$Be reaction (Singh *et al.*, 2004; Brown *et al.*, 2007; Costantini *et al.*, 2008; di Leva *et al.*, 2009; Carmona-Gallardo *et al.*, 2012; Bordeanu *et al.*, 2013; Kontos *et al.*, 2013) compared to the 68% intervals obtained in the N^{4}LO EFT calculation from Zhang, Nollett, and Phillips (2020) (solid gold line), which fits only capture data, and with R-matrix fits by Odell *et al.* (2022) that also simultaneously fits the scattering data of both Barnard, Jones, and Phillips (1964) and Paneru *et al.* (2024) (blue band) or simply the capture data and the scattering data of Paneru *et al.* (2024) (green band). Scattering data can provide additional constraints for phenomenological R-matrix fittings of radiative capture data, but the lack of detailed uncertainties can lead to erroneous results.

the cross section has been challenging. If only low-energy data are considered, a direct capture model (Tombrello and Parker, 1963) gives a good representation of the cross section, as observed by Parker and Kavanagh (1963), who found that the uncertainties were on the ≈10% level. However, as uncertainties decreased and measurements spanned a wider energy range (di Leva *et al.*, 2009), the external capture model (Holt *et al.*, 1978; Barker and Kajino, 1991; Angulo and Descouvemont, 2001; deBoer *et al.*, 2017) alone proved insufficient (Kontos *et al.*, 2013; deBoer *et al.*, 2014). A solution that naturally reproduced the energy dependence of the experimental data was the addition of a $1/2^+$ background level, which interfered with the $E1$ external capture. While the background contribution was relatively weak compared to the magnitude of the external capture, the interference term between the two was significant, making up ≈10% of the cross section. This contribution is significant considering that recent experiments report total uncertainties of ≈4%. While this phenomenological solution is able to give an excellent reproduction of the data, a better understanding of the physical interpretation of this background term is needed to add confidence to this modeling and the extrapolation to threshold energies. A recent higher energy measurement by Tóth *et al.* (2023) seemed to indicate the presence of one or more broad resonance structures, but the interpretation of the measurements remains unclear.

In recent years more emphasis has been placed on performing R-matrix fits that also include low-energy scattering data. In addition to constraining the energies and particle widths of resonances that are directly observed in the data, the small deviations of the data from Rutherford scattering over a wide energy range can also constrain the ANCs of bound states. Subthreshold state contributions in the ^{3}He$(\alpha,\gamma)^7$Be reaction may come from the first excited state in ^{7}Be, which has a pronounced cluster configuration but is too far removed from the threshold to promise significant impact. However, it served as a good case to study low-energy cross sections dominated by direct capture, and its relation to the external capture model supplemented by bound-state ANCs. This method was first used by deBoer *et al.* (2014) for the ^{3}He$(\alpha,\gamma)^7$Be reaction, although some tension was found between the ANCs obtained from the scattering and those obtained from the radiative capture data, which produced a significantly different low-energy extrapolation of the S factor as shown in Fig. 17. It was not until the reanalysis of Odell *et al.* (2022) used the new experimental scattering data of Paneru *et al.* (2024) that it was discovered that the older scattering data by Barnard, Jones, and Phillips (1964) had incomplete uncertainty characterization that likely caused this tension. This case presents both a cautionary tale and a demonstration of the power of this technique. While elastic scattering data (or any additional dataset) may add significant constraints to a phenomenological model, additional systematic uncertainties can be introduced. Nevertheless, these types of analyses, which include a wider range of data, should be pursued because if consistency can be achieved, they lead to increased confidence in both the data and models.

4. ^{7}Be$(p,\gamma)^8$B

Another reaction of great interest for the neutrino production in the Sun is the radiative capture process ^{7}Be$(p,\gamma)^8$B. This determines the relative strength of the pp-II and pp-III chains since the former generates neutrinos through the β decay of ^{8}B and the latter generates neutrinos through electron capture on ^{7}Be. The competition of the electron capture and radiative capture reactions thus determines the ratio of the neutrino flux from these two components of the pp chain (Johnson *et al.*, 1992).

The reaction has a low Q value of ≈137 keV and is dominated by direct capture to the ground state in ^{8}B. This makes it the third case of the weakly bound compound systems discussed here for which the cross section is primarily determined by direct capture to bound states. Only at higher energies does a single resonance at 720 keV contribute to the reaction rate, and this is relevant only at temperatures higher than those in the Sun. Dominated by a single direct capture transition, the ^{7}Be$(p,\gamma)^8$B low-energy cross section represents a perfect opportunity to test model predictions for extrapolating experimental low-energy laboratory data to the stellar energy range near the threshold.

The reaction was the focus of an experimental campaign in the 1960s to explore the reliability of the external capture model (Christy and Duck, 1961; Tombrello and Parker, 1963; Bertulani, 1996). The model did not support a flat S factor as tentatively implied from a continuation of the data but instead predicted an increase toward lower energies (Kavanagh, 1960; Parker, 1968). This effort in direct radiative capture studies was later complemented by Coulomb-dissociation measurements of radioactive ^{8}B beams using virtual photons (Motobayashi *et al.*, 1994; Iwasa *et al.*, 1999; Motobayashi, 2001; Schümann *et al.*, 2003, 2006). The modest rise of the S factor toward solar energies is due to the energy dependencies of the Whittaker function asymptotics of the ground state, the regular Coulomb functions describing the ^{7}Be $+\ p$ scattering states, and the E_γ^3 dipole phase-space factor. This behavior was confirmed in the framework of a single potential model by Tombrello (1965) and Bertulani (1996), microscopic cluster models (Descouvemont and Baye, 1988; Kolbe, Langanke, and Assenbaum, 1988; Johnson *et al.*, 1992; Descouvemont, 1993a; Csótó *et al.*, 1995; Csótó and Langanke, 1998), and early calculations based on the NCSM (Navrátil, Bertulani, and Caurier, 2006b). The reaction, together with the ^{7}Li$(n,\gamma)^8$Li mirror capture reaction, was one of the first examples to be analyzed in the framework of the SMEC (Bennaceur *et al.*, 1999). In these studies, which included $E1$, $E2$, and $M1$ contributions, the astrophysical S factor for the ^{7}Be$(p,\gamma)^8$B reaction at $E = 0$ is $S(0) = 0.0196$ keV b. The analysis of later experimental results was summarized by Adelberger *et al.* (1998, 2011). The S factor in the solar energy range, based on more recent data, averaged to $S = 0.019^{+0.004}_{-0.002}$ keV b, which is significantly lower than previously suggested. This value agrees well with the SMEC prediction for S by Bennaceur *et al.* (1999).

Figure 18 shows the results of a halo EFT analysis of data on the capture reaction ^{7}Be$(p,\gamma)^8$B at center-of-mass energies $E < 0.5$ MeV. Zhang, Nollett, and Phillips (2015) computed the amplitude for this reaction up to next-to-leading order and the Bayesian posterior probability density was determined by Markov chain Monte Carlo sampling; see also Zhang, Nollett, and Phillips (2018). The yellow band in Fig. 18 shows the 68% interval that was found for the S factor. The result for $S(0)$ is 0.0213 ± 0.0007 keV b. The small difference between the leading-order result (not shown) and the NLO result plotted in Fig. 18 confirms that halo EFT is converging well and higher-order terms are small. Higa, Premarathna, and Rupak (2022) subsequently calculated this reaction in halo EFT, including effects of both the excited state of the ^{7}Be core and the 1^+ resonance at 0.6 MeV. Results similar to the halo EFT ones shown in Fig. 18 were obtained for $E < 500$ keV.

The ^{7}Be$(p,\gamma)^8$B capture reaction was first investigated in an *ab initio* framework by Navrátil, Roth, and Quaglioni (2011) within the NCSM-RGM formalism starting from a similarity-renormalization-group- (SRG)evolved chiral NN interaction tuned to reproduce the experimental separation energy of the ^{8}B weakly bound $2^+_{\mathrm{g.s.}}$ with respect to the ^{7}Be $+\ p$ threshold. More advanced calculations using a set of six different chiral EFT NN and 3N interactions have since been performed within the NCSMC formalism (Kravvaris *et al.*, 2023). The NN interactions ranged from N^{2}LO through the original N^{3}LO (Entem and Machleidt, 2003) up to N^{4}LO (Entem, Machleidt, and Nosyk, 2017). These were combined with N^{2}LO chiral EFT 3N interactions of the type introduced by Navrátil (2007), Gazit, Quaglioni, and Navrátil (2019), and Somà *et al.* (2020), one of which, named $3\mathrm{N}^*_{\mathrm{lnl}}$, included a nominally N^{4}LO contact interaction that enhances the strength

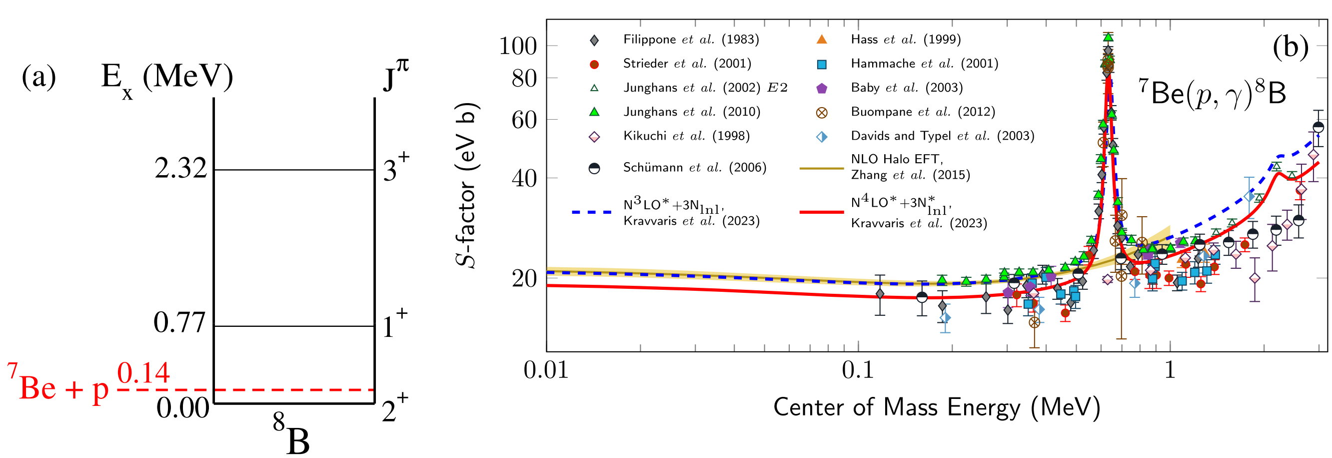

FIG. 18. (a) Level diagram of the ^{8}B system at low energies. (b) Comparison of the low-energy S-factor direct data (Filippone *et al.*, 1983; Hass *et al.*, 1999; Hammache *et al.*, 2001; Strieder *et al.*, 2001; Junghans *et al.*, 2002, 2010; Baby *et al.*, 2003; Buompane *et al.*, 2022) and those determined through Coulomb excitation (Kikuchi *et al.*, 1998; Davids and Typel, 2003; Schümann *et al.*, 2006) for the ^{7}Be$(p,\gamma)^8$B reaction compared to the NLO halo EFT calculations of Zhang, Nollett, and Phillips (2015), where the shaded region indicates the 68% confidence interval, and to *ab initio* calculations using chiral EFT NN and 3N forces by Kravvaris *et al.* (2023).

of spin-orbit splittings (Girlanda, Kievsky, and Viviani, 2011). Unlike the earlier NCSM-RGM calculations that focused only on the direct $E1$ capture, the new NCSMC calculations also include the $M1$ and $E2$ contributions from resonances. To reproduce the ^{8}B separation energy and positions of two low-lying resonances, the NCSMC-pheno approach was applied (Kravvaris et al., 2023).

The astrophysical S factor obtained with the N^{4}LO NN interaction and the $3\mathrm{N}^*_{\mathrm{lnl}}$ force and after this pheno adjustment is shown in Fig. 18. It accurately reproduces the resonance contributions due to the dominant $M1$ and smaller $E2$ transitions from the 1^+ resonance at ≈ 0.6 MeV and the 3^+ resonance at ≈ 2.2 MeV. This confirms that these resonances have no influence on the cross section at solar energies. The NCSMC *ab initio* calculation matches the Junghans direct measurement data well (Junghans et al., 2003), starting with the 1^+ resonance up to ≈ 2.5 MeV, including the 3^+ bump. At low energies below the 1^+ resonance, the NCSMC-pheno results are slightly below the Junghans data.

The application of a large set of chiral EFT interactions enabled a correlation study that examined the extent to which the *ab initio* S factor at higher energies is correlated with $S(0)$. Employing this correlation, as well as a combined result for the S factor at energies where it is measured (but below the 1^+ resonance), Kravvaris et al. (2023) arrived at a suggested value for the $^7\mathrm{Be}(p,\gamma)^8\mathrm{B}$ S factor at zero energy of $S(0) = 19.8 \pm 0.3$ eV b (Kravvaris et al., 2023).

5. $^{14}\mathrm{N}(p,\gamma)^{15}\mathrm{O}$

For massive main sequence stars ($M \geq 1.5 M_\odot$), the energy production is dominated by the CNO cycle, which is a catalytic process involving four subsequent proton capture reactions and two β decays with the emission of one α particle. This is a key nucleosynthesis process and was first suggested by Weizsäcker (1937), with a first quantitative calculation provided by Bethe (1939). The energy production of the CNO cycle in massive stars grows exponentially with temperature since it is limited only by the Coulomb barriers for proton capture on the stable CNO isotopes (Wiescher, Görres, and Schatz, 1999; Wiescher et al., 2010), while the relative contribution of the pp chains becomes smaller with increasing mass since the energy production rate is limited by the slow weak-interaction $p + p$ fusion process (Adelberger et al., 2011).

There are many cases in the CNO cycle where pronounced low-energy resonance states may serve as examples for near-threshold single-particle structures such as the $^{12}\mathrm{C}(p,\gamma)^{13}\mathrm{N}$ and $^{13}\mathrm{C}(p,\gamma)^{14}\mathrm{N}$ reactions, which are dominated by the associated resonance contributions (Csedreki, Gyürky, and Szücs, 2023; Skowronski et al., 2023), while the impact of bound subthreshold states may be seen in the low-energy cross section in the transition to the first excited halolike state in ^{17}F (Morlock et al., 1997).

In the following, however, we concentrate on the key reaction for the CNO cycle, the $^{14}\mathrm{N}(p,\gamma)^{15}\mathrm{O}$ reaction determining cycle time and equilibrium abundances in the cycle. The reaction was therefore of importance for the age determination of globular clusters as an independent way of deducing a lower limit for the age of the Universe (Chaboyer et al., 1996; Imbriani et al., 2004). With the first measurement of solar neutrinos associated with the β decay of ^{15}O (Agostini et al., 2020a; Appel et al., 2022; Basilico et al., 2023), interest in the low-energy cross section grew enormously since the flux information combined with reliable cross-section data in the solar energy range would provide an independent method for determining the metallicity of the solar core (Haxton and Serenelli, 2008; Haxton, Hamish Robertson, and Serenelli, 2013; Serenelli, Peña-Garay, and Haxton, 2013). Over the past few years, multiple experiments have been performed, in both aboveground and underground accelerator facilities, to map the cross section for the different reaction branches over a wide energy range (Schröder et al., 1987; Formicola, Costantini, and Imbriani, 2003; Formicola et al., 2004; Imbriani et al., 2005; Runkle et al., 2005; Lemut et al., 2006; Marta et al., 2008; Li et al., 2016; Frentz et al., 2022). The reaction analysis was performed primarily using R-matrix analysis techniques informed by indirect data for the possible contribution of near-threshold and subthreshold levels.

While several transitions contribute to the reaction, three are thought to dominate the low-energy cross section (Adelberger et al., 2011). These include external capture transitions but also resonant components interfering with the direct capture. This can be observed in the transition to the ground state in ^{15}O as well as in the transitions to the two excited states at 6.79 and 6.18 MeV excitation energy, as displayed by the S-factor curve shown in Fig. 19.

All three transitions exhibit a resonance at 278 keV corresponding to the unbound state at 7.556 MeV ($J^\pi = 1/2^+$). For the transitions to ground state and the state at 6.18 MeV, additional resonant contributions have been observed. For the direct capture, the transition to the $J^\pi = 3/2^+$ subthreshold state at 6.79 MeV makes the largest contribution. This state plays a particularly interesting role, not only for being strongly fed by the direct capture but also for exhibiting a pronounced subthreshold resonance contribution at $E_R = -505$ keV, tailing into the unbound excitation range of ^{15}O. This tail makes a strong contribution to the transition to the ground state ($J^\pi = 1/2^-$) and the 6.18 MeV state ($J^\pi = 3/2^-$), which are marked as subthreshold in Fig. 19. The 6.79 MeV level with a pronounced single-particle structure is an example of the near-threshold configuration impacting this reaction cross section at near-threshold energies.

This suggests that its strength is correlated to direct coupling to the continuum. Since the 6.79 MeV transition has consistent data and a simple theoretical description, it has been straightforward to determine the ANC using the capture data (Adelberger et al., 2011). In addition, proton transfer measurements (Bertone et al., 2002; Mukhamedzhanov et al., 2003) using the $^{14}\mathrm{N}(^3\mathrm{He},d)^{15}\mathrm{O}$ reaction have led to consistent determinations of ANCs for this state. However, to determine the strength of the subthreshold state, the γ-ray decay strength also needs to be known. As a bound state, the lifetime is determined by the transition strength of the γ-ray decay. There have been several experimental studies that have tried to measure it (Bertone et al., 2001; Schürmann et al., 2008; Galinski et al., 2014; Sharma et al., 2020; Frentz et al., 2021).

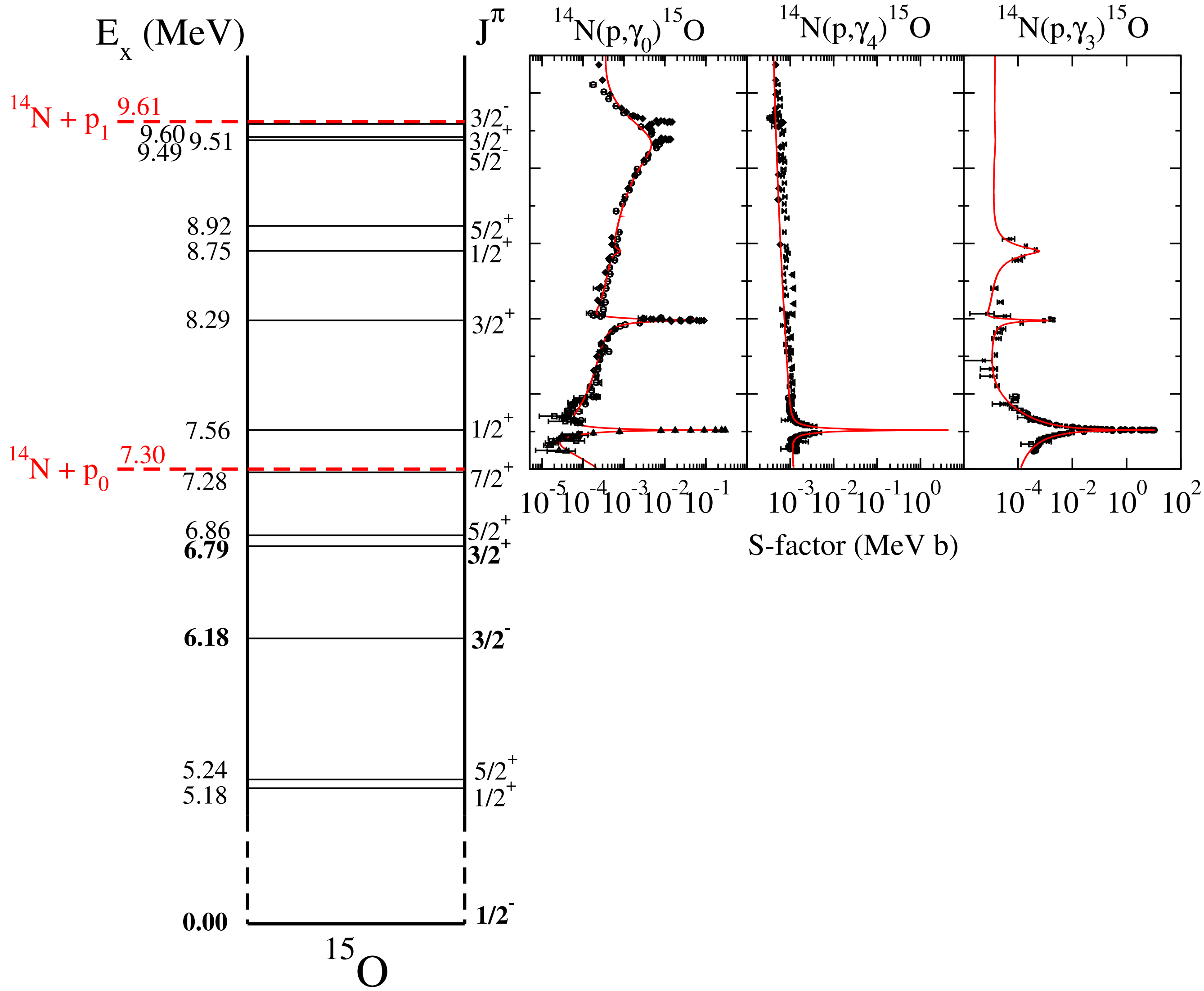

FIG. 19. Comparison between the R-matrix fit of deBoer *et al.* (2015) and the radiative capture data of Schröder *et al.* (1987), Runkle *et al.* (2005), Imbriani *et al.* (2005), Li *et al.* (2016), and Wagner *et al.* (2018) for the three strongest transitions in the $^{14}N(p,\gamma)^{15}O$ reaction.

The large acceptance angles of the detectors and uncertainties in the stopping powers typically limit lifetime measurements to femtoseconds. Because of the subfemtosecond lifetime of the ^{15}O subthreshold state, only upper limits have been reported.

6. $^{16}O(p,\gamma)^{17}F$

The $^{16}O(p,\gamma)^{17}F$ reaction has a low Q value ($Q = 600$ keV), suggesting that the additional proton is weakly bound to the ^{16}O core. The reaction cross section is dominated by direct capture to the $J^\pi = 5/2^+$ ground state and the $J^\pi = 1/2^+$ first excited state at 495 keV in ^{17}F, which was identified as a proton halo configuration in earlier work (Morlock *et al.*, 1997). Indeed, this $1/2^+$ subthreshold state can be identified as one of the threshold-aligned configurations on the basis of the pronounced single-particle configuration with an ANC $= 80.6(42)$ fm$^{-1/2}$ (Gagliardi *et al.*, 1999).

Figure 20 shows the level scheme and the associated R-matrix fit of the differential S factor of the two dominant γ-ray transitions feeding the two bound levels based on the elastic scattering (Amirikas, Jamieson, and Dooley, 1993; Morlock *et al.*, 1997) and radiative capture data (Chow, Griffiths, and Hall, 1975; Morlock *et al.*, 1997). The transition to the first excited state is characterized by a gradual enhancement in S factor that is similar to that observed in the $^7Be(p,\gamma)^8B$ reaction; see Sec. V.A.4. The uncertainty in the low-energy S factor was also recently investigated by Iliadis, Palanivelrajan, and de Souza (2022), who used the Bayesian methods described in Sec. III.A.2 but with a potential model instead of an R matrix.

7. $^{18}O(p,\gamma)^{19}F$ and $^{18}O(p,\alpha)^{15}O$

Proton capture on ^{18}O is a well studied process forming the compound nucleus at fairly high proton- and α-unbound excitation energies. As the $^{18}O(p,\alpha)^{19}F$ and the competing

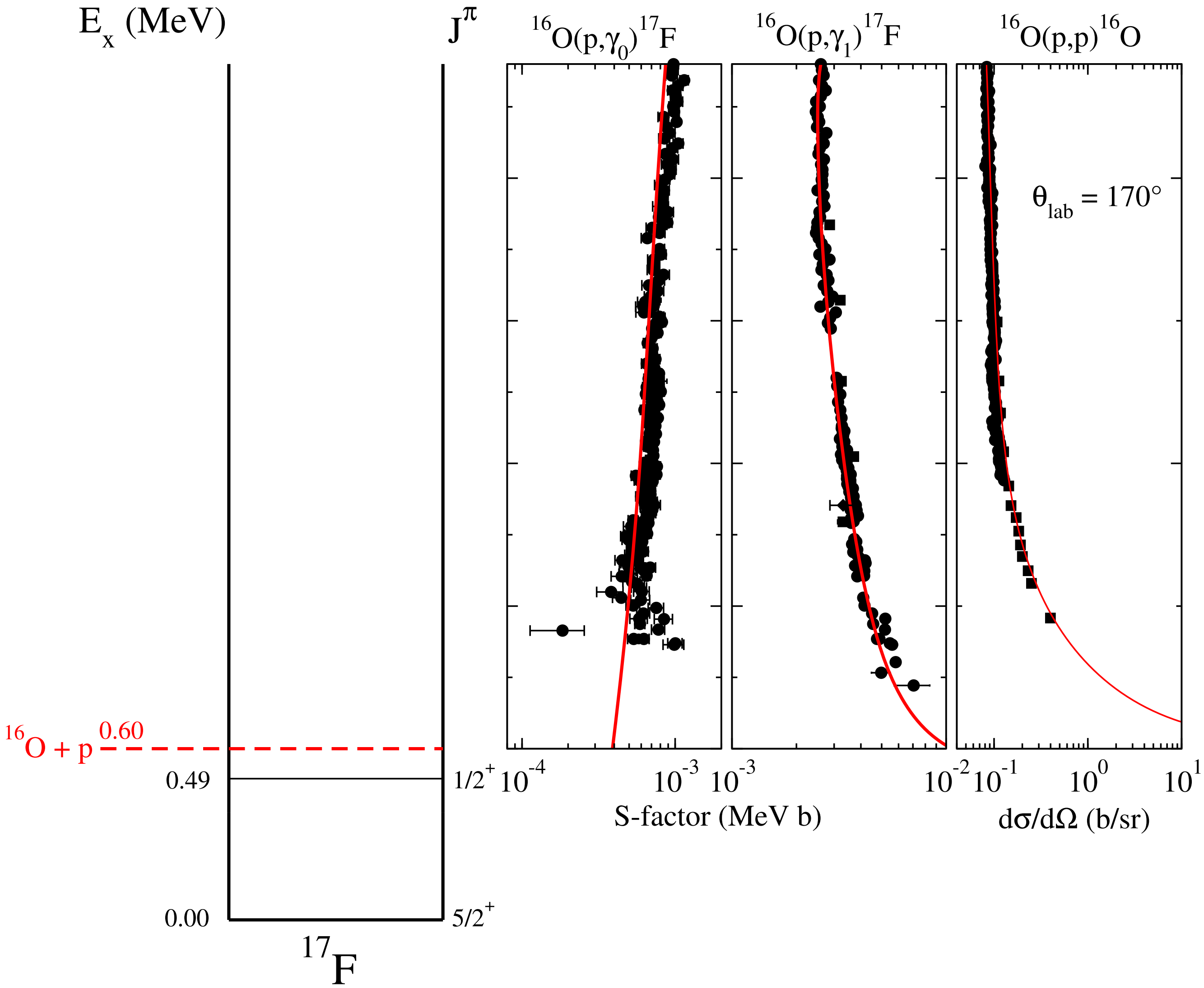

FIG. 20. Level diagram of the ^{17}F system up to an excitation energy of 3 MeV. Because of the lack of levels at low energy, the $^{16}O(p,\gamma)^{17}F$ reaction is completely dominated by direct capture that is shown as a red line based on an R-matrix calculation. The radiative capture data of Chow, Griffiths, and Hall (1975), Becker *et al.* (1982), and Morlock *et al.* (1997) and the scattering data of Amirikas, Jamieson, and Dooley (1993) and Morlock *et al.* (1997) is shown for comparison.

$^{18}O(p,\gamma)^{19}F$ radiative capture reactions are open, they create a more complex CNO cyclic burning pattern for hydrogen burning environments in massive stars (Wiescher and Kettner, 1982; Wiescher, Görres, and Schatz, 1999). Experimental studies for both reaction channels suggest a strong $1/2^+$ single-particle resonance state at 0.142 MeV center-of-mass energy both in the α-particle channel (Kettner *et al.*, 1977; Bruno *et al.*, 2019) and in the radiative capture channel (Wiescher *et al.*, 1980; Pantaleo *et al.*, 2021). This was confirmed by independent studies using the THM approach (La Cognata, Spitaleri, and Mukhamedzhanov, 2010). Based on the given data for the respective resonance strength, the Γ_α channel is about 170 times larger than the radiative Γ_γ channel. The proton spectroscopic factor has been determined to be ≈ 0.1 from single-particle transfer and direct capture measurements. The partial widths given by Wiescher *et al.* (1980), $\gamma_p = 0.17$ eV, $\gamma_\alpha = 220$ eV, and $\gamma_\gamma = 1.3$ eV, translate into a small α-particle spectroscopic factor of $\approx 2 \times 10^{-4}$, suggesting that this state in ^{19}F is one of the near-threshold configurations indicated in Fig. 8.

While the near-threshold resonances exhibit a large single-particle component, broad resonance structures at higher energies of more than 500 keV above the threshold suggest overlapping states with an appreciable α-particle width in both reaction channels, as shown in Fig. 21. This suggests the emergence of an α-cluster configuration in the ^{19}F compound nucleus at more than 8 MeV excitation energy. The exact nature of these states needs to be investigated (La Cognata *et al.*, 2008).

8. $^{20}Ne(p,\gamma)^{21}Na$

The $^{20}Ne(p,\gamma)^{21}Na$ reaction is another one of significance for our discussion of threshold phenomena since it refers to a pronounced subthreshold single-particle state located just below the proton threshold. It is one of the earliest examples

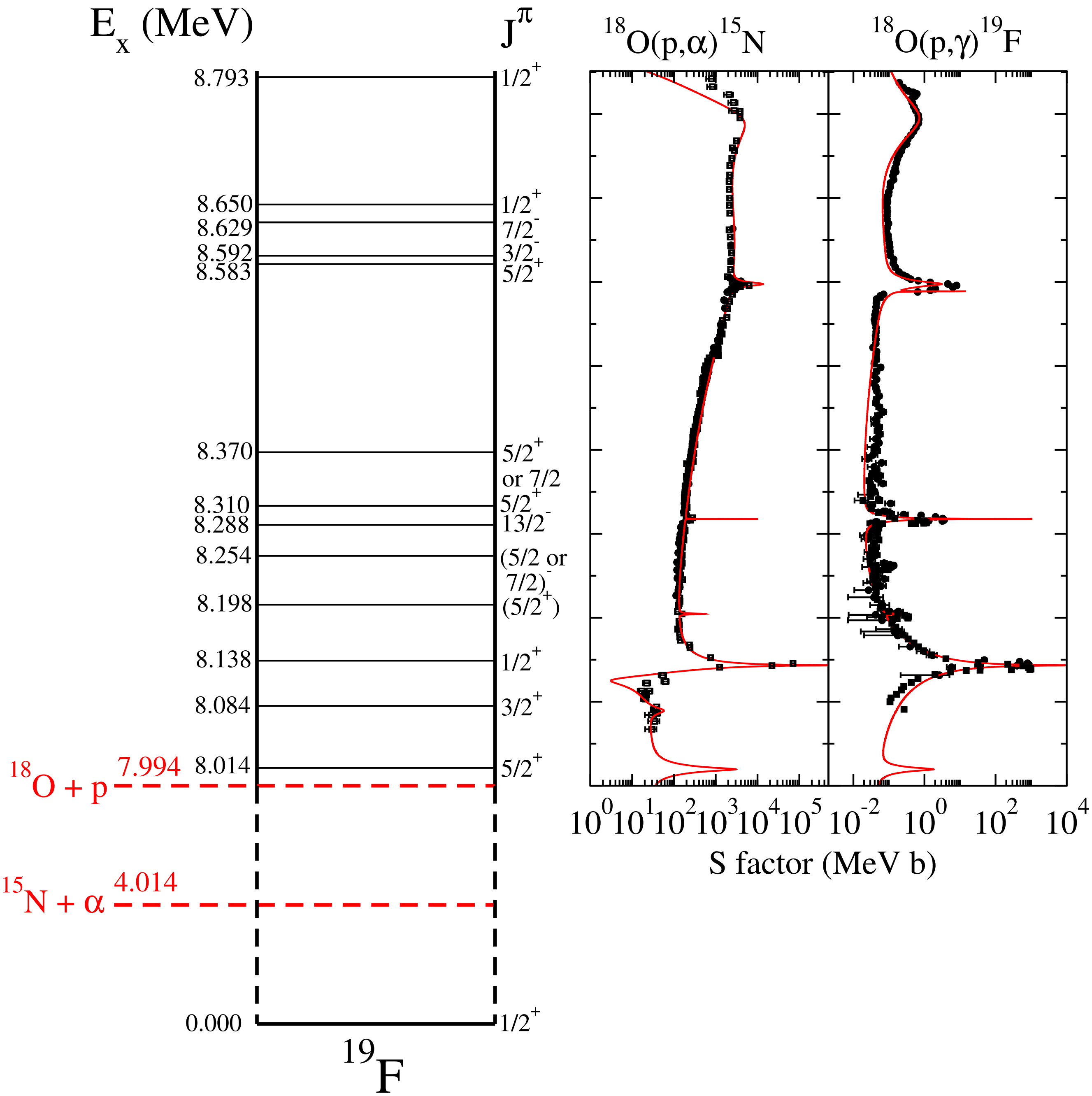

FIG. 21. Level diagram of the ^{19}F system compared with the S factors of the $^{18}O(p,\alpha)^{15}N$ (Lorenz-Wirzba, 1978; Mak et al., 1978) and $^{18}O(p,\gamma)^{19}F$ reactions (Wiescher et al., 1980; Pantaleo et al., 2021). For the radiative capture, the total radiative capture cross section obtained from an R-matrix fit of the individual primary γ-ray transitions is compared to the experimental data for the secondary γ-ray yield curve for the 197 keV excited state, which approximates the total radiative capture. The cross sections at lower energies are dominated by the impact of the near-threshold resonance at 142 keV. The contributions of the two lower resonance states have been analyzed through direct capture studies populating these levels (Wiescher and Kettner, 1982) and THM analysis (La Cognata, Spitaleri, and Mukhamedzhanov, 2010). The higher energy range is characterized by the contributions of a number of interfering resonances, which themselves are characterized by broad α-particle partial widths (La Cognata et al., 2008).

of a reaction where the high-energy tail of a subthreshold resonance has been clearly observed in the low-energy cross section (Rolfs et al., 1975; Lyons et al., 2018) and, more recently, confirmed in a deep-underground accelerator study (Masha et al., 2023). With its relatively low proton threshold of 2.432 MeV, the reaction rate is determined by several direct capture contributions as well as by the tail of a subthreshold resonance, as illustrated in Fig. 22.

This reaction is the slowest process in its NeNa nucleosynthesis cycle (Marion and Fowler, 1957) and therefore strongly impacts the energy production as well as the rate of nucleosynthesis for the entire cycle. The cycle may play a role

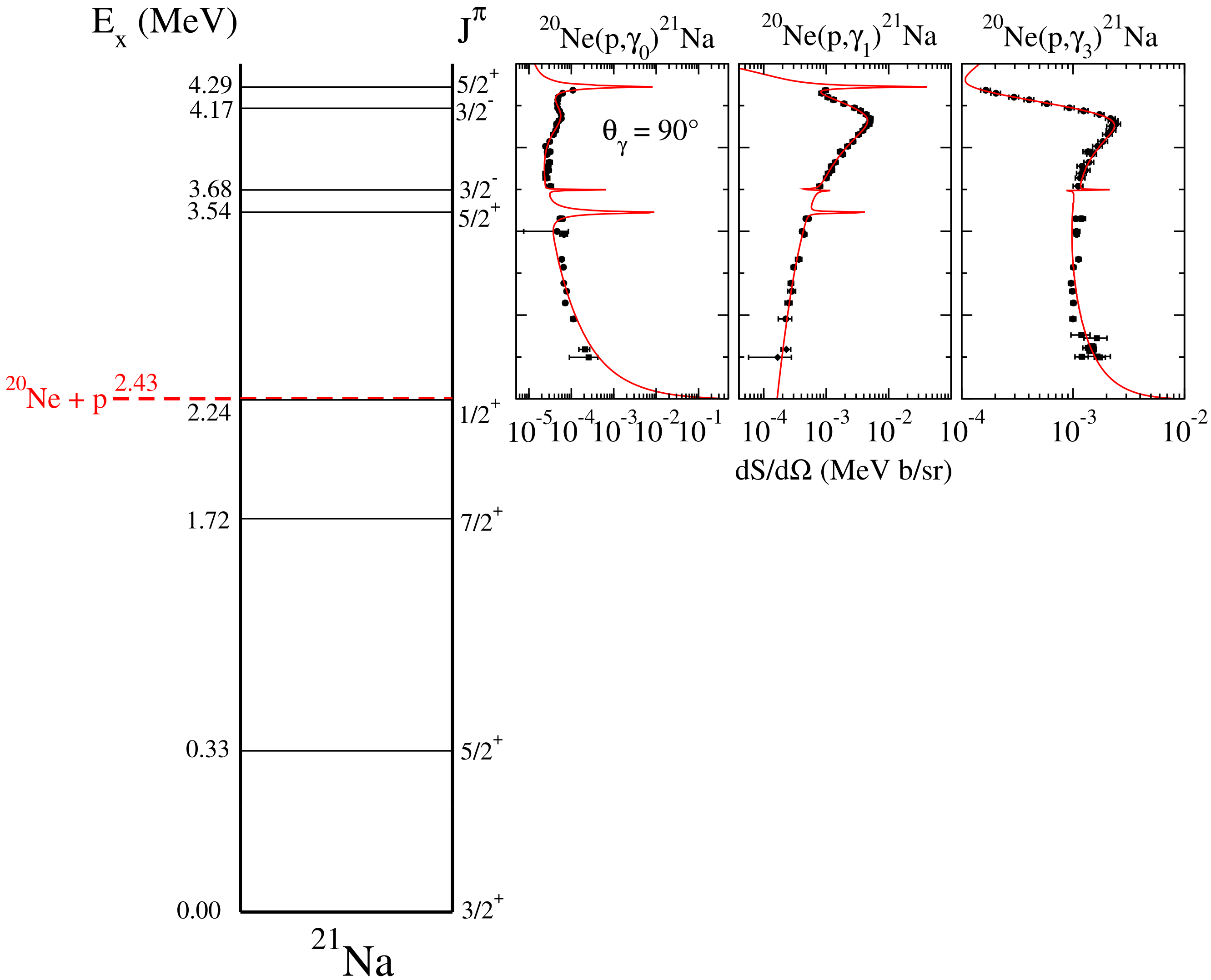

FIG. 22. Level diagram of the ^{21}Na system at low-energy compared to the ^{20}Ne$(p,\gamma)^{21}$Na data of Lyons *et al.* (2018) and Masha *et al.* (2023). Note that the angle integrated cross-section data (Masha *et al.*, 2023) have been scaled for comparison to the differential data (Lyons *et al.*, 2018).

in Ne-enriched hot environments such in carbon burning, where ^{20}Ne is produced as a main product of the ^{12}C$(^{12}$C$,\alpha)^{20}$Ne reaction and is processed further by proton capture, as further described in Sec. V.C. Since the ^{20}Ne$(p,\gamma)^{21}$Na reaction is important for determining the final abundance of ^{20}Ne in carbon burning, it affects another important scenario, Ne novas, which are driven by hydrogen accretion on oxygen-neon-magnesium white dwarf stars, the product of core carbon burning in medium-mass stars (Politano *et al.*, 1995; Starrfield *et al.*, 1997). Of particular interest is the possibility of the subsequent production of the long-lived ^{22}Na γ emitter (Fougères *et al.*, 2023), which would be a signature for Ne novas (Starrfield *et al.*, 1993; José, Coc, and Hernanz, 1999).

The formation of a full cycle depends, however, on the competition of the ^{23}Na$(p,\gamma)^{24}$Mg and ^{23}Na$(p,\alpha)^{20}$Ne reactions (Rowland *et al.*, 2004). A leak via the radiative capture reaction (Boeltzig *et al.*, 2019, 2022) would reduce the equilibrium abundance of ^{22}Ne in the Ne-Na cycle. Indeed, satellite-based γ-ray telescope missions like COMPTEL (Iyudin *et al.*, 2001) have found no evidence for ^{22}Na related activity, suggesting that the ^{20}Ne$(p,\gamma)^{21}$Na reaction might be smaller than anticipated or that the cycle may not be closed.

While the general trend of the ^{20}Ne$(p,\gamma)^{21}$Na low-energy cross section has been confirmed, measurements by Lyons *et al.* (2018) found substantial deviations from those reported by Rolfs *et al.* (1975) over the broad $J^\pi = 3/2^-$ resonance state at 4.170 MeV excitation energy. However, recent measurements toward threshold energies strongly support the claim of a subthreshold tail contributing to transitions to the ground state and the third excited state in ^{21}Na (Masha *et al.*, 2023). The latter state corresponds to the near-threshold $J^\pi = 1/2^+$ level at 2.425 MeV excitation energy.

The experimental data of Lyons *et al.* (2018) as well as the earlier data were reanalyzed using the R matrix in connection with Bayesian uncertainty analysis for a more reliable extrapolation into the low-energy range (Odell *et al.*, 2022). While the general fit presented by Lyons *et al.* (2018) was found to be robust, the treatment of the subthreshold state was not implemented correctly. The recommended values for the ANC obtained within the Bayesian framework are given in Table I; they are now found to be more consistent with those determined via transfer measurement (Mukhamedzhanov et al., 2006). The revised fit of the S factor and uncertainty bands are shown in Fig. 22. Compared to the extrapolated value of $S(0) = 3.5$ MeV b from Rolfs et al. (1975), the present analysis gives $S(0) = 5.0(7)$ MeV b, which highlights the difference resulting from systematic uncertainties in the different datasets.

B. Thermonuclear fusion reaction in stellar helium burning

Stellar helium burning is driven by the triple-α process: fusion of three α particles facilitated through the α-cluster configuration of the ^{8}Be ground state and the 7.65 MeV $J^{\pi} = 0_2^+$ state in ^{12}C, the Hoyle state, which is a prime example of an aligned-threshold α-cluster configuration (Freer et al., 2018), as indicated by the Ikeda diagram in Fig. 7.

While we do not discuss the three-particle-fusion mechanism in this review, we concentrate on the two subsequent α capture reactions $^{12}\mathrm{C}(\alpha,\gamma)^{16}\mathrm{O}$ and $^{16}\mathrm{O}(\alpha,\gamma)^{20}\mathrm{Ne}$, which determine the carbon/oxygen ratio in the Universe and also determine the high abundances of these two isotopes. We also later discuss the $^{10}\mathrm{B}(\alpha,d)^{12}\mathrm{C}$ reaction as an alternative path for producing ^{12}C in first stars. In addition, we discuss the $^{13}\mathrm{C}(\alpha,n)^{16}\mathrm{O}$ reaction since it is the dominant neutron source for the s process (Lugaro, Pignatari et al., 2023) and the i process (Clarkson, Herwig, and Pignatari, 2018; Denissenkov et al., 2019), which generate heavy elements in shell helium burning in different stellar environments.

1. $^{10}\mathrm{B}(\alpha,d)^{12}\mathrm{C}$

Before getting to the traditional mechanism of helium burning in massive red giant stars, we present a recently discussed threshold resonance phenomenon affecting the $^{10}\mathrm{B} + \alpha$ reactions (Liu et al., 2020; Gula et al., 2023). New low-energy studies of all three reaction channels $^{10}\mathrm{B}(\alpha,d)^{12}\mathrm{C}$, $^{10}\mathrm{B}(\alpha,n)^{13}\mathrm{N}$, and $^{10}\mathrm{B}(\alpha,p)^{13}\mathrm{C}$ suggest a strong increase in the S factor toward lower energies. While further reaction studies are being planned to map the full resonance structure, this feature is presently being interpreted as the high-energy tail of a pronounced resonance cluster near the threshold. These low-energy resonances may facilitate a complementary reaction path to the triple-α process by converting helium to carbon and may play a role in first star nucleosynthesis environments (Wiescher et al., 2021).

The α-separation energy of the ^{14}N compound nucleus corresponds to a fairly high excitation of $E_x = 11.612$ MeV in the tightly bound system, the proton threshold is at 7.551 MeV, and the neutron threshold is at 10.553 MeV. At these high excitation energies, the deuteron threshold opens at 10.272 MeV, while excited-state proton channels are accessible at 10.640, 11.236, and 11.405 MeV, thus allowing for multiple reaction channels, as indicated in Fig. 23.

A cluster of five resonance states between 11.676 and 11.998 MeV may be the underlying cause of the low-energy S-factor enhancement. The levels at 11.676 and 11.741 MeV have a spin and parity assignment of $J^{\pi} = 1^-$ or 2^-, while the state at 11.761 MeV is labeled with a $J^{\pi} = 3^-$ or 4^- assignment and the level at 11.807 MeV with $J^{\pi} = 1^+$ or 2^-. With the ground-state spin of ^{10}B being $J^{\pi} = 3^+$ this suggests that it is a cluster of p-wave resonances populating the compound nucleus ^{14}N. The state at 11.807 MeV might also contribute as a d-wave resonance in the $^{10}\mathrm{B} + \alpha$ reaction. However, these spin-parity assignments do not fit the observed increase because of their higher orbital-momentum value, as discussed by Gula et al. (2023), who found that a much improved deception of the experimental data could be obtained if the 11.807 MeV state's spin-parity was changed to 3^+ and an additional 3^+ state was added at 11.998 MeV, as shown in Fig. 23. In addition, Fig. 23 indicates approximate upper limits for the low-energy cross sections when the three lowest energy states are given α-particle widths equal to the Wigner limit.

The full complexity of the ^{14}N compound system at high excitation remains unresolved and requires additional measurements. Complementary structure information can be obtained from studies of $^{12}\mathrm{C} + d$ reaction channels populating this energy range in ^{14}N to probe for broad resonances. Some especially relevant previous measurements are those of $^{12}\mathrm{C}(d,d)$ and $^{12}\mathrm{C}(d,p)$ by McEllistrem et al. (1956) and Kashy, Perry, and Risser (1960). The results suggest a strong clustering of levels between the deuteron and α threshold around 11.3 and 11.4 MeV excitation energies, but Kashy, Perry, and Risser (1960) also demonstrated the importance of the 11.807 MeV as 1^+ state. The latter is confirmed in subsequent $^{12}\mathrm{C}(d,p\gamma)^{13}\mathrm{C}$ measurements by Tryti, Holtebekk, and Rekstad (1973) and Tryti, Holtebekk, and Ugletveit (1975), whose excitation curves are characterized by a strong broad resonance around 1.8 MeV deuteron energy, which is in the right range of corresponding excitation energy. However, preliminary R-matrix calculations over this region show that the observed structure is not reproduced by the levels reported in the literature, indicating that the level structure over this region has not been fully characterized. More detailed R-matrix analyses are presently underway to determine the complex multiple resonance features and contributions near the α threshold.

2. $^{12}\mathrm{C}(\alpha,\gamma)^{16}\mathrm{O}$

The $^{12}\mathrm{C}(\alpha,\gamma)^{16}\mathrm{O}$ reaction plays a particularly important role in nuclear astrophysics. The reaction converts the ^{12}C produced by the triple-α process in stellar helium burning to ^{16}O, with paramount importance for subsequent nucleosynthesis and stellar evolution (Fowler, 1983, 1984). The energy release of these two reactions stabilizes the core of a helium burning star against gravitational contraction, and the reaction rate of $^{12}\mathrm{C}(\alpha,\gamma)^{16}\mathrm{O}$ determines the carbon-to-oxygen ratio in the Universe through the subsequent phases of stellar burning. This is particularly important for the understanding of the composition of carbon-oxygen white dwarfs that develop after He burning in low-mass stars to an extent that it has been used to derive the reaction rate from observational astroseismology data on the carbon-oxygen abundance distribution of white dwarfs (Metcalfe, Salaris, and Winget,

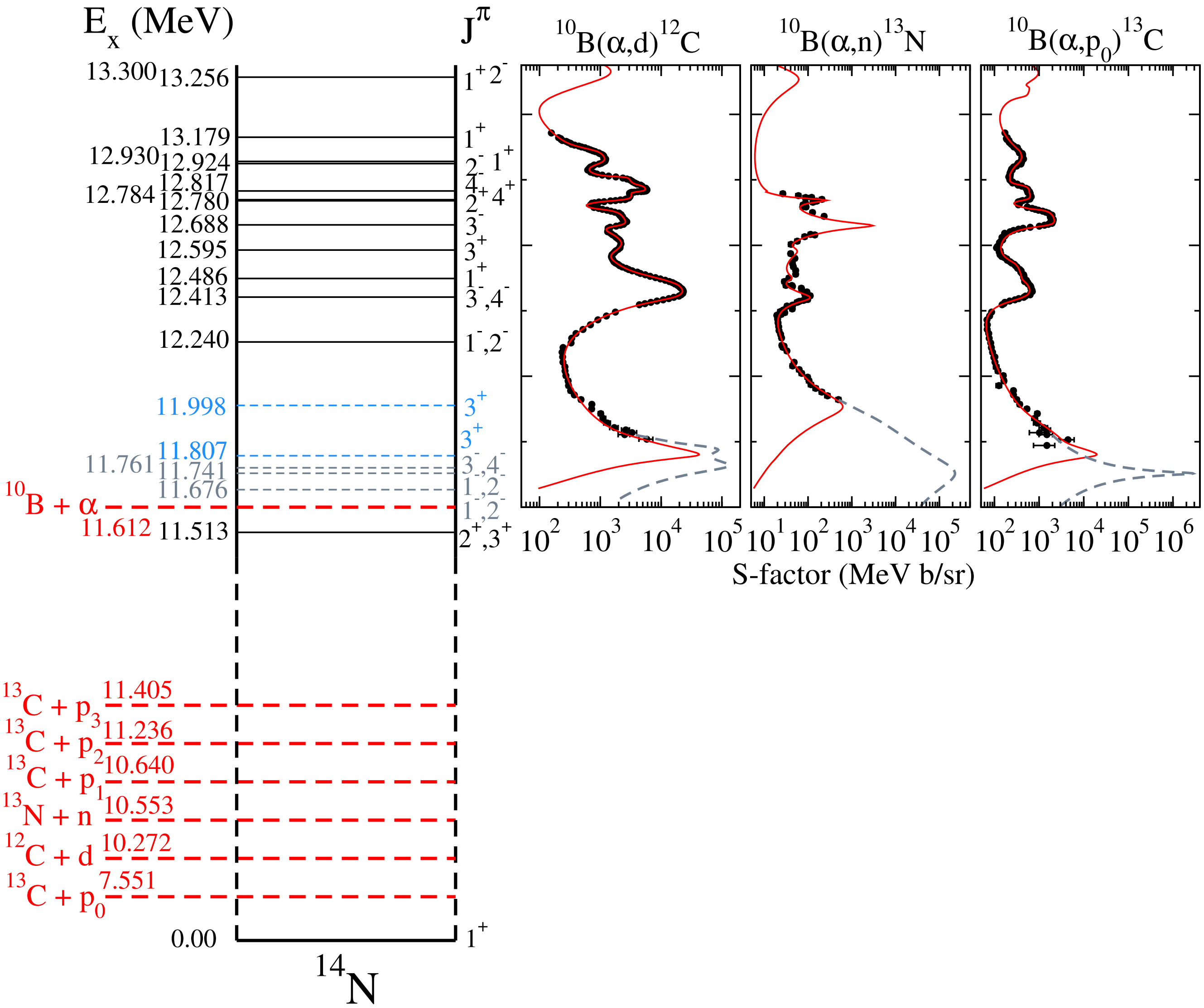

FIG. 23. Level diagram of the ^{14}N system over an approximately 2 MeV energy region above the α-particle separation energy, which is above several other open channels. The level structure is that adopted by Gula *et al.* (2023) for fits to ^{10}B + α data. The data of Liu *et al.* (2020) and Gula *et al.* (2023) are compared with the R-matrix extrapolation of the S factor from Gula *et al.* (2023) (the solid red lines). The observed increase in the low-energy S factors may be the result of strong resonances (possible upper limits indicated by the dashed gray lines). Candidate levels from the compilation (Ajzenberg-Selove, 1991) are indicated by dashed gray lines in the level diagram.

2002; Chidester, Timmes, and Farag, 2023). The rate also determines the nucleosynthesis of massive stars (Weaver and Woosley, 1993) and determines the ignition conditions of pair production supernovae and the boundaries of the second black-hole mass gap and in the Universe (Farmer *et al.*, 2020; Mehta *et al.*, 2022; Y. Shen *et al.*, 2023).

The low-energy S factor is characterized by strong interference effects between bound and unbound states, with 1^- and 2^+ states (see Fig. 24) determining the $E1$ and $E2$ multipolarity components as well as the $E2$ direct capture in the dominant ground state γ-ray transition as understood through several targeted studies of this reaction (Jaszczak, Gibbons, and Macklin, 1970; Jaszczak and Macklin, 1970; Dyer and Barnes, 1974; Kettner *et al.*, 1982; Redder *et al.*, 1987; Kremer *et al.*, 1988; Ouellet *et al.*, 1992; Roters *et al.*, 1999; Gialanella *et al.*, 2001; Heger, Langanke *et al.*, 2001; Heger, Woosley *et al.*, 2001; Kunz *et al.*, 2001; Fey, 2004; Assunção *et al.*, 2006; Makii *et al.*, 2009; Plag *et al.*, 2012; Hebborn *et al.*, 2022). The phenomenological R-matrix technique has played an important role in the analysis of this reaction over the years, particularly in the extrapolation of direct and indirect experimental data toward the stellar energy range (Buchmann and Barnes, 2006; Descouvemont and Baye, 2010; deBoer *et al.*, 2017), as more precise low-energy nuclear data have led to the use of a more rigorous model over polynomial and Breit-Wigner functions. In particular, one of its earliest measurements by Dyer and Barnes (1974) utilized the R-matrix technique, while a hybrid R-matrix–potential model was used by Koonin, Tombrello, and Fox (1974). The ^{12}C$(\alpha,\gamma)^{16}$O reaction therefore provides a good example for illustrating the R-matrix technique and the challenges of extrapolating its cross section to near-threshold energies,

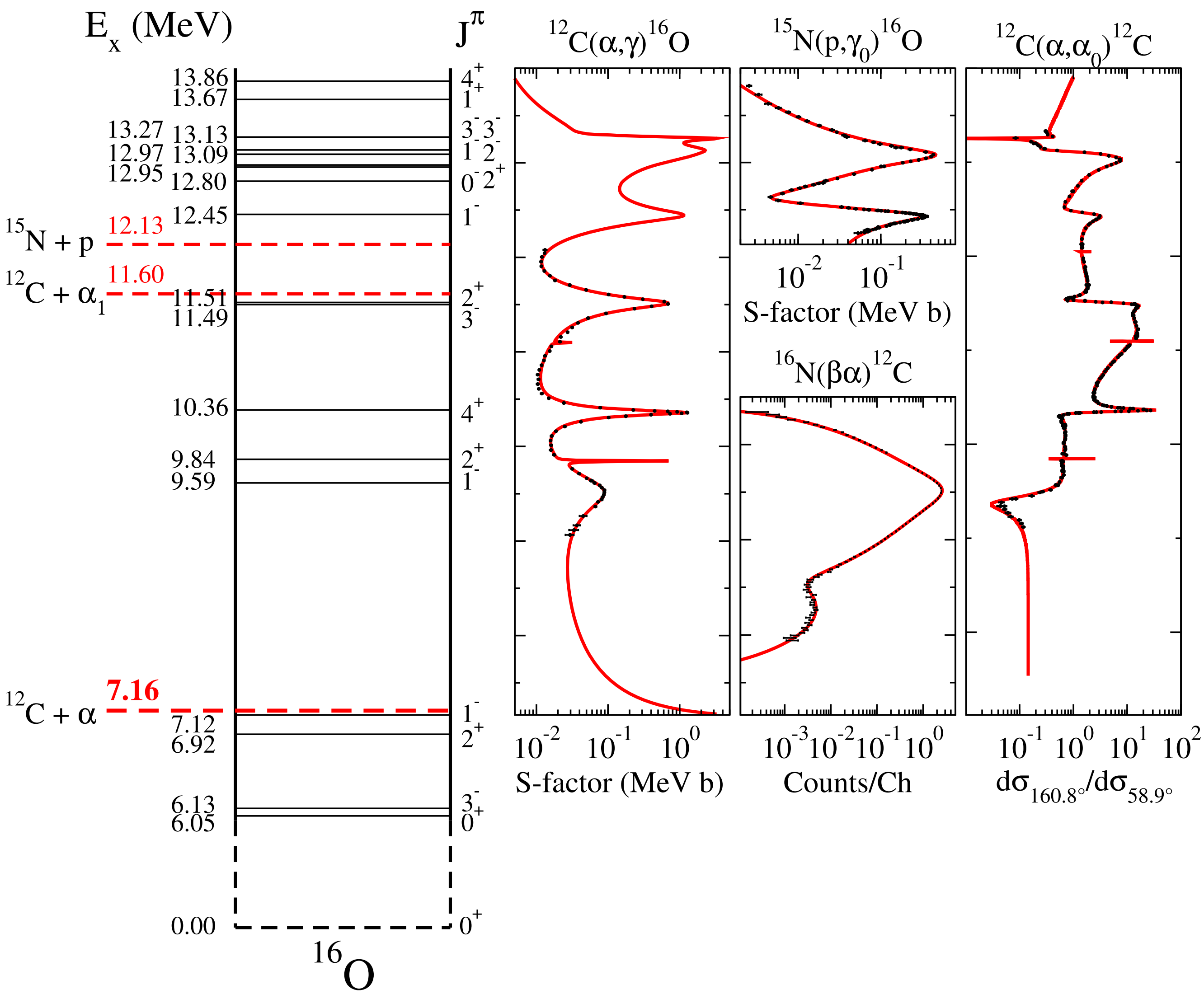

FIG. 24. Level structure of the ^{16}O system. Data for the reactions $^{12}C(\alpha,\gamma)^{16}O$ (Schürmann et al., 2005), $^{15}N(p,\gamma_0)^{16}O$ (Leblanc et al., 2010), the α-particle energy spectrum for $^{16}N(\beta\alpha)^{12}C$ (Buchmann et al., 1993), and the α-scattering yield ratios (Tischhauser et al., 2002) are compared with an R-matrix fit, as a function of excitation energy, to illustrate the correspondence between the unbound levels and resonances. Adapted from deBoer et al., 2017.

which was discussed in a lengthy review by deBoer et al. (2017).

Because of inconsistent direct measurements, current extrapolations of the $^{12}C(\alpha,\gamma)^{16}O$ cross section rely heavily on the ANCs of the bound states of ^{16}O. Thus, this aspect of threshold physics is of particular importance for this reaction. While it seemed that ANC determinations, especially for the 1^- and 2^+ subthreshold states, were becoming consistent at the time of deBoer et al. (2017), recent works have brought this more into question (Shen et al., 2019; Mukhamedzhanov et al., 2023; Hebborn et al., 2024) and for different reasons. Shen et al. (2019) noted a seeming inconsistency between their new determination of the ground-state ANC and that of the 2^+ subthreshold state that leads to a 20% increase in the extrapolation of the low-energy S factor. On the theory side, new first-principles calculations of the ANC of ^{6}Li by Hebborn et al. (2024) indicate a reduction of 20%. Finally, a new method of extracting ANCs from scattering data by Mukhamedzhanov et al. (2023) indicated an increase of 20%. Thus, it seems that previous estimates of the model uncertainties of these ANCs may have been underestimated. Some examples of differences in ANCs obtained from R-matrix fits of direct data versus those obtained from transfer reactions for ^{16}O are given in Table I.

3. $^{13}C(\alpha,n)^{16}O$

Like the $^{12}C(\alpha,\gamma)^{16}O$ reaction, the low-energy cross section of the $^{13}C(\alpha,n)^{16}O$ reaction is enhanced by a near-threshold resonance and the energy region of astrophysical interest lies in the valley between this and a broad resonance at higher energies, as shown in Fig. 25. This reaction is one of the main neutron sources for the s process in AGB stars (Bisterzo et al., 2015; Lugaro, Pignatari et al., 2023) and the i process in carbon enhanced metal-poor stars (Clarkson, Herwig, and Pignatari, 2018). The presence of the near-threshold state was

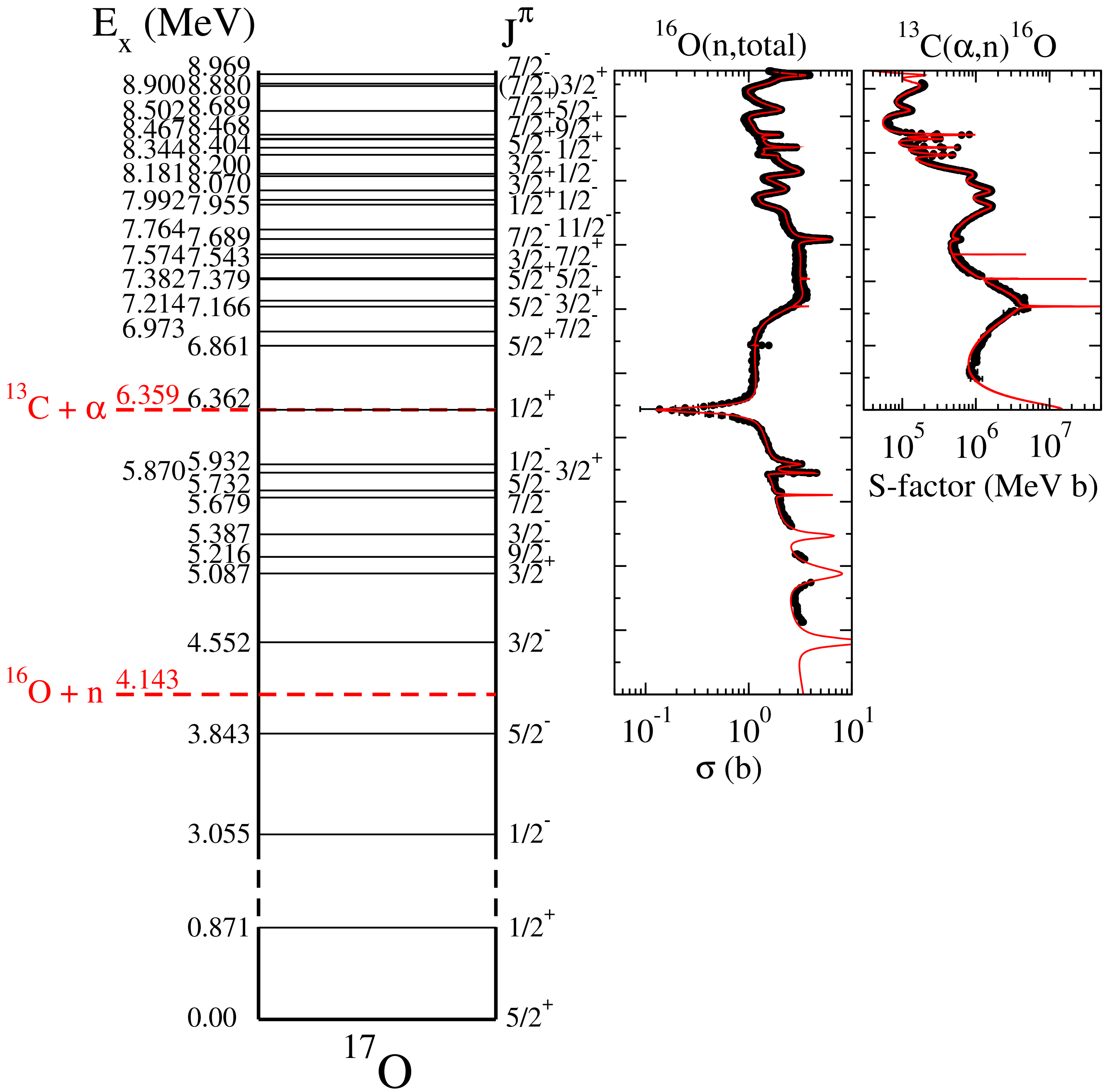

FIG. 25. Level diagram for the ^{17}O system. Representative experimental data for the $n + {}^{16}$O total cross section (Fowler, Johnson, and Feezel, 1973; Cierjacks et al., 1980) and the ^{13}C$(\alpha, n)^{16}$O S factors are shown for comparison (Bair and Haas, 1973; Gao et al., 2022).

first suggested by Descouvemont (1987), and subsequent indirect studies (Pellegriti et al., 2008; Guo et al., 2012; La Cognata et al., 2012, 2013; Avila et al., 2015b; Mezhevych et al., 2017; Trippella and La Cognata, 2017) confirmed its α-cluster nature [spectroscopic factor of ≈ 0.4 (Avila et al., 2015b)]. These studies put stringent constraints on the resonance's α-particle strength, although the accuracy of some of these measurements has been brought into question (Hebborn et al., 2024), while its (neutron) width is known from total neutron cross-section (Fowler, Johnson, and Feezel, 1973; Cierjacks et al., 1980) and transfer studies (Faestermann et al., 2015). Yet, despite the efforts of several low-energy measurements (Davids, 1968; Bair and Haas, 1973; Ramström and Wiedling, 1976, 1977; Kellogg, Vogelaar, and Kavanagh, 1989; Drotleff et al., 1993; Harissopulos et al., 2005; Heil et al., 2008; Ciani et al., 2021), the high-energy tail of the near-threshold resonance has only recently been observed directly by low-background underground measurements (Ciani et al., 2021; Gao et al., 2022). However, the interpretation of these direct measurements are now made more challenging because they have reached so low in energy that electron screening becomes significant, which is one reason why this reaction has also been investigated using the Trojan horse method (Mukhamedzhanov, Shubhchintak, and Bertulani, 2017; Trippella and La Cognata, 2017). Combining these experimental results has led to a significant decrease in the uncertainty in the extrapolated S factor (Ciani et al., 2021; Gao et al., 2022; deBoer et al., 2024), but a precise reevaluation is still underway.

Because of its role in neutron-induced astrophysical reaction processes, the $^{16}O + n$ reactions have also received a great deal of experimental attention as a strong neutron poison in s-process environments. These measurements, combined with an R-matrix analysis (Hale and Paris, 2017), constitute the low-energy portion of the ENDF/B nuclear data evaluation (Brown et al., 2018). This R-matrix analysis elucidates the underlying complexity of the different resonance contributions that make up both the total neutron and the $^{13}C(\alpha, n)^{16}O$ cross sections. While the near-threshold state in the $^{13}C(\alpha, n)^{16}O$ reaction and a higher energy broad resonance constitute the majority of the low-energy cross section, other, weaker resonances may also contribute at the level of the experimental uncertainties, especially now that those uncertainties have been reduced in recent measurements (Ciani et al., 2021; Gao et al., 2022; deBoer et al., 2024). These different resonance contributions can be more easily distinguished through differential cross-section measurements, but only one such low-energy measurement had been made (Walton, Clement, and Boreli, 1957) until recently (deBoer et al., 2024).

4. $^{16}O(\alpha,\gamma)^{20}Ne$

Helium burning stalls at the $^{16}O(\alpha, \gamma)^{20}Ne$ reaction. This seemingly does not meet the suggestion made in the Ikeda diagram shown in Fig. 7 that there should be a near-threshold state. In fact, ^{20}Ne still exhibits this characteristic, except that the threshold state happens to be of unnatural parity ($J^\pi = 2^-$ at $E_x = 4.97$ MeV and $S_\alpha = 4.73$ MeV), and its population is strongly suppressed by parity selection rules for $\alpha + {}^{16}O$ reactions. Because of its proximity to the threshold (-480 keV), the second excited state of ^{20}Ne ($J^\pi = 4^+$) could potentially enhance the low-energy cross section as a subthreshold state, but its amplitude is too strongly suppressed by its entrance-channel angular momentum; see Fig. 26. Mohr (2005) made a comprehensive estimate of the different possible contributions to the near-threshold cross section. Heavy-ion reactions such as $^{10}B(^{14}N, \alpha)^{20}Ne$ (Dück et al., 1978) demonstrate that both of these states are populated by α emission, presumably from highly excited compound states in ^{24}Mg, as discussed in Sec. V.C. More studies are needed to quantify the correlated α structure of these two levels.

Because of its small low-energy cross section, measurements are sparse and challenging (Hahn et al., 1987; Kunz et al., 1997; Costantini et al., 2010; Hager et al., 2011, 2012). With no near-threshold resonance enhancement, the low-energy cross section is thought to be dominated by direct capture (Mohr, 2005), where the dominant deexcitation is through the first excited state. The R-matrix analysis indicated in Fig. 26 is that of Costantini et al. (2010), and only data for the first excited-state transition fit. The direct capture contribution was included using an external capture model where the first excited state was estimated to be $75(10)\%$ of the total. While this indicates an estimate of the low-energy uncertainty of $\approx 10\%$, this should be viewed as a rough estimate; α-particle ANCs for low-lying states in ^{20}Ne would be useful for a better understanding of the extrapolation uncertainty. At higher energies the cross section is dominated by two narrow resonances at laboratory α-particle energies of 1.116 and 1.317 MeV that correspond to levels in ^{20}Ne of $J^\pi = 3^-$ and 1^-, respectively. These resonances have been well characterized (Almqvist and Kuehner, 1964; Pearson and Spear, 1964; Van Der Leun, Sheppard, and Smulders, 1965; Toevs, 1971; MacArthur et al., 1980; Mao, Fortune, and Lacaze, 1996; Avila et al., 2014) but are too high in energy to have any significant contribution to the reaction rate at helium burning temperatures.

5. $^{22}Ne(\alpha,\gamma)^{26}Mg$ and $^{22}Ne(\alpha,n)^{25}Mg$

The $^{22}Ne(\alpha, n)^{25}Mg$ reaction has been identified as the main neutron source for the weak s process in the contracting helium burning core of a massive red giant star, causing an increase in density and temperature (Kaeppeler et al., 1994). The reaction is also expected to serve as neutron source for the weak s-process component in the subsequent carbon burning phase of the star (Pignatari et al., 2010). In addition, the reaction may contribute to the neutron production for the main s process during the helium flash in AGB stars (Bisterzo et al., 2015). The release of the neutrons requires higher temperatures because of the negative Q value of the $^{22}Ne(\alpha, n)^{25}Mg$ reaction, $Q = -0.478$ MeV. A fourth important but frequently neglected scenario in which the reaction could play an important role is the n process (Blake and Schramm, 1976; Pignatari et al., 2018). This process is expected to be triggered by the shock front of the type II core collapse supernova traversing and compressing the helium and carbon shell of the presupernova star, in the process generating the necessary release of a high neutron flux contributing to the neutron-induced nucleosynthesis pattern in a core collapse supernova environment.

The impact of this neutron source, however, depends critically on the strength of the competing $^{22}Ne(\alpha, \gamma)^{26}Mg$ radiative capture reaction. These two α-capture-induced reactions, $^{22}Ne(\alpha, \gamma)^{26}Mg$ and $^{22}Ne(\alpha, n)^{25}Mg$, are both dominated by a strong resonance at about 702 keV center-of-mass energy; see Fig. 27. The existence of this state at such high excitation energies of $E_x = 11.32$ MeV has been a puzzle since its first discovery (Wolke et al., 1989) and its subsequent confirmation in the (α, n) reaction channel. Because of the negative Q value of the $^{22}Ne(\alpha, n)^{25}Mg$ reaction, this state may have substantial consequences for the efficiency of the neutron source, depending on the overall strength of the $^{22}Ne(\alpha, \gamma)^{26}Mg$ channel (Kaeppeler et al., 1994). However, despite substantial efforts using direct and indirect methods for identifying additional low-energy resonances in the $^{22}Ne(\alpha, \gamma)^{26}Mg$ channel, a solution to the issue remains elusive (Talwar et al., 2016; Adsley et al., 2021).

The comparable strength in both reaction channels has been puzzling for decades, and its identity as a single-resonance level has been questioned (Koehler, 2002). High-resolution measurements of neutron capture (Massimi et al., 2012) and neutron transfer reactions (Y. Chen et al., 2021), however, confirmed the identity of the resonance as a single level with an extremely small neutron width that is comparable to the γ width of the state. Based on current experimental observations

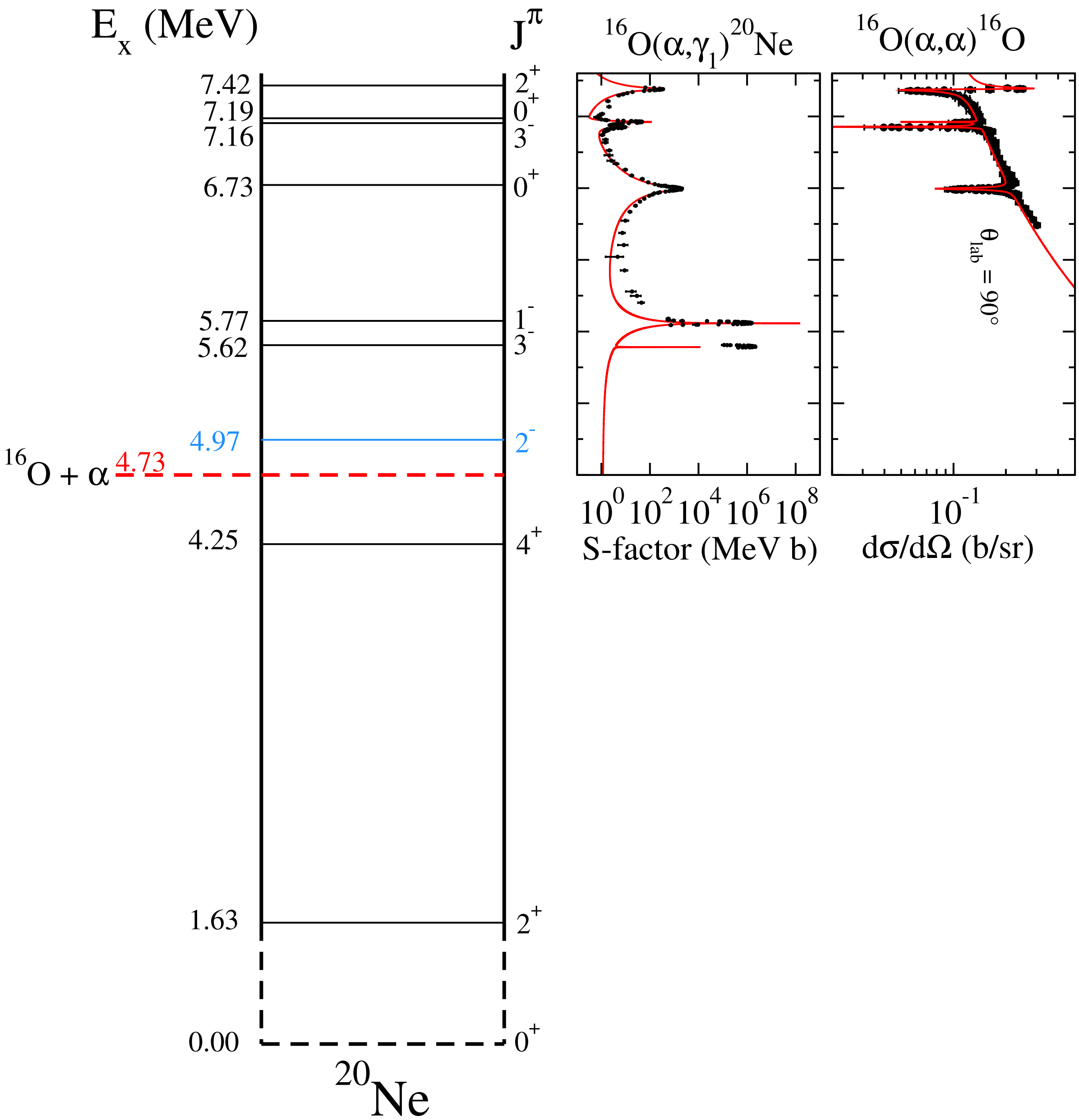

FIG. 26. Level diagram of the ^{20}Ne system with the S factor and differential cross sections of the $^{16}O(\alpha,\gamma)^{20}Ne$ reaction and $^{16}O(\alpha,\alpha)^{16}O$ elastic scattering, respectively. The experimental yield data and bare R-matrix extrapolations from Costantini *et al.* (2010) are shown. Note that the elevated yield compared to the R-matrix fit in the energy range above the strong resonances that corresponds to the 1^- level is attributed to the extended gas target. The two closest threshold states are 4^+, whose entrance-channel angular momentum suppresses its contribution as a subthreshold state and 2^- (unnatural parity), whose population is highly suppressed. In the absence of any kind of low-energy resonance enhancement, the radiative capture cross section is dominated by $E2$ direct capture.

(Shahina *et al.*, 2022; Shahina *et al.*, 2024), it seems that the 702 keV resonance dominates the rates of both channels (Wiescher, deBoer, and Görres, 2023). The observed strength of the resonance in both channels, however, characterizes this level as a pronounced α-cluster configuration, as expected for the near-threshold vicinity.

C. Clustering in nuclear molecules and its role in carbon burning

The study of light-ion (carbon-to-neon) fusion reactions emerged as an important research field in the 1950s as a side product of the nuclear test program associated with the development of the hydrogen bomb (Konopinski, Marvin, and Teller, 1946; Reynolds, Scott, and Zucker, 1953, 1956; Wyly and Zucker, 1953). The concern about possible atmospheric fusion processes (Wiescher and Langanke, 2024) has, however, triggered broader interest with the study of low-energy fusion reactions of carbon and oxygen isotopes, which showed a pronounced and rather unexpected resonance pattern that had not been observed in previous light-ion fusion studies (Reynolds, Scott, and Zucker, 1956; Almqvist, Bromley, and Kuehner, 1960). This behavior was also reflected in the elastic scattering channel (Bromley,

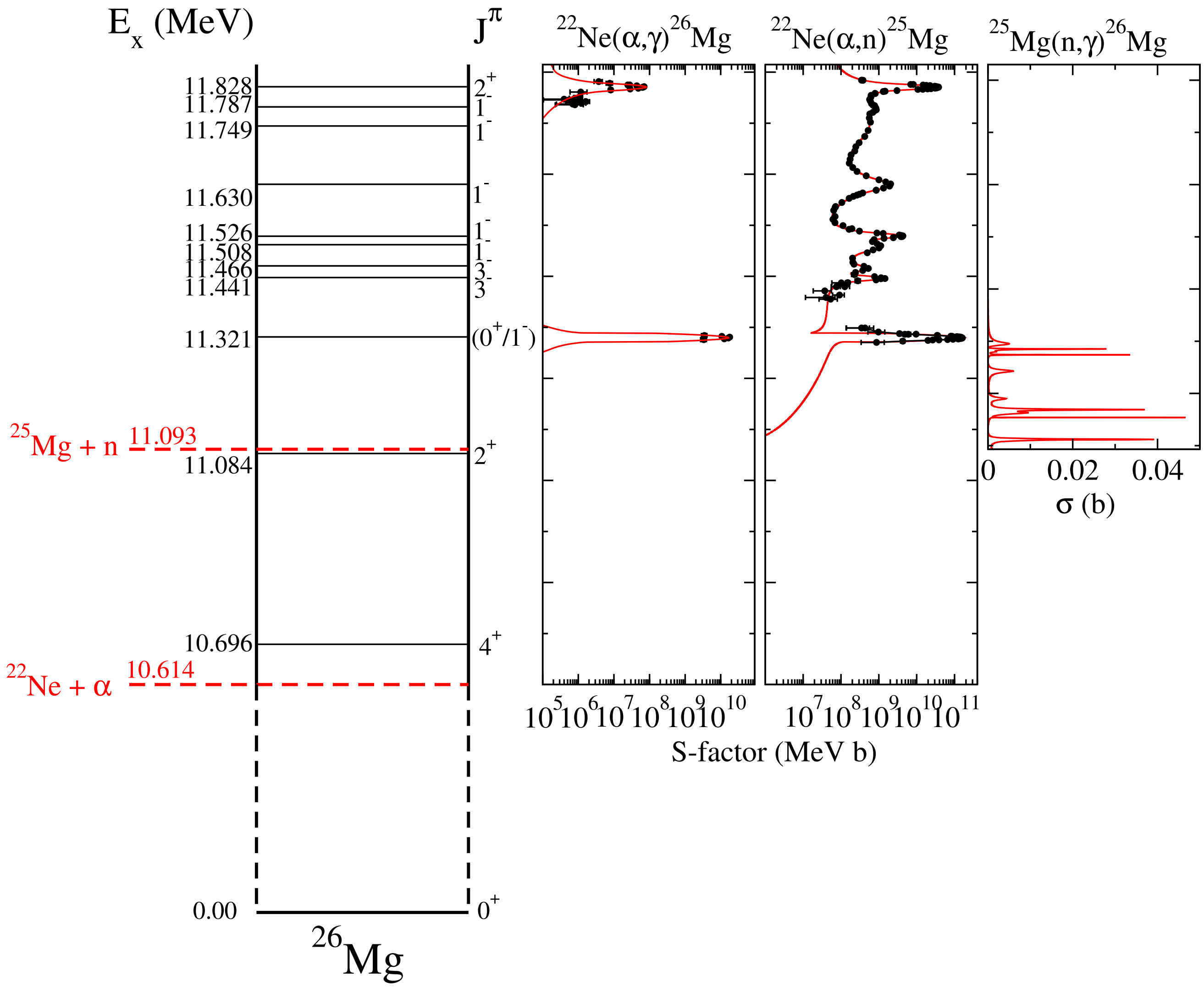

FIG. 27. Level diagram of the ^{26}Mg compound system relevant to the $^{22}Ne(\alpha,\gamma)^{26}Mg$ and $^{22}Ne(\alpha,n)^{25}Mg$ reactions, where the data from Jaeger *et al.* (2001) are shown for comparison. Also shown is an *R*-matrix calculation that reflects the known resonances in the $^{25}Mg(n,\gamma)^{26}Mg$ reaction (Massimi *et al.*, 2017). This reaction seems to be populated primarily by different states, and the measurements have been limited to low energies, thus making the correspondence of resonances populated through the $^{22}Ne + \alpha$ and $^{25}Mg + n$ reactions difficult.

Kuehner, and Almqvist, 1960). Initially, this phenomenon was discussed in the framework of a statistical model (Almqvist *et al.*, 1964; Shapira, Stokstad, and Bromley, 1974), but subsequent experiments (Patterson, Winkler, and Zaidins, 1969; Erb *et al.*, 1976; Becker *et al.*, 1981) suggested the existence of pronounced compound resonances, which were interpreted in terms of quasimolecular configurations near the $^{12}C + ^{12}C$ fusion threshold.

The interest in these fusion reactions was further amplified by their important roles in late-stage stellar evolution (Burbidge *et al.*, 1957; Reeves and Salpeter, 1959; Arnett and Truran, 1969) and the ignition of type Ia supernovae (Hoyle and Fowler, 1960; Arnett, 1969). A particularly interesting aspect was the interpretation of resonances in terms of near-threshold α-cluster configurations. Low-energy resonances may have been the reason for the observed enhancement in the low-energy cross section, a phenomenon initially called absorption below the barrier that was predicted to cause a significant enhancement in the fusion rate (Michaud and Vogt, 1972; Michaud, 1973). All this established the $^{12}C + ^{12}C$ fusion reaction as a unique phenomenon, triggering intense research efforts for at least a decade, as outlined in Sec. V.C.1.

1. Resonances below the barrier

The observed resonant structure in $^{12}C + ^{12}C$ elastic scattering (Almqvist, Bromley, and Kuehner, 1960; Bromley, Kuehner, and Almqvist, 1961; Kievsky *et al.*, 2008) and in the fusion cross sections is often prescribed to molecular states in these systems (Imanishi, 1968; Fink, Scheid, and Greiner, 1972; Park, Greiner, and Scheid, 1977). In contrast, these pronounced resonant structures are not observed in systems involving other carbon isotopes (Dasmahapatra, Čujec, and Lahlou, 1982; Trentalange *et al.*, 1988; Dasmahapatra and Čujec, 1993). This was initially interpreted as evidence that absorption plays a crucial role for the scattering and fusion processes (Esbensen et al., 1978). It was argued that absorption, i.e., coupling to other degrees of freedom, was particularly low for the fusion of inert nuclei like ^{12}C (or ^{16}O) (Mather et al., 1969), such that molecular states survived in the cross sections, while they are washed out in other systems by larger absorptive effects. This argumentation led to the introduction of imaginary parts in the optical potentials, which explicitly depended on a level density that was interpreted as a strength indicator of absorption (Helling, Scheid, and Greiner, 1971; Konnecke, 1982). The effect is further strengthened in systems of identical bosons like $^{12}\mathrm{C} + {}^{12}\mathrm{C}$ where molecular states can exist only for positive parities.

Note that the situation is similar to the anomalously large angle scattering (ALAS) effect in elastic α scattering on calcium isotopes where the cross sections at backward angles show a strong increase for ^{40}Ca that is much weaker or wholly not present for the other calcium isotopes (Gaul et al., 1969; Stock et al., 1972). The ALAS effect has been related to the appearance of α molecules (Friedrich and Langanke, 1975; Sünkel, 1976; Langanke and Frekers, 1978; Michel, Reidemeister, and Ohkubo, 1986; Delion and Suhonen, 2001), which were, however, visible only in the data due to the significantly smaller absorptive effects for ^{40}Ca compared to the other isotopes (Paneta et al., 1979; Langanke, 1982). These α-^{40}Ca molecules have been identified in elastic scattering and the parity dependence of their width has also been explained by absorptive effects caused by the parity dependence of the level density at low excitation energies (Frekers, Santo, and Langanke, 1983).

There have been attempts to identify the molecular nature of $^{12}\mathrm{C} + {}^{12}\mathrm{C}$ resonances by measuring the intraband γ transitions, which should be enhanced due to the collectivity of the states. Experiments that measured over the resonances above the Coulomb barrier could only determine upper limits (McGrath et al., 1981; Metag et al., 1982), while an experiment performed for the transition between two resonances close to barrier energies detected an enhanced $E2$ transition strength that was consistent with the molecular picture (Haas et al., 1997). In the argument that absorption is a crucial player for the observation of molecular states, it is envisioned that these states serve as doorways to more complicated configurations in the compound nucleus. This has been tested and confirmed in detailed investigations of the $^{16}\mathrm{O} + {}^{16}\mathrm{O}$ system at energies around the barrier that give clear evidence for a hierarchy of finer structures superimposed on top of broad resonances (Gaul and Bickel, 1986).

Potential models, with the inclusion of phenomenological imaginary potentials to account for absorption, were successful in describing elastic scattering data for various systems of carbon (and other medium-mass) isotopes (Canto and Hussein, 2013). However, when these models were applied to sub-barrier fusion, they noticeably underestimated measured cross sections. This became known as fusion enhancement. It became clear that inelastic excitations of the fragment nuclei were key to this enhancement (Esbensen, Tang, and Jiang, 2011). As elastic scattering was mainly proposed as a peripheral process and hence could be described by global potentials, sub-barrier fusion was sensitive to the internal part of the wave functions where inelastic excitations, even if they correspond to closed channels, could have significant amplitudes and couplings to the fusing wave function. Thus, it was concluded that single-channel approaches to sub-barrier fusion (Baye and Pecher, 1982; Baye and Descouvemont, 1984) were insufficient and that nuclear models had to be extended to multichannel approaches taking at least a few inelastic excitations explicitly into account. Indeed, the inclusion of inelastic excitations does enhance the sub-barrier fusion cross sections while having little effect on elastic scattering (Ito, Sakuragi, and Hirabayashi, 1999; Assunção and Descouvemont, 2013; Taniguchi and Kimura, 2021; Gasques, Chamon, and Cessel, 2022). However, in general, these models are not accurate enough to predict the sub-barrier fusion cross sections at astrophysically relevant energies. This is particularly true if the fusion cross section exhibits resonant structures such that their positions and strengths have to be experimentally determined.

We note that resonances also required a dedicated treatment to include electron screening effects (Salpeter and van Horn, 1969; Iliadis, 2023), which for the $^{12}\mathrm{C} + {}^{12}\mathrm{C}$ system is, however, relevant only at the degenerate conditions in white dwarf triggering type Ia supernovae (Cussons, Langanke, and Liolios, 2002; Gasques et al., 2005; Gasques, Brown et al., 2007; Chen et al., 2014). At these conditions, however, the density is so extreme that the enhancement of the reaction due to the screening effect will be overwhelmingly larger than the temperature-dependent modifications due to resonances, as further outlined in Sec. VI.A.3.

2. $^{12}\mathrm{C} + {}^{12}\mathrm{C}$ fusion cross section at stellar energies

The appearance of the pronounced resonant structures in the $^{12}\mathrm{C} + {}^{12}\mathrm{C}$ fusion cross sections, as well as the enhancement of the cross sections due to coupling to inelastic degrees of freedom, poses a serious challenge for deriving a reliable reaction rate. Therefore, predictions for hydrostatic carbon burning or for the onset of thermonuclear runaways in type Ia supernovae have carried a large uncertainty. Microscopic multichannel calculations have helped to illuminate the fusion mechanism but are not accurate enough to predict the resonant fusion cross sections in the astrophysical Gamow window (Bennett et al., 2012). Therefore, one usually relies on simple potential models or other parametrizations to extrapolate the cross sections to the stellar energy range (Caughlan and Fowler, 1988; Gasques et al., 2005).

A direct comparison of experimental fusion cross sections for the $^{12}\mathrm{C} + {}^{12}\mathrm{C}$ reaction reveals large deviations among the several available datasets, as illustrated in the upper panel of Fig. 28. Different techniques have been employed to measure the fusion excitation functions. While some experiments were designed for measuring charged particles with Si detectors (Patterson, Winkler, and Zaidins, 1969; Mazarakis and Stephens, 1973; Becker et al., 1981), others were based on detecting secondary γ rays from the evaporation residues (High and Čujec, 1977; Aguilera et al., 2006; Spillane et al., 2007). Most recently, using a more sophisticated technique, charged particles were measured in coincidence with γ rays (Jiang et al., 2018; Fruet et al., 2020; Tan et al., 2020, 2024).

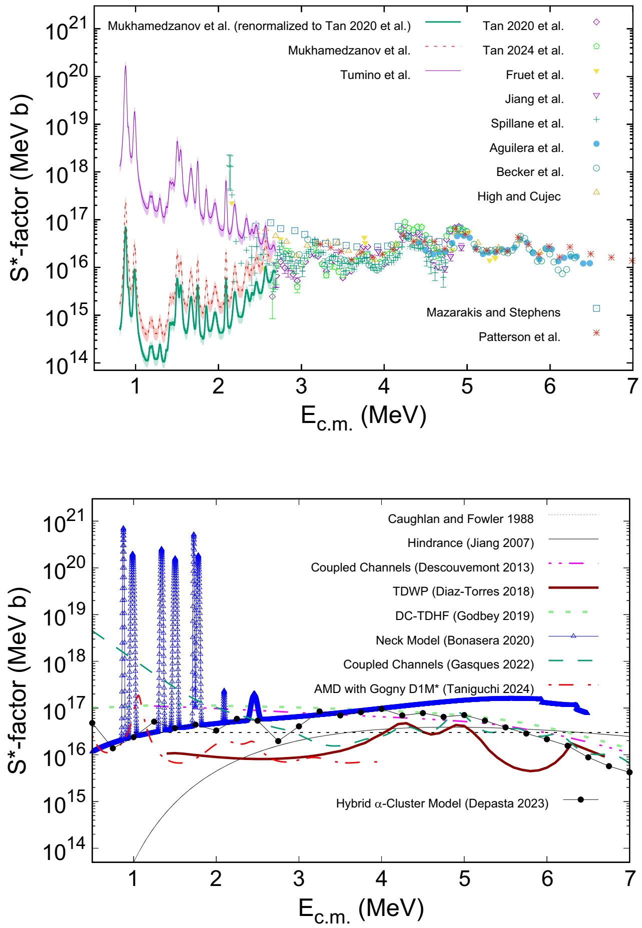

FIG. 28. Upper panel: direct (symbols) and indirect THM measurements (lines) of the modified astrophysical S factor for $^{12}C + ^{12}C$. Lower panel: model calculations of the S^* function. Large differences in model predictions exist at stellar energies (< 3 MeV), with most models describing the trend of observations at near-barrier energies (≈ 6 MeV) fairly well.

As mentioned, low-energy $^{12}C + ^{12}C$ fusion studies suggested a peculiar behavior in the S factor that seemed to increase toward lower energies (Mazarakis and Stephens, 1973), a pattern that was characterized as an absorption below the barrier phenomenon (Michaud, 1973). In-beam γ spectroscopy measurements obviated the suggested enhancement with fusion under the barrier (High and Čujec, 1977; Kettner et al., 1977; Kettner, Lorenz-Wirzba, and Rolfs, 1980) and seemed to necessitate a modification of the Coulomb transmission functions for the fusion process (Hussein, 1977). This was followed by extensive measurements of the different particle decay channels that provided more information about a possible compound resonant structure in the ^{24}Mg compound nucleus (Becker et al., 1981). Nevertheless, these observations led to the study of other fusion reactions such as $^{12}C + ^{16}O$ and $^{16}O + ^{16}O$ to search for similar phenomena associated with the ^{28}Si (Shapira et al., 1975; Stokstad et al., 1976; Christensen, Switkowskiw, and Dayras, 1977) and ^{32}S fusion compound nuclei (Stokstad et al., 1976; Hulke, Rolfs, and Trautvetter, 1980).

Interest in the role of near-threshold resonances was further amplified with the suggestion that the observation of superbursts, extended thermonuclear explosions in the crust of accreting neutron stars, are driven by the $^{12}C + ^{12}C$ reaction (Cumming and Bildsten, 2001; Strohmayer and Brown, 2002; Schatz, Bildsten, and Cumming, 2003; Cumming et al., 2006; Keek, Heger, and in 't Zand, 2012), namely, by a single resonance predicted in the lower, barely explored energy range (Cooper, Steiner, and Brown, 2009; Bravo et al., 2011). Renewed efforts were made to search for low-energy resonances, but the results were challenged by background contributions (Spillane et al., 2007; Morales-Gallegos et al., 2018; Zickefoose et al., 2018), while in other experimental efforts the resonance features were smeared out by thick-target effects, thus providing only averaged cross-section information for the observed reaction channels (Aguilera et al., 2006; Fruet et al., 2020; Morales-Gallegos et al., 2024). Correcting the averaged cross section for target thickness effects did reveal a more pronounced resonance structure over the lower energy range, as observed in multiple particle and γ-decay channels, confirming that the lower energy range was characterized by resonances (Tan et al., 2020, 2024).

3. Hindrance below the barrier

Difficulties regarding the reliable prediction for the low-energy extrapolation of $^{12}C + ^{12}C$ and other light-ion fusion reactions were further complicated by the suggestion that the low-energy cross section might actually be reduced due to a hindrance term associated with the incompressibility of nuclear matter (Mişicu and Esbensen, 2006). Under this concept the hindrance was an effect anticipated for the case of the fusion of two more massive nuclei (Jiang et al., 2007), an idea that developed from detailed experimental evidence observed in the fusion processes of heavier isotopes (Jiang et al., 2005, 2006). More detailed studies with respect to the viability of the hindrance factor followed (Dasgupta et al., 2007; Back et al., 2014; Jiang et al., 2021). An alternative explanation for the observed sudden decrease in cross section toward very low energies in heavy-ion fusion systems is the deformation or clusterization of reaction partners (Back et al., 2014; Montagnoli and Stefanini, 2017; Godbey, Simenel, and Umar, 2019), although there is evidence that such an effect exists in medium-mass systems toward very low sub-Coulomb energies. However, the extent of the effect for light-ion fusion systems such as $^{12}C + ^{12}C$ and $^{16}O + ^{16}O$ has not yet been experimentally verified (Tan et al., 2020, 2024), because the critical energy range has not been reached by direct measurements. Beyond the phenomenological models, such as those summarized by Hagino and Takigawa (2012) and Jiang et al. (2021), the hindrance effect has not been fully confirmed theoretically, as demonstrated by the time-dependent Hartree-Fock approach (Godbey, Simenel, and Umar, 2019) and by a combination of mean-field and cluster models (Umar, Godbey, and Simenel, 2023). Better microscopic techniques are necessary for a full theoretical evaluation. This hindrance factor in $^{12}C + ^{12}C$ fusion is indeed predicted to have a significant impact on the low-energy extrapolation of the cross section, as a number of stellar model simulations have demonstrated (Gasques, Brown et al., 2007; Pignatari et al., 2013; Chieffi et al., 2021; Monpribat et al., 2022). In some cases, such as the lower mass bound for core collapse type II supernovae progenitors (M*), these predictions are difficult to reconcile with astrophysical observations (Gasques, Brown et al., 2007). However, while it might reduce the overall transmission probability through the Coulomb barrier, it cannot be considered alone but instead needs to be considered in the context of possible low-energy resonances. Owing to the extremely and rapidly declining cross section, it seems unlikely that the direct experimental approach will reach these low energies in the near future, despite new efforts by the experimental community (Aliotta et al., 2022; Morales-Gallegos et al., 2023; Tan et al., 2024). However, interesting new results based on indirect reaction studies using the THM were presented that seem to provide the first look at the resonance pattern in the low-energy fusion range (Baur, 1986; Typel and Baur, 2003; Spitaleri et al., 2011; Tribble et al., 2014; Bertulani, Hussein, and Typel, 2018; Tumino et al., 2021).

4. Trojan horse method studies above the $^{12}C + ^{12}C$ threshold

The Trojan horse method has been successfully applied to study the low-energy contribution to the $^{12}C + ^{12}C$ fusion process (Tumino et al., 2018). The cross sections at astrophysical energies for the $\alpha_{0,1}$ and $p_{0,1}$ channels were determined from the measurement of the $^{12}C(^{14}N, \alpha^{20}Ne)^2H$ and $^{12}C(^{14}N, p^{23}Na)^2H$ three-body processes in quasifree kinematics with ^2H from ^{14}N spectator to the $^{12}C + ^{12}C$ reactions.

In the two-body reactions (α or p), the ejected particle was detected simultaneously with the spectator deuteron (d) particle using silicon telescopes positioned on both sides of the beam directions. These telescopes were strategically placed to cover angular regions optimized for the quasifree kinematics of the specific breakup process under investigation. Following the completion of various data analysis steps outlined by Tumino et al. (2018), the two-body cross section relevant to astrophysics was extracted for four specific channels: $^{20}Ne + \alpha_0$, $^{20}Ne + \alpha_1$, $^{23}Na + p_0$, and $^{23}Na + p_1$. A modified one-level many-channel R-matrix analysis taking into account the ^{24}Mg states as reported by Tumino et al. (2018) was conducted. Based on the findings presented by Becker et al. (1981) for energies up to $E \leq 3$ MeV and by closely monitoring the reduction of penetration factors associated with the relevant states, the modified R-matrix analysis neglected the contribution of α and p channels other than $\alpha_{0,1}$ and $p_{0,1}$ to the total fusion yield. The estimated errors for the α and p channels at center-of-mass energies E below 2 MeV were determined to be lower than 1% and 2%, respectively. The results suggested a sequence of pronounced resonance states. These resonance structures observed in the excitation functions align with the reported resonance energies for ^{24}Mg found in the literature (Abegg and Davis, 1991). Subsequently, the reduced widths obtained from the THM suggested a pronounced $^{12}C + ^{12}C$ α-cluster structure. Based on a subsequent R-matrix analysis, the $S(E)$ factor functions were obtained for the four reaction channels. THM results were normalized to the average of direct data over the energy range $E = 2.5$–2.63 MeV.

A theoretical Coulomb correction to the THM data, as described by Mukhamedzanov (2022), was proposed using a theory based on the DWBA without resonances. This reanalysis resulted in significantly lower values of the modified astrophysical S factor $S^*(E) = S(E)e^{(0.46E)}$, with differences of up to 4 orders of magnitude compared to previous findings. However, the convergence and numerical stability of calculations involving transfer to the continuum need to be critically examined so as not to incur results that are highly sensitive to the specifics of the model space. For instance, theoretical calculations utilizing the Feynman path-integral method produced S-factor values that exhibited agreement with the THM results (Bonasera and Natowitz, 2020).

A more recent paper by Taniguchi and Kimura (2024) based on the generator coordinate model that also takes into account the full coupling between the entrance and exit channels of the ^{24}Mg compound nucleus suggests the emergence of pronounced $^{12}C + ^{12}C$ molecular states, which are then fragmented into many narrower resonances—mostly 0^+ and 2^+ states—due to channel coupling. This agrees with the experimental spectrum of multiple states at low energies as suggested by the THM data. However, the application of the R-matrix formalism in deriving the cross sections yield results considerably below the values suggested by Tumino et al. (2018). This is not a final result, because the nonresonant contribution and possible interference effects have not been taken into account. In summary, the question about a reliable extrapolation is far from being solved. Knowledge about the nature of these states at low near-threshold energies, as well as possible interference effects, remains scarce. The upper panel of Fig. 28 shows an overall comparison of the modified S factor, S^*, from recent experiments. The S^* factor not only removes the exponential drop from tunneling through the repulsive Coulomb potential but also introduces a size-dependent correction factor for leveling the curve for easier extrapolation (Trentalange et al., 1988). It is defined as

$$S^* = \sigma E \exp(2\pi\eta + gE), \tag{23}$$

with $\eta = Z_1 Z_2 e/\hbar\nu$ the Sommerfeld parameter and $g = 1.22\sqrt{\mu R^3/Z_1 Z_2}$ the form factor for $^{12}C + ^{12}C$ collisions (Patterson, Winkler, and Zaidins, 1969). The constants $Z_{1,2}$ are the charges of the nuclei, while R and μ denote the square-well radius and the reduced mass of the system.

The current picture calls not only for additional experimental work to push direct measurements down the astrophysical energies but also for improved theoretical treatment in order to reconcile existing results and provide a reliable treatment that describes and models the observed phenomena. This is important not only for reactions such as $^{12}C + ^{12}C$ but also for the interpretation and treatment of other important fusion processes for stellar oxygen burning such as $^{12}C + ^{16}O$ and $^{16}O + ^{16}O$. In the following we provide a more detailed review of the different models that are presently being discussed for simulating sub-barrier fusion.

5. Models of $^{12}C + ^{12}C$ sub-barrier fusion

Several theoretical models have been used to study the probability of two colliding ^{12}C nuclei fusioning at energies well below the Coulomb barrier. For instance, the low-energy collision of heavy ions has been treated within a nuclear molecular picture (Fink, Scheid, and Greiner, 1972; Park, Greiner, and Scheid, 1977; Greiner, Park, and Scheid, 1995; Diaz-Torres, Gasques, and Wiescher, 2007), including the description of $^{12}C + ^{12}C$ fusion using different methods. The time-dependent wave-packet (TDWP) method directly solves the time-dependent Schrödinger equation with a multidimensional collective Hamiltonian, including the static quadrupole deformation and orientation of the ^{12}C nuclei (Diaz-Torres, 2008; Diaz-Torres and Wiescher, 2018). The equator-equator orientation of oblately deformed ^{12}C nuclei facilitates their capture in the corresponding potential pocket due to the lowest Coulomb barrier among all the orientations. This potential pocket supports doorway molecular states that feed the fusion process of the pole-pole dinuclear configuration (Diaz-Torres, 2008). In the TDWP model, the imaginary potential used to describe fusion for the pole-pole oriented dinuclear configuration is crucial for understanding the appearance of some molecular resonances in the fusion excitation function at energies near the Coulomb barrier (Diaz-Torres and Wiescher, 2018). The effects of compound-nucleus resonances on fusion cannot be included in this TDWP model, as it uses a strong, short-range imaginary potential to describe fusion. The latter only allows one to account for the average effect of the compound-nucleus resonances (Feshbach, Porter, and Weisskopf, 1954). The antisymmetrized molecular dynamics (AMD) approach combined with an R matrix has been successful in yielding some fusion resonances at stellar energies (Taniguchi and Kimura, 2021, 2024). In the AMD calculations, there is no short-range imaginary potential, but the compound-nucleus Hamiltonian is microscopically determined using different cluster configurations of ^{24}Mg. It is unclear how deformation, alignment, and multidimensional quantum tunneling of the ^{24}Mg clusters are rigorously addressed within a simple R-matrix model (Taniguchi and Kimura, 2021; Taniguchi and Kimura, 2024), which does not solve a coupled-channel tunneling problem for calculating the decay width of the compound-nucleus resonance. The AMD model has revealed a few fusion resonances at stellar energies, in agreement with the THM experiment (Tumino *et al.*, 2018). Some fusion resonances observed in the THM experiment are phenomenologically described within a classical neck model that uses both the nuclear Bass potential and the imaginary time method (Bonasera and Natowitz, 2020). This technique has been extended using a microscopic hybrid α-cluster model that is a molecular dynamics approach (Depastas *et al.*, 2023). The microscopic hybrid α-cluster model does not include the effects of ^{24}Mg resonances on carbon fusion.

Static coupled-channel calculations using a strong short-range absorption do not produce any resonant structure in the fusion excitation function and do not address specific alignments between the ^{12}C nuclei as in the TDWP model (Assunção and Descouvemont, 2013; Jiang *et al.*, 2013). They provide an average of the alignments (i.e., there is an integration over orientation angles in the coupling potentials), and the fusion absorption becomes isotropic. Potential model calculations that explicitly include quadrupole deformation and orientation of the ^{12}C nuclei and make an overall average of the alignments also produce a smooth S-factor function (Denisov and Pilipenko, 2010). The same happens with density-constraint time-dependent Hartree-Fock (DC-TDHF) calculations (Godbey, Simenel, and Umar, 2019) that use an ingoing-wave boundary condition, which is equivalent to a strong short-range absorption. The DC-TDHF fusion model resembles a two-body potential model in which the microscopically calculated $^{12}C - ^{12}C$ effective potential implicitly accounts for coupled-channel effects. Like the AMD model (Taniguchi and Kimura, 2021; Taniguchi and Kimura, 2024), the DC-TDHF approach uses Slater determinants for the many-particle wave function while obeying the Pauli exclusion principle and including effects of incompressibility of nuclear matter. Since the time-dependent Hartree-Fock model treats the internuclear distance coordinate classically, it is assumed that a DC-TDHF potential, determined at an incident energy above the Coulomb barrier, is the same at sub-Coulomb incident energies. The explicit treatment of the dynamics of the intermediate (nuclear molecule) configurations at sub-Coulomb energies is crucial. Coupled-channel calculations using a weak absorption may allow for that kind of treatment (Kondō, Matsuse, and Abe, 1978; Gasques, Chamon, and Cessel, 2022), which also requires the inclusion of highly excited states in the individual ^{12}C nuclei well beyond their first 2^+ excited states (Gasques, Chamon, and Cessel, 2022). Coupled-channel calculations in Gasques, Chamon, and Cessel (2022) described the $^{12}C + ^{12}C$ fusion resonances at energies around the Coulomb barrier well, which is partially due to an angular-momentum-dependent weak absorption that is adjusted to the experimental fusion data, including the THM measurements (Tumino *et al.*, 2018). There are some differences between the fusion resonances given by Gasques, Chamon, and Cessel (2022) and those discussed by Diaz-Torres and Wiescher (2018), which may be due to the absence of the ^{12}C intrinsic vibrations in the TDWP model (Diaz-Torres and Wiescher, 2018) that treats only rotational modes of statically deformed ^{12}C nuclei.

6. Challenges in the low-energy extrapolation

Two important questions regarding the extrapolation of the $^{12}C + ^{12}C$ fusion reaction are (1) What is the nature of the resonances observed in the THM approach? and (2) Can the analysis of multiple reaction channels provide reliable information? Several phenomenological calculations have attempted to describe the $^{12}C + ^{12}C$ fusion excitation function [see Assunção and Descouvemont (2013), Diaz-Torres and Wiescher (2018), Godbey, Simenel, and Umar (2019), Bonasera and Natowitz (2020), Taniguchi and Kimura (2021), Gasques, Chamon, and Cessel (2022), Depastas *et al.* (2023), and Taniguchi and Kimura (2024)], which further expands this question to the origin of the resonant structures: Are they due to a mechanism connected with the physics of the intermediate (nuclear molecule) compound structure, or do they arise from some other reaction mechanism? Some resonant structures in the $^{12}C + ^{12}C$ astrophysical S factor may be the result of the quantum partner dance, i.e., oscillations of the intrinsic symmetry axis of each ^{12}C nucleus relative to the internuclear axis in the nuclear molecule (Diaz-Torres and Wiescher, 2018). Some of the resonancelike features in the experimental data that are not yet explained could be due to compound-nucleus resonances (Jiang *et al.*,

2013) and/or cluster effects in the nuclear molecule (Diaz-Torres, Gasques, and Antonenko, 2024; Taniguchi and Kimura, 2024). The interpretation of the low-energy structures observed in the THM approach critically depends on the identification of these features as well as the impact of the cross-section extrapolation toward very low energies. This requires verification of the proposed obstacle effect that would reduce the cross section (Back *et al.*, 2014).

The lower panel of Fig. 28 shows different model predictions of the modified astrophysical S factor for $^{12}C + ^{12}C$, $S^*(E)$, such as those of TDWP, coupled-channel, neck model, microscopic hybrid α-cluster, DC-TDHF, and AMD calculations. Large discrepancies exist at stellar energies ($E < 3$ MeV), while most models describe the trend of experimental data (upper panel of Fig. 28) at energies near the Coulomb barrier (≈6 MeV) well. The standard estimation by Caughlan and Fowler (1988) (the dotted black line) assumes a constant S^* factor, whereas the hindrance model (the solid thin black line) suggests a strong suppression at stellar energies. The predictions of these different models differ by 2 orders of magnitude at the Gamow energy window ($E < 3$ MeV), which is centered at ≈1.5 MeV. In this astrophysically important energy region, most model calculations provide a smooth S^*-factor function, with the exception of two. Namely, (i) the AMD model that microscopically treats compound-nucleus resonances associated with different binary cluster configurations of ^{24}Mg (the dot-dashed red line) and (ii) the neck model model, which addresses a two-body potential model using the imaginary time method (the blue triangles). In the AMD model (Taniguchi and Kimura, 2021, 2024), the microscopic compound-nucleus Hamiltonian matrix is diagonalized. The R-matrix method, along with the Breit-Wigner formula for a single-resonance cross section, is then used for calculating the resonant S^* factor, which vastly changes depending on the different energy density functionals that are used (Taniguchi and Kimura, 2024). In the neck model approach (Bonasera and Natowitz, 2020), the Bass potential strength is increased at each 0^+ resonance observed in the THM data, phenomenologically adding resonance structures to a smooth S^* function that substantially deviates from other theoretical curves at energies around the Coulomb barrier. The microscopic hybrid α-cluster calculations (the solid circles) reveal oscillations whose origin seems to be numerical noise in the treatment of quantum tunneling with the imaginary time method (Depastas *et al.*, 2023). DC-TDHF calculations (the short-dashed light-green line) (Godbey, Simenel, and Umar, 2019) using the Skyrme energy density functional with the `SLy4d` parameter set predict an S^*-factor curve that is qualitatively similar to the one from the static coupled-channel calculations by Assunção and Descouvemont (2013) (the dot-dot-dashed magenta line), which included microscopic double-folding potentials using both the DDM3Y nucleon-nucleon interaction and transition densities from a triple-α cluster model. The coupled-channel calculations by Gasques, Chamon, and Cessel (2022) (the long-dashed green line) predict a strong increase in the S^* factor as the energy becomes smaller; this resembles the trend of the indirect THM measurements (Tumino *et al.*, 2018). This is because the set of parameters of the imaginary potential are chosen in such a way that they describe, on average, the THM measurements. These coupled-channel calculations use optical potentials based on the real São Paulo nuclear interaction, which is attractive at short radii (Chamon, Carlson, and Gasques, 2021), and a weak angular-momentum-dependent imaginary part, leading to resonant structures in the S^*-factor function at energies below and near the Coulomb barrier. Similar structures emerge from TDWP calculations (the dark-red solid line) (Diaz-Torres and Wiescher, 2018). However, discrepancies exist between the TDWP resonances and those in the coupled-channel calculations by Gasques, Chamon, and Cessel (2022). This might be due to the lack of the ^{12}C intrinsic vibration in the TDWP calculations.

In fusion calculations from outside to inside (i.e., in nuclear collisions)—such as those from coupled-channel, DC-TDHF, and TDWP models—the use of a strong, short-range imaginary potential to simulate fusion makes it difficult to account for the effects of compound-nucleus resonances on the fusion cross section. The latter is better described in fusion calculations from inside to outside (i.e., nuclear structure calculations linked to the R-matrix method), such as those within the AMD model, but the AMD model's description of the quantum tunneling process of heavy ions using the R-matrix method is simple. A great theoretical challenge is required to combine the strengths of the different fusion models, allowing one to account for the impact of both compound-nucleus and intermediate (nuclear molecule) resonances on the fusion cross section at stellar energies. The accurate calculation of small fusion probabilities at stellar energies is also numerically difficult. Any theoretical model aimed at investigating the existence of fusion resonances over the Gamow energy region should also be tested against observed resonances at energies around the Coulomb barrier.

VI. ELECTRON SCREENING EFFECTS

Thus far, we have discussed threshold quantum effects associated with the internal structure of a nucleus and the implications for the reaction rate. However, one of the best-known low-energy quantum effects is the so-called electron screening, which is caused by modifications in the Coulomb repulsion between the two interacting charged nuclei in hot plasmas. This includes not only gravitationally confined plasma in the interior of stars but also inertial and magnetic confined plasmas in fusion facilities. Electron screening by bound electrons also affects the cross sections obtained by very-low-energy accelerator-based reaction studies. Electron screening is a general phenomenon due to the Coulomb interaction of free or bound electrons with the nucleus, causing an increase in cross section by lowering the Coulomb repulsion between the ions that depends on the specific conditions. A particularly interesting situation occurs if the low-energy cross section is resonantly enhanced, as screening can effect both the position and the width of the resonance. Section VI.A discusses the present status of the mostly phenomenological models, which are presently being used by the low-energy-reaction community, in order to take such effects into account. Section VI.A expands on a recent summary on electron screening (Aliotta and Langanke, 2022) while also exploring the impact of cluster and structure phenomena and uncertainties in the stopping powers for light-particle reactions on screening.

A. Electron screening in stars

Astrophysical environments typically represent highly ionized plasma conditions. During hydrostatic stellar burning the density and temperature are such that the average Coulomb energy between ions in the plasma is much smaller than the average thermal energy. Screening in this "weak-screening" regime is discussed in Secs. VI.A.1 and VI.A.2. In contrast, "strong-screening" effects on nuclear reactions are expected in environments with high densities and low temperatures, as they are expected in cold neutron stars and white dwarfs; strong screening is discussed in Sec. VI.A.3.

Figure 29 describes several electron screening regimes in the stellar plasma. Different types of plasma screening by electrons in terms of the medium density and temperature are shown. E_G is the Gamow peak energy, E_{F} is the electron Fermi energy, $R_y = m_e e^4/(8\epsilon^2 h^3 c)$ is the Rydberg constant, and

$$E_0 \equiv \omega_p = \sqrt{\frac{4\pi Z^2 e^2 n_{\mathrm{ion}}}{m}} = 2.4726\lambda^{1/2} E_{\mathrm{Coul}} \tag{24}$$

is the ion-plasma oscillation frequency, where

$$\lambda = \frac{1}{ZA^2}\left(\frac{1}{\mu_A}\frac{\rho}{1.3574\times 10^{11}\ \mathrm{g\,cm^{-3}}}\right)^{1/3} \tag{25}$$

is a dimensionless inverse length parameter (Salpeter and van Horn, 1969), here $\mu_A = A(1 + Zm_e/AH)$, with H the unit of atomic mass. $E_{\mathrm{Coul}} = 1.819\,62 Z^2 e^2/a$ is the average Coulomb energy of the ions separated by an average distance a [the numerical constants apply for a Wigner-Seitz cell (described later)]. In the rectangular region, E_{F} and kT are both too small for complete ionization. If λ is small, the zero-point oscillation amplitude in a lattice of ions is also small at zero temperature, corresponding to the pycnonuclear regime. We discuss these features in the context of strong-screening regimes.

1. Weak screening and the Debye-Hückel model

The derivation of Debye screening using elementary concepts of classical physics was accomplished by Debye and Hückel (1923) with the aim of describing equilibrium processes in chemistry. At infinite dilution the Coulomb potential around an ion is given by $V_i(r) = Z_i e/r$. Because of the interaction between the charges, these concentrations are no longer spatially uniform, with negative charges tending to concentrate around positive ions. The potential V_i tends to attract a surplus of opposite charges with concentrations c_{j0} into the vicinity of the ion i. This reduces (shields) the magnitude of the potential. A time-averaged shielded potential $V_i(r)$ and a corresponding nonuniform charge density $\rho(r)$ emerges. This is a typical electrostatics problem that is solvable using Poisson's equation in spherical coordinates.

The interaction energy between an ion j and the potential created by the ion i is given by $E_{ij} = Z_j e V_i(r)$. The concentrations around the ion i are populated according to the statistical distribution of the individual charge j energies in the presence of an effective Coulomb field $V_i(r)$. In the weak-screening limit (see Fig. 29), the average Coulomb energy between the ions is much smaller than the thermal energy, i.e.,

$$\Gamma \equiv \frac{Z^2 e^2}{akT} \ll 1, \tag{26}$$

where a is the average inter-ion distance and Γ is known as the Coulomb coupling parameter. This implies that $Z_j e V_i(r)/kT \ll 1$ and therefore

$$V_i(r) = \frac{Z_i e}{r}\exp\left(-\frac{r}{R_D}\right), \tag{27}$$

with the *Debye radius* R_D defined as $R_D^2 = kT/[4\pi e^2 \sum_j Z_j^2 c_{j0}]$.

Screening modifies the Coulomb potential between the nuclear radius R and the classical turning point R_0 and consequently modifies the barrier penetration. For weak screening $R_D \gg R, R_0$. To first order the barrier energy for an incoming projectile with charge $Z_2 e$ is $V(r) \equiv Z_2 e V_1 = Z_1 Z_2 e^2/r + U(r)$, where the Debye-Hückel *screening potential* $U_0 \equiv U(0) = \mathrm{const}$ is given by $U_0 = -Z_1 Z_2 e^2/R_D$. The impact of the screening potential on the barrier penetrability and therefore on the astrophysical reaction rates can be approximated through a screening factor $f = \exp(U_0/kT)$ that, in the weak-screening limit, becomes $f \approx 1 + U_0/kT$. The Debye-Hückel screening model applied to electron screening in stellar plasmas was first studied by Salpeter (1954). In the decades since, Eq. (27) has been deduced using different theoretical approaches (Bahcall et al., 2002), including quantum-field theory (Brown and Sawyer, 1997).

In summary, for the weak-screening limit, the reaction rate is modified in the presence of electron screening, yielding $\langle\sigma v\rangle_{\mathrm{plasma}} = f(E)\langle\sigma v\rangle_{\mathrm{bare}}$ or, for a specific reaction, $i + j \to k + l + \cdots$,

$$\langle\sigma \mathrm{v}\rangle^*_{j,k} = f(Z_j, Z_k, \rho, T, Y_i)\langle\sigma \mathrm{v}\rangle_{j,k}, \tag{28}$$

where the screening factor f depends on the charges of the reacting nuclei, its density, its temperature, and its nuclear abundances Y_i. During stellar hydrostatic burning, the average Coulomb energy between the ions is usually smaller than the thermal energy, leading to weak screening, with

$$f = 1 + 0.188\frac{Z_1 Z_2 \rho^{1/2}\xi^{1/2}}{T_6^{3/2}}, \quad \xi = \sum_i (Z_i^2 + \mathcal{F}Z_i)^2 Y_i. \tag{29}$$

In Eq. (29) T_6 and ρ are the plasma temperature and density in units of 10^6 K and in $\mathrm{g/cm^3}$, respectively. $\mathcal{F}$ is a correction factor of the order unity accounting for electron degeneracy.

The Debye-Hückel approximation, which is shown schematically in Fig. 30, is valid for electron number densities n_e such as those within a radius R_D where a mean-field

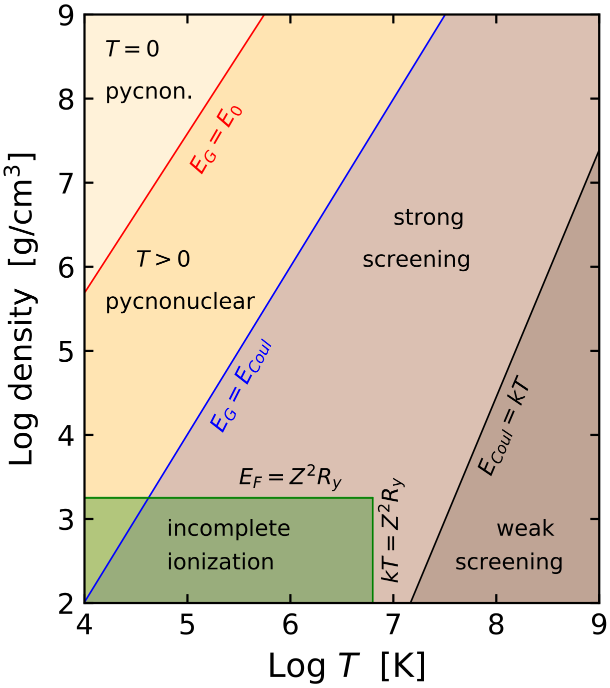

FIG. 29. Different types of plasma screening by electrons in terms of medium density and temperature. E_G is the Gamow peak energy, E_F is the electron Fermi energy, R_y is the Rydberg constant, and E_0 is the ion-plasma oscillation frequency for the density lattice environment that defines strong-screening and pycnonuclear reaction conditions. In the rectangular region, the electron Fermi energy E_F and kT are both too small for complete ionization. Adapted from Salpeter and van Horn (1969).

approximation is valid, $n_e R_D^3 \gg 1$. In the Sun for the $^7\mathrm{Be}(p,\gamma)^8\mathrm{B}$ reaction, $R_D \approx 0.218$ Å and $f \approx 1.2$. A 20% effect for this reaction is important for the high-energy neutrino production in the Sun. In comparison, the screening enhancement for the $^{12}\mathrm{C} + {}^{12}\mathrm{C}$ reaction during hydrostatic carbon burning with $T_6 \approx 700$ and $\rho = 3 \times 10^6$ g/cm^3 is about 60%, which is likely less than the uncertainty in the extrapolated low-energy cross section; see Sec. V.C. This example shows that electron screening is an important correction for nuclear reactions occurring in stellar environments. A laboratory study of the plasma-electron screening effect is highly desirable, and first experiments toward this goal are planned at the National Ignition Facility (Casey *et al.*, 2023). Langanke and Rolfs (1989) argued that the lowest data points measured for the $^2\mathrm{H}(t,n)^4\mathrm{He}$ reaction, which is important as fuel for fusion reactors, are likely slightly enhanced by screening.

The effects of electron screening on nuclear reaction rates occurring during the BBN epoch were assessed by Wang, Bertulani, and Balantekin (2011). They showed that electron screening does not produce noticeable results in the predictions of BBN elemental abundances unless the traditional Debye-Hückel model for its treatment in stellar environments in the weak-screening limit is enhanced by several orders of magnitude. The electron densities during the BBN epoch are too low to produce any relevant impact on the BBN

TABLE II. Dynamic screening factors for the pp chain (Carraro, Schafer, and Koonin, 1988). The second column is the ratio of the Gamow peak energy and the thermal kinetic energy kT, and the third column is the ratio between the weak polarization potential and the Debye potential U_0 (U_Debye), as defined in the text following Eq. (27). The last column is the ratio of the recalculated reaction rate due to dynamic screening with the static Debye screening model.

Reaction	E_G/kT	$U_\mathrm{pol}/U_\mathrm{Debye}$	$r_{12}/r_{12}^\mathrm{Debye}$
$p + p$	4.6	0.76	0.992
$^3\mathrm{He} + {}^3\mathrm{He}$	16.6	0.75	0.966
$^3\mathrm{He} + {}^4\mathrm{He}$	17.3	0.76	0.968
$p + {}^7\mathrm{Be}$	13.9	0.80	0.973
$p + {}^{14}\mathrm{N}$	20.6	0.82	0.958

nuclear reactions. Thus, it seems that electron screening is relevant only for astrophysical processes occurring in stellar environments and in the laboratory measurements of reaction cross sections.

2. Dynamic weak electron screening in plasmas

Carraro, Schafer, and Koonin (1988), Lavagno and Quarati (2000), Opher and Opher (2000), Tsytovich (2000), Savchenko (2001), Shaviv and Shaviv (2001), Weiss, Flaskamp, and Tsytovich (2001), and Fiorentini *et al.* (2003) calculated the factor $f(E)$ for weakly screened thermonuclear reactions, taking into account their dependence on the velocity of the colliding ions. They found enhancements that are appreciably different than those given by the standard adiabatic Debye-Hückel approximation if the Gamow velocity is greater than the ion thermal velocity. The mean-field approximation following the Debye-Hückel picture is not strictly valid under the conditions prevailing in the core of the Sun. A kinetic approach should be implemented, although the results by Carraro, Schafer, and Koonin (1988), Lavagno and Quarati (2000), Opher and Opher (2000), Tsytovich (2000), Savchenko (2001), Shaviv and Shaviv (2001), Weiss, Flaskamp, and Tsytovich (2001), and Fiorentini *et al.* (2003) were disputed by Bahcall *et al.* (2002).

Carraro, Schafer, and Koonin (1988) solved the Poisson equation for a plasma polarized by the motion of the ions corresponding to

$$\nabla^2 V = -4\pi(\rho_\mathrm{ion} + \rho_\mathrm{pol}), \tag{30}$$

with $\rho_\mathrm{ion} = Ze\delta(\mathbf{r} - \mathbf{v}t)$, where v is the relative energy between the ions. They calculated the plasma polarization density as a function of $\alpha = (mv^2/kT)^{1/2}$ using the framework of linear response theory. When $\alpha \to 0$, $V(r)$ reduces to the Debye result in Eq. (27). For $\alpha \approx 3$ and above, there is a considerable change in the polarization potential compared to the Debye model. The electron cloud density around the ions gets deformed, thus changing the value of the effective screening potential. Because the electron density spreads along a larger deformed volume behind the ion velocity direction, the polarization potential is reduced compared to the spherical Debye potential. Table II shows the effects of dynamic screening in the nuclear reactions of the pp chain operating in the Sun (Carraro, Schafer, and Koonin, 1988). The second column gives the ratio of the Gamow peak energy and the thermal kinetic energy kT, and the third column is the ratio between the weak polarization potential and the Debye potential U_0 ($U_{\rm Debye}$), as defined in the text following Eq. (27). The last column of Table II is the ratio of the recalculated reaction rate due to dynamic screening to that of the static Debye screening.

Carraro, Schafer, and Koonin (1988) argued that dynamical screening reduces the expected event rates in solar-neutrino detectors. The effect, however, is much too small to explain the well-known solar-neutrino puzzle, which, as we now know, is due to neutrino oscillations (Fukuda *et al.*, 1998; Ahmad *et al.*, 2001). Carraro, Schafer, and Koonin (1988) also claimed that dynamical screening is more likely to impact astrophysical plasmas made of heavier ions like ^{12}C.

Shaviv and Shaviv (1996, 1999, 2001) used a molecular dynamics approach to handle the dynamic screening in stellar plasmas. The basic idea is that inside the Debye sphere there are not enough particles to justify a mean-field approximation. For example, in the Sun $n_e R_D^3 \approx 3$–5, Shaviv and Shaviv claimed that one cannot derive the screening from thermodynamics but instead has to resort to kinetic equations. It was found that the energy exchange between any two scattering ions and the electron plasma is positive at low relative kinetic energies and negative at high energies. The turnover in a hydrogen plasma occurs at $E_{\text{kin-rel}} \approx 2kT < E_G \approx 6kT$ for the pp reaction. The net energy exchange, i.e., the sum over all pairs of scattering particles, vanishes in equilibrium.

Fluctuations and nonspherical effects crucially affect the screening. The derived screening corrections for the pp reaction enhance the transition rates, while higher Z reactions like $^7\mathrm{Be}(p,\gamma)^8\mathrm{B}$ are suppressed relative to the classical Salpeter or Debye-Hückel theory. Deviations from the Debye-Hückel theory were found to appreciably modify the reaction rates (Carraro, Schafer, and Koonin, 1988; Lavagno and Quarati, 2000; Opher and Opher, 2000; Tsytovich, 2000; Savchenko, 2001; Shaviv and Shaviv, 2001; Weiss, Flaskamp, and Tsytovich, 2001; Fiorentini *et al.*, 2003).

Brown and Sawyer (1997) used a quantum-field theoretical method to calculate the reaction rates in stellar environments using

$$r_{12} = \int_{-\infty}^{\infty} dt \int d^3 r \langle \Psi_1^\dagger(\mathbf{r},t)\Psi_2^\dagger(\mathbf{r},t) W(\mathbf{r},t). \times \Psi_1(0,t)\Psi_2(0,t)\rangle_\beta, \tag{31}$$

where Ψ_i are the particle fields, Q is the energy transfer, and W is an effective operator for nuclear reactions in the plasma-state space. They (a) concluded that there was a reduction in the fusion rate of about 10% compared to the Salpeter enhancement factor, but (b) found no "dynamical screening" modification of the Salpeter enhancement factor.

Bahcall *et al.* (2002) rederived the Salpeter factor using five different theoretical formulations. They concluded that no dynamical screening modification was necessary. Moreover, they claimed that all publications questioning the validity of the Debye approximation, including (Dewitt, Graboske, and Cooper (1973), Graboske *et al.* (1973), Carraro, Schafer, and Koonin (1988), Shaviv and Shaviv (1996, 1999; 2001), Lavagno and Quarati (2000), Opher and Opher (2000), Tsytovich (2000), Savchenko (2001), and Weiss, Flaskamp, and Tsytovich (2001), were either wrong or ill formulated.

Kushnir, Waxman, and Chugunov (2019) rederived a useful relation between the plasma screening factor and the chemical potentials of the ions, originally attributed to Dewitt, Graboske, and Cooper (1973) and Graboske *et al.* (1973), based on the plasma pair distribution functions. They used the principle of detailed balance and generalized the relation to reactions involving N fusing ions, where the screening factor for the p-e-p reaction, $p + e + p \to 2d + \nu_e$, was calculated. For the plasma conditions near the center of the Sun, the reaction was found to be suppressed by roughly the same amount ($\approx$10%) that the $p + p \to 2d + e^+ + \nu_e$ reaction was enhanced.

Another detailed discussion of weak screening in stellar plasmas was given by Adelberger *et al.* (2011), who reached no conclusion on the apparent contradictions among the several models existing in the literature (Bahcall *et al.*, 2002). The models used by Carraro, Schafer, and Koonin (1988) and Shaviv and Shaviv (2001) have not been adopted by other researchers and it is presently unclear whether their claims were substantiated. These two works were only a couple of the examples found in the literature, where contentious claims have been made and remain unverified (Lavagno and Quarati, 2000; Opher and Opher, 2000; Tsytovich, 2000; Savchenko, 2001; Weiss, Flaskamp, and Tsytovich, 2001; Fiorentini *et al.*, 2003).

3. Strong screening and pycnonuclear reactions

In the strong screening and pycnonuclear regimes (see Fig. 29), the average Coulomb energy between the ions is comparable to or larger than the thermal energy, i.e., $\Gamma \gtrsim 1$ [Γ is defined in Eq. (26)]. Under such conditions the screening corrections can enhance the nuclear cross sections by several orders of magnitude. At high temperatures and low densities such that $\Gamma \ll 1$, the nuclei and electrons form a gas and the weak-screening regime applies, as previously discussed. But for $\Gamma \gg 1$ the nuclei form a condensed phase. At sufficiently low temperatures, one can reach values of $\Gamma \approx 50$–150, and one has a genuine lattice with full long-range order. For $1 \lessapprox \Gamma \lessapprox 50$ one deals with a liquid phase. Even in this case, the same short-range order occurs as in a crystalline

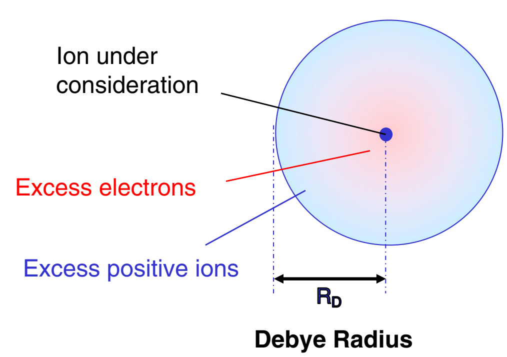

FIG. 30. Schematic of the Debye-Hückel sphere approximation used to describe electron screening in plasmas.

solid, and the nuclear reaction rates are affected mainly by nearby nuclei.

As proposed by Salpeter and van Horn (1969), the electrostatic interaction energies of the ions in the $\Gamma \gg 1$ regime can be of sufficient magnitude to "freeze" the nuclei into a Coulomb lattice structure. As with a hypothetical electron solid, one can assume this lattice to be a body-centered-cubic (bcc) structure, leading to the greatest binding energy per nucleus in the pycnonuclear regime (Cameron, 1959; Harrison, 1964; Jain *et al.*, 2023). Sometimes, researchers also use the face-centered-cubic (fcc) lattice. It is, however, better to replace the polyhedral lattice of a crystal with a concatenation of the so-called Wigner-Seitz cell, which is a lattice cell with radial size a containing a total distributed negative charge $-Ze$, $(4/3)\pi a^3 n_e = Z$, plus one single ion of charge $+Ze$ at the center (Wigner and Seitz, 1933). The Wigner-Seitz cell is used to treat the effects of electron screening across the range of validity of strong screening, $\Gamma \gtrsim 1$. This is a complementary version of the weak-screening Debye sphere that is schematically shown in Fig. 30. The Wigner-Seitz cell is well known in lattice theory and immensely helpful for understanding the geometric symmetry of a crystal. A two-dimensional sketch of the Wigner-Seitz cell is shown in Fig. 31 and constructed in the following way (Kittel, 2004): from one of the lattice ions, draw straight lines to all closest lattice ions. At the middle of these lines, draw a perpendicular line. The area inside is the Wigner-Seitz cell. In three dimensions one replaces the middle lines by planes. Examples of 3D Wigner-Seitz cells are as follows: (a) for a primitive cubic lattice, it is a cube; (b) for a bcc lattice, it is a truncated octathedron; and (c) for a fcc lattice it is a rhombic dodecahedron. All the cells are perfectly connected without interstitial gaps, and they have the advantage that they always have only one ion at the center, which is appropriate for treating the screening by electrons. For the number density of nuclei n_a and a bcc lattice constant $a = (n_a/2)^{1/3}$, the total electrostatic interaction energy per nucleus in a Wigner-Seitz cell is $E_{\mathrm{Coul}} = 1.819\,62 Z^2 e^2/a$.

Most models for strong screening assume that the ion-ion potential is changed from a pure Coulomb repulsion with the addition of a background potential $H(r)$, i.e., for two identical ions,

$$V(r) = \frac{Z^2 e^2}{r} - H(r), \tag{32}$$

where for simplicity H is taken as spherically symmetric around the ion. Salpeter (1954) assumed a constant background and obtained

$$H(r) = H_0 = 1.0573 Z^2 e^2 \left(\frac{4\pi n_e}{3Z}\right)^{1/3}, \tag{33}$$

where the probability for tunneling through the barrier is increased by a factor $f_{\mathrm{scr}} = \exp(H_0/kT)$. At high densities and sufficiently low temperatures, nuclei settle into a Coulombic lattice. A schematic representation of a lattice with background electrons is shown in Fig. 32. The Coulomb lattice is formed by ions (carbon, oxygen, nitrogen, etc.) and background electrons. The background electrons give rise to a usually inhomogeneous background Coulomb field $H(r)$ as a function of the distance to a particular ion.

In Fig. 33 we show the S factor for $^{12}\mathrm{C} + {}^{12}\mathrm{C}$ fusion in carbon matter as a function of the center-of-mass energy E. The solid line neglects plasma screening. The dashed, dotted, and dot-dashed lines are S factors calculated using the homogeneous background Salpeter's model for plasma screening in the strong regime at $\rho = 10^8$, 10^9, and $10^{10}\ \mathrm{g\,cm^{-3}}$, respectively, and vanishing temperature. The importance of screening is evident, as it increases the S factors exponentially to large values at the typical densities. This also means that one needs to develop an accurate theory if one wants to get the numbers right, as a small change in the description of the background function $H(r)$ leads to enormous changes in the screening enhancement (note the logarithmic scale).

Since Salpeter's pioneering work, others have studied the same problem and observed that the field H is not homogeneous. The typical tunneling times in the low-temperature regime are much smaller than the plasma oscillation period $\approx \omega_p^{-1}$, which justifies the assumption of an almost constant and static plasma potential during a tunneling event. As the

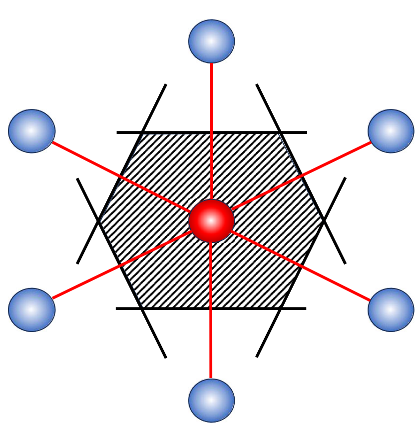

FIG. 31. Two-dimensional representation of the Wigner-Seitz cell.

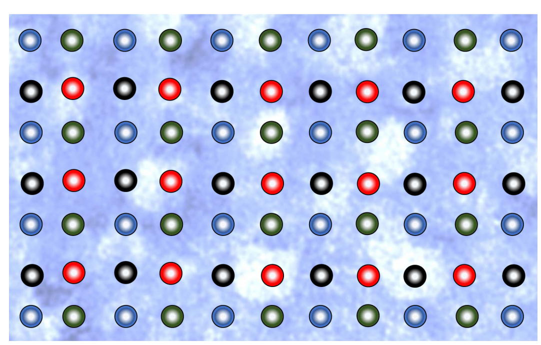

FIG. 32. Schematic of a Coulomb lattice formed by ions (carbon, oxygen, nitrogen, etc.) and background electrons. The background electrons give rise to an inhomogeneous background Coulomb field $H(r)$ as a function of the distance to a particular ion.

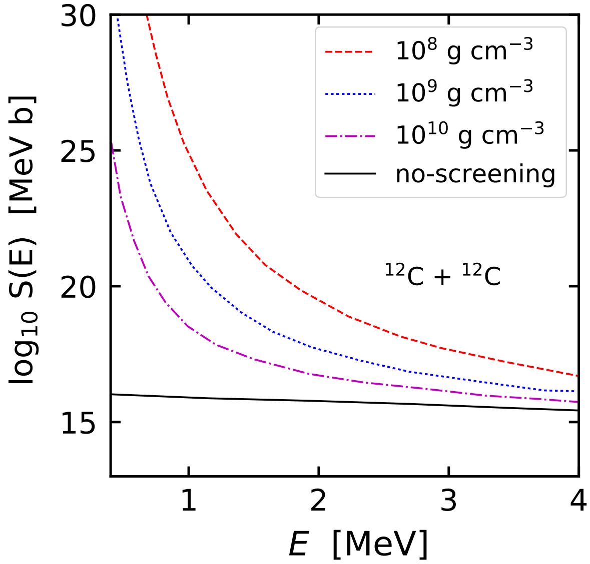

FIG. 33. S factor for $^{12}C + ^{12}C$ fusion in carbon matter as a function of the center-of-mass energy E. The solid line neglects plasma screening. The dashed, dotted, and dot-dashed lines are S factors calculated using Salpeter's model for plasma screening in the strong regime at $\rho = 10^8$, 10^9, and 10^{10} g cm^{-3}, respectively. Adapted from Kravchuk and Yakovlev, 2014.

temperature T increases, the ionic lattice can be excited to higher frequency modes, as discussed by Salpeter and van Horn (1969). The lattice frequency, or zero-point energy, discussed near Eq. (25) is $E_0 = \omega_p \approx \rho^{1/6} A^{1/3} Z^3$, thus also increasing with the density; see Fig. 29. The oscillation frequency of the lattice acts as an effective spring force between the ions and the electrons with an average spring constant of the order of $k \approx \omega_p^2 m_e$. This has an additional effect on the background potential H_0 given by Eq. (33).

More detailed treatments of the background potential $H(r)$ were given by Dewitt, Graboske, and Cooper (1973), Graboske et al. (1973), Jancovici (1978), Ogata, Iyetomi, and Ichimaru (1991), Ichimaru, Ogata, and van Horn (1992), Ogata, Ichimaru, and van Horn (1993), Kitamura and Ichimaru (1995), Rosenfeld (1996), Kitamura (2000), Potekhin and Chabrier (2000), Fiorentini et al. (2003), Pollock and Militzer (2004), and Kravchuk and Yakovlev (2014). In the mean-field approximation, the background potential can be written as

$$H(r) = \frac{Z_1 Z_2 e^2}{a} h(x),$$
$$h(x) = b_0 + b_2 x^2 + b_4 x^4 + \cdots, \tag{34}$$

where a is the inter-ion distance and $h(x)$ is a dimensionless function of a dimensionless radial coordinate $x = r/a$. At $x \ll 2$ the function $h(x)$ can be expanded, as shown in Eq. (34). The expansion coefficients b_0, b_2, b_4, etc., tend to depend on only one parameter $z = Z_1/Z_2$. Their values were given by Kravchuk and Yakovlev (2014). The normalized potential $h(x)$ is symmetric with respect to $z \to 1/z$, so it is sufficient to consider the case of $z \geq 1$. The models to calculate $h(x)$ include numerous techniques, such as Monte Carlo sampling in a generalized path integral (Dewitt, Graboske, and Cooper, 1973; Graboske et al., 1973; Ogata, Iyetomi, and Ichimaru, 1991; Ichimaru, Ogata, and van Horn, 1992; Ogata, Ichimaru, and van Horn, 1993; Kitamura and Ichimaru, 1995; Fiorentini et al., 2003) or simple semi-analytical models such as the electron drop model (Kravchuk and Yakovlev, 2014). Note that strong plasma screening is still a contentious subject, with enhancement factors differing in some cases by factors of 50. At low temperatures the screening factors can be as large as $f_{\rm scr} \approx 10^{70}$ for $\Gamma \approx 170$. This is basically due to the fact that tunneling through the Coulomb barrier is extremely small when nuclei are organized in a lattice such as those thought to exist in a white dwarf. Electron screening enhances the tunneling probability by a large factor, thus allowing nuclear fusion to proceed in the pycnonuclear regime.

An important example in which strong screening plays a crucial role is the $^{12}C + ^{12}C$ fusion reaction under highly degenerate white dwarf conditions at which the reaction is predicted to ignite thermonuclear supernovae (Hillebrandt et al., 2013). Reviews about strong screening in astrophysical conditions were given by Itoh et al. (1979) and Fiorentini et al. (2003).

At even higher densities and even at vanishing temperature, the lattice is destroyed due to the zero-point motion of the nuclei, and the system becomes a quantum fluid. This zero-point motion also allows the nuclei to tunnel through the Coulomb barrier, which is significantly modified due to the interaction with other ions and the neutralizing electron background (Salpeter and van Horn, 1969). Such density-induced reactions are the so-called pycnonuclear reactions (Salpeter and van Horn, 1969), and they are the reason why no Coulomb crystal exists at arbitrarily large densities. Parametrizations of pycnonuclear reaction rates were proposed by Gasques et al. (2005), Beard et al. (2010), and Yakovlev et al. (2010).

With respect to the theme of this review, a particularly interesting role is played by pycnonuclear reactions in a ^{4}He plasma, as might occur on the surface of isolated neutron stars that accrete matter from the interstellar medium (Blaes et al., 1992). For the evolution of a ^{4}He plasma with growing density, a crucial role is played by the α-cluster states that appear just above threshold in ^{8}Be and ^{12}C. In ^{8}Be this is the ground state just 92.2 keV above the $\alpha + \alpha$ threshold in ^{12}C, the well-known Hoyle state, which lies 285 keV above the $3 - \alpha$ threshold. In a series of papers with increasing sophistication, it was shown that at densities around 3×10^9 g/cm^3 the ^{4}He plasma transforms into ^{8}Be matter, which is caused by the screening energy equaling the ^{8}Be resonance energy. However, this phase transition will not be realized, because the pyconuclear reaction of three α particles transforms the plasma into ^{12}C matter at even slightly lower densities (Schramm and Koonin, 1990; Langanke et al., 1991; Schramm, Langanke, and Koonin, 1992; Müller and Langanke, 1994). Accretion processes in binary systems including neutron stars lead to thermonuclear runaway processes that are observed as x-ray bursts (Woosley and Taam, 1976; Woosley et al., 2004). Further processing of the ashes (Schatz et al., 1999) in an increasingly dense environment

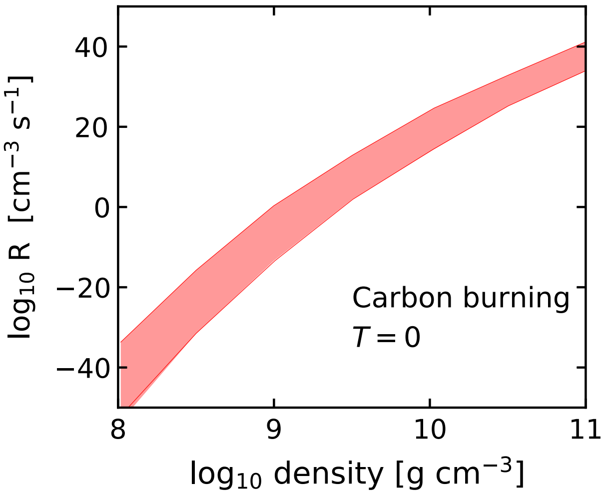

FIG. 34. Reaction rates of pycnonuclear carbon burning at $T = 0$ as a function of density for the different theoretical models studied by Fiorentini *et al.* (2003). The band refers to the uncertainty region of reactions for carbon burning using bcc and fcc Wigner-Seitz cells.

causes pycnonuclear fusion processes in the deeper layers of the neutron-star crust. These reactions influence the cooling of the observed transients (Haensel and Zdunik, 1990; Jain *et al.*, 2023). The associated pycnonuclear reaction rates thus far are estimated only in a framework of nuclear potential models (Gasques, Afanasjev *et al.*, 2007) and carry considerable uncertainties (Horowitz, Dussan, and Berry, 2008; Beard *et al.*, 2010; Afanasjev *et al.*, 2012). Figure 34 shows the present uncertainty of reaction rates of pycnonuclear carbon burning at $T = 0$ as a function of density for the different theoretical models studied by Fiorentini *et al.* (2003) and Gasques *et al.* (2005). The uncertainty band arises due to the treatment of reactions using either bcc or fcc Wigner-Seitz cells and due to the different assumptions used in various theories. It is evident that more theoretical work needs to be done to decrease such uncertainties. However, experimental studies suggest a reasonable agreement between the theoretical predictions and observed data within the given uncertainties of the model parameters (Carnelli *et al.*, 2014; Avila *et al.*, 2016; Hudan *et al.*, 2020).

B. Electron screening in laboratory experiments

1. Data and models of screened cross sections

Reaction rates of astrophysical interest measured in the laboratory are also increased by the presence of atomic electrons bound in the nuclei (Assenbaum, Langanke, and Rolfs, 1987; Rolfs and Somorjai, 1995; Rolfs, 2001), which reduce the Coulomb barrier. The "adiabatic model" for laboratory screening assumes that the center-of-mass energy E between the ions increases when the incident ion comes within range of the strong interaction of the target, thus leading to a larger tunneling probability (Assenbaum, Langanke, and Rolfs, 1987). Owing to energy conservation, this increase has to be equal to the difference between the binding energy of the atomic electrons in the two configurations. This is schematically shown in Fig. 35. The screening potential entering Eq. (35) is then equal to $U_e = E' - E$. Experimental findings on the incremental factors are at odds with some apparently well-founded electron screening theories, such as the adiabatic model (Engstler *et al.*, 1988, 1992a; Angulo, Engstler *et al.*, 1993; Prati *et al.*, 1994; Greife *et al.*, 1995; Aliotta *et al.*, 2001). Owing to screening the fusion cross section is equal to that at energy $E + U_e$ (Assenbaum, Langanke, and Rolfs, 1987). That is,

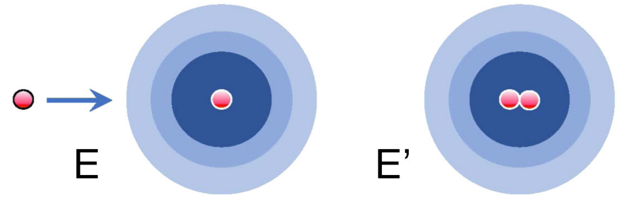

FIG. 35. The adiabatic model (Assenbaum, Langanke, and Rolfs, 1987) for laboratory screening assumes that the relative energy E between the ions increases when the incident ion comes within range of the strong interaction with the target, leading to a larger tunneling probability. Owing to energy conservation, this increase has to be equal to the difference between the binding of the atomic electrons in the two configurations. The screening potential entering Eq. (35) is then equal to $U_e = E' - E$.

$$\sigma(E + U_e) = \exp\left[\pi\eta(E)\frac{U_e}{E}\right]\sigma(E) \qquad (35)$$

since the factor $S(E)/E$ has a much smaller dependence on the energy than the term $\exp[-2\pi\eta(E)]$. Figure 36 shows the effects of laboratory screening on $S(E)$ for the reaction $^3\mathrm{He}(d,p)^4\mathrm{He}$. As expected, the screening effect increases the S factor in an exponential manner as the energy decreases. What is unexpected is the value of the screening potential U_e, which is a factor of 2 larger than that obtained with the adiabatic model, which yields the upper limit for U_e. Dynamical effects, including atomic excitation and polarization as the ions approach each other, will reduce their relative

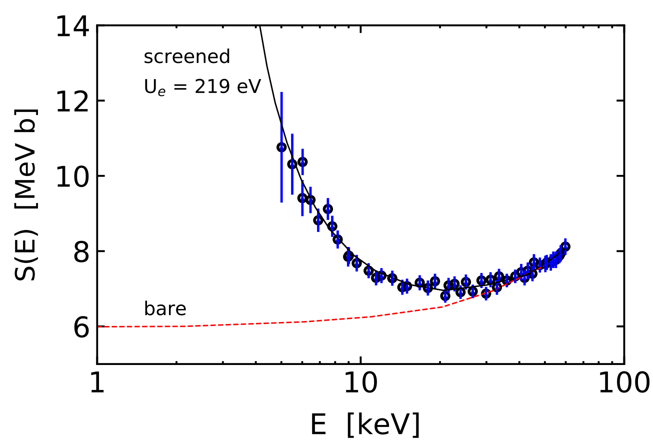

FIG. 36. Experimental data for the $^3\mathrm{He}(d,p)^4\mathrm{He}$ S factor as a function of the relative energy. The dashed curve represents the bare S factor and the solid curve is for screened nuclei with $U_e = 219$ eV. Adapted from Aliotta *et al.*, 2001.

TABLE III. Experimental values of the electron screening potentials U_e^{exp} and the theoretical adiabatic limits U_e^{adlim}.

	Reaction	U_e^{adlim} (eV)	U_e^{exp} (eV)	Note	Reference(s)
(a)	$^2\mathrm{H}(d,t)^1\mathrm{H}$	14	19.1 ± 3.4		Greife *et al.* (1995) and Tumino *et al.* (2014)
(b)	$^3\mathrm{He}(d,p)^4\mathrm{He}$	65	109 ± 9	D_2 gas target	Aliotta *et al.* (2001)
(c)	$^3\mathrm{He}(d,p)^4\mathrm{He}$	120	219 ± 7		Aliotta *et al.* (2001)
(d)	$^3\mathrm{He}(^3\mathrm{He},2p)^4\mathrm{He}$	240	305 ± 90	Compilation	Adelberger *et al.* (2011)
(e)	$^6\mathrm{Li}(d,\alpha)^4\mathrm{He}$	175	330 ± 120	H gas target	Engstler *et al.* (1992a)
(f)	$^6\mathrm{Li}(d,\alpha)^4\mathrm{He}$	175	330 ± 49		Engstler *et al.* (1992a) and Spitaleri *et al.* (2001)
(g)	$^6\mathrm{Li}(p,\alpha)^3\mathrm{He}$	175	440 ± 150	H gas target	Engstler *et al.* (1992a)
(h)	$^6\mathrm{Li}(p,\alpha)^3\mathrm{He}$	175	355 ± 67		Engstler *et al.* (1992a), Cruz *et al.* (2008), and Lamia *et al.* (2013)
(i)	$^7\mathrm{Li}(p,\alpha)^4\mathrm{He}$	175	300 ± 160	H gas target	Engstler *et al.* (1992a)
(j)	$^7\mathrm{Li}(p,\alpha)^4\mathrm{He}$	175	363 ± 52		Engstler *et al.* (1992a), Cruz *et al.* (2008), and Lamia, Spitaleri *et al.* (2012)
(k)	$^9\mathrm{Be}(p,\alpha_0)^6\mathrm{Li}$	240	788 ± 70		Zahnow *et al.* (1997) and Wen *et al.* (2008)
(l)	$^{10}\mathrm{B}(p,\alpha_0)^7\mathrm{Be}$	340	376 ± 75		Angulo, Engstler *et al.* (1993) and Spitaleri *et al.* (2014)
(m)	$^{11}\mathrm{B}(p,\alpha_0)^8\mathrm{Be}$	340	447 ± 67		Angulo, Engstler *et al.* (1993) and Lamia *et al.* (2012)

energy and consequently reduce the value of U_e. In fact, dynamical calculations together with the consideration of several atomic effects have not been able to explain the fact that U_e, as measured experimentally, is substantially larger than that obtained theoretically (Assenbaum, Langanke, and Rolfs, 1987; Shoppa *et al.*, 1993; Rolfs and Somorjai, 1995; Balantekin, Bertulani, and Hussein, 1997; Flambaum and Zelevinsky, 1999; Rolfs, 2001; Hagino and Balantekin, 2002; Fiorentini *et al.*, 2003). This fact is displayed in Table III and Fig. 37.

As an atomic effect, screening should not show an isotope dependence. This was confirmed by Engstler *et al.* (1992b), who investigated the proton fusion on different Li isotopes at low energies and found identical screening potentials. In specific fusion reactions, for example, on deuterium, the target is a molecule. Electron screening in molecular fusion reactions was investigated theoretically for low-energy collisions of $Z = 1$ nuclei with hydrogen molecules by Shoppa *et al.* (1996). They dynamically evolved the electron wave functions using the time-dependent Hartree-Fock model, while the motion of the nuclei was treated classically. They revealed two relevant results. First, at low energies, where screening effects change the cross sections, the electron response can be treated adiabatically. However, the adiabatic screening energies show a striking dependence on the scattering angle. They are found to be largest if the projectile approaches the molecule perpendicularly, while it is smallest if the projectile has to pass the spectator nucleus before fusion. Shoppa *et al.* (1996) pointed to an exceptional difference in the screening effect for the fusion of deuterons (d) with deuterium (D) atoms and D_2 molecules. Owing to reflection symmetry, the $d + \mathrm{D}$ system is asymptotically a 50% mixture of positive and negative parity configurations (Bracci, Fiorentini, and Mezzorani, 1990; Bracci *et al.*, 1991), with the result that the screening energy at low energies for atomic targets is only about half of that found for molecular targets.

Bang *et al.* (1996) and Langanke *et al.* (1996) questioned whether the stopping-power corrections used in the experimental analysis were properly accounted. As shown in the left image of Fig. 38, the fusion of a low-energy ion can occur at any point within the target, and the stopping power S accounts for the energy loss $S = -dE/dx$ of the ions as they penetrate the target. The proper reaction energy $E_{\mathrm{eff}} = E_{\mathrm{ion}} - \langle Sdx \rangle$, in laboratory experiments of fusion reactions, needs to account for the average energy loss $\langle Sdx \rangle$. The stopping power at very low energies was further studied by Bertulani and de Paula (2000) and Bertulani (2004) for $\mathrm{H}^+ + \mathrm{H}$, $\mathrm{H}^+ + \mathrm{He}$, and $\mathrm{He}^+ + \mathrm{He}$ collisions. These are the simplest few-electron systems that can be treated with a relatively accurate theory, and it has been verified that the stopping power is in fact smaller than those predicted by the experimental extrapolations of the Ziegler tables (Ziegler, Ziegler, and Biersack, 2010). This is shown as a solid line in the right panel of Fig. 38. Also shown as a dashed line in the figure is the "nuclear stopping power" due to straggling by Coulomb collisions with the target nuclei. Another dashed line displays

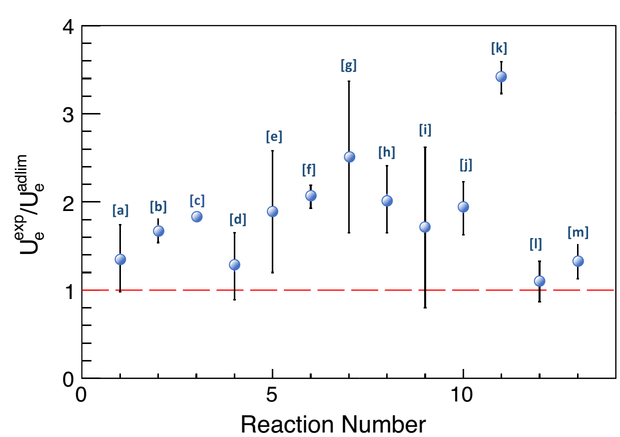

FIG. 37. Ratio of the experimental electron screening potential U_e^{exp} and the theoretical adiabatic limit of the electron screening potential U_e^{adlim} as a function of the main reaction present in the literature. The vertical bars are the total uncertainties of the measurements. The letters in brackets correspond to those in Table III. Adapted from Spitaleri *et al.*, 2016.

the extrapolations of Andersen-Ziegler stopping-power tables to low energies (Ziegler, Ziegler, and Biersack, 2010).

Because at very low ion energies the electrons in the atoms respond nearly adiabatically to the time-dependent interaction, the main cause of stopping is charge exchange, i.e., when an electron jumps from one atom to the other, or by Rutherford scattering, i.e., straggling, in the target (usually denoted as nuclear stopping). Such findings are in agreement with previously determined stopping-power values reported by Golser and Semrad (1991). This is shown in the right panel of Fig. 38 based on a dynamical calculation (Bertulani, 2004). The same trend was found for atomic $\mathrm{He}^+ + \mathrm{He}$ (Bertulani, 2004). A "quenching" of the nuclear recoil contribution to the stopping power was observed experimentally by Formicola *et al.* (2003) and explained by Bertulani (2004). Several fusion reactions were further studied in deuterated metals, and a large increase of the cross sections were found (Czerski *et al.*, 2004; Kasagi, 2004; Raiola *et al.*, 2004, 2006; Huke *et al.*, 2008; Cvetinović *et al.*, 2015). No plausible theoretical explanation seems to exist to explain such discrepancies. However, the adiabatic limit, as derived for isolated atomic cases by Assenbaum, Langanke, and Rolfs (1987), should not apply for fusion reactions in metallic environments.

2. Resonant screening

An interesting situation occurs if the nuclear reaction proceeds through a resonance in the low-energy regime, where the resonance is characterized by its energy position E_R and its width Γ_R. As pointed out by Salpeter (1954), screening modifies the resonance energy. In the weak-screening limit, one usually finds that the screening scale (R_D for Debye screening) is much larger than the nuclear scale, i.e., the screening potential does not vary over the extension of the nucleus and can there be replaced by the screening energy U_0. As a consequence, in the presence of screening the resonance energy is lowered to $E_R - U_0$ (Salpeter, 1954), shifting it closer to the reaction threshold. In the exceptional case in which $U_0 > E_R$, the resonance can even be changed into a particle-bound state. We note that the lowering of the resonance energy by screening is a general behavior that also applies for screening of resonant reactions in metallic environments (Zinner, 2007) or in the strong-screening case. For the latter we have already discussed the behavior of a ^{4}He plasma at high densities where the screening energy gets larger than the ^{8}Be resonance energy at densities above $\rho = 3 \times 10^9\ \mathrm{g/cm^3}$. Screening also affects the width of the resonance. The resonance width is mainly determined by the penetration through the barrier. The barrier that needs to be penetrated is generally getting wider as the screening potential decreases with radius r. However, if $U(r) \approx U_0$ until the outer turning point R_0, the width is unmodified. This exceptional case might occur for resonances at energies close to the barrier and for weak screening. Such a situation was discussed by Salpeter (1954), and the screening enhancement was obtained as $f = \exp(U_0/kT)$. If the width of the entrance fusion channel is noticeably smaller than the one of the exit channel (which is usually the case), the entrance-channel width determines the resonance strength. In such a situation, the screening enhancement of a resonant cross section is less than that given by f due to the decrease in the resonance width. This applies, in particular, to low-energy (i.e., narrow) resonances where the assumption of a constant screening energy is not valid and the radial dependence of the screening potential has to be explicitly considered (Iliadis, 2023), resulting in a significant lowering of the screening enhancement. Cussons, Langanke, and Liolios (2002) pointed out that the modification of screening has to be taken into account for the $^{12}\mathrm{C} + {}^{12}\mathrm{C}$ fusion reaction in type Ia supernova simulations if the resonance behavior in carbon fusion extends to low energies.

An experimental verification of the screening effects on resonances has not yet been given. A possible candidate to observe the shift of the resonance energy is the $J^\pi = 5/2_2^+$ resonance state at 10 keV in $p + {}^{11}\mathrm{B}$ that was discussed in Sec. II.E.5. Based on the adiabatic model, screening should shift the resonance position by nearly 350 eV, which would translate into a change of resonance strength by about 2%. In this context a reliable quantification of the role of electron screening in the $p + {}^{10}\mathrm{B}$ reaction is still missing, although an experimental analysis using indirect methods has been reported in the literature (Bertulani and Gade, 2010; Tribble *et al.*, 2014; Caciolli *et al.*, 2016; Aumann and Bertulani, 2020). In fact, (p,α) reactions on boron, in particular, $^{11}\mathrm{B}(p,\alpha)^8\mathrm{Be}$, play an important role as a source of neutron-free energy production, which would be a solution with respect to the deuteron-tritium reaction where a large emerging neutron flux occurs (Labaune *et al.*, 2013).

In-medium effects should alter α-decay half-lives when the decaying nucleus is immersed within a metal (Emery, 1972). Relying on established screening models such as the Thomas-Fermi model and the Debye approach, it has been shown (Zinner, 2007) that these anticipated effects should be minimal (Wan, Xu, and Ren, 2015, 2016), as confirmed by experimental studies (Jeppesen *et al.*, 2007; Raiola *et al.*, 2007; Su *et al.*, 2010).

3. Clusterization in light nuclei

In Table III and Fig. 37, we show typical cases for the screening potential of reactions at ultralow energies where clusterization fusion enhancements might have been observed: the first is for the case of $Z = 1$ nuclei reacting with nuclei that do not present an evident nuclear cluster structure; the second is for the case of clusterlike nuclei. Only reactions involving protons and deuterons have been considered to simplify the analysis because deviations from the adiabatic screening model must be related to the atomic and nuclear structure of the He, Li, Be, and B isotopes. The main conclusion drawn from Table III is that there is a clear correlation between the cluster structure of nuclei involved in reactions at ultralow energies and the discrepancy between the value of the upper limit (adiabatic approximation) of the screening potential U_e^{adlim} and its experimental value U_e^{exp}. The disagreement increases as the cluster structure is more pronounced (a larger cluster spectroscopic factor).

It has been proposed that a possible solution to the *electron screening puzzle* may be due to clusterization and polarization effects in nuclear reactions involving light nuclei at very low energies (Spitaleri *et al.*, 2016; Bertulani and Spitaleri, 2017).

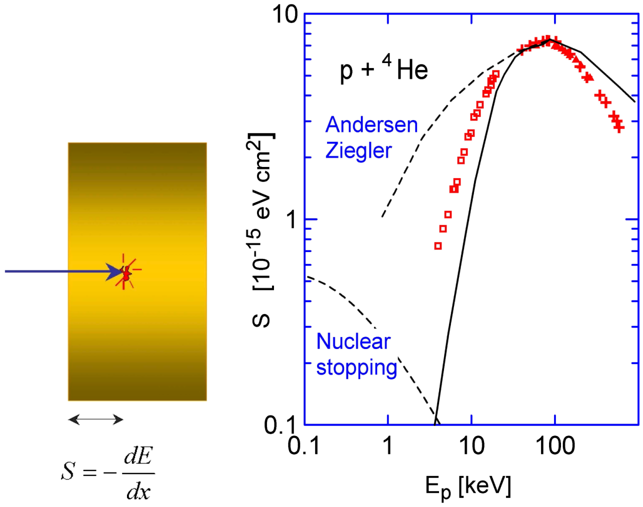

FIG. 38. Left image: schematic of the stopping of low-energy ions in nuclear targets. Right panel: calculated stopping power in $p + {}^4$He collisions at energies of astrophysical relevance (solid line) (Bertulani and de Paula, 2000; Bertulani, 2004). The nuclear stopping power due to straggling by Coulomb collisions with the target nuclei is shown as a dashed line. Another dashed line displays the extrapolations to low energies of the Andersen-Ziegler stopping-power tables (Ziegler, Ziegler, and Biersack, 2010).

Different tunneling distances for each cluster induce a reduction of the overall tunneling probability. Such clustering effects can also be induced by polarization as the nuclei approach each other, as shown in Fig. 39. It was shown that this is possibly the only way to explain why the reaction ^{6}Li + ^{6}Li $\rightarrow 3\alpha$ yields the experimentally observed cross sections (Lattuada *et al.*, 1988), which are much higher in value than one expects for estimates of tunneling in the ^{6}Li + ^{6}Li system. In fact, if the Coulomb barrier penetrability used in the ^{6}Li + ^{6}Li were due to structureless ^{6}Li ions, the cross section for ^{6}Li + ^{6}Li $\rightarrow 3\alpha$ would nearly vanish, or at least one could not measure it; however, it is observed experimentally at low energies.

It is highly probable that the deuterons within ^{6}Li come close together and penetrate a smaller barrier and form α particles, thus explaining the puzzle. This is likely to occur adiabatically and with large probabilities for clusterlike structures as they approach each other. The barrier penetrabilities for $d + d$ and $d + {}^6$Li reactions as a function of the relative-motion energy are also displayed in Fig. 39. Spitaleri *et al.* (2016) and Bertulani and Spitaleri (2017) showed that several reactions of astrophysical interest with light nuclei can be explained in this way. This indicates that more precise experiments need to be carried out to allow for a critical review of theory versus experimental values of the electronic screening potentials U_e and the role of clusterization in astrophysical reactions.

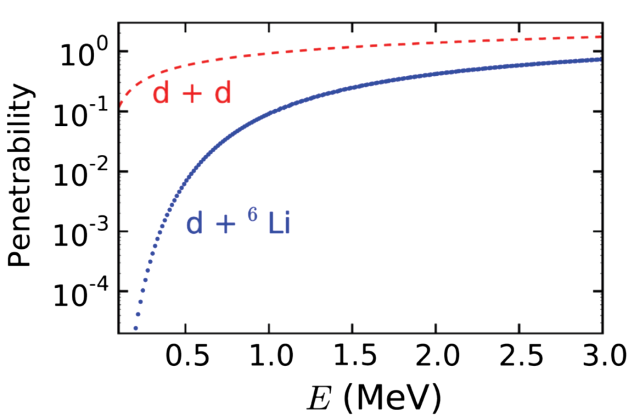

FIG. 39. Barrier penetrabilities for $d + d$ and for $d + {}^6$Li reactions as a function of the relative-motion energy.

The previously discussed clusterization is not the only effect that might play a role in astrophysical reactions and electron screening. Owing to polarization the ground-state shape deformation of nuclei is also important in capture reactions in stars (Wong, 1973; Schmidt and Scheid, 1996; Denisov and Pilipenko, 2010; Soylu *et al.*, 2018). The fusion cross sections depend on the orientation of incoming nuclei, leading to various barrier heights. Small barrier heights that increase the transmission probability and nonaxial symmetric configurations can be the reason for the molecular resonances observed for the ^{12}C + ^{12}C reaction (Spillane *et al.*, 2007; Diaz-Torres, 2008; Tumino *et al.*, 2018). The magnitude of the screening effect strongly depends on an accurate quantification of the polarization, reorientation, and deformation roles in fusion and rearrangement reactions.

C. Electron screening effects on weak-interaction processes

Screening induced by the astrophysical environment also plays an important role for reactions induced by the weak interaction. A prominent example is electron capture on ^{7}Be in the solar interior where the reaction rate is slightly enhanced due to plasma screening, which affects both the continuum and the bound electron contributions to the rate (Iben, Kalata, and Schwartz, 1967; Bahcall and Moeller, 1969; Johnson *et al.*, 1992; Brown and Sawyer, 1997; Gruzinov and Bahcall, 1997; Adelberger *et al.*, 1998, 2011).

Electron capture on nuclei is also the main mechanism working against gravitational core collapse in the late stages of intermediate and massive stars (Bethe *et al.*, 1979; Langanke and Martínez-Pinedo, 2000, 2003; Hix *et al.*, 2003; Langanke *et al.*, 2003; Janka *et al.*, 2007). The relevant rates are modified by Coulomb corrections in the dense astrophysical environment (Bravo and García-Senz, 1999; Liu, Yuan, and Zhang, 2009; Juodagalvis *et al.*, 2010): the threshold energy between parent and daughter nuclei is enhanced, while the chemical potential of the electrons is reduced. Both effects decrease the electron capture rates under core conditions and are considered in the modern rate tabulations used in supernova simulations (Juodagalvis *et al.*, 2010). In contrast, the two effects increase β-decay rates. This increase is unimportant for the late-stage evolution of massive stars, as at high densities β decays are Pauli blocked due to the presence of a relativistic electron gas with sizable electron chemical potential (Janka *et al.*, 2007). This is, however, not true during silicon burning in massive stars where β decays and electron captures compete, leading to something like a generalized

Urca process[1] involving an ensemble of nuclei (Heger, Langanke et al., 2001; Heger, Woosley et al., 2001). The Urca process on selected pairs like ^{23}Na-^{23}Ne, ^{25}Mg-^{25}Na, and ^{25}Na-^{25}Ne play a crucial role in the final core evolution of intermediate-mass stars ($\approx 7M_{\odot}$–$11M_{\odot}$), where they act as an efficient cooling mechanism (Nomoto, 1984, 1987; Strömberg, Martínez-Pinedo, and Nowacki, 2022). As Coulomb corrections have opposite effects on β-decay and electron capture rates, Urca pairs operate at slightly larger densities when screening effects are considered (Martínez-Pinedo et al., 2014; Kirsebom et al., 2019; Zha et al., 2019; Leung, Nomoto, and Suzuki, 2020).

Environmental corrections also play a role for selected nuclei, like ^{56}Ni and ^{44}Ti, which power the light curve of supernovae at different times. Here the rates depend on density, temperature, and also the ionization of the atoms (Takahashi and Yokoi, 1983; Takahashi et al., 1987).

D. Outlook on electron screening in experiment and stars

Electron screening in the laboratory has been observed in low-energy data of a few light-particle reactions; however, there seems to be a mismatch between the effects predicted by existing screening models and observed screening patterns. The discrepancy between data and theoretical predictions must be resolved to avoid uncertainties in the determination of "bare" S factors from future experiments planned at underground facilities that promise the measurement of astrophysically relevant fusion cross sections at energies that are at or near the Gamow window. These efforts should also include experimental and theoretical work on low-energy stopping powers, which typically carry significant uncertainties in the low-energy range (Paul, 2006; Lee, Gosselin, and Diaz-Torres, 2023) and may affect the experimental screening analysis. THM measurements promise to deliver low-energy cross-section data obtained by studies in a "screening-free environment" since the Coulomb barrier has been removed (Pizzone et al., 2010; Spitaleri, 2015). This offers a complementary approach in distinguishing between screening and nuclear threshold phenomena.

The screening effects anticipated for stellar hydrostatic burning conditions currently rely entirely on theoretical modeling based on the Debye-Hückel theory. The development of laser-confined plasma facilities (Cerjan et al., 2018) reaching temperature and density conditions of the stellar interior (Casey et al., 2017) offers a unique opportunity to compare the predictions with the observations made at facilities like NIF or OMEGA (Casey et al., 2023). This allows for a direct determination of reaction rates in certain stellar plasmas and can be used to indirectly check the screening effects deduced from accelerator-based reaction data (Wiescher, deBoer, and Görres, 2022). Screening effects at the high-density conditions expected for the ignition of thermonuclear supernovae and pycnonuclear burning in the neutron-star crust must rely on observations to test theoretical predictions. Observations are sparse, but the long timescale for the cooling of transients due to pycnonuclear processes might offer a path toward testing the theoretical predictions for such extreme conditions (Gupta et al., 2007; Brown and Cumming, 2009).

VII. DERIVATION FROM OBSERVATION

With the increasingly accurate and complementary observational techniques that have emerged in today's multimessenger era, observational results indeed offer tantalizing opportunities to provide observation-based information on reaction rates. Information relies on the determination of specific abundance distributions, spectral observations, light or cooling curves, neutrino flux, helioseismological and astroseismological data, and gravitational wave signals. This allows for the derivation of reaction rates from a number of complementary observational signatures, given that the hydrodynamical and thermodynamical conditions of the specific environments are reasonably well known. The uncertainty of the extracted reaction rate is therefore determined primarily by the uncertainties associated with the observed dataset and the model conditions assumed for the stellar environment.

A discussion of this link between experiment-based reaction rates and observational results is timely because a comparison of the CNO neutrino flux from the Sun (Agostini et al., 2020a) with the predicted flux from low-energy nuclear cross-section measurements shows some discrepancy. This might be due to the uncertainties associated with the extraction of the CNO neutrino signal from the neutrino background in the Borexino detector (Basilico et al., 2023), but it might also be due to uncertainties in the contributions of the high-energy tail of the ^{15}O subthreshold state to the reaction cross section of ^{14}N$(p,\gamma)^{15}$O (Bertone et al., 2001; Frentz et al., 2021).

The determination of the C/O ratio in white dwarfs with astroseismology techniques (Metcalfe, Salaris, and Winget, 2002) also disagrees with predictions based on the best available extrapolation of the ^{12}C$(\alpha,\gamma)^{16}$O cross section. These deviations could be caused by inadequacies in the standard solar model or the simulation of white dwarf material, but they could also be caused by quantum threshold effects at very low energies that render the nuclear reaction rates used in these contexts inaccurate. In the following we discuss some of the atomic and nuclear phenomena that may modify the reaction cross section at very low energies and therefore influence the predictions for stellar reaction rates.

An early example of such a low-energy modification in the literature was the derivation of the ^{12}C$(\alpha,\gamma)^{16}$O rate on the basis of an analysis of the nucleosynthesis products for a grid of massive stars by Weaver and Woosley (1993) followed by a comparison with the known solar abundance distribution. The conclusion was that the rate should have been higher by a factor of 1.7 ± 0.5 times, which was previously suggested by Caughlan and Fowler (1988). This caused a flurry of subsequent studies on the reliability of the approach and the possible impact of other rates and environmental phenomena;

[1]Named by Mario Schoenberg and George Gamow after the former Urca Casino in Rio de Janeiro, where it was well known that money disappears as fast as the thermal energy from the interior of a star by means of reactions that emit neutrinos (Gamow, 1970).

see Hoffman et al. (1999), Rauscher et al. (2002), and Tur, Heger, and Austin (2007). The analysis of astroseismology data on the ^{12}C and ^{16}O abundances and distributions in white dwarfs has been suggested as a unique tool that can be used to derive the $^{12}\mathrm{C}(\alpha,\gamma)^{16}\mathrm{O}$ rate (Metcalfe, Salaris, and Winget, 2002). These deductions have been challenged for not taking into account convection-induced mixing, which introduces large uncertainties in the resulting reaction rate (Straniero et al., 2003). It was suggested that diffusion effects between the different white dwarf layers require a more complex theoretical model approach for deducing a single reaction rate (Fontaine and Brassard, 2002). It has been pointed out, however, that the analysis of lower modes of seismological signals may well allow for the derivation of a rate from the data (Chidester, Timmes, and Farag, 2023). More recent attempts in modeling the white dwarf carbon-oxygen compositions do indeed look more promising, albeit they seem to suggest a slightly enhanced $^{12}\mathrm{C}(\alpha,\gamma)^{16}\mathrm{O}$ reaction rate (Giammichele, Charpinet, and Brassard, 2022) than suggested by the extrapolation of the accelerator-based cross-section data.

The black-hole mass gap is predicted to be the result of pair-instability supernovae (Fowler and Hoyle, 1964; Woosley and Heger, 2021) and may provide independent information about the strength of the $^{12}\mathrm{C}(\alpha,\gamma)^{16}\mathrm{O}$ rate. The high temperatures generated by helium burning in massive stars increases the high-energy photon flux in the Planck distribution, causing internal energy loss by $e^+ + e^-$ pair production. This reduces the internal radiation pressure causing the stellar core to rapidly contract while increasing the temperature. This causes the ignition of the $^{16}\mathrm{O} + {}^{16}\mathrm{O}$ fusion reaction, generating expansion by radiation pressure, thus balancing and reversing the contraction. This phenomenon can occur several times, depending on the helium-core mass and temperature, and is labeled as the pair instability of massive stars. For stars with helium-core masses above $\approx 50 M_\odot$, explosive oxygen burning via the $^{16}\mathrm{O} + {}^{16}\mathrm{O}$ fusion process causes total disruption of the star resulting in pair-instability supernovae without a neutron-star or black-hole remnant. The strength of the $^{12}\mathrm{C}(\alpha,\gamma)^{16}\mathrm{O}$ rate determines the onset of pair instability as well as the mass limit of pair-instability supernova leading to the black-hole mass gap (Timmes, Woosley, and Weaver, 1996; Farmer et al., 2020; Mehta et al., 2022). Yet, all these studies rely on model predictions for the reaction rates of $^{12}\mathrm{C}(\alpha,\gamma)^{16}\mathrm{O}$ to provide theoretical limits for the mass gap without taking into account reverse reaction-rate analysis.

Because of the dominant role of helium burning in massive stars and AGB stars, the impact of the $^{12}\mathrm{C}(\alpha,\gamma)^{16}\mathrm{O}$ reaction and the triple-α process was even analyzed in terms of its influence on the slow neutron capture or s process (Tur, Heger, and Austin, 2009), but no reverse analysis was provided. The existence of the s process itself was confirmed by observation of the element technetium in stellar spectra (Merrill, 1952). Since there is no stable technetium isotope in the Universe, the conclusion was that it must have been produced on site by neutron capture processes, serving as observational evidence for the existence of such a reaction mechanism (Iben and Renzini, 1983). The s process is now considered a well-established nucleosynthesis environment, with neutrons produced by the $^{13}\mathrm{C}(\alpha,n)^{16}\mathrm{O}$ or $^{22}\mathrm{Ne}(\alpha,n)^{25}\mathrm{Mg}$ reaction depending on the seed abundances and the temperature conditions in the stellar environment (Lugaro, Pignatari et al., 2023). Isotopic abundance distributions in meteoritic grains provide information about neutron capture branchings on long-lived isotopes (Palmerini et al., 2021; Lugaro, Ek et al., 2023), information that can be utilized for evaluating the neutron flux and temperature conditions at the s-process site (Bisterzo et al., 2015). However, because of the hydrodynamical complexity of the neutron production environment, no conclusive determination of the reaction rates for the neutron production has yet been provided.

The detection and analysis of solar neutrinos associated with the decay of ^{13}N, ^{15}O, and ^{17}F were suggested by Haxton and Serenelli (2008) and Serenelli, Peña-Garay, and Haxton (2013) as an independent approach to deduce the metallicity of the Sun (Asplund, Amarsi, and Grevesse, 2021; Magg et al., 2022). Such measurements may also be utilized to test the current predictions of the associated reaction rates for the $^{12}\mathrm{C}(p,\gamma)^{13}\mathrm{N}$, $^{14}\mathrm{N}(p,\gamma)^{15}\mathrm{O}$, and $^{16}\mathrm{O}(p,\gamma)^{17}\mathrm{F}$ reactions, respectively (Adelberger et al., 2011). These rates still carry substantial uncertainties and inspire new experimental efforts to expand the data range toward lower energies for the $^{12}\mathrm{C}(p,\gamma)^{13}\mathrm{N}$ (Skowronski et al., 2023), $^{14}\mathrm{N}(p,\gamma)^{15}\mathrm{O}$ reactions (Frentz et al., 2022), and new efforts for the $^{16}\mathrm{O}(p,\gamma)^{17}\mathrm{F}$ reaction are in preparation.

While it is a major challenge to identify the single CNO neutrino components in the solar-neutrino flux (Agostini et al., 2020b), in view of the inherent background conditions, the observation of solar CNO neutrinos from the decay of ^{15}O provide direct insight into the metallicity of the Sun, as well as the reaction rate of $^{14}\mathrm{N}(p,\gamma)^{15}\mathrm{O}$ (Agostini et al., 2020a; Appel et al., 2022). Results seem to favor the high solar metallicity predictions of Grevesse and Sauval (1998) and Magg et al. (2022) versus the low solar metallicity prediction by Asplund, Amarsi, and Grevesse (2021) and references therein. This result is not conclusive with respect to the inner structure of the Sun (Buldgen et al., 2023) and also relies on the assumption that the neutrino signal is generated primarily by the decay of ^{15}O. The reaction rate for $^{14}\mathrm{N}(p,\gamma)^{15}\mathrm{O}$ is the largest nuclear physics related uncertainty in the evaluation of solar metallicity but does not provide any direct information on the $^{14}\mathrm{N}(p,\gamma)^{15}\mathrm{O}$ rate that is used in the analysis.

In view of the uncertainties associated with the detailed conditions of the stellar environment and the computational difficulties in modeling it, a major challenge still remains in reliably extracting nuclear reaction rates from stellar observations. This is a different range of uncertainties that are based primarily on model assumptions about the stellar environment, while the uncertainties associated with experimental data are used primarily in regard to the theoretical ways and means to extrapolate this data toward a lower energy range. One can consider it a complementary approach, but given our limited capability to model the stellar environment with the necessary accuracy, there is a long way to go before constraints on nuclear physics data can come from stellar observations.

VIII. PERSPECTIVES

Near-threshold resonances are abundant in atomic nuclei. Their presence is important for low-temperature plasma environments and may significantly affect the fusion rates in anthropogenic and stellar plasmas. Threshold effects are experimentally challenging. Transfer reaction studies have traditionally concentrated on energy regions below the threshold, with the primary objective of understanding the nuclear shell structure, while low-energy capture studies are limited to the excitation range above the threshold, as they are handicapped by the presence of the Coulomb barrier. This makes the threshold region difficult or impossible to access. In recent years deep-underground accelerator experiments have allowed for a reduction of the cosmic-ray-induced background and have succeeded in expanding the experimental data toward lower energies. Complementary to that, the application of the THM approach and the direct determination of ANC values for near-threshold configurations (Mukhamedzhanov *et al.*, 2007) have made it possible to quantify and translate indirect structure data into reaction data, albeit with some model-dependent uncertainties.

Considerable theoretical progress has been achieved in recent years in describing nuclear reactions at low or subthreshold energies, from which also the astrophysically required extrapolation of data has benefited. The first step was taken with the development of microscopic cluster models, but more recently a plethora of so-called *ab initio* A-body methods based on realistic interactions have been formulated and applied. Significant progress in the description of low-energy reactions has been made using EFT-based models and multichannel R-matrix techniques coupled with a Bayesian uncertainty analysis. A microscopic approach that accounts for the influence of near-threshold states on low-energy cross sections is the continuum shell model, which explicitly involves the coupling between bound states and the scattering continuum. In the most sophisticated realizations, this method can be combined with *ab initio* multichannel techniques.

Despite important advances, none of the existing theoretical models have the necessary predictive power to accurately calculate the energies of resonances or subthreshold states, which dramatically impact low-energy cross sections. The limitations are in the exponential energy dependence of the Coulomb penetration factor. Thus, resonance energies have to be determined experimentally. Here important advances have been made through the development of indirect experimental techniques. Another quantity of considerable importance for the description of resonant contributions to cross sections is the width of the resonance. For the fusion of light particles with intermediate-mass nuclei, the resonance strength is often distributed over several states. Here the interacting shell model has been used as a promising method to determine the proton width for astrophysically relevant reactions involving medium-mass nuclei that are of relevance in hydrogen burning in x-ray bursts or novas. Thus far, however, no formalisms have been proposed to determine the α widths of resonances within the shell model. For the determination of low-energy cross sections that are dominated by a single-resonance or subthreshold state, the ANC method has been established as a powerful tool using Coulomb insensitive transfer reactions (Mukhamedzhanov and Tribble, 1999; Tribble *et al.*, 2014).

As pointed out, a direct probing of the near-threshold regions is difficult, both for charged-particle reactions and for high-ℓ neutron-induced resonances. The reactions with low Z or low ℓ can be studied directly in underground accelerator measurements and laser plasma studies. Traditionally, direct measurements have been complemented by indirect studies that aim at determination of the relevant resonance parameters (i.e., energy, angular momentum, width, etc.). A promising experimental alternative was recently introduced as the Trojan horse method. To overcome the sensitivity to the dominating Coulomb repulsion, the light projectile is brought into fusion range with the desired nucleus as part of a larger nucleus and at higher energies. With carefully chosen kinematics, the desired low-energy fusion cross section can be derived from the reaction data. Although the method holds promise and has been successfully applied in some cases, a proper description of the reaction is lacking, as treatment of the kinematics of the spectator particles, the orbital momenta, the spin and parity of the populated resonances, Coulomb barrier effects, and other features such as nuclear incompressibility for heavy-ion fusion reactions remain major theoretical challenges (Mukhamedzhanov, Kadyrov, and Pang, 2020).

While many examples discussed in this review pertain to stable beams, note that we consider the emergence of threshold effects a generally valid quantum phenomena based on the coupling of bound-state configurations to the continuum. Therefore, nuclear reactions far from stability will also be affected. Much less is known about these processes due to the limitations in beam intensity and the associated lack of experimental data, but the features discussed in Sec. II.E highlight the importance for both proton and neutron capture reaction on unstable particles.

Neutron captures for r-process simulations are the most prominent example (Cowan *et al.*, 2021). Published reaction rates often rely on Hauser-Feshbach predictions (Cyburt *et al.*, 2010), even for systems with low level density (Randhawa *et al.*, 2020). This approach carries potentially large uncertainties that are frequently unaccounted for. Nuclear reactions at low energies are expected to become considerably more complex when one takes into account neutron skin and halo effects, which affect nuclear properties (Dobaczewski and Nazarewicz, 1998) and further may influence the reaction cross section near the threshold (Signorini, Mazzocco, and Pierroutsakou, 2020). Halo effects may become particularly pronounced for the predictions of neutron capture rates (Goriely, 1998; Litvinova *et al.*, 2009; Loens *et al.*, 2012; Tanihata, Savajols, and Kanungo, 2013); these rely mostly on statistical model calculations where the uncertainties in the collective model parameters provide a limit for extrapolating reaction cross sections away from the range of stability. A specific case for reactions involving neutron-rich nuclei with a potential halo structure are the pycnonuclear fusion processes that are expected to occur in the deep crust of neutron-star transients.

In contrast to stellar fusion reactions during hydrostatic burning, pycnonuclear reactions are facilitated not by the finite temperature of the stellar environment but rather by the increase in density in an electron, if not the neutron degenerated environment (Shternin et al., 2012). Pycnonuclear fusion rates depend sensitively on the extension of the neutron halo and need to be calculated based on the realistic proton-neutron density distribution of the fusing isotopes (Gasques, Afanasjev et al., 2007; Beard et al., 2010; Afanasjev et al., 2012). The actual rate is dominated by extensive electron and neutron screening in the local high-density environment (Yakovlev et al., 2006). These reactions provide an internal energy source and modify the internal composition of the crust material (Jain et al., 2023). This is reflected in the cooling behavior of x-ray burst transients (Brown and Cumming, 2009).

Electron screening effects also impact the low-energy cross sections in experiments and in plasma. In laboratory experiments, the screening is induced by the bound electrons in the target and projectile, while in the anthropogenic and stellar plasma environment, the screening is due mainly to continuum electrons. Thus, these two reactions represent different situations requiring different descriptions. In laboratory settings there is currently a serious mismatch between theoretical predictions and experimental data. A solution to this shortcoming might involve better data and better models for low-energy stopping powers, in particular, for hydrogen and helium targets. An alternative is offered by the THM, which provides direct access to the bare-nucleus S factor. Plasma screening, which for hydrostatic burning is traditionally described on the basis of the weak-screening approach, can be tested by inertial fusion studies. First studies in this direction have already been presented (Cerjan et al., 2018; Casey et al., 2023). Screening effects become significant in high-density systems such as nuclear reactions in the atmosphere, the crust, the interior of white dwarfs, and the outer and deeper layers of neutron stars. Nuclear processes at high-density environments affect (or drive) explosive phenomena ranging from novas and thermonuclear supernovae to x-ray bursts.

The development of deep-underground high-intensity accelerators allows for expanded direct studies toward lower energies in a cosmic-ray-shielded environment. New innovative and indirect methods open new avenues for studying the quantum features that emerge in the threshold region. The rapid improvement in inertial confined laser techniques has enabled direct studies of low-energy nuclear reactions in plasma environments. The outcome is a new path to direct exploration of the plasma screening effects. Finally, advanced theoretical techniques have been proposed to reliably extrapolate the reaction cross sections into important near-threshold regions. New technical developments and theoretical efforts discussed in this review pave the way to understanding the impact of nuclear and atomic low-energy effects on nuclear reaction rates in stellar environments.

ACKNOWLEDGMENTS

The authors thank Daniel Odell and Xilin Zhang for supplying comparison model calculations. This research utilized resources from the Notre Dame Center for Research Computing and was supported by the National Science Foundation through Grants No. PHY-2310059 (University of Notre Dame Nuclear Science Laboratory), No. PHY-1430152 (the Joint Institute for Nuclear Astrophysics—Center for the Evolution of the Elements), and No. OISE-1927130 (IReNA). This work was supported in part by the National Science Foundation CSSI program under Award No. OAC-2004601 (BAND Collaboration) and the U.S. Department of Energy, Office of Science, Office of Nuclear Physics under Awards No. DE-SC0013365, No. DE-FG02-88ER40387, No. DE-FG02-08ER41533, No. DE-FG02-93ER40756, and No. DE-NA0004065 and under Work Proposal No. SCW0498. This work was prepared in part by LLNL under Contract No. DE-AC52-07NA27344. Computing support for this work came in part from the LLNL institutional Computing Grand Challenge Program. A. D.-T.'s work was supported by the United Kingdom Science and Technology Facilities Council (STFC) under Grants No. ST/P005314/1 and No. ST/V001108/1. P. N. acknowledges support from NSERC Grant No. SAPIN-2022-00019 and computing support from an INCITE Award on the Summit and Frontier supercomputers of the Oak Ridge Leadership Computing Facility (OLCF) at ORNL, from Livermore Computing, and from the Digital Research Alliance of Canada. TRIUMF receives federal funding via a contribution agreement with the National Research Council Canada.

REFERENCES

Abegg, R., and C. A. Davis, 1991, "^{24}Mg states observed via ^{20}Ne$(\alpha, \alpha_0)^{20}$Ne," Phys. Rev. C **43**, 2523–2540.

Abramovich, S. N., 2015, "Threshold phenomena in few-nucleon systems," Bull. Russ. Acad. Sci. Phys. **79**, 823–828.

Abramovich, S. N., B. Y. Guzhovsky, and L. M. Lazarev, 1992, "Threshold phenomena in nuclear reactions," Sov. J. Part. Nucl. **23**, 129.

Abu-Shawareb, H., et al., 2022, "Lawson Criterion for Ignition Exceeded in an Inertial Fusion Experiment," Phys. Rev. Lett. **129**, 075001.

Acharya, B., and D. R. Phillips, 2013, "^{19}C in halo EFT: Effective-range parameters from Coulomb dissociation experiments," Nucl. Phys. **A913**, 103–115.

Adair, R. K., 1958, "Production of strange particles by π-nucleon and photonucleon interactions near threshold," Phys. Rev. **111**, 632–639.

Adelberger, E. G., et al., 1998, "Solar fusion cross sections," Rev. Mod. Phys. **70**, 1265–1291.

Adelberger, E. G., et al., 2011, "Solar fusion cross sections. II. The pp chain and CNO cycles," Rev. Mod. Phys. **83**, 195–245.

Adsley, P., et al., 2021, "Reevaluation of the ^{22}Ne$(\alpha,\gamma)^{26}$Mg and ^{22}Ne$(\alpha,n)^{25}$Mg reaction rates," Phys. Rev. C **103**, 015805.

Afanasjev, A. V., M. Beard, A. I. Chugunov, M. Wiescher, and D. G. Yakovlev, 2012, "Large collection of astrophysical S factors and their compact representation," Phys. Rev. C **85**, 054615.

Agostini, M., et al. (Borexino Collaboration), 2020a, "Experimental evidence of neutrinos produced in the CNO fusion cycle in the Sun," Nature (London) **587**, 577–582.

Agostini, M., et al. (BOREXINO Collaboration), 2020b, "Sensitivity to neutrinos from the solar CNO cycle in Borexino," Eur. Phys. J. C **80**, 1091.

Aguilera, E. F., et al., 2006, "New γ-ray measurements for ^{12}C + ^{12}C sub-Coulomb fusion: Toward data unification," Phys. Rev. C **73**, 064601.

Ahmad, Q. R., *et al.*, 2001, "Measurement of the Rate of $\nu_e + d \to p + p + e^-$ Interactions Produced by ^{8}B Solar Neutrinos at the Sudbury Neutrino Observatory," Phys. Rev. Lett. **87**, 071301.

Ajzenberg-Selove, F., 1991, "Energy levels of light nuclei $A = 13$–15," Nucl. Phys. **A523**, 1–196.

Alexander, T. K., G. C. Ball, W. N. Lennard, H. Geissel, and H. B. Mak, 1984, "Measurement of the absolute cross section of the ^{3}He(^{4}He, γ)^{7}Be reaction at $E_{c.m.} = 525$ keV," Nucl. Phys. **A427**, 526–544.

Aliotta, M., and K. Langanke, 2022, "Screening effects in stars and in the laboratory," Front. Phys. **10**, 942726.

Aliotta, M., *et al.*, 2001, "Electron screening effect in the reactions ^{3}He(d,p)^{4}He and d(^{3}He, p)^{4}He*," Nucl. Phys. **A690**, 790–800.

Aliotta, M., *et al.*, 2022, "The status and future of direct nuclear reaction measurements for stellar burning," J. Phys. G **49**, 010501.

Almqvist, E., D. A. Bromley, and J. A. Kuehner, 1960, "Resonances in C^{12} on Carbon Reactions," Phys. Rev. Lett. **4**, 515–517.

Almqvist, E., and J. A. Kuehner, 1964, "5.63 and 5.80 MeV levels of Ne^{20}; de-excitation branching," Nucl. Phys. **55**, 145–154.

Almqvist, E., J. A. Kuehner, D. McPherson, and E. W. Vogt, 1964, "Effects of sample size and statistical weights on fluctuations in the C^{12}(C^{12}, α)Ne^{20} reactions," Phys. Rev. **136**, B84.

Altmeyer, T., E. Kolbe, T. Warmann, K. Langanke, and H. J. Assenbaum, 1988, "On discrepancies within the experimental and theoretical low energy ^{3}H(α,γ)^{7}Li cross sections," Z. Phys. A **330**, 277–282.

Amirikas, R., D. N. Jamieson, and S. P. Dooley, 1993, "Measurement of (p,p) elastic cross sections for C, O and Si in the energy range 1.0–3.5 MeV," Nucl. Instrum. Methods Phys. Res., Sect. B **77**, 110–116.

Anders, M., *et al.* (LUNA Collaboration), 2014, "First Direct Measurement of the ^{2}H(α,γ)^{6}Li Cross Section at Big Bang Energies and the Primordial Lithium Problem," Phys. Rev. Lett. **113**, 042501.

Angulo, C., and P. Descouvemont, 2000, "*R*-matrix analysis of interference effects in ^{12}C(α,α)^{12}C and ^{12}C(α,γ)^{16}O," Phys. Rev. C **61**, 064611.

Angulo, C., and P. Descouvemont, 2001, "The ^{14}N(p,γ)^{15}O low-energy *S*-factor," Nucl. Phys. **A690**, 755–768.

Angulo, C., S. Engstler, G. Raimann, C. Rolfs, W. H. Schulte, and E. Somorjai, 1993, "The effects of electron screening and resonances in (p,α) reactions on ^{10}B and ^{11}B at thermal energies," Z. Phys. A **345**, 231–242.

Angulo, C., W. H. Schulte, D. Zahnow, G. Raimann, and C. Rolfs, 1993, "Astrophysical $S(E)$ factor of ^{10}B(p,α_1)^{7}Be at low energies," Z. Phys. A **345**, 333–334.

Antoine, J.-P., 2021, "Quantum mechanics and its evolving formulations," Entropy **23**, 124.

Appel, S., *et al.* (Borexino Collaboration), 2022, "Improved Measurement of Solar Neutrinos from the Carbon-Nitrogen-Oxygen Cycle by Borexino and Its Implications for the Standard Solar Model," Phys. Rev. Lett. **129**, 252701.

Arnett, W. D., 1969, "A possible model of supernovae: Detonation of ^{12}C," Astrophys. Space Sci. **5**, 180–212.

Arnett, W. D., and J. W. Truran, 1969, "Carbon-burning nucleosynthesis at constant temperature," Astrophys. J. **157**, 339.

Artemov, S. V., *et al.*, 2022, "Asymptotic normalization coefficient for ^{12}C + $p \to {}^{13}$N from the ^{12}C(^{10}B, ^{9}Be)^{13}N reaction and the ^{12}C(p,γ)^{13}N astrophysical *S* factor," Eur. Phys. J. A **58**, 24.

Asplund, M., A. M. Amarsi, and N. Grevesse, 2021, "The chemical make-up of the Sun: A 2020 vision," Astron. Astrophys. **653**, A141.

Asplund, M., D. L. Lambert, P. E. Nissen, F. Primas, and V. V. Smith, 2006, "Lithium isotopic abundances in metal-poor halo stars," Astrophys. J. **644**, 229–259.

Assenbaum, H. J., K. Langanke, and C. Rolfs, 1987, "Effects of electron screening on low-energy fusion cross sections," Z. Phys. A **327**, 461–468.

Assunção, M., and P. Descouvemont, 2013, "Role of the Hoyle state in ^{12}C + ^{12}C fusion," Phys. Lett. B **723**, 355–359.

Assunção, M., *et al.*, 2006, "*E*1 and *E*2 *S* factors of ^{12}C(α,γ_0)^{16}O from γ-ray angular distributions with a 4π-detector array," Phys. Rev. C **73**, 055801.

Atkinson, M. C., K. Kravvaris, S. Quaglioni, and P. Navrátil, 2025, "*Ab initio* calculation of the ^{3}He(α,γ)^{7}Be astrophysical *S* factor with chiral two- and three-nucleon forces," Phys. Lett. B **860**, 139189.

Atkinson, R. D. E., and F. G. Houtermans, 1929, "Zur Frage der Aufbaumöglichkeit der Elemente in Sternen," Z. Phys. **54**, 656–665.

Auerbach, N., and N. Vinh Mau, 2000, "About Coulomb energy shifts in halo nuclei," Phys. Rev. C **63**, 017301.

Auerbach, N., and V. Zelevinsky, 2011, "Super-radiant dynamics, doorways and resonances in nuclei and other open mesoscopic systems," Rep. Prog. Phys. **74**, 106301.

Aumann, T., and C. A. Bertulani, 2020, "Indirect methods in nuclear astrophysics with relativistic radioactive beams," Prog. Part. Nucl. Phys. **112**, 103753.

Avila, M. L., G. V. Rogachev, E. Koshchiy, L. T. Baby, J. Belarge, K. W. Kemper, A. N. Kuchera, A. M. Mukhamedzhanov, D. Santiago-Gonzalez, and E. Uberseder, 2015a, "Constraining the 6.05 MeV 0^+ and 6.13 MeV 3^- Cascade Transitions in the ^{12}C(α,γ)^{16}O Reaction Using the Asymptotic Normalization Coefficients," Phys. Rev. Lett. **114**, 071101.

Avila, M. L., G. V. Rogachev, E. Koshchiy, L. T. Baby, J. Belarge, K. W. Kemper, A. N. Kuchera, and D. Santiago-Gonzalez, 2015b, "New measurement of the α asymptotic normalization coefficient of the $1/2^+$ state in ^{17}O at 6.356 MeV that dominates the ^{13}C(α,n)^{16}O reaction rate at temperatures relevant for the *s* process," Phys. Rev. C **91**, 048801.

Avila, M. L., G. V. Rogachev, E. Koshchiy, L. T. Baby, J. Belarge, K. W. Kemper, A. N. Kuchera, and D. Santiago-Gonzalez, 2014, "α-cluster asymptotic normalization coefficients for nuclear astrophysics," Phys. Rev. C **90**, 042801.

Avila, M. L., *et al.*, 2016, "Study of the ^{20,22}Ne + ^{20,22}Ne and ^{10,12,13,14,15}C + ^{12}C fusion reactions with MUSIC," EPJ Web Conf. **117**, 08009.

Ayyad, Y., *et al.*, 2019, "Direct Observation of Proton Emission in ^{11}Be," Phys. Rev. Lett. **123**, 082501.

Ayyad, Y., *et al.*, 2022, "Evidence of a Near-Threshold Resonance in ^{11}B Relevant to the β -Delayed Proton Emission of ^{11}Be," Phys. Rev. Lett. **129**, 012501.

Azuma, R. E., *et al.*, 2010, "AZURE: An *R*-matrix code for nuclear astrophysics," Phys. Rev. C **81**, 045805.

Babenko, V. A., and N. M. Petrov, 2013, "Low-energy parameters of neutron-neutron interaction in the effective-range approximation," Phys. At. Nucl. **76**, 684–689.

Baby, L. T., *et al.*, 2003, "Precision Measurement of the ^{7}Be(p,γ)^{8}B Cross Section with an Implanted ^{7}Be Target," Phys. Rev. Lett. **90**, 022501.

Back, B. B., H. Esbensen, C. L. Jiang, and K. E. Rehm, 2014, "Recent developments in heavy-ion fusion reactions," Rev. Mod. Phys. **86**, 317–360.

Bahcall, J. N., L. S. Brown, A. Gruzinov, and R. F. Sawyer, 2002, "The Salpeter plasma correction for solar fusion reactions," Astron. Astrophys. **383**, 291–295.

Bahcall, J. N., and C. P. Moeller, 1969, "The ^{7}Be Electron-capture rate," Astrophys. J. **155**, 511.

Bair, J. K., and F. X. Haas, 1973, "Total neutron yield from the reactions ^{13}C$(\alpha,n)^{16}$O and ^{17,18}O$(\alpha,n)^{20,21}$Ne," Phys. Rev. C **7**, 1356–1364.

Bak, P., C. Tang, and K. Wiesenfeld, 1987, "Self-Organized Criticality: An Explanation of the $1/f$ Noise," Phys. Rev. Lett. **59**, 381–384.

Balantekin, A. B., C. A. Bertulani, and M. S. Hussein, 1997, "Small effects in astrophysical fusion reactions," Nucl. Phys. **A627**, 324–333.

Banerjee, P., R. Chatterjee, and R. Shyam, 2008, "Coulomb dissociation of ^{9}Li and the rate of the ^{8}Li$(n,\gamma)^{9}$Li reaction," Phys. Rev. C **78**, 035804.

Bang, J. M., L. S. Ferreira, E. Maglione, and J. M. Hansteen, 1996, "Energy dependence of fusion cross sections," Phys. Rev. C **53**, R18–R19.

Barker, F. C., 1964, "A model for nuclear threshold levels," Proc. Phys. Soc. London **84**, 681–687.

Barker, F. C., and T. Kajino, 1991, "The ^{12}C$(\alpha,\gamma)^{16}$O cross section at low energies," Aust. J. Phys. **44**, 369.

Barnard, A. C. L., C. M. Jones, and G. C. Phillips, 1964, "The scattering of He^{3} by He^{4}," Nucl. Phys. **50**, 629–640.

Baroni, S., P. Navrátil, and S. Quaglioni, 2013a, "*Ab Initio* Description of the Exotic Unbound ^{7}He Nucleus," Phys. Rev. Lett. **110**, 022505.

Baroni, S., P. Navrátil, and S. Quaglioni, 2013b, "Unified *ab initio* approach to bound and unbound states: No-core shell model with continuum and its application to ^{7}He," Phys. Rev. C **87**, 034326.

Barrett, B. R., P. Navrátil, and J. P. Vary, 2013, "*Ab initio* no core shell model," Prog. Part. Nucl. Phys. **69**, 131–181.

Bartlett, A., J. Görres, G. J. Mathews, K. Otsuki, M. Wiescher, D. Frekers, A. Mengoni, and J. Tostevin, 2006, "Two-neutron capture reactions and the r process," Phys. Rev. C **74**, 015802.

Basilico, D., *et al.* (Borexino Collaboration), 2023, "Final results of Borexino on CNO solar neutrinos," Phys. Rev. D **108**, 102005.

Batley, J. R., *et al.* (NA48/2 Collaboration), 2006, "Observation of a cusp-like structure in the $\pi^0\pi^0$ invariant mass distribution from $K^{\pm}\to\pi^{\pm}\pi^0\pi^0$ decay and determination of the $\pi\pi$ scattering lengths," Phys. Lett. B **633**, 173–182.

Bauhoff, W., E. Caurier, B. Grammaticos, and M. Ploszajczak, 1985, "Description of light-ion collisions in the time-dependent cluster model," Phys. Rev. C **32**, 1915–1926.

Baur, G., 1986, "Breakup reactions as an indirect method to investigate low-energy charged-particle reactions relevant for nuclear astrophysics," Phys. Lett. B **178**, 135–138.

Baur, G., C. A. Bertulani, and H. Rebel, 1986, "Coulomb dissociation as a source of information on radiative capture processes of astrophysical interest," Nucl. Phys. **A458**, 188–204.

Baye, D., and E. Brainis, 2000, "Zero-energy determination of the astrophysical S factor and effective-range expansions," Phys. Rev. C **61**, 025801.

Baye, D., and P. Descouvemont, 1984, "Electromagnetic properties of the ^{12}C + ^{12}C and ^{16}O + ^{16}O quasimolecules in the generator coordinate method," Nucl. Phys. **A419**, 397–411.

Baye, D., and N. Pecher, 1982, "Microscopic investigation of the ^{12}C + ^{12}C interaction," Nucl. Phys. **A379**, 330–348.

Baz, A., 1957, "The energy dependence of a scattering cross section near the threshold of a reaction," J. Exp. Theor. Phys. **33**, 923, http://jetp.ras.ru/cgi-bin/dn/e_006_04_0709.pdf.

Baz', A. I., Y. B. Zel'dovich, and A. M. Perelomov, 1969, *Scattering, Reactions and Decay in Nonrelativistic Quantum Mechanics* (Israel Program for Scientific Translation, Jerusalem).

Beard, M., A. V. Afanasjev, L. C. Chamon, L. R. Gasques, M. Wiescher, and D. G. Yakovlev, 2010, "Astrophysical S factors for fusion reactions involving C, O, Ne, and Mg isotopes," At. Data Nucl. Data Tables **96**, 541–566.

Beard, M., E. Uberseder, R. Crowter, and M. Wiescher, 2014, "Comparison of statistical model calculations for stable isotope neutron capture," Phys. Rev. C **90**, 034619.

Becker, H. W., K. U. Kettner, C. Rolfs, and H. P. Trautvetter, 1981, "The ^{12}C + ^{12}C reaction at subcoulomb energies. II," Z. Phys. A **303**, 305–312.

Becker, H. W., W. E. Kieser, C. Rolfs, H. P. Trautvetter, and M. Wiescher, 1982, "Resonance strengths of some light nuclei," Z. Phys. A **305**, 319–323.

Bedaque, P. F., H. W. Hammer, and U. van Kolck, 2003, "Narrow resonances in effective field theory," Phys. Lett. B **569**, 159–167.

Bedaque, P. F., and U. van Kolck, 2002, "Effective field theory for few-nucleon systems," Annu. Rev. Nucl. Part. Sci. **52**, 339–396.

Bemmerer, D., *et al.*, 2006, "Activation Measurement of the ^{3}He$(\alpha,\gamma)^{7}$Be Cross Section at Low Energy," Phys. Rev. Lett. **97**, 122502.

Bennaceur, K., F. Nowacki, J. Okołowicz, and M. Płoszajczak, 1999, "Study of the ^{7}Be$(p,\gamma)^{8}$B and ^{7}Li$(n,\gamma)^{8}$Li capture reactions using the shell model embedded in the continuum," Nucl. Phys. **A651**, 289–319.

Bennaceur, K., F. Nowacki, J. Okołowicz, and M. Płoszajczak, 2000, "Analysis of the ^{16}O$(p,\gamma)^{17}$F capture reaction using the shell model embedded in the continuum," Nucl. Phys. **A671**, 203–232.

Bennett, C. H., and P. W. Shor, 1998, "Quantum information theory," IEEE Trans. Inf. Theory **44**, 2724–2742.

Bennett, M. E., *et al.*, 2012, "The effect of ^{12}C + ^{12}C rate uncertainties on the evolution and nucleosynthesis of massive stars," Mon. Not. R. Astron. Soc. **420**, 3047–3070.

Bergervoet, J. R., P. C. van Campen, W. A. van der Sanden, and J. J. de Swart, 1988, "Phase shift analysis of 0–30 MeV pp scattering data," Phys. Rev. C **38**, 15–50.

Berggren, T., 1968, "On the use of resonant states in eigenfunction expansions of scattering and reaction amplitudes," Nucl. Phys. **A109**, 265–287.

Berggren, T., 1978, "On the interpretation of complex cross sections for production of resonant final states," Phys. Lett. **73B**, 389–392.

Berggren, T., 1996, "Expectation value of an operator in a resonant state," Phys. Lett. B **373**, 1–4.

Berggren, T., and P. Lind, 1993, "Resonant state expansion of the resolvent," Phys. Rev. C **47**, 768–778.

Berrones-Santos, A., L. Benavides-Vázquez, E. Schaeffer, and J. Almaguer, 2022, "Fragmentation instability in aggregating systems," Physica (Amsterdam) **594A**, 127021.

Bertone, P. F., A. E. Champagne, M. Boswell, C. Iliadis, S. E. Hale, V. Y. Hansper, and D. C. Powell, 2002, "^{14}N(^{3}He, d)^{15}O as a probe of direct capture in the ^{14}N$(p,\gamma)^{15}$O reaction," Phys. Rev. C **66**, 055804.

Bertone, P. F., A. E. Champagne, D. C. Powell, C. Iliadis, S. E. Hale, and V. Y. Hansper, 2001, "Lifetime of the 6793-keV State in ^{15}O," Phys. Rev. Lett. **87**, 152501.

Bertulani, C., and P. Danielewicz, 2021, *Introduction to Nuclear Reactions*, 2nd ed. (Taylor & Francis, Bristol, England).

Bertulani, C. A., 1996, "^{7}Be$(p,\gamma)^{8}$B cross section from indirect breakup experiments," Z. Phys. A **356**, 293–297.

Bertulani, C. A., 1999, "The astrophysical reaction ^{8}Li$(n,\gamma)^{9}$Li from measurements by reverse kinematics," J. Phys. G **25**, 1959–1963.

Bertulani, C. A., 2004, "Electronic stopping in astrophysical fusion reactions," Phys. Lett. B **585**, 35–41.

Bertulani, C. A., and D. T. de Paula, 2000, "Stopping of swift protons in matter and its implication for astrophysical fusion reactions," Phys. Rev. C **62**, 045802.

Bertulani, C. A., and A. Gade, 2010, "Nuclear astrophysics with radioactive beams," Phys. Rep. **485**, 195–259.

Bertulani, C. A., H. W. Hammer, and U. van Kolck, 2002, "Effective field theory for halo nuclei: Shallow p-wave states," Nucl. Phys. **A712**, 37–58.

Bertulani, C. A., M. S. Hussein, and S. Typel, 2018, "Assessing the foundation of the Trojan horse method," Phys. Lett. B **776**, 217–221.

Bertulani, C. A., and T. Kajino, 2016, "Frontiers in nuclear astrophysics," Prog. Part. Nucl. Phys. **89**, 56–100.

Bertulani, C. A., and C. Spitaleri, 2017, "Nuclear clustering and the electron screening puzzle," EPJ Web Conf. **165**, 02002.

Bestelmeyer, B. T., 2006, "Threshold concepts and their use in rangeland management and restoration: The good, the bad, and the insidious," Restor. Ecol. **14**, 325–329.

Beth, E., and G. E. Uhlenbeck, 1937, "The quantum theory of the non-ideal gas. II. Behaviour at low temperatures," Physica (Amsterdam) **4**, 915–924.

Bethe, H. A., 1937, "Nuclear physics B. Nuclear dynamics, theoretical," Rev. Mod. Phys. **9**, 69–244.

Bethe, H. A., 1939, "Energy production in stars," Phys. Rev. **55**, 434–456.

Bethe, H. A., 1949, "Theory of the effective range in nuclear scattering," Phys. Rev. **76**, 38–50.

Bethe, H. A., G. E. Brown, J. Applegate, and J. M. Lattimer, 1979, "Equation of state in the gravitational collapse of stars," Nucl. Phys. **A324**, 487–533.

Bilodeau, R. C., I. Dumitriu, N. D. Gibson, C. W. Walter, and N. Berrah, 2009, "Promoting a core electron to fill a d-shell in negative ions: Shape versus Feshbach resonances and a novel threshold law," J. Phys. Conf. Ser. **194**, 022095.

Birse, M. C., 1999, "A renormalisation-group treatment of two-body scattering," Phys. Lett. B **464**, 169–176.

Bisterzo, S., R. Gallino, F. Käppeler, M. Wiescher, G. Imbriani, O. Straniero, S. Cristallo, J. Görres, and R. J. deBoer, 2015, "The branchings of the main s-process: Their sensitivity to α-induced reactions on ^{13}C and ^{22}Ne and to the uncertainties of the nuclear network," Mon. Not. R. Astron. Soc. **449**, 506–527.

Blaes, O. M., R. D. Blandford, P. Madau, and L. Yan, 1992, "On the evolution of slowly accreting neutron stars," Astrophys. J. **399**, 634.

Blake, J. B., and D. N. Schramm, 1976, "A possible alternative to the R-process," Astrophys. J. **209**, 846–849.

Blatt, S. L., A. M. Young, S. C. Ling, K. J. Moon, and C. D. Porterfield, 1968, "Reaction $t(^{3}\mathrm{He},\gamma)^{6}$Li in the energy range 0.5–11 MeV," Phys. Rev. **176**, 1147–1153.

Bloch, C., 1957, "Une formulation unifiée de la théorie des réactions nucléaires," Nucl. Phys. **4**, 503–528.

Bloch, I., M. H. Hull, A. A. Broyles, W. G. Bouricius, B. E. Freeman, and G. Breit, 1951, "Coulomb functions for reactions of protons and alpha-particles with the lighter nuclei," Rev. Mod. Phys. **23**, 147–182.

Bodansky, D., D. D. Clayton, and W. A. Fowler, 1968, "Nuclear quasi-equilibrium during silicon burning," Astrophys. J. Suppl. Ser. **16**, 299.

Boeltzig, A., *et al.*, 2019, "Direct measurements of low-energy resonance strengths of the ^{23}Na$(p,\gamma)^{24}$Mg reaction for astrophysics," Phys. Lett. B **795**, 122–128.

Boeltzig, A., *et al.*, 2022, "Investigation of direct capture in the ^{23}Na$(p,\gamma)^{24}$Mg reaction," Phys. Rev. C **106**, 045801.

Bohm, A., 1978, *The Rigged Hilbert Space and Quantum Mechanics: Lectures in Mathematical Physics at the University of Texas*, Lecture Notes in Physics Vol. 78 (Springer-Verlag, New York).

Bohm, A., J. D. Dollard, and M. Gadella, 1989, *Dirac Kets, Gamow Vectors and Gel'fand Triplets: The Rigged Hilbert Space Formulation of Quantum Mechanics*, Lecture Notes in Physics Vol. 348 (Springer-Verlag, Berlin).

Bonasera, A., and J. B. Natowitz, 2020, "Calculation of the $^{12}\mathrm{C}+{}^{12}\mathrm{C}$ sub-barrier fusion cross section in an imaginary-time-dependent mean field theory," Phys. Rev. C **102**, 061602.

Bonetti, R., *et al.*, 1999, "First Measurement of the ^{3}He$(^{3}\mathrm{He},2p)^{4}$He Cross Section down to the Lower Edge of the Solar Gamow Peak," Phys. Rev. Lett. **82**, 5205–5208.

Bordeanu, C., G. Gyürky, Z. Halász, T. Szücs, G. G. Kiss, Z. Elekes, J. Farkas, Z. Fülöp, and E. Somorjai, 2013, "Activation measurement of the ^{3}He$(\alpha,\gamma)^{7}$Be reaction cross section at high energies," Nucl. Phys. **A908**, 1–11.

Bosch, H. S., and G. M. Hale, 1992, "Improved formulas for fusion cross-sections and thermal reactivities," Nucl. Fusion **32**, 611–631.

Bracci, L., G. Fiorentini, V. S. Melezhik, G. Mezzorani, and P. Pasini, 1991, "Quantum mechanical calculation of the electron screening in d-D fusion," Phys. Lett. A **153**, 456–460.

Bracci, L., G. Fiorentini, and G. Mezzorani, 1990, "A dynamical calculation of the electron shielding for d-D fusion," Phys. Lett. A **146**, 128–133.

Bravo, E., and D. García-Senz, 1999, "Coulomb corrections to the equation of state of nuclear statistical equilibrium matter: implications for SNIa nucleosynthesis and the accretion-induced collapse of white dwarfs," Mon. Not. R. Astron. Soc. **307**, 984–992.

Bravo, E., L. Piersanti, I. Domínguez, O. Straniero, J. Isern, and J. A. Escartin, 2011, "Type Ia supernovae and the $^{12}\mathrm{C}+{}^{12}\mathrm{C}$ reaction rate," Astron. Astrophys. **535**, A114.

Breit, G., 1957, "Energy dependence of reactions at thresholds," Phys. Rev. **107**, 1612–1615.

Breit, G., and E. Wigner, 1936, "Capture of slow neutrons," Phys. Rev. **49**, 519–531.

Brenig, W., 1959, "Two particle approximations of the many body problem (II)," Nucl. Phys. **13**, 333–349.

Bretscher, E., and A. P. French, 1949, "Low energy cross section of the $D-T$ reaction and angular distribution of the alpha-particles emitted," Phys. Rev. **75**, 1154–1160.

Bromley, D. A., J. A. Kuehner, and E. Almqvist, 1960, "Resonant Elastic Scattering of C^{12} by Carbon," Phys. Rev. Lett. **4**, 365–367.

Bromley, D. A., J. A. Kuehner, and E. Almqvist, 1961, "Elastic scattering of identical spin-zero nuclei," Phys. Rev. **123**, 878–893.

Brookes, J. C., 2017, "Quantum effects in biology: Golden rule in enzymes, olfaction, photosynthesis and magnetodetection," Proc. R. Soc. A **473**, 20160822.

Brown, D. A., *et al.*, 2018, "ENDF/B-VIII.0: The 8th major release of the nuclear reaction data library with CIELO-project cross sections, new standards and thermal scattering data," Nucl. Data Sheets **148**, 1–142.

Brown, E. F., and A. Cumming, 2009, "Mapping crustal heating with the cooling light curves of quasi-persistent transients," Astrophys. J. **698**, 1020–1032.

Brown, L. S., and R. F. Sawyer, 1997, "Nuclear reaction rates in a plasma," Rev. Mod. Phys. **69**, 411–436.

Brown, T. A. D., C. Bordeanu, K. A. Snover, D. W. Storm, D. Melconian, A. L. Sallaska, S. K. L. Sjue, and S. Triambak, 2007, "^{3}He + ^{4}He^{7}Be astrophysical *S* factor," Phys. Rev. C **76**, 055801.

Brune, C. R., 2020, "Spectroscopic factors, overlaps, and isospin symmetry from an *R*-matrix point of view," Phys. Rev. C **102**, 034328.

Brune, C. R., W. H. Geist, R. W. Kavanagh, and A. K. Veal, 1999, "Sub-Coulomb α Transfers on ^{12}C and the $^{12}C(\alpha,\gamma)^{16}$OS Factor," Phys. Rev. Lett. **83**, 4025–4028.

Bruno, C. G., *et al.*, 2019, "Improved astrophysical rate for the $^{18}O(p,\alpha)^{15}$N reaction by underground measurements," Phys. Lett. B **790**, 237–242.

Buchmann, L., R. E. Azuma, C. A. Barnes, J. M. D'Auria, M. Dombsky, U. Giesen, K. P. Jackson, J. D. King, R. G. Korteling, and P. McNeely, 1993, "β-Delayed α Spectrum of ^{16}N and the $^{12}C(\alpha,\gamma)^{16}$O Cross Section at Low Energies," Phys. Rev. Lett. **70**, 726–729.

Buchmann, L. R., and C. A. Barnes, 2006, "Nuclear reactions in stellar helium burning and later hydrostatic burning stages," Nucl. Phys. **A777**, 254–290.

Buldgen, G., P. Eggenberger, A. Noels, R. Scuflaire, A. M. Amarsi, N. Grevesse, and S. Salmon, 2023, "Higher metal abundances do not solve the solar problem," Astron. Astrophys. **669**, L9.

Buompane, R., *et al.*, 2022, "Determination of the $^7Be(p,\gamma)^8$B cross section at astrophysical energies using a radioactive ^{7}Be ion beam," Phys. Lett. B **824**, 136819.

Burbidge, E. M., G. R. Burbidge, W. A. Fowler, and F. Hoyle, 1957, "Synthesis of the elements in stars," Rev. Mod. Phys. **29**, 547–650.

Caciolli, A., *et al.*, 2016, "A new study of $^{10}B(p,\alpha)^7$Be reaction at low energies," Eur. Phys. J. A **52**, 136.

Cameron, A. G. W., 1959, "Pycnonuclear reactions and nova explosions," Astrophys. J. **130**, 916.

Canto, L. F., and M. S. Hussein, 2013, *Scattering Theory of Molecules, Atoms and Nuclei* (World Scientific, Singapore).

Capel, P., D. R. Phillips, and H. W. Hammer, 2018, "Dissecting reaction calculations using halo effective field theory and *ab initio* input," Phys. Rev. C **98**, 034610.

Capel, P., *et al.*, 2023, "Effective field theory analysis of the Coulomb breakup of the one-neutron halo nucleus ^{19}C," Eur. Phys. J. A **59**, 273.

Caradonna, P., C. Makochekanwa, A. Jones, J. R. Machacek, J. P. Sullivan, and S. J. Buckman, 2012, "A search for Wigner cusps and resonances in positron scattering by atoms and molecules," J. Phys. Conf. Ser. **388**, 072012.

Carmona-Gallardo, M., *et al.*, 2012, "New measurement of the $^3He(\alpha,\gamma)^7$Be cross section at medium energies," Phys. Rev. C **86**, 032801.

Carnelli, P. F. F., *et al.*, 2014, "Measurements of Fusion Reactions of Low-Intensity Radioactive Carbon Beams on ^{12}C and Their Implications for the Understanding of X-Ray Bursts," Phys. Rev. Lett. **112**, 192701.

Carraro, C., A. Schafer, and S. E. Koonin, 1988, "Dynamic screening of thermonuclear reactions," Astrophys. J. **331**, 565.

Casey, D. T., *et al.*, 2017, "Thermonuclear reactions probed at stellar-core conditions with laser-based inertial-confinement fusion," Nat. Phys. **13**, 1227–1231.

Casey, D. T., *et al.*, 2023, "Towards the first plasma-electron screening experiment," Front. Phys. **10**, 1057603.

Caughlan, G. R., and W. A. Fowler, 1988, "Thermonuclear reaction rates V," At. Data Nucl. Data Tables **40**, 283.

Caurier, E., B. Grammaticos, and T. Sami, 1982, "The time dependent cluster model," Phys. Lett. **109B**, 150–154.

Celardo, G. L., N. Auerbach, F. M. Izrailev, and V. G. Zelevinsky, 2011, "Distribution of Resonance Widths and Dynamics of Continuum Coupling," Phys. Rev. Lett. **106**, 042501.

Cerjan, C. J., *et al.*, 2018, "Dynamic high energy density plasma environments at the National Ignition Facility for nuclear science research," J. Phys. G **45**, 033003.

Chaboyer, B., P. Demarque, P. J. Kernan, and L. M. Krauss, 1996, "A lower limit on the age of the Universe," Science **271**, 957–961.

Chadwick, M. B., G. M. Hale, M. W. Paris, J. P. Lestone, C. Bates, J. B. Wilhelmy, S. A. Andrews, W. Tornow, and S. W. Finch, 2023, "The earliest DT nuclear fusion discoveries," arXiv:2302.04206.

Chadwick, M. B., M. W. Paris, and B. M. Haines, 2023, "*dt* fusion through the ^{5}He $3/2^+$ 'Bretscher state' accounts for $\geq 25\%$ of our existence via nucleosynthesis and for the possibility of fusion energy," arXiv:2305.00647.

Chae, K. Y., *et al.*, 2012, "Searching for resonances in the unbound ^{6}Be nucleus by using a radioactive ^{7}Be beam," J. Korean Phys. Soc. **61**, 1786–1791.

Chamon, L. C., B. V. Carlson, and L. R. Gasques, 2021, "São Paulo potential version 2 (SPP2) and Brazilian nuclear potential (BNP)," Comput. Phys. Commun. **267**, 108061.

Charity, R. J., *et al.*, 2019, "Invariant-mass spectroscopy of ^{14}O excited states," Phys. Rev. C **100**, 064305.

Charity, R. J., *et al.*, 2021, "Observation of the Exotic Isotope ^{13}F Located Four Neutrons beyond the Proton Drip Line," Phys. Rev. Lett. **126**, 132501.

Charity, R. J., *et al.*, 2023, "Strong Evidence for ^{9}N and the Limits of Existence of Atomic Nuclei," Phys. Rev. Lett. **131**, 172501.

Chen, J., *et al.*, 2021, "Observation of the near-threshold intruder 0^- resonance in ^{12}Be," Phys. Rev. C **103**, L031302.

Chen, J.-W., H. W. Grießhammer, M. J. Savage, and R. P. Springer, 1998, "The polarizability of the deuteron," Nucl. Phys. **A644**, 221–234.

Chen, J.-W., G. Rupak, and M. J. Savage, 1999, "Nucleon-nucleon effective field theory without pions," Nucl. Phys. **A653**, 386–412.

Chen, M. C., F. Herwig, P. A. Denissenkov, and B. Paxton, 2014, "The dependence of the evolution of Type Ia SN progenitors on the C-burning rate uncertainty and parameters of convective boundary mixing," Mon. Not. R. Astron. Soc. **440**, 1274–1280.

Chen, Y., *et al.*, 2021, "Neutron transfer studies on ^{25}Mg and its correlation to neutron radiative capture processes," Phys. Rev. C **103**, 035809.

Chernykh, M., H. Feldmeier, T. Neff, P. von Neumann-Cosel, and A. Richter, 2007, "Structure of the Hoyle State in ^{12}C," Phys. Rev. Lett. **98**, 032501.

Chidester, M. T., F. X. Timmes, and E. Farag, 2023, "Seismic signatures of the $^{12}C(\alpha,\gamma)^{16}$O reaction rate in white dwarf models with overshooting," Astrophys. J. **954**, 51.

Chieffi, A., L. Roberti, M. Limongi, M. La Cognata, L. Lamia, S. Palmerini, R. G. Pizzone, R. Spartà, and A. Tumino, 2021, "Impact of the new measurement of the $^{12}C + ^{12}$C fusion cross section on the final compactness of massive stars," Astrophys. J. **916**, 79.

Chow, H. C., G. M. Griffiths, and T. H. Hall, 1975, "The $^{16}O(p,\gamma)^{17}$F direct capture cross section with an extrapolation to astrophysical energies," Can. J. Phys. **53**, 1672–1686.

Christensen, P. R., Z. E. Switkowskiw, and R. A. Dayras, 1977, "Sub-barrier fusion measurements for $^{12}C + ^{16}$O," Nucl. Phys. **A280**, 189–204.

Christy, R. F., and I. Duck, 1961, "γ rays from an extranuclear direct capture process," Nucl. Phys. **24**, 89–101.

Ciani, G. F., *et al.* (LUNA Collaboration), 2021, "Direct Measurement of the $^{13}C(\alpha,n)^{16}$O Cross Section into the *s*-Process Gamow Peak," Phys. Rev. Lett. **127**, 152701.

Cierjacks, S., F. Hinterberger, G. Schmalz, D. Erbe, P. v. Rossen, and B. Leugers, 1980, "High precision time-of-flight measurements of neutron resonance energies in carbon and oxygen between 3 and 30 MeV," Nucl. Instrum. Methods **169**, 185–198.

Clarkson, O., F. Herwig, and M. Pignatari, 2018, "Pop III *i*-process nucleosynthesis and the elemental abundances of SMSS J0313-6708 and the most iron-poor stars," Mon. Not. R. Astron. Soc. **474**, L37–L41.

Clifford, F. E., and R. J. Tayler, 1965, "The equilibrium distribution of nuclides in matter at high temperatures," Mon. Not. R. Astron. Soc. **129**, 104.

Confortola, F., *et al.*, 2007, "Astrophysical S factor of the $^3\mathrm{He}(\alpha,\gamma)^7\mathrm{Be}$ reaction measured at low energy via detection of prompt and delayed γ rays," Phys. Rev. C **75**, 065803.

Cooper, M. D., W. Galati, and W. F. Hornyak, 1974, "Extraction of spectroscopic factors using R-matrix theory," Nucl. Phys. **A221**, 528–540.

Cooper, R. L., A. W. Steiner, and E. F. Brown, 2009, "Possible resonances in the $^{12}\mathrm{C}+{}^{12}\mathrm{C}$ fusion rate and superburst ignition," Astrophys. J. **702**, 660–671.

Corbari, G., *et al.*, 2023, "γ decay from the near-neutron-threshold 2^+ state in $^{14}\mathrm{C}$: A probe of collectivization phenomena in light nuclei," Acta Phys. Pol. B Proc. Suppl. **16**, 4–A33.

Costantini, H., *et al.*, 2008, "The $^3\mathrm{He}(\alpha,\gamma)^7\mathrm{Be}$ S-factor at solar energies: The prompt γ experiment at LUNA," Nucl. Phys. **A814**, 144–158.

Costantini, H., *et al.*, 2010, "$^{16}\mathrm{O}(\alpha,\gamma)^{20}\mathrm{Ne}$ S factor: Measurements and R-matrix analysis," Phys. Rev. C **82**, 035802.

Cowan, J. J., C. Sneden, J. E. Lawler, A. Aprahamian, M. Wiescher, K. Langanke, G. Martínez-Pinedo, and F.-K. Thielemann, 2021, "Origin of the heaviest elements: The rapid neutron-capture process," Rev. Mod. Phys. **93**, 015002.

Cruz, J., *et al.*, 2008, "Experimental study of proton-induced nuclear reactions in $^{6,7}\mathrm{Li}$," J. Phys. G **35**, 014004.

Csedreki, L., G. Gyürky, and T. Szücs, 2023, "Precise resonance parameter measurement in the $^{12}\mathrm{C}(p,\gamma)^{13}\mathrm{N}$ astrophysically important reaction," Nucl. Phys. **A1037**, 122705.

Csótó, A., and K. Langanke, 1998, "Effects of $^8\mathrm{B}$ size on the low-energy $^7\mathrm{Be}(p,\gamma)^8\mathrm{B}$ cross section," Nucl. Phys. **A636**, 240–246.

Csótó, A., and K. Langanke, 2000, "Study of the $^3\mathrm{He}(^4\mathrm{He},\gamma)^7\mathrm{Be}$ and $^3\mathrm{H}(^4\mathrm{He},\gamma)^7\mathrm{Li}$ reactions in an extended two-cluster model," Few-Body Syst. **29**, 121–130.

Csótó, A., K. Langanke, S. E. Koonin, and T. D. Shoppa, 1995, "$^7\mathrm{Be}(p,\gamma)^8\mathrm{B}$ cross section and the properties of $^7\mathrm{Be}$," Phys. Rev. C **52**, 1130–1133.

Cumming, A., and L. Bildsten, 2001, "Carbon flashes in the heavy-element ocean on accreting neutron stars," Astrophys. J. Lett. **559**, L127–L130.

Cumming, A., J. Macbeth, J. J. M. in 't Zand, and D. Page, 2006, "Long type I x-ray bursts and neutron star interior physics," Astrophys. J. **646**, 429–451.

Cussons, R., K. Langanke, and T. Liolios, 2002, "Potential resonant screening effects on stellar $^{12}\mathrm{C}+{}^{12}\mathrm{C}$ reaction rates," Eur. Phys. J. A **15**, 291–293.

Cvetinović, A., M. Lipoglavšek, S. Markelj, and J. Vesić, 2015, "Large electron screening effect in different environments," AIP Conf. Ser. **1681**, 060002.

Cvetinović, A., *et al.*, 2018, "Trojan horse measurement of the $^{10}\mathrm{B}(p,\alpha_0)^7\mathrm{Be}$ cross section in the energy range from 3 keV to 2.2 MeV," Phys. Rev. C **97**, 065801.

Cyburt, R. H., B. D. Fields, K. A. Olive, and T.-H. Yeh, 2016, "Big bang nucleosynthesis: Present status," Rev. Mod. Phys. **88**, 015004.

Cyburt, R. H., *et al.*, 2010, "The JINA REACLIB database: Its recent updates and impact on type-I x-ray bursts," Astrophys. J. Suppl. Ser. **189**, 240–252.

Czerski, K., A. Huke, P. Heide, and G. Ruprecht, 2004, "The $^2\mathrm{H}(d,p)^3\mathrm{H}$ reaction in metallic media at very low energies," Europhys. Lett. **68**, 363–369.

Dasgupta, M., D. J. Hinde, A. Diaz-Torres, B. Bouriquet, C. I. Low, G. J. Milburn, and J. O. Newton, 2007, "Beyond the Coherent Coupled Channels Description of Nuclear Fusion," Phys. Rev. Lett. **99**, 192701.

Dasmahapatra, B., and B. Čujec, 1993, "Measurement of cross sections for $^{12}\mathrm{C}+{}^{14}\mathrm{C}$ reaction at subbarrier energies," Nucl. Phys. **A565**, 657–670.

Dasmahapatra, B., B. Čujec, and F. Lahlou, 1982, "Fusion cross sections for $^{12}\mathrm{C}+{}^{12}\mathrm{C}$, $^{12}\mathrm{C}+{}^{13}\mathrm{C}$ and $^{13}\mathrm{C}+{}^{13}\mathrm{C}$ at low energies," Nucl. Phys. **A384**, 257–272.

Davids, B., and S. Typel, 2003, "Electromagnetic dissociation of $^8\mathrm{B}$ and the astrophysical S factor for $^7\mathrm{Be}(p,\gamma)^8\mathrm{B}$," Phys. Rev. C **68**, 045802.

Davids, C. N., 1968, "A study of (α,n) reactions on $^9\mathrm{Be}$ and $^{13}\mathrm{C}$ at low energies," Nucl. Phys. **A110**, 619–636.

deBoer, R. J., C. R. Brune, M. Febrarro, J. Görres, I. J. Thompson, and M. Wiescher, 2020, "Sensitivity of the $^{13}\mathrm{C}(\alpha,n)^{16}\mathrm{O}$ S factor to the uncertainty in the level parameters of the near-threshold state," Phys. Rev. C **101**, 045802.

deBoer, R. J., O. Clarkson, A. J. Couture, J. Görres, F. Herwig, I. Lombardo, P. Scholz, and M. Wiescher, 2021, "$^{19}\mathrm{F}(p,\gamma)^{20}\mathrm{Ne}$ and $^{19}\mathrm{F}(p,\alpha\gamma)^{16}\mathrm{O}$ reaction rates and their effect on calcium production in Population III stars from hot CNO breakout," Phys. Rev. C **103**, 055815.

deBoer, R. J., J. Görres, K. Smith, E. Uberseder, M. Wiescher, A. Kontos, G. Imbriani, A. Di Leva, and F. Strieder, 2014, "Monte Carlo uncertainty of the $^3\mathrm{He}(\alpha,\gamma)^7\mathrm{Be}$ reaction rate," Phys. Rev. C **90**, 035804.

deBoer, R. J., *et al.*, 2015, "Low energy scattering cross section ratios of $^{14}\mathrm{N}(p,p)^{14}\mathrm{N}$," Phys. Rev. C **91**, 045804.

deBoer, R. J., *et al.*, 2017, "The $^{12}\mathrm{C}(\alpha,\gamma)^{16}\mathrm{O}$ reaction and its implications for stellar helium burning," Rev. Mod. Phys. **89**, 035007.

deBoer, R. J., *et al.*, 2024, "Measurement of the $^{13}\mathrm{C}(\alpha,n_0)^{16}\mathrm{O}$ Differential Cross Section from 0.8 to 6.5 MeV," Phys. Rev. Lett. **132**, 062702.

Debye, P., and E. Hückel, 1923, "De la theorie des electrolytes. I. Abaissement du point de congelation et phenomenes associes," Phys. Z. **24**, 185–206, https://perso.uclouvain.be/ernest.matagne/SOLAIRE/SEM11/Debye.doc.

de Grancey, F., *et al.*, 2016, "An above-barrier narrow resonance in $^{15}\mathrm{F}$," Phys. Lett. B **758**, 26–31.

de la Madrid, R., 2005, "The role of the rigged Hilbert space in quantum mechanics," Eur. J. Phys. **26**, 287–312.

de la Madrid, R., 2012, "The rigged Hilbert space approach to the Gamow states," J. Math. Phys. (N.Y.) **53**, 102113–102113.

Delion, D. S., and J. Suhonen, 2001, "Microscopic description of $\alpha+{}^{40}\mathrm{Ca}$ quasimolecular resonances," Phys. Rev. C **63**, 061306.

Deltuva, A., 2018, "Tetraneutron: Rigorous continuum calculation," Phys. Lett. B **782**, 238–241.

Deltuva, A., and A. C. Fonseca, 2007, "Four-Body Calculation of Proton-$^3\mathrm{He}$ Scattering," Phys. Rev. Lett. **98**, 162502.

Denisov, V. Y., and N. A. Pilipenko, 2010, "Fusion of deformed nuclei: $^{12}\mathrm{C}+{}^{12}\mathrm{C}$," Phys. Rev. C **81**, 025805.

Denissenkov, P. A., F. Herwig, U. Battino, C. Ritter, M. Pignatari, S. Jones, and B. Paxton, 2017, "*i*-process nucleosynthesis and mass retention efficiency in He-shell flash evolution of rapidly accreting white dwarfs," Astrophys. J. Lett. **834**, L10.

Denissenkov, P. A., F. Herwig, P. Woodward, R. Andrassy, M. Pignatari, and S. Jones, 2019, "The i-process yields of rapidly accreting white dwarfs from multicycle He-shell flash stellar evolution models with mixing parametrizations from 3D hydrodynamics simulations," Mon. Not. R. Astron. Soc. **488**, 4258–4270.

Depastas, T., S. T. Sun, H. Zheng, and A. Bonasera, 2023, "α-cluster microscopic study of $^{12}C + ^{12}C$ fusion toward the zero energy limit," Phys. Rev. C **108**, 035806.

Descouvemont, P., 1987, "Microscopic analysis of the $^{13}C(\alpha,n)^{16}O$ and $^{13}C(\alpha,\alpha)^{13}C$ reactions," Phys. Rev. C **36**, 2206–2211.

Descouvemont, P., 1993a, "Microscopic models for nuclear reaction rates," J. Phys. G **19**, S141–S152.

Descouvemont, P., 1993b, "The $^{8}Li(n,\gamma)^{9}Li$ and $^{8}B(p,\gamma)^{9}C$ mirror reactions in a microscopic cluster model," Astrophys. J. **405**, 518.

Descouvemont, P., 2004, "Reanalysis of the $^{7}Be(p,\gamma)^{8}Be$ S factor in a microscopic model," Phys. Rev. C **70**, 065802.

Descouvemont, P., A. Adahchour, C. Angulo, A. Coc, and E. Vangioni-Flam, 2004, "Compilation and R-matrix analysis of big bang nuclear reaction rates," At. Data Nucl. Data Tables **88**, 203–236.

Descouvemont, P., and D. Baye, 1987, "$^{12}C(\alpha,\gamma)^{16}O$ reaction in a multiconfiguration microscopic model," Phys. Rev. C **36**, 1249–1255.

Descouvemont, P., and D. Baye, 1988, "The $^{7}Be(p,\gamma)^{8}B$ reaction in a microscopic three-cluster model," Nucl. Phys. **A487**, 420–432.

Descouvemont, P., and D. Baye, 2010, "The R-matrix theory," Rep. Prog. Phys. **73**, 036301.

Descouvemont, P., D. Baye, and P. H. Heenen, 1984, "Microscopic analysis of the $^{12}C(\alpha,\gamma)^{16}O$ reaction," Nucl. Phys. **A430**, 426–444.

de Souza, R. S., S. R. Boston, A. Coc, and C. Iliadis, 2019, "Thermonuclear fusion rates for tritium + deuterium using Bayesian methods," Phys. Rev. C **99**, 014619.

Dewitt, H. E., H. C. Graboske, and M. S. Cooper, 1973, "Screening factors for nuclear reactions. I. General theory," Astrophys. J. **181**, 439–456.

Diaz-Torres, A., 2008, "Solving the Two-Center Nuclear Shell-Model Problem with Arbitrarily Oriented Deformed Potentials," Phys. Rev. Lett. **101**, 122501.

Diaz-Torres, A., L. R. Gasques, and N. V. Antonenko, 2024, "Cluster effects on low-energy carbon burning," Phys. Lett. B **849**, 138476.

Diaz-Torres, A., L. R. Gasques, and M. Wiescher, 2007, "Effects of nuclear molecular configurations on the astrophysical S-factor for $^{16}O + ^{16}O$," Phys. Lett. B **652**, 255–258.

Diaz-Torres, A., and M. Wiescher, 2018, "Characterizing the astrophysical S factor for $^{12}C + ^{12}C$ fusion with wave-packet dynamics," Phys. Rev. C **97**, 055802.

Dicke, R. H., 1954, "Coherence in spontaneous radiation processes," Phys. Rev. **93**, 99–110.

Dickhoff, W. H., 2010, "Determining and calculating spectroscopic factors from stable nuclei to the drip lines," J. Phys. G **37**, 064007.

di Leva, A., et al., 2009, "Stellar and Primordial Nucleosynthesis of ^{7}Be: Measurement of $^{3}He(\alpha,\gamma)^{7}Be$," Phys. Rev. Lett. **102**, 232502.

Dobaczewski, J., N. Michel, W. Nazarewicz, M. Płoszajczak, and J. Rotureau, 2007, "Shell structure of exotic nuclei," Prog. Part. Nucl. Phys. **59**, 432–445.

Dobaczewski, J., and W. Nazarewicz, 1998, "Theoretical aspects of science with radioactive nuclear beams," Phil. Trans. R. Soc. A **356**, 2007–2031.

Dohet-Eraly, J., P. Navrátil, S. Quaglioni, W. Horiuchi, G. Hupin, and F. Raimondi, 2016, "$^{3}He(\alpha,\gamma)^{7}Be$ and $^{3}H(\alpha,\gamma)^{7}Li$ astrophysical S factors from the no-core shell model with continuum," Phys. Lett. B **757**, 430–436.

Domcke, W., 1981, "Analytic theory of resonances, virtual states and bound states ion electron-molecule scattering and related processes," J. Phys. B **14**, 4889–4922.

Dong, G. X., X. B. Wang, N. Michel, and M. Płoszajczak, 2022, "Gamow shell model description of the radiative capture reaction $^{8}Li(n,\gamma)^{9}Li$," Phys. Rev. C **105**, 064608.

Dong, G. X., X. B. Wang, N. Michel, and M. Płoszajczak, 2023a, "Erratum: Gamow shell model description of the radiative capture reaction $^{8}B(p,\gamma)^{9}C$ [Phys. Rev. C **107**, 044613 (2023)]," Phys. Rev. C **108**, 049903.

Dong, G. X., X. B. Wang, N. Michel, and M. Płoszajczak, 2023b, "Erratum: Gamow shell model description of the radiative capture reaction $^{8}Li(n,\gamma)^{9}Li$ [Phys. Rev. C **105**, 064608 (2022)]," Phys. Rev. C **108**, 049902.

Dong, G. X., X. B. Wang, N. Michel, and M. Płoszajczak, 2023c, "Gamow shell model description of the radiative capture reaction $^{8}B(p,\gamma)^{9}C$," Phys. Rev. C **107**, 044613.

Drotleff, H. W., A. Denker, H. Knee, M. Soine, G. Wolf, J. W. Hammer, U. Greife, C. Rolfs, and H. P. Trautvetter, 1993, "Reaction rates of the s-process neutron sources $^{22}Ne(\alpha,n)^{25}Mg$ and $^{13}C(\alpha,n)^{16}O$," Astrophys. J. **414**, 735.

Drożdż, S., J. Okołowicz, and M. Płoszajczak, 1982, "The time-dependent cluster theory—Application to the α-α collision," Phys. Lett. **109B**, 145–149.

Drożdż, S., J. Okołowicz, M. Płoszajczak, and I. Rotter, 2000, "Statistical aspects of nuclear coupling to continuum," Phys. Rev. C **62**, 024313.

Dubovichenko, S. B., 2010, "Astrophysical S factors of radiative $^{3}He^{4}He$, $^{3}H^{4}He$, and $^{2}H^{4}He$ capture," Phys. At. Nucl. **73**, 1526–1538.

Dubovichenko, S. B., and A. V. Dzhazairov-Kakhramanov, 2016, "The reaction $^{8}Li(n,\gamma)^{9}Li$ at astrophysical energies and its role in primordial nucleosynthesis," Astrophys. J. **819**, 78.

Dück, P., H. Fröhlich, W. Galster, W. Treu, and H. Voit, 1978, "Reaction $^{10}B(^{14}N,\alpha)^{20}Ne$ at $E_{c.m.} \approx 10$ MeV," Phys. Rev. C **18**, 290–292.

Duer, M., et al., 2022, "Observation of a correlated free four-neutron system," Nature (London) **606**, 678–682.

Dufour, M., and P. Descouvemont, 2008, "$^{12}C(\alpha,\gamma)^{16}O$ $E2$ cross section: R-matrix fits combined with a microscopic cluster model," Phys. Rev. C **78**, 015808.

Dyer, P., and C. A. Barnes, 1974, "The $^{12}C(\alpha,\gamma)^{16}O$ reaction and stellar helium burning," Nucl. Phys. **A233**, 495–520.

Dytrych, T., K. D. Launey, J. P. Draayer, D. J. Rowe, J. L. Wood, G. Rosensteel, C. Bahri, D. Langr, and R. B. Baker, 2020, "Physics of Nuclei: Key Role of an Emergent Symmetry," Phys. Rev. Lett. **124**, 042501.

Ehrman, J. B., 1951, "On the displacement of corresponding energy levels of C^{13} and N^{13}," Phys. Rev. **81**, 412–416.

Ekström, A., C. Forssén, G. Hagen, G. R. Jansen, W. Jiang, and T. Papenbrock, 2023, "What is *ab initio* in nuclear theory?," Front. Phys. **11**, 1129094.

Elhatisari, S., D. Lee, G. Rupak, E. Epelbaum, H. Krebs, T. A. Lähde, T. Luu, and U.-G. Meißner, 2015, "*Ab initio* alpha-alpha scattering," Nature (London) **528**, 111–114.

Emery, G. T., 1972, "Perturbation of nuclear decay rates," Annu. Rev. Nucl. Part. Sci. **22**, 165–202.

Engstler, S., A. Krauss, K. Neldner, C. Rolfs, U. Schröder, and K. Langanke, 1988, "Effects of electron screening on the $^{3}He(d,p)^{4}He$ low-energy cross sections," Phys. Lett. B **202**, 179–184.

Engstler, S., G. Raimann, C. Angulo, U. Greife, C. Rolfs, U. Schröder, E. Somorjai, B. Kirch, and K. Langanke, 1992a,

"Isotopic dependence of electron screening in fusion reactions," Z. Phys. A **342**, 471–482.
Engstler, S., G. Raimann, C. Angulo, U. Greife, C. Rolfs, U. Schröder, E. Somorjai, B. Kirch, and K. Langanke, 1992b, "Test for isotopic dependence of electron screening in fusion reactions," Phys. Lett. B **279**, 20–24.
Entem, D. R., and R. Machleidt, 2003, "Accurate charge-dependent nucleon-nucleon potential at fourth order of chiral perturbation theory," Phys. Rev. C **68**, 041001.
Entem, D. R., R. Machleidt, and Y. Nosyk, 2017, "High-quality two-nucleon potentials up to fifth order of the chiral expansion," Phys. Rev. C **96**, 024004.
Epelbaum, E., H. W. Hammer, and U.-G. Meißner, 2009, "Modern theory of nuclear forces," Rev. Mod. Phys. **81**, 1773–1825.
Epelbaum, E., H. Krebs, D. Lee, and U.-G. Meißner, 2011, "*Ab Initio* Calculation of the Hoyle State," Phys. Rev. Lett. **106**, 192501.
Erb, K. A., R. R. Betts, D. L. Hanson, M. W. Sachs, R. L. White, P. P. Tung, and D. A. Bromley, 1976, "New Resonances in the Low-Energy ^{12}C-^{12}C Spectrum," Phys. Rev. Lett. **37**, 670–673.
Esbensen, H., X. Tang, and C. L. Jiang, 2011, "Effects of mutual excitations in the fusion of carbon isotopes," Phys. Rev. C **84**, 064613.
Esbensen, H., A. Winther, R. A. Broglia, and C. H. Dasso, 1978, "Fluctuations due to Zero-Point Motion of Surface Vibrations in Deep-Inelastic Rections," Phys. Rev. Lett. **41**, 296–298.
Faestermann, T., P. Mohr, R. Hertenberger, and H. F. Wirth, 2015, "Broad levels in ^{17}O and their relevance for the astrophysical s process," Phys. Rev. C **92**, 052802.
Fano, U., 1961, "Effects of configuration interaction on intensities and phase shifts," Phys. Rev. **124**, 1866–1878.
Farmer, R., M. Renzo, S. E. de Mink, M. Fishbach, and S. Justham, 2020, "Constraints from gravitational-wave detections of binary black hole mergers on the $^{12}\mathrm{C}(\alpha,\gamma)^{16}\mathrm{O}$ rate," Astrophys. J. Lett. **902**, L36.
Feldmeier, H., 1990, "Fermionic molecular dynamics," Nucl. Phys. **A515**, 147–172.
Fernandez, J. P. L., N. Michel, M. Płoszajczak, and A. Mercenne, 2023, "Description of ^{7}Be and ^{7}Li within the Gamow shell model," Phys. Rev. C **108**, 044616.
Feshbach, H., 1958, "Unified theory of nuclear reactions," Ann. Phys. (N.Y.) **5**, 357–390.
Feshbach, H., 1962, "A unified theory of nuclear reactions. II," Ann. Phys. (N.Y.) **19**, 287–313.
Feshbach, H., C. E. Porter, and V. F. Weisskopf, 1954, "Model for nuclear reactions with neutrons," Phys. Rev. **96**, 448–464.
Fetisov, V. N., and Y. S. Kopysov, 1975, "Solar neutrinos and experiments to search for the hypothetical level in ^{6}Be," Nucl. Phys. **A239**, 511–529.
Fey, M., 2004, "Im brennpunkt der nuklearen astrophysik: Die reaktion $^{12}\mathrm{C}(\alpha,\gamma)^{16}\mathrm{O}$ [In the focus of nuclear astrophysics: The $^{12}\mathrm{C}(\alpha,\gamma)^{16}\mathrm{O}$ reaction]," Ph.D. thesis (University of Stuttgart).
Fick, D., 1978, "Narrow resonances in the continuum," in *Few Body Systems and Nuclear Forces II*, Lecture Notes in Physics Vol. 87, edited by H. Høgaasen and P. Sorba (Springer-Verlag, Berlin), pp. 414–426.
Fields, B. D., 2011, "The primordial lithium problem," Annu. Rev. Nucl. Part. Sci. **61**, 47–68.
Filippone, B. W., A. J. Elwyn, C. N. Davids, and D. D. Koetke, 1983, "Proton capture cross section of ^{7}Be and the flux of high energy solar neutrinos," Phys. Rev. C **28**, 2222–2229.
Fink, H. J., W. Scheid, and W. Greiner, 1972, "Nuclear molecular structure in ^{12}C-^{12}C scattering," Nucl. Phys. **A188**, 259–288.
Fiorentini, G., C. Rolfs, F. L. Villante, and B. Ricci, 2003, "Fusion rate enhancement due to energy spread of colliding nuclei," Phys. Rev. C **67**, 014603.
Flambaum, V. V., and V. G. Zelevinsky, 1999, "Radiation Corrections Increase Tunneling Probability," Phys. Rev. Lett. **83**, 3108–3111.
Fonda, L., 1961, "Inelastic collisions and threshold effects," Nuovo Cimento **20**, 116–145.
Fonda, L., and G. C. Ghirardi, 1964, "Threshold effects and unstable particles," Nucl. Phys. **58**, 374–384.
Fontaine, G., and P. Brassard, 2002, "Can white dwarf asteroseismology really constrain the $^{12}\mathrm{C}(\alpha,\gamma)^{16}\mathrm{O}$ reaction rate?," Astrophys. J. Lett. **581**, L33–L37.
Formicola, A., H. Costantini, and G. Imbriani, 2003, "A new study of the $^{14}\mathrm{N}(p,\gamma)^{15}\mathrm{O}$ reaction at low energy," Nucl. Phys. **A719**, C94–C98.
Formicola, A., *et al.*, 2003, "The LUNA II 400 kV accelerator," Nucl. Instrum. Methods Phys. Res., Sect. A **507**, 609–616.
Formicola, A., *et al.*, 2004, "Astrophysical S-factor of $^{14}\mathrm{N}(p,\gamma)^{15}\mathrm{O}$," Phys. Lett. B **591**, 61–68.
Fortune, H. T., and R. Sherr, 2005, "Energy shifts and configuration mixing in the $A = 15$ quartet," Phys. Rev. C **72**, 024319.
Fossez, K., N. Michel, M. Płoszajczak, Y. Jaganathen, and R. M. Id Betan, 2015, "Description of the proton and neutron radiative capture reactions in the Gamow shell model," Phys. Rev. C **91**, 034609.
Fossez, K., J. Rotureau, N. Michel, and M. Płoszajczak, 2017, "Can Tetraneutron Be a Narrow Resonance?," Phys. Rev. Lett. **119**, 032501.
Fougères, C., *et al.*, 2023, "Search for ^{22}Na in novae supported by a novel method for measuring femtosecond nuclear lifetimes," Nat. Commun. **14**, 4536.
Fowler, J. L., C. H. Johnson, and R. M. Feezel, 1973, "Level structure of ^{17}O from neutron total cross sections," Phys. Rev. C **8**, 545–562.
Fowler, W. A., 1972, "What cooks with solar neutrinos?," Nature (London) **238**, 24–26.
Fowler, W. A., 1983, "Experimental and theoretical nuclear astrophysics; the quest for the origin of the elements," Nobel Lecture, https://www.nobelprize.org/prizes/physics/1983/fowler/lecture/.
Fowler, W. A., 1984, "Experimental and theoretical nuclear astrophysics: The quest for the origin of the elements," Rev. Mod. Phys. **56**, 149–179.
Fowler, W. A., G. R. Caughlan, and B. A. Zimmerman, 1967, "Thermonuclear reaction rates," Annu. Rev. Astron. Astrophys. **5**, 525.
Fowler, W. A., G. R. Caughlan, and B. A. Zimmerman, 1975, "Thermonuclear reaction rates, II," Annu. Rev. Astron. Astrophys. **13**, 69.
Fowler, W. A., and F. Hoyle, 1964, "Neutrino processes and pair formation in massive stars and supernovae," Astrophys. J. Suppl. Ser. **9**, 201.
Freer, M., and H. O. U. Fynbo, 2014, "The Hoyle state in ^{12}C," Prog. Part. Nucl. Phys. **78**, 1–23.
Freer, M., H. Horiuchi, Y. Kanada-En'yo, D. Lee, and U.-G. Meißner, 2018, "Microscopic clustering in light nuclei," Rev. Mod. Phys. **90**, 035004.
Frekers, D., R. Santo, and K. Langanke, 1983, "Identification of quasimolecular resonances in low energy α-^{40}Ca scattering and effects of compound nucleus excitation," Nucl. Phys. **A394**, 189–220.
Frentz, B., *et al.*, 2021, "Lifetime measurements of excited states in ^{15}O," Phys. Rev. C **103**, 045802.
Frentz, B., *et al.*, 2022, "Investigation of the $^{14}\mathrm{N}(p,\gamma)^{15}\mathrm{O}$ reaction and its impact on the CNO cycle," Phys. Rev. C **106**, 065803.

Friedrich, H., and K. Langanke, 1975, "Description of elastic α-^{40}Ca scattering by the resonating group method," Nucl. Phys. **A252**, 47–61.

Fröhlich, C., G. Martínez-Pinedo, M. Liebendörfer, F. K. Thielemann, E. Bravo, W. R. Hix, K. Langanke, and N. T. Zinner, 2006, "Neutrino-Induced Nucleosynthesis of $A > 64$ Nuclei: The νp Process," Phys. Rev. Lett. **96**, 142502.

Fruet, G., *et al.*, 2020, "Advances in the Direct Study of Carbon Burning in Massive Stars," Phys. Rev. Lett. **124**, 192701.

Fukuda, Y., *et al.*, 1998, "Evidence for Oscillation of Atmospheric Neutrinos," Phys. Rev. Lett. **81**, 1562–1567.

Fukui, T., K. Ogata, and M. Yahiro, 2015, "Breakup and finite-range effects on the ^{8}B$(d,n)^{9}$C reaction," Phys. Rev. C **91**, 014604.

Funck, C., K. Langanke, and A. Weiguny, 1985, "The $E2$ contribution to the ^{12}C$(\alpha,\gamma)^{16}$O reaction at stellar energies in a coupled channel approach," Phys. Lett. **152B**, 11–16.

Fyodorov, Y. V., and B. A. Khoruzhenko, 1999, "Systematic Analytical Approach to Correlation Functions of Resonances in Quantum Chaotic Scattering," Phys. Rev. Lett. **83**, 65–68.

Gagliardi, C. A., *et al.*, 1999, "Tests of transfer reaction determinations of astrophysical S factors," Phys. Rev. C **59**, 1149–1153.

Galinski, N., *et al.*, 2014, "Lifetime measurements of states in ^{15}O," Phys. Rev. C **90**, 035803.

Gamow, G., 1928, "Zur Quantentheorie des Atomkernes," Z. Phys. **51**, 204–212.

Gamow, G., 1970, *My World Line: An Informal Autobiography* (Viking, New York).

Gamow, G., and E. Teller, 1938, "The rate of selective thermonuclear reactions," Phys. Rev. **53**, 608–609.

Gao, B., *et al.* (JUNA Collaboration), 2022, "Deep Underground Laboratory Measurement of ^{13}C$(\alpha,n)^{16}$O in the Gamow Windows of the s and i Processes," Phys. Rev. Lett. **129**, 132701.

Gasques, L. R., A. V. Afanasjev, E. F. Aguilera, M. Beard, L. C. Chamon, P. Ring, M. Wiescher, and D. G. Yakovlev, 2005, "Nuclear fusion in dense matter: Reaction rate and carbon burning," Phys. Rev. C **72**, 025806.

Gasques, L. R., A. V. Afanasjev, M. Beard, J. Lubian, T. Neff, M. Wiescher, and D. G. Yakovlev, 2007, "São Paulo potential as a tool for calculating S factors of fusion reactions in dense stellar matter," Phys. Rev. C **76**, 045802.

Gasques, L. R., E. F. Brown, A. Chieffi, C. L. Jiang, M. Limongi, C. Rolfs, M. Wiescher, and D. G. Yakovlev, 2007, "Implications of low-energy fusion hindrance on stellar burning and nucleosynthesis," Phys. Rev. C **76**, 035802.

Gasques, L. R., L. C. Chamon, and G. P. Cessel, 2022, "The role of inelastic couplings on the ^{12}C + ^{12}C fusion at sub-barrier energies," Eur. Phys. J. A **58**, 102.

Gatu Johnson, M., G. Hale, M. Paris, M. Wiescher, and A. Zylstra, 2023, "Editorial: Using high energy density plasmas for nuclear experiments relevant to nuclear astrophysics," Front. Phys. **11**, 1180821.

Gatu Johnson, M., *et al.*, 2017, "Development of an inertial confinement fusion platform to study charged-particle-producing nuclear reactions relevant to nuclear astrophysics," Phys. Plasmas **24**, 041407.

Gaul, G., and W. Bickel, 1986, "Intermediate and compound structure in the ^{16}O system," Phys. Rev. C **34**, 326–329.

Gaul, G., H. Lüdecke, R. Santo, H. Schmeing, and R. Stock, 1969, "Effects of α-particle correlations in elastic α-scattering," Nucl. Phys. **A137**, 177–192.

Gazit, D., S. Quaglioni, and P. Navrátil, 2019, "Erratum: Three-Nucleon Low-Energy Constants from the Consistency of Interactions and Currents in Chiral Effective Field Theory [Phys. Rev. Lett. **103**, 102502 (2009)]," Phys. Rev. Lett. **122**, 029901.

Gel'fand, I. M., and N. Y. Vilenkin, 1964, *Generalized Functions, Vol. 4: Applications of Harmonic Analysis* (Academic Press, New York).

Gialanella, L., *et al.*, 2001, "The $E1$ capture amplitude in ^{12}C$(\alpha,\gamma_0)^{16}$O," Eur. Phys. J. A **11**, 357–370.

Giammichele, N., S. Charpinet, and P. Brassard, 2022, "Seismic cartography of white-dwarf interiors from the Toulouse-Montréal optimal-design approach," Front. Astron. Space Sci. **9**, 879045.

Girard-Alcindor, V., *et al.*, 2022, "New narrow resonances observed in the unbound nucleus ^{15}F," Phys. Rev. C **105**, L051301.

Girlanda, L., A. Kievsky, and M. Viviani, 2011, "Subleading contributions to the three-nucleon contact interaction," Phys. Rev. C **84**, 014001.

Godbey, K., C. Simenel, and A. S. Umar, 2019, "Absence of hindrance in a microscopic ^{12}C + ^{12}C fusion study," Phys. Rev. C **100**, 024619.

Golser, R., and D. Semrad, 1991, "Observation of a Striking Departure from Velocity Proportionality in Low-Energy Electronic Stopping," Phys. Rev. Lett. **66**, 1831–1833.

Goriely, S., 1998, "Radiative neutron captures by neutron-rich nuclei and the r-process nucleosynthesis," Phys. Lett. B **436**, 10–18.

Görres, J., H. Herndl, I. J. Thompson, and M. Wiescher, 1995, "Two-neutron capture reactions in supernovae neutrino bubbles," Phys. Rev. C **52**, 2231–2235.

Graboske, H. C., H. E. Dewitt, A. S. Grossman, and M. S. Cooper, 1973, "Screening factors for nuclear reactions. II. Intermediate screening and astrophysical applications," Astrophys. J. **181**, 457–474.

Greife, U., F. Gorris, M. Junker, C. Rolfs, and D. Zahnow, 1995, "Oppenheimer-Phillips effect and electron screening in $d + d$ fusion reactions," Z. Phys. A **351**, 107–112.

Greiner, W., J. Y. Park, and W. Scheid, 1995, *Nuclear Molecules* (World Scientific, Singapore).

Grevesse, N., and A. J. Sauval, 1998, "Standard solar composition," Space Sci. Rev. **85**, 161–174.

Grigorenko, L. V., I. G. Mukha, I. J. Thompson, and M. V. Zhukov, 2002, "Two-Proton Widths of ^{12}O, ^{16}Ne, and Three-Body Mechanism of Thomas-Ehrman Shift," Phys. Rev. Lett. **88**, 042502.

Gruzinov, A. V., and J. N. Bahcall, 1997, "The ^{7}Be electron capture rate in the Sun," Astrophys. J. **490**, 437–441.

Guardalben, M. J., M. Barczys, B. E. Kruschwitz, M. Spilatro, L. J. Waxer, and E. M. Hill, 2020, "Laser-system model for enhanced operational performance and flexibility on OMEGA EP," High Power Laser Sci. Eng. **8**, e8.

Guimarães, V., *et al.*, 2007, "Neutron transfer reactions induced by ^{8}Li on ^{9}Be," Phys. Rev. C **75**, 054602.

Gula, A., *et al.*, 2023, "^{10}B + α reactions at low energies," Phys. Rev. C **107**, 025805.

Guo, B., *et al.*, 2012, "New determination of the ^{13}C$(\alpha,n)^{16}$O reaction rate and its influence on the s-process nucleosynthesis in AGB stars," Astrophys. J. **756**, 193.

Gupta, S., E. F. Brown, H. Schatz, P. Möller, and K.-L. Kratz, 2007, "Heating in the accreted neutron star ocean: Implications for superburst ignition," Astrophys. J. **662**, 1188–1197.

Gurney, R. W., and E. U. Condon, 1928, "Wave mechanics and radioactive disintegration," Nature (London) **122**, 439.

Gyürky, G., *et al.*, 2007, "^{3}He$(\alpha,\gamma)^{7}$Be cross section at low energies," Phys. Rev. C **75**, 035805.

Haas, F., A. Elanique, R. M. Freeman, C. Beck, R. Nouicer, D. L. Watson, C. Jones, R. Cowin, P. Lee, and Z. Basrak, 1997, "Search for electromagnetic transitions between ^{12}C–^{12}C cluster states in ^{24}Mg," Nuovo Cimento Soc. Ital. Fis. **110A**, 989.

Haensel, P., and J. L. Zdunik, 1990, "Non-equilibrium processes in the crust of an accreting neutron star," Astron. Astrophys. **227**, 431–436, https://articles.adsabs.harvard.edu/pdf/1990A%26A...227..431H.

Hagen, G., and N. Michel, 2012, "Elastic proton scattering of medium mass nuclei from coupled-cluster theory," Phys. Rev. C **86**, 021602(R).

Hager, U., *et al.*, 2011, "Direct total cross section measurement of the ^{16}O$(\alpha,\gamma)^{20}$Ne reaction at $E_{\mathrm{c.m.}} = 2.26$ MeV," Phys. Rev. C **84**, 022801.

Hager, U., *et al.*, 2012, "Direct measurement of the ^{16}O$(\alpha,\gamma)^{20}$Ne reaction at $E_{\mathrm{c.m.}} = 2.43$ MeV and 1.69 MeV," Phys. Rev. C **86**, 055802.

Hagino, K., and A. B. Balantekin, 2002, "Radiation correction to astrophysical fusion reactions and the electron screening problem," Phys. Rev. C **66**, 055801.

Hagino, K., and N. Takigawa, 2012, "Subbarrier fusion reactions and many-particle quantum tunneling," Prog. Theor. Phys. **128**, 1061–1106.

Hahn, K. H., K. H. Chang, T. R. Donoghue, and B. W. Filippone, 1987, "Search for nonresonant capture in the ^{16}O$(\alpha,\gamma)^{20}$Ne reaction at low energies," Phys. Rev. C **36**, 892–898.

Hale, G. M., and M. W. Paris, 2017, "Neutron cross sections for carbon and oxygen from new *R*-matrix analyses of the ^{13,14}C and ^{17}O systems," EPJ Web Conf. **146**, 02027.

Halliwell, J. J., 1991, "Introductory lectures on quantum cosmology," in *Quantum Cosmology and Baby Universes*, edited by S. Coleman, J. B. Hartle, T. Piran, and S. Weinberg (World Scientific, Singapore), pp. 159–243.

Hammache, F., *et al.*, 2001, "Low-Energy Measurement of the ^{7}Be$(p,\gamma)^{8}$B Cross Section," Phys. Rev. Lett. **86**, 3985–3988.

Hammache, F., *et al.*, 2010, "High-energy breakup of ^{6}Li as a tool to study the big bang nucleosynthesis reaction ^{2}H$(\alpha,\gamma)^{6}$Li," Phys. Rev. C **82**, 065803.

Hammer, H. W., C. Ji, and D. R. Phillips, 2017, "Effective field theory description of halo nuclei," J. Phys. G **44**, 103002.

Hammer, H. W., and D. R. Phillips, 2011, "Electric properties of the beryllium-11 system in halo EFT," Nucl. Phys. **A865**, 17–42.

Harissopulos, S., H. W. Becker, J. W. Hammer, A. Lagoyannis, C. Rolfs, and F. Strieder, 2005, "Cross section of the ^{13}C$(\alpha,n)^{16}$O reaction: A background for the measurement of geo-neutrinos," Phys. Rev. C **72**, 062801.

Harrison, E. R., 1964, "Thermonuclear and pycnonuclear reactions," Proc. Phys. Soc. London **84**, 213–229.

Hass, M., C. Broude, V. Fedoseev, G. Goldring, G. Huber, J. Lettry, V. Mishin, H. Ravn, V. Sebastian, and L. Weissman (ISOLDE Collaboration), 1999, "A new measurement of the ^{7}Be$(p,\gamma)^{8}$B cross-section with an implanted ^{7}Be target," Phys. Lett. B **462**, 237–242.

Hategan, C., 1973, "Threshold phenomena and their observation," Phys. Lett. **46B**, 23–26.

Hategan, C., 1978, "Threshold phenomena in *R*-matrix theory," Ann. Phys. (N.Y.) **116**, 77–85.

Hauser, W., and H. Feshbach, 1952, "The inelastic scattering of neutrons," Phys. Rev. **87**, 366–373.

Haxton, W. C., R. G. Hamish Robertson, and A. M. Serenelli, 2013, "Solar neutrinos: Status and prospects," Annu. Rev. Astron. Astrophys. **51**, 21–61.

Haxton, W. C., and A. M. Serenelli, 2008, "CN cycle solar neutrinos and the Sun's primordial core metallicity," Astrophys. J. **687**, 678–691.

Hayakawa, S., *et al.*, 2021, "Constraining the primordial lithium abundance: New cross section measurement of the ^{7}Be + n reactions updates the total ^{7}Be destruction rate," Astrophys. J. Lett. **915**, L13.

Hebborn, C., M. L. Avila, K. Kravvaris, G. Potel, and S. Quaglioni, 2024, "Impact of the ^{6}Li asymptotic normalization constant onto α-induced reactions of astrophysical interest," Phys. Rev. C **109**, L061601.

Hebborn, C., G. Hupin, K. Kravvaris, S. Quaglioni, P. Navrátil, and P. Gysbers, 2022, "*Ab Initio* Prediction of the ^{4}He$(d,\gamma)^{6}$Li Big Bang Radiative Capture," Phys. Rev. Lett. **129**, 042503.

Heger, A., K. Langanke, G. Martínez-Pinedo, and S. E. Woosley, 2001, "Presupernova Collapse Models with Improved Weak-Interaction Rates," Phys. Rev. Lett. **86**, 1678–1681.

Heger, A., S. E. Woosley, G. Martínez-Pinedo, and K. Langanke, 2001, "Presupernova evolution with improved rates for weak interactions," Astrophys. J. **560**, 307–325.

Heil, M., F. Käppeler, M. Wiescher, and A. Mengoni, 1998, "The (n,γ) cross section of ^{7}Li," Astrophys. J. **507**, 997–1002.

Heil, M., *et al.*, 2008, "The ^{13}C(α,n) reaction and its role as a neutron source for the *s* process," Phys. Rev. C **78**, 025803.

Helling, G., W. Scheid, and W. Greiner, 1971, "Angular momentum dependence of the optical potential in heavy-ion scattering," Phys. Lett. **36B**, 64–67.

Hergert, H., 2020, "A guided tour of *ab initio* nuclear many-body theory," Front. Phys. **8**, 379.

Herndl, H., R. Hofinger, J. Jank, H. Oberhummer, J. Görres, M. Wiescher, F. K. Thielemann, and B. A. Brown, 1999, "Reaction rates for neutron capture reactions to C, N, and O isotopes to the neutron rich side of stability," Phys. Rev. C **60**, 064614.

Higa, R., H. W. Hammer, and U. van Kolck, 2008, "$\alpha\alpha$ scattering in halo effective field theory," Nucl. Phys. **A809**, 171–188.

Higa, R., P. Premarathna, and G. Rupak, 2022, "Coupled-channels treatment of ^{7}Be$(p,\gamma)^{8}$B in effective field theory," Phys. Rev. C **106**, 014601.

Higa, R., G. Rupak, and A. Vaghani, 2018, "Radiative ^{3}He$(\alpha,\gamma)^{7}$Be reaction in halo effective field theory," Eur. Phys. J. A **54**, 89.

Higgins, M. D., C. H. Greene, A. Kievsky, and M. Viviani, 2020, "Nonresonant Density of States Enhancement at Low Energies for Three or Four Neutrons," Phys. Rev. Lett. **125**, 052501.

High, M. D., and B. Čujec, 1977, "The ^{12}C + ^{12}C sub-Coulomb fusion cross section," Nucl. Phys. **A282**, 181–188.

Hilgemeier, M., H. W. Becker, C. Rolfs, H. P. Trautvetter, and J. W. Hammer, 1988, "Absolute cross section of the ^{3}He$(\alpha,\gamma)^{7}$Be reaction," Z. Phys. A **329**, 243–254.

Hillebrandt, W., M. Kromer, F. K. Röpke, and A. J. Ruiter, 2013, "Towards an understanding of type Ia supernovae from a synthesis of theory and observations," Front. Phys. **8**, 116–143.

Hix, W. R., O. E. Messer, A. Mezzacappa, M. Liebendörfer, J. Sampaio, K. Langanke, D. J. Dean, and G. Martínez-Pinedo, 2003, "Consequences of Nuclear Electron Capture in Core Collapse Supernovae," Phys. Rev. Lett. **91**, 201102.

Hix, W. R., and F.-K. Thielemann, 1996, "Silicon burning. I. Neutronization and the physics of quasi-equilibrium," Astrophys. J. **460**, 869.

Hodgson, P., 1976, "Wigner cusps in nuclear reactions," Nature (London) **259**, 364–365.

Hoffman, R. D., S. E. Woosley, T. A. Weaver, T. Rauscher, and F. K. Thielemann, 1999, "The reaction rate sensitivity of nucleosynthesis in type II supernovae," Astrophys. J. **521**, 735–752.

Hogan, W. J., E. I. Moses, B. E. Warner, M. S. Sorem, and J. M. Soures, 2001, "The National Ignition Facility," Nucl. Fusion **41**, 567–573.

Hogan, W. S., and R. G. Seyler, 1970, "Effect of the Mott-Schwinger interaction on neutron-proton scattering," Phys. Rev. C **1**, 17–27.
Holmes, J. A., S. E. Woosley, W. A. Fowler, and B. A. Zimmerman, 1976, "Tables of thermonuclear-reaction-rate data for neutron-induced reactions on heavy nuclei," At. Data Nucl. Data Tables **18**, 305.
Holt, R. J., H. E. Jackson, R. M. Laszewski, J. E. Monahan, and J. R. Specht, 1978, "Effects of channel and potential radiative transitions in the $^{17}O(\gamma, n_0)^{16}O$ reaction," Phys. Rev. C **18**, 1962–1972.
Horowitz, C. J., H. Dussan, and D. K. Berry, 2008, "Fusion of neutron-rich oxygen isotopes in the crust of accreting neutron stars," Phys. Rev. C **77**, 045807.
Hoyle, F., 1954, "On nuclear reactions occurring in very hot STARS. I. The synthesis of elements from carbon to nickel," Astrophys. J. Suppl. Ser. **1**, 121.
Hoyle, F., and W. A. Fowler, 1960, "Nucleosynthesis in supernovae," Astrophys. J. **132**, 565.
Hu, B., *et al.*, 2022, "*Ab initio* predictions link the neutron skin of ^{208}Pb to nuclear forces," Nat. Phys. **18**, 1196–1200.
Hudan, S., R. T. deSouza, A. S. Umar, Z. Lin, and C. J. Horowitz, 2020, "Enhanced dynamics in fusion of neutron-rich oxygen nuclei at above-barrier energies," Phys. Rev. C **101**, 061601(R).
Huke, A., K. Czerski, P. Heide, G. Ruprecht, N. Targosz, and W. Żebrowski, 2008, "Enhancement of deuteron-fusion reactions in metals and experimental implications," Phys. Rev. C **78**, 015803.
Hulke, G., C. Rolfs, and H. P. Trautvetter, 1980, "Comparison of the fusion reactions $^{12}C + ^{20}Ne$ and $^{16}O + ^{16}O$ near the Coulomb barrier," Z. Phys. A **297**, 161–183.
Humblet, J., W. A. Fowler, and B. A. Zimmerman, 1987, "Approximate penetration factors for nuclear reactions of astrophysical interest," Astron. Astrophys. **177**, 317–325, https://articles.adsabs.harvard.edu/pdf/1987A%26A...177..317H.
Humblet, J., and L. Rosenfeld, 1961, "Theory of nuclear reactions. I. Resonant states and collision matrix," Nucl. Phys. **26**, 529–578.
Hupin, G., S. Quaglioni, and P. Navrátil, 2019, "*Ab initio* predictions for polarized deuterium-tritium thermonuclear fusion," Nat. Commun. **10**, 351.
Hussein, M. S., 1977, "Under-the-barrier absorption effects in low energy heavy ion fusion reactions," Phys. Lett. **71B**, 249–251.
Hwang, E., H. Ko, K. Heo, M.-K. Cheoun, and D. Jang, 2023, "Reinvestigating the Gamow factor of reactions on light nuclei," Astrophys. J. **955**, 79.
Iben, Jr., I., K. Kalata, and J. Schwartz, 1967, "The effect of ^7Be K-capture on the solar neutrino flux," Astrophys. J. **150**, 1001.
Iben, Jr., I., and A. Renzini, 1983, "Asymptotic giant branch evolution and beyond," Annu. Rev. Astron. Astrophys. **21**, 271–342.
Ichimaru, S., S. Ogata, and H. M. van Horn, 1992, "Pycnonuclear reaction rates for binary ionic mixtures," Astrophys. J. Lett. **401**, L35.
Id Betan, R., R. J. Liotta, N. Sandulescu, and T. Vertse, 2002, "Two-Particle Resonant States in a Many-Body Mean Field," Phys. Rev. Lett. **89**, 042501.
Igamov, S. B., and R. Yarmukhamedov, 2000, "Triple-differential cross section of the $^{208}Pb(^6Li, \alpha d)^{208}Pb$ Coulomb breakup and astrophysical S-factor of the $d(\alpha, \gamma)^6Li$ reaction at extremely low energies," Nucl. Phys. **A673**, 509–525.
Ikeda, K., N. Takigawa, and H. Horiuchi, 1968, "The systematic structure-change into the molecule-like structures in the self-conjugate $4n$ nuclei," Prog. Theor. Phys. Suppl. **E68**, 464–475.
Iliadis, C., 2023, "Laboratory electron screening in nuclear resonance reactions," Phys. Rev. C **107**, 044610.
Iliadis, C., J. M. D'Auria, S. Starrfield, W. J. Thompson, and M. Wiescher, 2001, "Proton-induced thermonuclear reaction rates for $A = 20$–40 nuclei," Astrophys. J. Suppl. Ser. **134**, 151–171.
Iliadis, C., V. Palanivelrajan, and R. S. de Souza, 2022, "Bayesian estimation of the S factor and thermonuclear reaction rate for $^{16}O(p, \gamma)^{17}F$," Phys. Rev. C **106**, 055802.
Imanishi, B., 1968, "Resonance energies and partial widths of quasimolecular states formed by the two carbon nuclei," Phys. Lett. **27B**, 267–270.
Imbriani, G., *et al.*, 2004, "The bottleneck of CNO burning and the age of globular clusters," Astron. Astrophys. **420**, 625–629.
Imbriani, G., *et al.*, 2005, "S-factor of $^{14}N(p, \gamma)^{15}O$ at astrophysical energies*," Eur. Phys. J. A **25**, 455–466.
Inglis, D. R., 1962, "Nuclear models, threshold states and rearrangement energy," Nucl. Phys. **30**, 1–29.
Ishigami, M., B. Blue, R. Tsuchikawa, A. Ahmadi, D. Heligman, Z. Zhang, J. Hone, and E. Mucciolo, 2018, "Experimental observation of the Wigner cusps in a metallic carbon nanotube," in *Proceedings of the APS March Meeting, Los Angeles, 2018*, p. H40.014, https://meetings.aps.org/Meeting/MAR18/Session/H40.14.
Ito, M., Y. Sakuragi, and Y. Hirabayashi, 1999, "Dynamic polarization potential of $^{12}C + ^{12}C$ system at molecular-resonance energies," Eur. Phys. J. A **5**, 373–383.
Itoh, N., H. Totsuji, S. Ichimaru, and H. E. Dewitt, 1979, "Enhancement of thermonuclear reaction rate due to strong screening. II—Ionic mixtures," Astrophys. J. **234**, 1079–1084.
Iwasa, N., *et al.*, 1999, "Measurement of the Coulomb Dissociation of ^8B at 254 MeV/nucleon and the ^8B Solar Neutrino Flux," Phys. Rev. Lett. **83**, 2910–2913.
Iyudin, A. F., V. Schönfelder, A. W. Strong, K. Bennett, R. Diehl, W. Hermsen, G. G. Lichti, and J. Ryan, 2001, "Study of the Galactic distribution of nova-produced ^{22}Na with COMPTEL," AIP Conf. Ser. **587**, 508–512.
Jaeger, M., R. Kunz, A. Mayer, J. W. Hammer, G. Staudt, K. L. Kratz, and B. Pfeiffer, 2001, "$^{22}Ne(\alpha, n)^{25}Mg$: The Key Neutron Source in Massive Stars," Phys. Rev. Lett. **87**, 202501.
Jaganathen, Y., N. Michel, and M. Płoszajczak, 2014, "Gamow shell model description of proton scattering on ^{18}Ne," Phys. Rev. C **89**, 034624.
Jain, R., *et al.*, 2023, "Impact of pycnonuclear fusion uncertainties on the cooling of accreting neutron star crusts," Astrophys. J. **955**, 51.
Jancovici, B., 1978, "Exchange quantum corrections in the one-component plasma," Physica (Amsterdam) **91A**, 152–160.
Janka, H. T., K. Langanke, A. Marek, G. Martínez-Pinedo, and B. Müller, 2007, "Theory of core-collapse supernovae," Phys. Rep. **442**, 38–74.
Jaszczak, R. J., J. H. Gibbons, and R. L. Macklin, 1970, "$^{12}C(\alpha, \gamma)^{16}O$ Capture cross section below 3.2 MeV," Phys. Rev. C **2**, 63–69.
Jaszczak, R. J., and R. L. Macklin, 1970, "$^{12}C(\alpha, \gamma)^{16}O$ Capture cross section below 4.1 MeV," Phys. Rev. C **2**, 2452–2453.
Jeppesen, H. B., J. Byskov-Nielsen, P. Wright, J. G. Correia, L. M. Fraile, H. O. U. Fynbo, K. Johnston, and K. Riisager, 2007, "Alpha-decay half-life of ^{221}Fr in different environments," Eur. Phys. J. A **32**, 31–34.
Jiang, C. L., B. B. Back, H. Esbensen, R. V. Janssens, and K. E. Rehm, 2006, "Systematics of heavy-ion fusion hindrance at extreme sub-barrier energies," Phys. Rev. C **73**, 014613.
Jiang, C. L., B. B. Back, H. Esbensen, R. V. F. Janssens, K. E. Rehm, and R. J. Charity, 2013, "Origin and Consequences of $^{12}C + ^{12}C$ Fusion Resonances at Deep Sub-barrier Energies," Phys. Rev. Lett. **110**, 072701.

Jiang, C. L., B. B. Back, K. E. Rehm, K. Hagino, G. Montagnoli, and A. M. Stefanini, 2021, "Heavy-ion fusion reactions at extreme sub-barrier energies," Eur. Phys. J. A **57**, 235.

Jiang, C. L., K. E. Rehm, B. B. Back, and R. V. F. Janssens, 2007, "Expectations for ^{12}C and ^{16}O induced fusion cross sections at energies of astrophysical interest," Phys. Rev. C **75**, 015803.

Jiang, C. L., *et al.*, 2005, "Hindrance of heavy-ion fusion at extreme sub-barrier energies in open-shell colliding systems," Phys. Rev. C **71**, 044613.

Jiang, C. L., *et al.*, 2018, "Reaction rate for carbon burning in massive stars," Phys. Rev. C **97**, 012801.

Johnson, C. H., 1973, "Unified R-matrix-plus-potential analysis for $^{16}\mathrm{O}+n$ cross sections," Phys. Rev. C **7**, 561–573.

Johnson, C. W., E. Kolbe, S. E. Koonin, and K. Langanke, 1992, "The fate of ^{7}Be in the Sun," Astrophys. J. **392**, 320.

José, J., A. Coc, and M. Hernanz, 1999, "Nuclear uncertainties in the NeNa-MgAl cycles and production of ^{22}Na and ^{26}Al during nova outbursts," Astrophys. J. **520**, 347–360.

Junghans, A. R., E. C. Mohrmann, K. A. Snover, T. D. Steiger, E. G. Adelberger, J. M. Casandjian, H. E. Swanson, L. Buchmann, S. H. Park, and A. Zyuzin, 2002, "$^7\mathrm{Be}(p,\gamma)^8\mathrm{B}$ Astrophysical S Factor from Precision Cross Section Measurements," Phys. Rev. Lett. **88**, 041101.

Junghans, A. R., K. A. Snover, E. C. Mohrmann, E. G. Adelberger, and L. Buchmann, 2010, "Updated S factors for the $^7\mathrm{Be}(p,\gamma)^8\mathrm{B}$ reaction," Phys. Rev. C **81**, 012801.

Junghans, A. R., *et al.*, 2003, "Precise measurement of the $^7\mathrm{Be}(p,\gamma)^8\mathrm{B}$ S factor," Phys. Rev. C **68**, 065803.

Junker, M., *et al.*, 1998, "Cross section of $^3\mathrm{He}(^3\mathrm{He},2p)^4\mathrm{He}$ measured at solar energies," Phys. Rev. C **57**, 2700–2710.

Juodagalvis, A., K. Langanke, W. R. Hix, G. Martínez-Pinedo, and J. M. Sampaio, 2010, "Improved estimate of electron capture rates on nuclei during stellar core collapse," Nucl. Phys. **A848**, 454–478.

Kaeppeler, F., *et al.*, 1994, "Reaction rates for 18O(alpha, gamma) 22Ne, 22Ne (alpha, gamma) 26Mg, and 22Ne (alpha, n) 25Mg in stellar helium burning and s-process nucleosynthesis in massive stars," Astrophys. J. **437**, 396.

Kajino, T., 1986, "The $^3\mathrm{He}(\alpha,\gamma)^7\mathrm{Be}$ and $^3\mathrm{He}(\alpha,\gamma)^7\mathrm{Li}$ reactions at astrophysical energies," Nucl. Phys. **A460**, 559–580.

Kajino, T., and A. Arima, 1984, "Resonating-Group Calculation of Radiative Capture Reactions $\alpha(^3\mathrm{He},\gamma)^7\mathrm{Be}$ and $\alpha(t,\gamma)^7\mathrm{Li}$ at Astrophysical Low Energies," Phys. Rev. Lett. **52**, 739–742.

Kajino, T., G. F. Bertsch, and F. C. Barker, 1989, "Energy dependence of astrophysical S-factor for radiative charged particle reactions," in *Proceedings of the Fifth International Conference on Clustering Aspects in Nuclear and Subnuclear Systems, Kyoto, Japan, 1988*, edited by K. Ikeda, K. Katori, and Y. Suzuki (Physical Society of Japan, Tokyo), pp. 639–645, https://www.jps.or.jp//books/jpsjs/58/jpsj.58s.639.pdf.

Kajino, T., H. Toki, and S. M. Austin, 1987, "Radiative alpha-capture rates leading to $A=7$ nuclei: Applications to the solar neutrino problem and big bang nucleosynthesis," Astrophys. J. **319**, 531.

Kalai, G., and S. Safra, 2006, "Threshold phenomena and influence: Perspectives from mathematics, computer science, and economics," in *Computational Complexity and Statistical Physics*, edited by A. Percus, G. Istrate, and C. Moore (Oxford University Press, New York), 10.1093/oso/9780195177374.003.0008.

Kamionkowski, M., and J. N. Bahcall, 1994, "Vacuum-polarization corrections to solar-fusion rates," Phys. Rev. C **49**, 545–547.

Kanada-En'yo, Y., 2007, "The structure of ground and excited states of ^{12}C," Prog. Theor. Phys. **117**, 655–680.

Kanada-En'yo, Y., M. Kimura, and A. Ono, 2012, "Antisymmetrized molecular dynamics and its applications to cluster phenomena," Prog. Theor. Exp. Phys. 01A202.

Kanada-En'yo, Y., T. Suhara, and Y. Taniguchi, 2014, "Approximation of reduced width amplitude and application to cluster decay width," Prog. Theor. Exp. Phys. 073E02.

Kaplan, D. B., M. J. Savage, and M. B. Wise, 1998a, "A new expansion for nucleon-nucleon interactions," Phys. Lett. B **424**, 390–396.

Kaplan, D. B., M. J. Savage, and M. B. Wise, 1998b, "Two-nucleon systems from effective field theory," Nucl. Phys. **B534**, 329–355.

Kasagi, J., 2004, "Low-energy nuclear reactions in metals," Prog. Theor. Phys. Suppl. **154**, 365–372.

Kashy, E., R. R. Perry, and J. R. Risser, 1960, "Excited states in N^{14} from $\mathrm{C}^{12}(d,d)\mathrm{C}^{12}$, $\mathrm{C}^{12}(d,p_0)\mathrm{C}^{13}$, and $\mathrm{C}^{12}(d,p_1)\mathrm{C}^{13*}$," Phys. Rev. **117**, 1289–1296.

Katsuma, M., 2008, "Low-energy cross sections in the $^{12}\mathrm{C}(\alpha,\gamma)^{16}\mathrm{O}$ reaction," Phys. Rev. C **78**, 034606.

Kavanagh, R. W., 1960, "Proton capture in ^{7}Be," Nucl. Phys. **15**, 411–420.

Keek, L., A. Heger, and J. J. M. in 't Zand, 2012, "Superburst models for neutron stars with hydrogen- and helium-rich atmospheres," Astrophys. J. **752**, 150.

Keim-Malpass, J., M. Clark, D. Lake, and R. Moorman, 2020, "Towards development of alert thresholds for clinical deterioration using continuous predictive analytics monitoring," J. Clin. Monit. Comput. **34**, 797–804.

Kellogg, S., R. Vogelaar, and R. Kavanagh, 1989, "$^{13}\mathrm{C}(\alpha,n)$ and $^{14}\mathrm{C}(p,n)$: Astrophysical neutron sources and sinks," Bull. Am. Phys. Soc. **34**, 1192.

Kettner, K. U., H. W. Becker, L. Buchmann, J. Görres, H. Kräwinkel, C. Rolfs, P. Schmalbrock, H. P. Trautvetter, and A. Vlieks, 1982, "The $^4\mathrm{He}(^{12}\mathrm{C},\gamma)^{16}\mathrm{O}$ reaction at stellar energies," Z. Phys. A **308**, 73–94.

Kettner, K. U., H. Lorenz-Wirzba, and C. Rolfs, 1980, "The $^{12}\mathrm{C}+{}^{12}\mathrm{C}$ reaction at subcoulomb energies (I)," Z. Phys. A **298**, 65–75.

Kettner, K. U., H. Lorenz-Wirzba, C. Rolfs, and H. Winkler, 1977, "Study of the Fusion Reaction $^{12}\mathrm{C}+{}^{12}\mathrm{C}$ below the Coulomb Barrier," Phys. Rev. Lett. **38**, 337–340.

Kharbach, A., and P. Descouvemont, 1998, "Microscopic study of the $^2\mathrm{H}(\alpha,\gamma)^6\mathrm{Li}$ reaction in a multicluster model," Phys. Rev. C **58**, 1066–1072.

Kiener, J., H. J. Gils, H. Rebel, S. Zagromski, G. Gsottschneider, N. Heide, H. Jelitto, J. Wentz, and G. Baur, 1991, "Measurements of the Coulomb dissociation cross section of 156 MeV ^{6}Li projectiles at extremely low relative fragment energies of astrophysical interest," Phys. Rev. C **44**, 2195–2208.

Kievsky, A., S. Rosati, M. Viviani, L. E. Marcucci, and L. Girlanda, 2008, "Topical review: A high-precision variational approach to three- and four-nucleon bound and zero-energy scattering states," J. Phys. G **35**, 063101.

Kikuchi, T., *et al.*, 1998, "Further measurement of the $^7\mathrm{Be}(p,\gamma)^8\mathrm{B}$ cross section at low energies with the Coulomb dissociation of ^{8}B," Eur. Phys. J. A **3**, 213–215.

Kim, B. T., T. Izumoto, and K. Nagatani, 1981, "Radiative capture reaction $^3\mathrm{He}(\alpha,\gamma)^7\mathrm{Be}$ at low energies," Phys. Rev. C **23**, 33–41.

Kirsebom, O. S., *et al.*, 2019, "Discovery of an Exceptionally Strong β-Decay Transition of ^{20}F and Implications for the Fate of Intermediate-Mass Stars," Phys. Rev. Lett. **123**, 262701.

Kiss, G. G., *et al.*, 2020, "Astrophysical S-factor for the $^3\mathrm{He}(\alpha,\gamma)^7\mathrm{Be}$ reaction via the asymptotic normalization coefficient (ANC) method," Phys. Lett. B **807**, 135606.

Kitamura, H., 2000, "Pycnonuclear reactions in dense matter near solidification," Astrophys. J. **539**, 888–901.

Kitamura, H., and S. Ichimaru, 1995, "Pycnonuclear reaction rates in stellar interiors: Thermal enhancement," Astrophys. J. **438**, 300.

Kittel, C., 2004, *Introduction to Solid State Physics*, 8th ed. (Wiley, New York).

Kleinwachter, P., and I. Rotter, 1985, "Spectroscopic properties of highly excited states," Phys. Rev. C **32**, 1742–1744.

Kobayashi, H., *et al.*, 2003, "Astrophysical reaction rate for the $^{8}\mathrm{Li}(n,\gamma)^{9}\mathrm{Li}$ reaction," Phys. Rev. C **67**, 015806.

Koehler, P. E., 2002, "Constraints on the $^{22}\mathrm{Ne}(\alpha,n)^{25}\mathrm{Mg}$ s-process neutron source from analysis of $^{\mathrm{nat}}\mathrm{Mg}+\mathrm{n}$ total and $^{25}\mathrm{Mg}(n,\gamma)$ cross sections," Phys. Rev. C **66**, 055805.

Koehler, P. E., F. Bečvář, M. Krtička, J. A. Harvey, and K. H. Guber, 2010, "Anomalous Fluctuations of s-Wave Reduced Neutron Widths of ^{192,194}Pt Resonances," Phys. Rev. Lett. **105**, 072502.

Kohley, Z., *et al.*, 2013, "Study of Two-Neutron Radioactivity in the Decay of ^{26}O," Phys. Rev. Lett. **110**, 152501.

Kok, L. P., 1980, "Accurate Determination of the Ground-State Level of the ^{2}He Nucleus," Phys. Rev. Lett. **45**, 427–430.

Kolbe, E., K. Langanke, and H. J. Assenbaum, 1988, "Microscopic study of the low-energy $^{7}\mathrm{Be}(p,\gamma)^{8}\mathrm{B}$ reaction," Phys. Lett. B **214**, 169–172.

Kolk, B. V., *et al.*, 2022, "Investigation of the $^{10}\mathrm{B}(p,\alpha)^{7}\mathrm{Be}$ reaction from 0.8 to 2.0 MeV," Phys. Rev. C **105**, 055802.

Kondo, Y., *et al.*, 2016, "Nucleus ^{26}O: A Barely Unbound System beyond the Drip Line," Phys. Rev. Lett. **116**, 102503.

Kondo, Y., *et al.*, 2023, "First observation of ^{28}O," Nature (London) **620**, 965–970.

Kondō, Y., T. Matsuse, and Y. Abe, 1978, "A study of resonances in the sub-Coulomb ^{12}C-^{12}C reaction from the viewpoint of nuclear molecule," Prog. Theor. Phys. **59**, 465–479.

Kong, X., and F. Ravndal, 2000, "Coulomb effects in low energy proton proton scattering," Nucl. Phys. **A665**, 137–163.

Koning, A. J., and D. Rochman, 2012, "Modern nuclear data evaluation with the TALYS code system," Nucl. Data Sheets **113**, 2841–2934.

Konnecke, R., 1982, "A consistent imaginary potential treatment in the nuclear molecular channel picture," J. Phys. G **8**, L11–L16.

Konopinski, E. J., C. Marvin, and E. Teller, 1946, "Ignition of the atmosphere with nuclear bombs," Los Alamos National Laboratory Technical Report No. LA-602.

Kontos, A., E. Uberseder, R. deBoer, J. Görres, C. Akers, A. Best, M. Couder, and M. Wiescher, 2013, "Astrophysical S factor of $^{3}\mathrm{He}(\alpha,\gamma)^{7}\mathrm{Be}$," Phys. Rev. C **87**, 065804.

Koonin, S. E., T. A. Tombrello, and G. Fox, 1974, "A 'hybrid' R-matrix-optical model parametrization of the $^{12}\mathrm{C}(\alpha,\gamma)^{16}\mathrm{O}$ cross section," Nucl. Phys. **A220**, 221–232.

Kravchuk, P. A., and D. G. Yakovlev, 2014, "Strong plasma screening in thermonuclear reactions: Electron drop model," Phys. Rev. C **89**, 015802.

Kravvaris, K., P. Navrátil, S. Quaglioni, C. Hebborn, and G. Hupin, 2023, "*Ab initio* informed evaluation of the radiative capture of protons on ^{7}Be," Phys. Lett. B **845**, 138156.

Kräwinkel, H., *et al.*, 1982, "The $^{3}\mathrm{He}(\alpha,\gamma)^{7}\mathrm{Be}$ reaction and the solar neutrino problem," Z. Phys. A **304**, 307–332.

Kremer, R. M., C. A. Barnes, K. H. Chang, H. C. Evans, and B. W. Filippone, 1988, "Coincidence Measurement of the $^{12}\mathrm{C}(\alpha,\gamma)^{16}\mathrm{O}$ Cross Section at Low Energies," Phys. Rev. Lett. **60**, 1475–1478.

Kritcher, A. L., *et al.*, 2022, "Design of inertial fusion implosions reaching the burning plasma regime," Nat. Phys. **18**, 251–258.

Kruppa, A. T., and K. Arai, 1999, "Resonances and the continuum level density," Phys. Rev. A **59**, 3556–3561.

Kruppa, A. T., G. Papadimitriou, W. Nazarewicz, and N. Michel, 2014, "Nuclear three-body problem in the complex energy plane: Complex-scaling Slater method," Phys. Rev. C **89**, 014330.

Kunz, R., M. Jaeger, A. Mayer, J. W. Hammer, G. Staudt, S. Harissopulos, and T. Paradellis, 2001, "$^{12}\mathrm{C}(\alpha,\gamma)^{16}\mathrm{O}$: The Key Reaction in Stellar Nucleosynthesis," Phys. Rev. Lett. **86**, 3244–3247.

Kunz, R., *et al.*, 1997, "Capture reactions in the helium burning of stars," Nucl. Phys. **A621**, 149–152.

Kushnir, D., E. Waxman, and A. I. Chugunov, 2019, "Screening of fusion reactions from the principle of detailed balance and application to the pep reaction," Mon. Not. R. Astron. Soc. **486**, 449–452.

Labaune, C., C. Baccou, S. Depierreux, C. Goyon, G. Loisel, V. Yahia, and J. Rafelski, 2013, "Fusion reactions initiated by laser-accelerated particle beams in a laser-produced plasma," Nat. Commun. **4**, 2506.

La Cognata, M., S. Palmerini, C. Spitaleri, I. Indelicato, A. M. Mukhamedzhanov, I. Lombardo, and O. Trippella, 2015, "Updated THM astrophysical factor of the $^{19}\mathrm{F}(p,\alpha)^{16}\mathrm{O}$ reaction and influence of new direct data at astrophysical energies," Astrophys. J. **805**, 128.

La Cognata, M., C. Spitaleri, and A. M. Mukhamedzhanov, 2010, "Effect of high-energy resonances on the $^{18}\mathrm{O}(p,\alpha)^{15}\mathrm{N}$ reaction rate at AGB and post-AGB relevant temperatures," Astrophys. J. **723**, 1512–1522.

La Cognata, M., *et al.*, 2008, "Indirect measurement of the $^{18}\mathrm{O}(p,\alpha)^{15}\mathrm{N}$ reaction rate through the THM," J. Phys. G **35**, 014014.

La Cognata, M., *et al.*, 2010, "A novel approach to measure the cross section of the $^{18}\mathrm{O}(p,\alpha)^{15}\mathrm{N}$ resonant reaction in the 0–200 keV energy range," Astrophys. J. **708**, 796–811.

La Cognata, M., *et al.*, 2012, "Measurement of the -3 keV Resonance in the Reaction $^{13}\mathrm{C}(\alpha,n)^{16}\mathrm{O}$ of Importance in the s-Process," Phys. Rev. Lett. **109**, 232701.

La Cognata, M., *et al.*, 2013, "On the measurement of the $^{13}\mathrm{C}(\alpha,n)^{16}\mathrm{O}$ S-factor at negative energies and its influence on the s-process," Astrophys. J. **777**, 143.

La Cognata, M., *et al.*, 2022, "A new reaction rate of the $^{27}\mathrm{Al}(p,\alpha)^{24}\mathrm{Mg}$ reaction based on indirect measurements at astrophysical energies and implications for ^{27}Al yields of intermediate-mass stars," Astrophys. J. **941**, 96.

Lamia, L., C. Spitaleri, M. La Cognata, S. Palmerini, and R. G. Pizzone, 2012, "Recent evaluation of the $^{7}\mathrm{Li}(p,\alpha)^{4}\mathrm{He}$ reaction rate at astrophysical energies via the Trojan horse method," Astron. Astrophys. **541**, A158.

Lamia, L., C. Spitaleri, R. G. Pizzone, E. Tognelli, A. Tumino, S. Degl'Innocenti, P. G. Prada Moroni, M. La Cognata, L. Pappalardo, and M. L. Sergi, 2013, "An updated $^{6}\mathrm{Li}(p,\alpha)^{3}\mathrm{He}$ reaction rate at astrophysical energies with the Trojan horse method," Astrophys. J. **768**, 65.

Lamia, L., *et al.*, 2007, "Boron depletion: Indirect measurement of the $^{10}\mathrm{B}(p,\alpha)^{7}\mathrm{Be}$ $S(E)$-factor," Nucl. Phys. **A787**, 309–314.

Lamia, L., *et al.*, 2012, "New measurement of the $^{11}\mathrm{B}(p,\alpha_0)^{8}\mathrm{Be}$ bare-nucleus $S(E)$ factor via the Trojan horse method," J. Phys. G **39**, 015106.

Lamia, L., *et al.*, 2020, "Overview on the Trojan horse method in nuclear astrophysics," J. Phys. Conf. Ser. **1643**, 012051.

Lane, A. M., 1970, "A theory of anomalies observed in (d,p) excitation curves at thresholds for neutron analogue channels," Phys. Lett. **33B**, 274–278.

Lane, A. M., and R. G. Thomas, 1958, "*R*-matrix theory of nuclear reactions," Rev. Mod. Phys. **30**, 257–353.

Langanke, K., 1982, "Explanation of the backangle anomaly and the isotope effect within a microscopic study of elastic α-scattering on the even Ca isotopes," Nucl. Phys. **A377**, 53–83.

Langanke, K., 1986, "Microscopic potential model studies of light nuclear capture reactions," Nucl. Phys. **A457**, 351–366.

Langanke, K., 1994, *The Third Generation of Nuclear-Physics with the Microacopic Cluster Model* (Springer, Boston), pp. 85–226.

Langanke, K., and D. Frekers, 1978, "Microscopic investigations of the backward angle anomaly in elastic α-^{40}Ca scattering," Nucl. Phys. **A302**, 134–158.

Langanke, K., and H. Friedrich, 1986, "Microscopic description of nucleus-nucleus collisions," Adv. Nucl. Phys. **17**, 223–363.

Langanke, K., and S. E. Koonin, 1983, "The ^{12}C$(\alpha,\gamma)^{16}$O reaction at stellar energies," Nucl. Phys. **A410**, 334–348.

Langanke, K., and S. E. Koonin, 1985, "^{12}C$(\alpha,\gamma)^{16}$O revisited," Nucl. Phys. **A439**, 384–396.

Langanke, K., D. Lukas, H. M. Müller, S. Schramm, and S. E. Koonin, 1991, "Phase transition from a ^{4}He plasma to stable ^{8}Be matter," Z. Phys. A **339**, 419–420.

Langanke, K., and G. Martínez-Pinedo, 2000, "Shell-model calculations of stellar weak interaction rates: II. Weak rates for nuclei in the mass range $A = 45$–65 in supernovae environments," Nucl. Phys. **A673**, 481–508.

Langanke, K., and G. Martínez-Pinedo, 2003, "Nuclear weak-interaction processes in stars," Rev. Mod. Phys. **75**, 819–862.

Langanke, K., G. Martínez-Pinedo, J. M. Sampaio, D. J. Dean, W. R. Hix, O. E. Messer, A. Mezzacappa, M. Liebendörfer, H. T. Janka, and M. Rampp, 2003, "Electron Capture Rates on Nuclei and Implications for Stellar Core Collapse," Phys. Rev. Lett. **90**, 241102.

Langanke, K., and C. Rolfs, 1989, "On the $t(d,n)\alpha$ Reactivity in fusion reactors," Mod. Phys. Lett. A **04**, 2101–2112.

Langanke, K., T. D. Shoppa, C. A. Barnes, and C. Rolfs, 1996, "Energy loss, electron screening and the astrophysical ^{3}He$(d,p)^4$He cross section," Phys. Lett. B **369**, 211–214.

Langanke, K., R. Stademann, and A. Weiguny, 1983, "Microscopic study of heavy-particle transfer reactions: The $(^{16}$O$,\alpha)$ reactions on ^{16}O and ^{28}Si," Nucl. Phys. **A406**, 574–590.

Lashko, Y. A., V. S. Vasilevsky, and V. I. Zhaba, 2024, "Many-channel microscopic theory of resonance states and scattering processes in ^{9}Be and ^{9}B," Phys. Rev. C **109**, 045803.

Lattuada, M., F. Riggi, D. Vinciguerra, C. Spitaleri, G. Vourvopoulos, D. Miljanić, and E. Norbeck, 1988, "Energy dependence of direct effects in the ^{6}Li + ^{6}Li $\rightarrow 3\alpha$ reaction around the Coulomb barrier," Z. Phys. A **330**, 183–188.

Lau, R., *et al.*, 2018, "Nuclear reactions in the crusts of accreting neutron stars," Astrophys. J. **859**, 62.

Launey, K. D., A. Mercenne, and T. Dytrych, 2021, "Nuclear dynamics and reactions in the *ab initio* symmetry-adapted framework," Annu. Rev. Nucl. Part. Sci. **71**, 253–277.

Lavagno, A., and P. Quarati, 2000, "Nonextensive statistics in stellar plasma and solar neutrinos," Nucl. Phys. B, Proc. Suppl. **87**, 209–211.

Lazauskas, R., 2018, "Solution of the n-^{4}He elastic scattering problem using the Faddeev-Yakubovsky equations," Phys. Rev. C **97**, 044002.

Lazauskas, R., and J. Carbonell, 2004, "Testing nonlocal nucleon-nucleon interactions in four-nucleon systems," Phys. Rev. C **70**, 044002.

Leblanc, P. J., *et al.*, 2010, "Constraining the *S* factor of ^{15}N$(p,\gamma)^{16}$O at astrophysical energies," Phys. Rev. C **82**, 055804.

Lee, I., G. Gosselin, and A. Diaz-Torres, 2023, "Thermal and atomic effects on coupled-channels heavy-ion fusion," Phys. Rev. C **107**, 054609.

, Lemut, A., *et al.* (LUNA Collaboration), 2006, "First measurement of the ^{14}N$(p,\gamma)^{15}$O cross section down to 70 keV," Phys. Lett. B **634**, 483–487.

Leung, S.-C., K. Nomoto, and T. Suzuki, 2020, "Electron-capture supernovae of super-AGB stars: Sensitivity on input physics," Astrophys. J. **889**, 34.

Li, J. G., N. Michel, W. Zuo, and F. R. Xu, 2021, "Resonances of $A = 4$ $T = 1$ isospin triplet states within the *ab initio* no-core Gamow shell model," Phys. Rev. C **104**, 024319.

Li, Q., J. Görres, R. J. deBoer, G. Imbriani, A. Best, A. Kontos, P. J. LeBlanc, E. Uberseder, and M. Wiescher, 2016, "Cross section measurement of ^{14}N$(p,\gamma)^{15}$O in the CNO cycle," Phys. Rev. C **93**, 055806.

Li, Z. H., *et al.*, 2005, "The ^{8}Li$(d,p)^9$Li reaction and the astrophysical ^{8}Li$(n,\gamma)^9$Li reaction rate," Phys. Rev. C **71**, 052801.

Lind, P., 1993, "Completeness relations and resonant state expansions," Phys. Rev. C **47**, 1903–1920.

Litvinova, E., H. P. Loens, K. Langanke, G. Martínez-Pinedo, T. Rauscher, P. Ring, F. K. Thielemann, and V. Tselyaev, 2009, "Low-lying dipole response in the relativistic quasiparticle time blocking approximation and its influence on neutron capture cross sections," Nucl. Phys. **A823**, 26–37.

Liu, M.-Q., Y.-F. Yuan, and J. Zhang, 2009, "Effect of electron screening on the collapsing process of core-collapse supernovae," Mon. Not. R. Astron. Soc. **400**, 815–819.

Liu, Q., *et al.*, 2020, "Low-energy cross-section measurement of the ^{10}B$(\alpha,n)^{13}$N reaction and its impact on neutron production in first-generation stars," Phys. Rev. C **101**, 025808.

Liu, Q. K. K., H. Kanada, and Y. C. Tang, 1981, "Microscopic study of ^{3}He$(\alpha,\gamma)^7$Be electric-dipole capture reaction," Phys. Rev. C **23**, 645–656.

Loens, H. P., K. Langanke, G. Martínez-Pinedo, and K. Sieja, 2012, "*M*1 strength functions from large-scale shell-model calculations and their effect on astrophysical neutron capture cross-sections," Eur. Phys. J. A **48**, 34.

Lomnitz-Adler, J., 1993, "Automaton models of seismic fracture: Constraints imposed by the magnitude-frequency relation," J. Geophys. Res. **98**, 17745–17756.

Lopez-Saavedra, E., *et al.*, 2022, "Observation of a Near-Threshold Proton Resonance in ^{11}B," Phys. Rev. Lett. **129**, 012502.

Lorenz-Wirzba, H., 1978, "Untersuchung von (p,α) Reaktionen Unterhalb der Coulombbarriere," Ph.D. thesis (Westfälischen Wilhelms-Universität zu Münster).

Lorenz-Wirzba, H., P. Schmalbrock, H. P. Trautvetter, M. Wiescher, C. Rolfs, and W. S. Rodney, 1979, "The ^{18}O$(p,\alpha)^{15}$N reaction at stellar energies," Nucl. Phys. **A313**, 346–362.

Lovas, R. G., N. Tanaka, Y. Suzuki, and K. Varga, 2002, "Nuclear resonances by extrapolation of bound states," in *Resonances in Few-Body Systems*, Vol. 13, edited by A. T. Kruppa and R. G. Lovas (Springer, New York), pp. 76–85, 10.1007/978-3-7091-6114-2_8.

Lovato, A., S. Gandolfi, J. Carlson, S. C. Pieper, and R. Schiavilla, 2016, "Electromagnetic Response of ^{12}C: A First-Principles Calculation," Phys. Rev. Lett. **117**, 082501.

Ludwig, G., 1983a, *An Axiomatic Basis of Quantum Mechanics*, Vols. I and II (Springer-Verlag, New York).

Ludwig, G., 1983b, *Foundations of Quantum Mechanics*, Vols. I and II (Springer-Verlag, New York).

Lugaro, M., M. Ek, M. Pető, M. Pignatari, G. V. Makhatadze, I. J. Onyett, and M. Schönbächler, 2023, "Representation of *s*-process abundances for comparison to data from bulk meteorites," Eur. Phys. J. A **59**, 53.

Lugaro, M., M. Pignatari, R. Reifarth, and M. Wiescher, 2023, "The s process and beyond," Annu. Rev. Nucl. Part. Sci. **73**, 315–340.

Lynn, J. E., I. Tews, J. Carlson, S. Gandolfi, A. Gezerlis, K. E. Schmidt, and A. Schwenk, 2016, "Chiral Three-Nucleon Interactions in Light Nuclei, Neutron-α Scattering, and Neutron Matter," Phys. Rev. Lett. **116**, 062501.

Lyons, S., *et al.*, 2018, "Determination of $^{20}\mathrm{Ne}(p,\gamma)^{21}\mathrm{Na}$ cross sections from $E_p = 500$–2000 keV," Phys. Rev. C **97**, 065802.

Ma, W. H., *et al.*, 2021, "Observation of $^6\mathrm{He} + t$ cluster states in $^9\mathrm{Li}$," Phys. Rev. C **103**, L061302.

MacArthur, J. D., H. C. Evans, J. R. Leslie, and H. B. Mak, 1980, "First two members of the $\mathrm{K}^\pi = 0^-$ band in $^{20}\mathrm{Ne}$," Phys. Rev. C **22**, 356–361.

MacDonald, W. M., 1964a, "Antisymmetrization of a unified nuclear reaction theory," Nucl. Phys. **56**, 636–646.

MacDonald, W. M., 1964b, "A unified nuclear reaction theory for phenomenological analyses," Nucl. Phys. **54**, 393–404.

Macfarlane, M. H., and J. B. French, 1960, "Stripping reactions and the structure of light and intermediate nuclei," Rev. Mod. Phys. **32**, 567–691.

Magee, R. M., *et al.*, 2023, "First measurements of $p^{11}\mathrm{B}$ fusion in a magnetically confined plasma," Nat. Commun. **14**, 955.

Magg, E., *et al.*, 2022, "Observational constraints on the origin of the elements. IV. Standard composition of the Sun," Astron. Astrophys. **661**, A140.

Magunov, A. I., I. Rotter, and S. I. Strakhova, 1999, "Laser-induced resonance trapping in atoms," J. Phys. B **32**, 1669–1684.

Mahaux, C., and H. A. Weidenmüller, 1969, *Shell-Model Approach to Nuclear Reactions* (North-Holland, Amsterdam).

Mak, H. B., H. C. Evans, G. T. Ewan, and J. D. Macarthur, 1978, "The $^{18}\mathrm{O}(p,\alpha)^{15}\mathrm{N}$ cross section at low energies," Nucl. Phys. **A304**, 210–220.

Makii, H., Y. Nagai, T. Shima, M. Segawa, K. Mishima, H. Ueda, M. Igashira, and T. Ohsaki, 2009, "$E1$ and $E2$ cross sections of the $^{12}\mathrm{C}(\alpha,\gamma_0)^{16}\mathrm{O}$ reaction using pulsed α beams," Phys. Rev. C **80**, 065802.

Mao, X., K. Fossez, and W. Nazarewicz, 2018, "Resonant spectra of multipole-bound anions," Phys. Rev. A **98**, 062515.

Mao, Z. Q., H. T. Fortune, and A. G. Lacaze, 1996, "Alpha-particle spectroscopic strengths in $^{19}\mathrm{F}$ and $^{20}\mathrm{Ne}$," Phys. Rev. C **53**, 1197–1204.

Marion, J. B., and W. A. Fowler, 1957, "Nuclear reactions with the neon isotopes in stars," Astrophys. J. **125**, 221.

Marković, D., and C. Gros, 2014, "Power laws and self-organized criticality in theory and nature," Phys. Rep. **536**, 41–74.

Marta, M., *et al.*, 2008, "Precision study of ground state capture in the $^{14}\mathrm{N}(p,\gamma)^{15}\mathrm{O}$ reaction," Phys. Rev. C **78**, 022802.

Martínez-Pinedo, G., Y. H. Lam, K. Langanke, R. G. T. Zegers, and C. Sullivan, 2014, "Astrophysical weak-interaction rates for selected $A = 20$ and $A = 24$ nuclei," Phys. Rev. C **89**, 045806.

Masha, E., *et al.* (LUNA Collaboration), 2023, "First measurement of the low-energy direct capture in $^{20}\mathrm{Ne}(p,\gamma)^{21}\mathrm{Na}$ and improved energy and strength of the $E_{\mathrm{c.m.}} = 368$ keV resonance," Phys. Rev. C **108**, L052801.

Massimi, C., *et al.*, 2012, "Resonance neutron-capture cross sections of stable magnesium isotopes and their astrophysical implications," Phys. Rev. C **85**, 044615.

Massimi, C., *et al.*, 2017, "Neutron spectroscopy of $^{26}\mathrm{Mg}$ states: Constraining the stellar neutron source $^{22}\mathrm{Ne}(\alpha,n)^{25}\mathrm{Mg}$," Phys. Lett. B **768**, 1–6.

Masui, H., K. Katō, N. Michel, and M. Płoszajczak, 2014, "Precise comparison of the Gaussian expansion method and the Gamow shell model," Phys. Rev. C **89**, 044317.

Mather, J. V., M. W. Sachs, R. H. Siemssen, A. Weidinger, and D. A. Bromley, 1969, "Nuclear interaction of oxygen with oxygen," Phys. Rev. **188**, 1665–1682.

Maurin, K., 1968, *Generalized Eigenfunction Expansions and Unitary Representations of Topological Groups*, Vol. 48 (Polish Scientific Publishers, Warsaw).

Mazarakis, M. G., and W. E. Stephens, 1973, "Experimental measurements of the $^{12}\mathrm{C} + {}^{12}\mathrm{C}$ nuclear reactions at low energies," Phys. Rev. C **7**, 1280–1287.

McCracken, C., P. Navrátil, A. McCoy, S. Quaglioni, and G. Hupin, 2021, "Microscopic investigation of the $^8\mathrm{Li}(n,\gamma)^9\mathrm{Li}$ reaction," Phys. Rev. C **103**, 035801.

McEllistrem, M. T., K. W. Jones, R. Chiba, R. A. Douglas, D. F. Herring, and E. A. Silverstein, 1956, "Differential cross sections for $^{12}\mathrm{C}(d,d)^{12}\mathrm{C}$ and $^{12}\mathrm{C}(d,p)^{13}\mathrm{C}$," Phys. Rev. **104**, 1008–1017.

McGrath, R. L., D. Abriola, J. Karp, T. Renner, and S. Y. Zhu, 1981, "Direct γ transitions in $^{12}\mathrm{C} + {}^{12}\mathrm{C}$," Phys. Rev. C **24**, 2374–2377.

Mehta, A. K., A. Buonanno, J. Gair, M. C. Miller, E. Farag, R. J. deBoer, M. Wiescher, and F. X. Timmes, 2022, "Observing intermediate-mass black holes and the upper stellar-mass gap with LIGO and Virgo," Astrophys. J. **924**, 39.

Mercenne, A., N. Michel, J. P. Linares Fernández, and M. Płoszajczak, 2023, "Gamow shell model description of the $^{40}\mathrm{Ca}(d,p)$ transfer reaction," Phys. Rev. C **107**, L011603.

Mercenne, A., N. Michel, and M. Płoszajczak, 2019, "Gamow shell model description of $^4\mathrm{He}(d,d)$ elastic scattering reactions," Phys. Rev. C **99**, 044606.

Merrill, P. W., 1952, "Techetium in the stars," Science **115**, 479–489.

Metag, V., A. Lazzarini, K. Lesko, and R. Vandenbosch, 1982, "Search for γ rays from the quasimolecular $^{12}\mathrm{C} + {}^{12}\mathrm{C}$ system," Phys. Rev. C **25**, 1486–1493.

Metcalfe, T. S., M. Salaris, and D. E. Winget, 2002, "Measuring $^{12}\mathrm{C}(\alpha,\gamma)^{16}\mathrm{O}$ from white dwarf asteroseismology," Astrophys. J. **573**, 803–811.

Meyerhof, W. E., 1963, "Threshold effects in average cross sections according to R-matrix theory," Phys. Rev. **129**, 692–702.

Mezhevych, S. Y., A. T. Rudchik, A. A. Rudchik, O. A. Ponkratenko, N. Keeley, K. W. Kemper, M. Mazzocco, K. Rusek, and S. B. Sakuta, 2017, "Cluster structure of $^{17}\mathrm{O}$," Phys. Rev. C **95**, 034607.

Michaud, G., 1973, "Experimental evidence for repulsive cores in heavy-ion reactions," Phys. Rev. C **8**, 525–533.

Michaud, G. J., and E. W. Vogt, 1972, "Phenomenological analysis of the $^{12}\mathrm{C} + {}^{12}\mathrm{C}$ reaction," Phys. Rev. C **5**, 350–368.

Michel, F., G. Reidemeister, and S. Ohkubo, 1986, "Evidence for Alpha-Particle Clustering in the $^{44}\mathrm{Ti}$ Nucleus," Phys. Rev. Lett. **57**, 1215–1218.

Michel, N., W. Nazarewicz, and M. Płoszajczak, 2007, "Threshold effects in multichannel coupling and spectroscopic factors in exotic nuclei," Phys. Rev. C **75**, 031301.

Michel, N., W. Nazarewicz, and M. Płoszajczak, 2010, "Isospin mixing and the continuum coupling in weakly bound nuclei," Phys. Rev. C **82**, 044315.

Michel, N., W. Nazarewicz, and M. Płoszajczak, 2023, "Description of the Proton-Decaying 0_2^+ Resonance of the α Particle," Phys. Rev. Lett. **131**, 242502.

Michel, N., W. Nazarewicz, M. Płoszajczak, and K. Bennaceur, 2002, "Gamow Shell Model Description of Neutron-Rich Nuclei," Phys. Rev. Lett. **89**, 042502.

Michel, N., W. Nazarewicz, M. Płoszajczak, and J. Okołowicz, 2003, "Gamow shell model description of weakly bound nuclei and unbound nuclear states," Phys. Rev. C **67**, 054311.

Michel, N., W. Nazarewicz, M. Płoszajczak, and T. Vertse, 2009, "Topical review: Shell model in the complex energy plane," J. Phys. G **36**, 013101.

Michel, N., and M. Płoszajczak, 2021, *Gamow Shell Model: The Unified Theory of Nuclear Structure and Reactions*, Lecture Notes in Physics Vol. 983 (Springer, New York), 10.1007/978-3-030-69356-5.

Minea, A., and P. Villieu, 2009, "Threshold effects in monetary and fiscal policies in a growth model: Assessing the importance of the financial system," J. Macroecon. **31**, 304–319.

Mişicu, Ş., and H. Esbensen, 2006, "Hindrance of Heavy-Ion Fusion due to Nuclear Incompressibility," Phys. Rev. Lett. **96**, 112701.

Mohr, P., 2003, "Low-energy direct capture in the ^{8}Li$(n,\gamma)^9$Li and ^{8}B$(p,\gamma)^9$C reactions," Phys. Rev. C **67**, 065802.

Mohr, P., 2005, "Low-energy direct capture in the ^{16}O$(\alpha,\gamma)^{20}$Ne reaction," Phys. Rev. C **72**, 035803.

Mohr, P., H. Abele, R. Zwiebel, G. Staudt, H. Krauss, H. Oberhummer, A. Denker, J. W. Hammer, and G. Wolf, 1993, "Alpha scattering and capture reactions in the $A = 7$ system at low energies," Phys. Rev. C **48**, 1420–1427.

Mohr, P., Z. Fülöp, G. Gyürky, G. G. Kiss, and T. Szücs, 2020, "Successful Prediction of Total α -Induced Reaction Cross Sections at Astrophysically Relevant Sub-Coulomb Energies Using a Novel Approach," Phys. Rev. Lett. **124**, 252701.

Mohr, P., V. Kölle, S. Wilmes, U. Atzrott, G. Staudt, J. W. Hammer, H. Krauss, and H. Oberhummer, 1994, "Direct capture in the 3^+ resonance of ^{2}H$(\alpha,\gamma)^6$Li," Phys. Rev. C **50**, 1543–1549.

Moiseyev, N., 2011, *Non-Hermitian Quantum Mechanics* (Cambridge University Press, New York).

Monpribat, E., *et al.*, 2022, "A new ^{12}C + ^{12}C nuclear reaction rate: Impact on stellar evolution," Astron. Astrophys. **660**, A47.

Montagnoli, G., and A. M. Stefanini, 2017, "Recent experimental results in sub- and near-barrier heavy-ion fusion reactions," Eur. Phys. J. A **53**, 169.

Moore, C. F., C. E. Watson, S. A. Zaidi, J. J. Kent, and J. G. Kulleck, 1966, "Experimental Observation of the Coupling of the Analogous Channels in a (d,p) and (d,n) Reaction," Phys. Rev. Lett. **17**, 926–928.

Morales-Gallegos, L., *et al.*, 2018, "Reduction of deuterium content in carbon targets for ^{12}C + ^{12}C reaction studies of astrophysical interest," Eur. Phys. J. A **54**, 132.

Morales-Gallegos, L., *et al.*, 2023, "^{12}C + ^{12}C reactions for nuclear astrophysics," EPJ Web Conf. **279**, 11005.

Morales-Gallegos, L., *et al.*, 2024, "Direct measurements of the ^{12}C + ^{12}C reactions cross-sections towards astrophysical energies," Eur. Phys. J. A **60**, 11.

Morlock, R., R. Kunz, A. Mayer, M. Jaeger, A. Müller, J. W. Hammer, P. Mohr, H. Oberhummer, G. Staudt, and V. Kölle, 1997, "Halo Properties of the First $1/2^+$ State in ^{17}F from the ^{16}O$(p,\gamma)^{17}$F Reaction," Phys. Rev. Lett. **79**, 3837–3840.

Moschini, L., J. Yang, and P. Capel, 2019, "^{15}C: From halo effective field theory structure to the study of transfer, breakup, and radiative-capture reactions," Phys. Rev. C **100**, 044615.

Moscoso, J., R. S. de Souza, A. Coc, and C. Iliadis, 2021, "Bayesian estimation of the $d(p,\gamma)^3$He thermonuclear reaction rate," Astrophys. J. **923**, 49.

Motobayashi, T., 2001, "Indirect measurements of the solar-neutrino production reaction ^{7}Be$(p,\gamma)^8$B," Nucl. Phys. **A693**, 258–268.

Motobayashi, T., *et al.*, 1994, "Coulomb Dissociation of ^{8}B and the ^{7}Be$(p,\gamma)^8$B Reaction at Low Energies," Phys. Rev. Lett. **73**, 2680–2683.

Mughabghab, S., M. Divadeenam, and N. Holden, 1982, *Neutron Cross Sections: Neutron Resonance Parameters and Thermal Cross Sections, Part A: Z = 1–60*, Vol. 1 (Academic Press, New York).

Mukhamedzanov, A. M., 2022, "Status of deep subbarrier ^{12}C + ^{12}C fusion and advancing the Trojan horse method," Eur. Phys. J. A **58**, 71.

Mukhamedzhanov, A. M., 2023, "Proton 0.01 MeV resonance width and low-energy S factor of $p + {}^{10}$B fusion," Phys. Rev. C **108**, 054603.

Mukhamedzhanov, A. M., and L. D. Blokhintsev, 2022, "Asymptotic normalization coefficients in nuclear reactions and nuclear astrophysics," Eur. Phys. J. A **58**, 29.

Mukhamedzhanov, A. M., R. J. deBoer, B. F. Irgaziev, L. D. Blokhintsev, A. S. Kadyrov, and D. A. Savin, 2023, "Asymptotic normalization coefficients for $\alpha + {}^{12}$C synthesis and the S-factor for ^{12}C$(\alpha,\gamma)^{16}$O radiative capture," arXiv:2310.20255.

Mukhamedzhanov, A. M., C. A. Gagliardi, and R. E. Tribble, 2001, "Asymptotic normalization coefficients, spectroscopic factors, and direct radiative capture rates," Phys. Rev. C **63**, 024612.

Mukhamedzhanov, A. M., B. F. Irgaziev, V. Z. Goldberg, Y. V. Orlov, and I. Qazi, 2010, "Bound, virtual, and resonance S-matrix poles from the Schrödinger equation," Phys. Rev. C **81**, 054314.

Mukhamedzhanov, A. M., A. S. Kadyrov, and D. Y. Pang, 2020, "Trojan horse method as an indirect approach to study resonant reactions in nuclear astrophysics," Eur. Phys. J. A **56**, 233.

Mukhamedzhanov, A. M., Shubhchintak, and C. A. Bertulani, 2017, "Subthreshold resonances and resonances in the R-matrix method for binary reactions and in the Trojan horse method," Phys. Rev. C **96**, 024623.

Mukhamedzhanov, A. M., and R. E. Tribble, 1999, "Connection between asymptotic normalization coefficients, subthreshold bound states, and resonances," Phys. Rev. C **59**, 3418–3424.

Mukhamedzhanov, A. M., *et al.*, 2003, "Asymptotic normalization coefficients for ^{14}N + p^{15}O and the astrophysical S factor for ^{14}N$(p,\gamma)^{15}$O," Phys. Rev. C **67**, 065804.

Mukhamedzhanov, A. M., *et al.*, 2006, "Asymptotic normalization coefficients from the ^{20}Ne$(^3$He$,d)^{21}$Na reaction and astrophysical factor for ^{20}Ne$(p,\gamma)^{21}$Na," Phys. Rev. C **73**, 035806.

Mukhamedzhanov, A. M., *et al.*, 2007, "Indirect techniques in nuclear astrophysics. Asymptotic normalization coefficient and Trojan horse," Nucl. Phys. **A787**, 321–328.

Müller, H. M., and K. Langanke, 1994, "Study of dense helium plasma in the optimal hypernetted chain approximation," Phys. Rev. C **49**, 524–532.

Myo, T., and K. Katō, 2020, "Complex scaling: Physics of unbound light nuclei and perspective," Prog. Theor. Exp. Phys. 12A101.

Nagatani, K., M. R. Dwarakanath, and D. Ashery, 1969, "The ^{3}He$(\alpha,\gamma)^7$Be reaction at very low energy," Nucl. Phys. **A128**, 325–332.

Navrátil, P., 2007, "Local three-nucleon interaction from chiral effective field theory," Few-Body Syst. **41**, 117–140.

Navrátil, P., C. A. Bertulani, and E. Caurier, 2006a, "^{7}Be$(p,\gamma)^8$B S-factor from *ab initio* wave functions," J. Phys. Conf. Ser. **49**, 15–20.

Navrátil, P., C. A. Bertulani, and E. Caurier, 2006b, "^{7}Be$(p,\gamma)^8$B S-factor from *ab initio* wave functions," Phys. Lett. B **634**, 191–194.

Navrátil, P., and S. Quaglioni, 2012, "*Ab Initio* Many-Body Calculations of the ^{3}H$(d,n)^4$He and ^{3}He$(d,p)^4$He Fusion Reactions," Phys. Rev. Lett. **108**, 042503.

Navrátil, P., and S. Quaglioni, 2020, "*Ab initio* nuclear reaction theory with applications to astrophysics," in *Handbook of Nuclear Physics*, edited by I. Tanihata, H. Toki, and T. Kajino (Springer Nature, Singapore), pp. 1–46.

Navrátil, P., S. Quaglioni, G. Hupin, C. Romero-Redondo, and A. Calci, 2016, "Unified *ab initio* approaches to nuclear structure and reactions," Phys. Scr. **91**, 053002.

Navrátil, P., R. Roth, and S. Quaglioni, 2011, "*Ab initio* many-body calculation of the ^{7}Be$(p,\gamma)^8$B radiative capture," Phys. Lett. B **704**, 379–383.

Navrátil, P., J. P. Vary, and B. R. Barrett, 2000a, "Large-basis *ab initio* no-core shell model and its application to ^{12}C," Phys. Rev. C **62**, 054311.

Navrátil, P., J. P. Vary, and B. R. Barrett, 2000b, "Properties of ^{12}C in the *Ab Initio* Nuclear Shell Model," Phys. Rev. Lett. **84**, 5728–5731.

Neff, T., 2011, "Microscopic Calculation of the ^{3}He$(\alpha,\gamma)^7$Be and ^{3}H$(\alpha,\gamma)^7$Li Capture Cross Sections Using Realistic Interactions," Phys. Rev. Lett. **106**, 042502.

Neff, T., and H. Feldmeier, 2003, "Tensor correlations in the unitary correlation operator method," Nucl. Phys. **A713**, 311–371.

Neff, T., and H. Feldmeier, 2009, "Microscopic description of few-body systems in the fermionic molecular dynamics approach," Few-Body Syst. **45**, 145–147.

Newton, J. O., R. D. Butt, M. Dasgupta, D. J. Hinde, I. I. Gontchar, C. R. Morton, and K. Hagino, 2004, "Systematics of precise nuclear fusion cross sections: The need for a new dynamical treatment of fusion?," Phys. Lett. B **586**, 219–224.

Newton, R. G., 1958, "Inelastic scattering," Ann. Phys. (N.Y.) **4**, 29–56.

Newton, R. G., 1959, "Threshold properties of scattering and reaction cross sections," Phys. Rev. **114**, 1611–1618.

Nollett, K. M., 2001, "Radiative α-capture cross sections from realistic nucleon-nucleon interactions and variational Monte Carlo wave functions," Phys. Rev. C **63**, 054002.

Nollett, K. M., S. C. Pieper, R. B. Wiringa, J. Carlson, and G. M. Hale, 2007, "Quantum Monte Carlo Calculations of Neutron-α Scattering," Phys. Rev. Lett. **99**, 022502.

Nomoto, K., 1984, "Evolution of 8–10 solar mass stars toward electron capture supernovae. I—Formation of electron-degenerate O + Ne + Mg cores," Astrophys. J. **277**, 791–805.

Nomoto, K., 1987, "Evolution of 8–10 M_{sun} Stars toward electron capture supernovae. II. Collapse of an O + Ne + Mg core," Astrophys. J. **322**, 206.

Odell, D., C. R. Brune, and D. R. Phillips, 2022, "How Bayesian methods can improve *R*-matrix analyses of data: The example of the *dt* reaction," Phys. Rev. C **105**, 014625.

Odell, D., C. R. Brune, D. R. Phillips, R. J. deBoer, and S. N. Paneru, 2022, "Performing Bayesian analyses with `AZURE2` using `BRICK`: An application to the ^{7}Be system," Front. Phys. **10**, 888476.

Ogata, S., S. Ichimaru, and H. M. van Horn, 1993, "Thermonuclear reaction rates for dense binary-ionic mixtures," Astrophys. J. **417**, 265.

Ogata, S., H. Iyetomi, and S. Ichimaru, 1991, "Nuclear reaction rates in dense carbon-oxygen mixtures," Astrophys. J. **372**, 259.

Ohanian, H. C., and C. G. Ginsburg, 1974, "Antibound 'states' and resonances," Am. J. Phys. **42**, 310–315.

Okołowicz, J., N. Michel, W. Nazarewicz, and M. Płoszajczak, 2012, "Asymptotic normalization coefficients and continuum coupling in mirror nuclei," Phys. Rev. C **85**, 064320.

Okołowicz, J., W. Nazarewicz, and M. Płoszajczak, 2013, "Toward understanding the microscopic origin of nuclear clustering," Fortschr. Phys. **61**, 66–79.

Okołowicz, J., M. Płoszajczak, R. J. Charity, and L. G. Sobotka, 2018, "Collectivization of anti-analog strength above charged particle thresholds," Phys. Rev. C **97**, 044303.

Okołowicz, J., M. Płoszajczak, and W. Nazarewicz, 2012, "On the origin of nuclear clustering," Prog. Theor. Phys. Suppl. **196**, 230–243.

Okołowicz, J., M. Płoszajczak, and W. Nazarewicz, 2020, "Convenient Location of a Near-Threshold Proton-Emitting Resonance in ^{11}B," Phys. Rev. Lett. **124**, 042502.

Okołowicz, J., M. Płoszajczak, and W. Nazarewicz, 2022, "$\beta^- p$ and $\beta^- \alpha$ decay of the ^{11}Be neutron halo ground state," J. Phys. G **49**, 10LT01.

Okołowicz, J., M. Płoszajczak, and W. Nazarewicz, 2023, "Near-threshold resonances in ^{11}C and the ^{10}B$(p,\alpha)^7$Be aneutronic reaction," Phys. Rev. C **107**, L021305.

Okołowicz, J., M. Płoszajczak, and W. Nazarewicz, 2024, "Erratum: Near-threshold resonances in ^{11}C and the ^{10}B$(p,\alpha)^7$Be aneutronic reaction [Phys. Rev. C **107**, L021305 (2023)]," Phys. Rev. C **109**, 059902.

Okołowicz, J., M. Płoszajczak, and I. Rotter, 2003, "Dynamics of quantum systems embedded in a continuum," Phys. Rep. **374**, 271–383.

Oliva, A. A., and G. L. Guardo, 2024, "Shedding light on ^{17}O$(n,\alpha)^{14}$C reaction at astrophysical energies with Trojan horse method and asymptotic normalization coefficient," EPJ Web Conf. **297**, 02008.

Opher, M., and R. Opher, 2000, "Dynamic screening in thermonuclear reactions," Astrophys. J. **535**, 473–474.

Osborne, J. L., C. A. Barnes, R. W. Kavanagh, R. M. Kremer, G. J. Mathews, J. L. Zyskind, P. D. Parker, and A. J. Howard, 1982, "Low Energy ^{3}He$(\alpha,\gamma)^7$Be Cross-Section Measurements," Phys. Rev. Lett. **48**, 1664–1666.

Osborne, J. L., C. A. Barnes, R. W. Kavanagh, R. M. Kremer, G. J. Mathews, J. L. Zyskind, P. D. Parker, and A. J. Howard, 1984, "Low-energy behavior of the ^{3}He$(\alpha,\gamma)^7$Be cross section," Nucl. Phys. **A419**, 115–132.

Otsuka, T., T. Abe, T. Yoshida, Y. Tsunoda, N. Shimizu, N. Itagaki, Y. Utsuno, J. Vary, P. Maris, and H. Ueno, 2022, "α-clustering in atomic nuclei from first principles with statistical learning and the Hoyle state character," Nat. Commun. **13**, 2234.

Otsuki, K., J. Truran, M. Wiescher, J. Gorres, G. Mathews, D. Frekers, A. Mengoni, A. Bartlett, and J. Tostevin, 2006, "Origin of the main *r*-process elements," AIP Conf. Proc. **847**, 227–232.

Ouellet, J. M. L., *et al.*, 1992, "^{12}C$(\alpha,\gamma)^{16}$O Cross Sections at Stellar Energies," Phys. Rev. Lett. **69**, 1896–1899.

Palmerini, S., *et al.*, 2021, "Presolar grain isotopic ratios as constraints to nuclear and stellar parameters of asymptotic giant branch star nucleosynthesis," Astrophys. J. **921**, 7.

Paneru, S. N., *et al.*, 2024, "Elastic scattering of ^{3}He + ^{4}He with the SONIK scattering chamber," Phys. Rev. C **109**, 015802.

Paneta, R., H. Dabrowski, L. Freindl, and K. Grotowski, 1979, "Explanation of the anomalously small absorption of α-particles in ^{40}Ca nuclei," Nucl. Phys. **A326**, 97–107.

Pantaleo, F. R., *et al.* (LUNA Collaboration), 2021, "Low-energy resonances in the ^{18}O$(p,\gamma)^{19}$F reaction," Phys. Rev. C **104**, 025802.

Papadimitriou, G., J. Rotureau, N. Michel, M. Płoszajczak, and B. R. Barrett, 2013, "*Ab initio* no-core Gamow shell model calculations with realistic interactions," Phys. Rev. C **88**, 044318.

Paris, M. W., and M. B. Chadwick, 2023, "A lost detail in D–T fusion history," Phys. Today **76**, No. 10, 10–11.

Paris, M. W., and M. B. Chadwick, 2024, "Anthropic importance of the 'Bretscher state' in DT fusion," Fusion Sci. Technol. **80**, S110–S119.

Park, J. Y., W. Greiner, and W. Scheid, 1977, “Quasimolecular states in the ^{12}C-^{12}C system,” Phys. Rev. C **16**, 2276–2290.

Parker, P. D., 1968, “Reanalysis of the Be$^7(p,\gamma)$B^8 cross-section data,” Astrophys. J. Lett. **153**, L85.

Parker, P. D., and R. W. Kavanagh, 1963, “He$^3(\alpha,\gamma)$Be^7 reaction,” Phys. Rev. **131**, 2578–2582.

Patterson, J. R., H. Winkler, and C. S. Zaidins, 1969, “Experimental investigation of the stellar nuclear reaction ^{12}C + ^{12}C at low energies,” Astrophys. J. **157**, 367.

Paul, H., 2006, “A comparison of recent stopping power tables for light and medium-heavy ions with experimental data, and applications to radiotherapy dosimetry,” Nucl. Instrum. Methods Phys. Res., Sect. B **247**, 166–172.

Pearson, J. D., and R. H. Spear, 1964, “A study of the gamma radiation produced in the alpha-particle bombardment of O^{16},” Nucl. Phys. **54**, 434–464.

Pellegriti, M. G., *et al.*, 2008, “Indirect study of the ^{13}C$(\alpha,n)^{16}$O reaction via the ^{13}C(^{7}Li, t)^{17}O transfer reaction,” Phys. Rev. C **77**, 042801.

Persson, E., M. Müller, and I. Rotter, 1996, “Resonance phenomena near thresholds,” Phys. Rev. C **53**, 3002–3008.

Philpott, R., 1977, Fizika (Zegreb) **9**, 109.

Pignatari, M., R. Gallino, M. Heil, M. Wiescher, F. Käppeler, F. Herwig, and S. Bisterzo, 2010, “The weak *s*-process in massive stars and its dependence on the neutron capture cross sections,” Astrophys. J. **710**, 1557–1577.

Pignatari, M., R. Hirschi, M. Wiescher, R. Gallino, M. Bennett, M. Beard, C. Fryer, F. Herwig, G. Rockefeller, and F. X. Timmes, 2013, “The ^{12}C + ^{12}C reaction and the impact on nucleosynthesis in massive stars,” Astrophys. J. **762**, 31.

Pignatari, M., P. Hoppe, R. Trappitsch, C. Fryer, F. Timmes, F. Herwig, and R. Hirschi, 2018, “The neutron capture process in the He shell in core-collapse supernovae: Presolar silicon carbide grains as a diagnostic tool for nuclear astrophysics,” Geochim. Cosmochim. Acta **221**, 37–46.

Pitrou, C., and M. Pospelov, 2020, “QED corrections to big-bang nucleosynthesis reaction rates,” Phys. Rev. C **102**, 015803.

Pizzone, R. G., C. A. Bertulani, L. Lamia, M. L. Cognata, M. L. Sergi, R. Spartá, and A. Tumino, 2020, “Clusters and their fundamental role for Trojan horse method,” Eur. Phys. J. A **56**, 283.

Pizzone, R. G., *et al.*, 2010, “Trojan horse method: A useful tool for electron screening effect investigation,” Nucl. Phys. **A834**, 673–675.

Plag, R., R. Reifarth, M. Heil, F. Käppeler, G. Rupp, F. Voss, and K. Wisshak, 2012, “^{12}C$(\alpha,\gamma)^{16}$O studied with the Karlsruhe 4πBaF$_2$ detector,” Phys. Rev. C **86**, 015805.

Płoszajczak, M., and J. Okołowicz, 2020, “Collectivity of the electromagnetic transitions in near-threshold resonances,” J. Phys. Conf. Ser. **1643**, 012156.

Politano, M., S. Starrfield, J. W. Truran, A. Weiss, and W. M. Sparks, 1995, “Hydrodynamic studies of accretion onto massive white dwarfs: ONeMg-enriched nova outbursts. I. Dependence on white dwarf mass,” Astrophys. J. **448**, 807.

Pollock, E. L., and B. Militzer, 2004, “Dense Plasma Effects on Nuclear Reaction Rates,” Phys. Rev. Lett. **92**, 021101.

Potekhin, A. Y., and G. Chabrier, 2000, “Equation of state of fully ionized electron-ion plasmas. II. Extension to relativistic densities and to the solid phase,” Phys. Rev. E. **62**, 8554–8563.

Poudel, M., and D. R. Phillips, 2022, “Effective field theory analysis of ^{3}He-α scattering data,” J. Phys. G **49**, 045102.

Prati, P., *et al.*, 1994, “Electron screening in the $d + {}^3$He fusion reaction,” Z. Phys. A **350**, 171–176.

Premarathna, P., and G. Rupak, 2020, “Bayesian analysis of capture reactions ^{3}He$(\alpha,\gamma)^7$Be and ^{3}H$(\alpha,\gamma)^7$Li,” Eur. Phys. J. A **56**, 166.

Pruet, J., R. D. Hoffman, S. E. Woosley, H. T. Janka, and R. Buras, 2006, “Nucleosynthesis in early supernova winds. II. The role of neutrinos,” Astrophys. J. **644**, 1028–1039.

Quaglioni, S., and P. Navrátil, 2009, “*Ab initio* many-body calculations of nucleon-nucleus scattering,” Phys. Rev. C **79**, 044606.

Raiola, F., *et al.*, 2004, “Enhanced electron screening in $d(d,p)t$ for deuterated metals,” Eur. Phys. J. A **19**, 283–287.

Raiola, F., *et al.*, 2006, “Enhanced $d(d,p)t$ fusion reaction in metals,” Eur. Phys. J. A **27**, 79–82.

Raiola, F., *et al.*, 2007, “First hint on a change of the ^{210}Po alpha-decay half-life in the metal Cu,” Eur. Phys. J. A **32**, 51–53.

Raman, S., M. Igashira, Y. Dozono, H. Kitazawa, M. Mizumoto, and J. E. Lynn, 1990, “Valence capture mechanism in resonance neutron capture by ^{13}C,” Phys. Rev. C **41**, 458–471.

Ramírez Jiménez, D. F., and N. G. Kelkar, 2018, “Different manifestations of *S*-matrix poles,” Ann. Phys. (Amsterdam) **396**, 18–43.

Ramström, E., and T. Wiedling, 1976, “The excitation function of the ^{13}C$(\alpha,n)^{16}$O reaction and its astrophysical application,” Nucl. Phys. **A272**, 259–268.

Ramström, E., and T. Wiedling, 1977, “The reaction rate of the ^{13}C$(\alpha,n)^{16}$O process,” Astrophys. J. **211**, 223–225.

Randhawa, J. S., *et al.*, 2020, “First Direct Measurement of ^{22}Mg$(\alpha,p)^{25}$Al and Implications for X-Ray Burst Model-Observation Comparisons,” Phys. Rev. Lett. **125**, 202701.

Rauscher, T., 2011, “The path to improved reaction rates for astrophysics,” Int. J. Mod. Phys. E **20**, 1071–1169.

Rauscher, T., A. Heger, R. D. Hoffman, and S. E. Woosley, 2002, “Nucleosynthesis in massive stars with improved nuclear and stellar physics,” Astrophys. J. **576**, 323–348.

Rauscher, T., and F.-K. Thielemann, 2000, “Astrophysical reaction rates from statistical model calculations,” At. Data Nucl. Data Tables **75**, 1–351.

Redder, A., H. W. Becker, C. Rolfs, H. P. Trautvetter, T. R. Donoghue, T. C. Rinckel, J. W. Hammer, and K. Langanke, 1987, “The ^{12}C$(\alpha,\gamma)^{16}$O cross section at stellar energies,” Nucl. Phys. **A462**, 385–412.

Reeves, H., and E. E. Salpeter, 1959, “Nuclear reactions in stars. IV. Buildup from carbon,” Phys. Rev. **116**, 1505–1516.

Refsgaard, J., J. Büscher, A. Arokiaraj, H. O. U. Fynbo, R. Raabe, and K. Riisager, 2019, “Clarification of large-strength transitions in the β decay of ^{11}Be,” Phys. Rev. C **99**, 044316.

Reyment, R. A., 1982, “Threshold characters in a Cretaceous foraminifer,” Palaeogeogr., Palaeoclimatol., Palaeoecol. **38**, 1–7.

Reynolds, H. L., D. W. Scott, and A. Zucker, 1953, “Nuclear reactions with energetic nitrogen ions,” Proc. Natl. Acad. Sci. U.S.A. **39**, 975–985.

Reynolds, H. L., D. W. Scott, and A. Zucker, 1956, “Nuclear reactions produced by nitrogen on boron and oxygen,” Phys. Rev. **102**, 237–241.

Riisager, K., *et al.*, 2014, “^{11}Be(βp), a quasi-free neutron decay?,” Phys. Lett. B **732**, 305–308.

Riisager, K., *et al.*, 2020, “Search for beta-delayed proton emission from ^{11}Be,” Eur. Phys. J. A **56**, 100.

Robertson, R. G. H., P. Dyer, T. J. Bowles, R. E. Brown, N. Jarmie, C. J. Maggiore, and S. M. Austin, 1983, “Cross section of the capture reaction ^{3}He$(\alpha,\gamma)^7$Be,” Phys. Rev. C **27**, 11–17.

Robertson, R. G. H., P. Dyer, R. A. Warner, R. C. Melin, T. J. Bowles, A. B. McDonald, G. C. Ball, W. G. Davies, and E. D. Earle, 1981, “Observation of the Capture Reaction ^{2}H$(\alpha,\gamma)^6$Li and Its Role in Production of ^{6}Li in the Big Bang,” Phys. Rev. Lett. **47**, 1867–1870.

Rodberg, L. S., 1961, "Calculable model for compound nucleus-direct interaction interference," Phys. Rev. **124**, 210–212.

Rolfs, C., 1973, "Spectroscopic factors from radiative capture reactions," Nucl. Phys. **A217**, 29–70.

Rolfs, C., 2001, "Nuclear reactions in stars," Prog. Part. Nucl. Phys. **46**, 23–35.

Rolfs, C., W. S. Rodney, M. H. Shapiro, and H. Winkler, 1975, "Hydrogen burning of ^{20}Ne and ^{22}Ne in stars," Nucl. Phys. **A241**, 460–486.

Rolfs, C., and E. Somorjai, 1995, "Status report on electron screening," Nucl. Instrum. Methods Phys. Res., Sect. B **99**, 297–300.

Rosenfeld, Y., 1996, "Short-range screening potentials for classical Coulomb fluids: Reanalysis of Monte Carlo sampling and cluster model studies," Phys. Rev. E. **53**, 2000–2007.

Rossignol, R., B. Faustin, C. Rocher, M. Malgat, J. Mazat, and T. Letellier, 2003, "Mitochondrial threshold effects," Biochem. J. **370**, 751–762.

Roters, G., C. Rolfs, F. Strieder, and H. P. Trautvetter, 1999, "The $E1$ and $E2$ capture amplitudes in $^{12}C(\alpha,\gamma_0)^{16}O$," Eur. Phys. J. A **6**, 451–461.

Rothman, D. H., 2017, "Thresholds of catastrophe in the Earth system," Sci. Adv. **3**, e1700906.

Rotter, I., 1991, "A continuum shell model for the open quantum mechanical nuclear system," Rep. Prog. Phys. **54**, 635–682.

Rotter, I., H. W. Barz, and J. Höhn, 1978, "Threshold effects in nuclear reactions and the line shape of resonances," Nucl. Phys. **A297**, 237–253.

Rotureau, J., J. Okołowicz, and M. Płoszajczak, 2006, "Theory of the two-proton radioactivity in the continuum shell model," Nucl. Phys. **A767**, 13–57.

Rowland, C., C. Iliadis, A. E. Champagne, C. Fox, J. José, and R. Runkle, 2004, "Does an NeNa cycle exist in explosive hydrogen burning?," Astrophys. J. Lett. **615**, L37–L40.

Runkle, R. C., A. E. Champagne, C. Angulo, C. Fox, C. Iliadis, R. Longland, and J. Pollanen, 2005, "Direct Measurement of the $^{14}N(p,\gamma)^{15}O$ S Factor," Phys. Rev. Lett. **94**, 082503.

Rupak, G., L. Fernando, and A. Vaghani, 2012, "Radiative neutron capture on carbon-14 in effective field theory," Phys. Rev. C **86**, 044608.

Rupak, G., and R. Higa, 2011, "Model-Independent Calculation of Radiative Neutron Capture on Lithium-7," Phys. Rev. Lett. **106**, 222501.

Sadeghpour, H. R., J. L. Bohn, M. J. Cavagnero, B. D. Esry, I. I. Fabrikant, J. H. Macek, and A. R. P. Rau, 2000, "Topical review: Collisions near threshold in atomic and molecular physics," J. Phys. B **33**, R93–R140.

Sallaska, A. L., C. Iliadis, A. E. Champange, S. Goriely, S. Starrfield, and F. X. Timmes, 2013, "STARLIB: A next-generation reaction-rate library for nuclear astrophysics," Astrophys. J. Suppl. Ser. **207**, 18.

Salpeter, E. E., 1952, "Nuclear reactions in the stars. I. Proton-proton chain," Phys. Rev. **88**, 547–553.

Salpeter, E. E., 1954, "Electrons screening and thermonuclear reactions," Aust. J. Phys. **7**, 373.

Salpeter, E. E., and H. M. van Horn, 1969, "Nuclear reaction rates at high densities," Astrophys. J. **155**, 183.

Savchenko, V. I., 2001, "Quantum, multibody effects and nuclear reaction rates in plasmas," Phys. Plasmas **8**, 82–91.

Sayre, D. B., C. R. Brune, D. E. Carter, D. K. Jacobs, T. N. Massey, and J. E. O'Donnell, 2012, "$E2$ Interference Effects in the $^{12}C(\alpha,\gamma_0)^{16}O$ Reaction," Phys. Rev. Lett. **109**, 142501.

Schatz, H., L. Bildsten, and A. Cumming, 2003, "Photodisintegration-triggered nuclear energy release in superbursts," Astrophys. J. Lett. **583**, L87–L90.

Schatz, H., L. Bildsten, A. Cumming, and M. Wiescher, 1999, "The rapid proton process ashes from stable nuclear burning on an accreting neutron star," Astrophys. J. **524**, 1014–1029.

Schatz, H., F. Kaeppeler, P. E. Koehler, M. Wiescher, and H. P. Trautvetter, 1993, "17O(n, alpha) 14C: Closure of a primordial CNO bi-cycle?," Astrophys. J. **413**, 750.

Schatz, H., *et al.*, 1998, "rp-process nucleosynthesis at extreme temperature and density conditions," Phys. Rep. **294**, 167–264.

Schmidt, J., and W. Scheid, 1996, "Molecular states in the equator-equator orientation of two oblately deformed ^{12}C nuclei," Phys. Rev. C **53**, 322–333.

Schramm, S., and S. E. Koonin, 1990, "Pycnonuclear fusion rates," Astrophys. J. **365**, 296.

Schramm, S., K. Langanke, and S. E. Koonin, 1992, "Pycnonuclear triple-alpha fusion rates," Astrophys. J. **397**, 579.

Schröder, U., H. W. Becker, G. Bogaert, J. Görres, C. Rolfs, H. P. Trautvetter, R. E. Azuma, C. Campbell, J. D. King, and J. Vise, 1987, "Stellar reaction rate of $^{14}N(p,\gamma)^{15}O$ and hydrogen burning in massive stars," Nucl. Phys. **A467**, 240–260.

Schümann, F., *et al.*, 2003, "Coulomb Dissociation of ^{8}B and the Low-Energy Cross Section of the $^{7}Be(p,\gamma)^{8}B$ Solar Fusion Reaction," Phys. Rev. Lett. **90**, 232501.

Schümann, F., *et al.*, 2006, "Low-energy cross section of the $^{7}Be(p,\gamma)^{8}B$ solar fusion reaction from the Coulomb dissociation of ^{8}B," Phys. Rev. C **73**, 015806.

Schürmann, D., R. Kunz, I. Lingner, C. Rolfs, F. Schümann, F. Strieder, and H. P. Trautvetter, 2008, "Lifetime measurement of the 6792 keV state in ^{15}O, important for the astrophysical S factor extrapolation in $^{14}N(p,\gamma)^{15}O$," Phys. Rev. C **77**, 055803.

Schürmann, D., *et al.*, 2005, "First direct measurement of the total cross-section of $^{12}C(\alpha,\gamma)^{16}O$," Eur. Phys. J. A **26**, 301–305.

Serenelli, A., C. Peña-Garay, and W. C. Haxton, 2013, "Using the standard solar model to constrain solar composition and nuclear reaction S factors," Phys. Rev. D **87**, 043001.

Serpico, P. D., S. Esposito, F. Iocco, G. Mangano, G. Miele, and O. Pisanti, 2004, "Nuclear reaction network for primordial nucleosynthesis: A detailed analysis of rates, uncertainties and light nuclei yields," J. Cosmol. Astropart. Phys. 12, 010.

Shahina, *et al.*, 2022, "Direct measurement of the low-energy resonances in $^{22}Ne(\alpha,\gamma)^{26}Mg$ reaction," Phys. Rev. C **106**, 025805.

Shahina, *et al.*, 2024, "Strength measurement of the $E_\alpha{}^{\mathrm{lab}} = 830$ keV resonance in the $^{22}Ne(\alpha,n)^{25}Mg$ reaction using a stilbene detector," Phys. Rev. C **110**, 015801.

Shapira, D., R. G. Stokstad, and D. A. Bromley, 1974, "Statistical analysis of the energy dependence of $^{12}C + {}^{12}C$ cross sections," Phys. Rev. C **10**, 1063–1082.

Shapira, D., R. G. Stokstad, M. W. Sachs, A. Gobbi, and D. A. Bromley, 1975, "Experimental studies of the resonance at $E_{\mathrm{c.m.}} = 19.7$ MeV in the $^{12}C + {}^{16}O$ system," Phys. Rev. C **12**, 1907–1917.

Sharma, S., A. Gupta, M. R. Chowdhury, A. Mandal, A. Bisoi, V. Nanal, L. C. Tribedi, and M. S. Sarkar, 2020, "Proton capture resonant state of ^{15}O at 7556 keV," Phys. Rev. C **102**, 024308.

Shaviv, G., and N. J. Shaviv, 1999, "Is there a dynamic effect in the screening of nuclear reactions in stellar plasmas?," Phys. Rep. **311**, 99–114.

Shaviv, N. J., and G. Shaviv, 1996, "The electrostatic screening of thermonuclear reactions in astrophysical plasmas. I.," Astrophys. J. **468**, 433.

Shaviv, N. J., and G. Shaviv, 2001, "The electrostatic screening of nuclear reactions in the Sun," Astrophys. J. **558**, 925–942.

Shen, S., S. Elhatisari, T. A. Lähde, D. Lee, B.-N. Lu, and U.-G. Meißner, 2023, "Emergent geometry and duality in the carbon nucleus," Nat. Commun. **14**, 2777.

Shen, Y., *et al.*, 2023, "New determination of the $^{12}C(\alpha,\gamma)^{16}O$ reaction rate and its impact on the black-hole mass gap," Astrophys. J. **945**, 41.

Shen, Y. P., *et al.*, 2019, "Astrophysical S_{E2} factor of the $^{12}C(\alpha,\gamma)^{16}O$ reaction through the $^{12}C(^{11}B,{}^7Li)^{16}O$ transfer reaction," Phys. Rev. C **99**, 025805.

Shen, Y. P., *et al.*, 2020, "Constraining the External Capture to the ^{16}O Ground State and the $E2$ S Factor of the $^{12}C(\alpha,\gamma)^{16}O$ Reaction," Phys. Rev. Lett. **124**, 162701.

Shima, T., F. Okazaki, T. Kikuchi, T. Kobayashi, T. Kii, T. Baba, Y. Nagai, and M. Igashira, 1997, "Measurement of the $^{13}C(n,\gamma)^{14}C$ cross section at stellar energies," Nucl. Phys. **A621**, 231–234.

Shoppa, T. D., M. Jeng, S. E. Koonin, K. Langanke, and R. Seki, 1996, "Electron screening in molecular fusion reactions," Nucl. Phys. **A605**, 387–402.

Shoppa, T. D., S. E. Koonin, K. Langanke, and R. Seki, 1993, "One- and two-electron atomic screening in fusion reactions," Phys. Rev. C **48**, 837–840.

Shternin, P. S., M. Beard, M. Wiescher, and D. G. Yakovlev, 2012, "Neutron degeneracy and plasma physics effects on radiative neutron captures in neutron star crust," Phys. Rev. C **86**, 015808.

Siegert, A. J., 1939, "On the derivation of the dispersion formula for nuclear reactions," Phys. Rev. **56**, 750–752.

Signorini, C., M. Mazzocco, and D. Pierroutsakou, 2020, "Low-energy reactions with halo nuclei," in *Handbook of Nuclear Physics*, edited by I. Tanihata, H. Toki, and T. Kajino (Springer Nature, Singapore), pp. 1–80.

Singh, B. S., M. Hass, Y. Nir-El, and G. Haquin, 2004, "New Precision Measurement of the $^3He(^4He,\gamma)^7Be$ Cross Section," Phys. Rev. Lett. **93**, 262503.

Skowronski, J., *et al.*, 2023, "Improved S factor of the $^{12}C(p,\gamma)^{13}N$ reaction at $E = 320$–620 keV and the 422 keV resonance," Phys. Rev. C **107**, L062801.

Smith, M. S., L. H. Kawano, and R. A. Malaney, 1993, "Experimental, computational, and observational analysis of primordial nucleosynthesis," Astrophys. J. Suppl. Ser. **85**, 219.

Sokolov, V. V., and V. G. Zelevinsky, 1988, "On a statistical theory of overlapping resonances," Phys. Lett. B **202**, 10–14.

Sokołowska, N., *et al.*, 2024, "Decay study of ^{11}Be with an optical TPC detector," arXiv:2407.09846.

Somà, V., P. Navrátil, F. Raimondi, C. Barbieri, and T. Duguet, 2020, "Novel chiral Hamiltonian and observables in light and medium-mass nuclei," Phys. Rev. C **101**, 014318.

Soylu, A., F. Koyuncu, A. Coban, O. Bayrak, and M. Freer, 2018, "Investigation of deformation effects on the decay properties of $^{12}C + \alpha$ cluster states in ^{16}O," Ann. Phys. (Amsterdam) **391**, 263–277.

Spillane, T., *et al.*, 2007, "$^{12}C + {}^{12}C$ Fusion Reactions near the Gamow Energy," Phys. Rev. Lett. **98**, 122501.

Spitaleri, C., 2015, "Nuclear astrophysics with the Trojan horse method," J. Phys. Conf. Ser. **590**, 012013.

Spitaleri, C., C. A. Bertulani, L. Fortunato, and A. Vitturi, 2016, "The electron screening puzzle and nuclear clustering," Phys. Lett. B **755**, 275–278.

Spitaleri, C., A. M. Mukhamedzhanov, L. D. Blokhintsev, M. La Cognata, R. G. Pizzone, and A. Tumino, 2011, "The Trojan horse method in nuclear astrophysics," Phys. At. Nucl. **74**, 1725–1739.

Spitaleri, C., *et al.*, 2001, "'Trojan horse' method applied to $^2H(^6Li,\alpha)^4He$ at astrophysical energies," Phys. Rev. C **63**, 055801.

Spitaleri, C., *et al.*, 2014, "Measurement of the 10 keV resonance in the $^{10}B(p,\alpha_0)^7Be$ reaction via the Trojan horse method," Phys. Rev. C **90**, 035801.

Spitaleri, C., *et al.*, 2017, "Measurement of the $^{10}B(p,\alpha_0)^7Be$ cross section from 5 keV to 1.5 MeV in a single experiment using the Trojan horse method," Phys. Rev. C **95**, 035801.

Spite, M., and F. Spite, 1982, "Lithium abundance at the formation of the Galaxy," Nature (London) **297**, 483–485.

Starostin, A., *et al.*, 2005, "Measurement of $\pi^- p \to \pi^0 n$ in the vicinity of the η threshold," Phys. Rev. C **72**, 015205.

Starrfield, S., J. W. Truran, M. Politano, W. M. Sparks, I. Nofar, and G. Shaviv, 1993, "^{22}Na and ^{26}Al production in nova outbursts," Phys. Rep. **227**, 223–234.

Starrfield, S., J. W. Truran, M. Wiescher, and W. M. Sparks, 1997, "Nova nucleosynthesis," Nucl. Phys. **A621**, 495–498.

Stock, R., G. Gaul, R. Santo, M. Bernas, B. Harvey, D. Hendrie, J. Mahoney, J. Sherman, J. Steyaert, and M. Zisman, 1972, "Anomalous backward α scattering," Phys. Rev. C **6**, 1226–1234.

Stöckmann, H. J., E. Persson, Y. H. Kim, M. Barth, U. Kuhl, and I. Rotter, 2002, "Effective Hamiltonian for a microwave billiard with attached waveguide," Phys. Rev. E. **65**, 066211.

Stoks, V. G. J., and J. J. de Swart, 1990, "Magnetic moment interaction in nucleon-nucleon phase-shift analyses," Phys. Rev. C **42**, 1235–1248.

Stokstad, R. G., Z. E. Switkowski, R. A. Dayras, and R. M. Wieland, 1976, "Measurements of Fusion Cross Sections for Heavy-Ion Systems at Very Low Energies," Phys. Rev. Lett. **37**, 888–891.

Straniero, O., I. Domínguez, G. Imbriani, and L. Piersanti, 2003, "The chemical composition of white dwarfs as a test of convective efficiency during core helium burning," Astrophys. J. **583**, 878–884.

Strieder, F., *et al.*, 2001, "Absolute cross section of $^7Be(p,\gamma)^8B$," Nucl. Phys. **A696**, 219–230.

Strohmayer, T. E., and E. F. Brown, 2002, "A remarkable 3 hour thermonuclear burst from 4U 1820-30," Astrophys. J. **566**, 1045–1059.

Strömberg, D. F., G. Martínez-Pinedo, and F. Nowacki, 2022, "Forbidden electron capture on ^{24}Na and ^{27}Al in degenerate oxygen-neon stellar cores," Phys. Rev. C **105**, 025803.

Su, J., *et al.*, 2010, "Alpha decay half-life of ^{147}Sm in metal samarium and Sm_2O_3," Eur. Phys. J. A **46**, 69–72.

Sünkel, W., 1976, "A generator coordinate technique for arbitrary cluster widths," Phys. Lett. **65B**, 419–422.

Suzuki, Y., 2021, "Calculable microscopic theory for $^{12}C(\alpha,\gamma)^{16}O$ cross section near Gamow window," Few-Body Syst. **62**, 2.

Suzuki, Y., 2023, "Correction to: Calculable microscopic theory for $^{12}C(\alpha,\gamma)^{16}O$ cross section near Gamow window," Few-Body Syst. **64**, 73.

Suzuki, Y., and K. Ikeda, 1988, "Cluster-orbital shell model and its application to the He isotopes," Phys. Rev. C **38**, 410–413.

Suzuki, Y., H. Matsumura, M. Orabi, Y. Fujiwara, P. Descouvemont, M. Theeten, and D. Baye, 2008, "Local versus nonlocal $\alpha\alpha$ interactions in a 3α description of ^{12}C," Phys. Lett. B **659**, 160–164.

Switkowski, Z. E., J. C. P. Heggie, and F. M. Mann, 1978, "Wigner cusps in the $^{65}Cu(p,\gamma)^{66}Zn$ and $^{65}Cu(p,\alpha_0)^{62}Ni$ reactions," Phys. Rev. C **17**, 392–395.

Takahashi, K., R. N. Boyd, G. J. Mathews, and K. Yokoi, 1987, "Bound-state beta decay of highly ionized atoms," Phys. Rev. C **36**, 1522–1528.

Takahashi, K., and K. Yokoi, 1983, "Nuclear β-decays of highly ionized heavy atoms in stellar interiors," Nucl. Phys. **A404**, 578–598.

Talwar, R., *et al.*, 2016, "Probing astrophysically important states in the ^{26}Mg nucleus to study neutron sources for the *s* process," Phys. Rev. C **93**, 055803.

Tan, W. P., *et al.*, 2020, "New Measurement of $^{12}C + {}^{12}C$ Fusion Reaction at Astrophysical Energies," Phys. Rev. Lett. **124**, 192702.

Tan, W. P., *et al.*, 2024, "Coincident measurement of the $^{12}C + {}^{12}C$ fusion cross section via the differential thick-target technique," Phys. Rev. C **110**, 035808.

Tang, Y. C., M. LeMere, and D. R. Thompsom, 1978, "Resonating-group method for nuclear many-body problems," Phys. Rep. **47**, 167–223.

Taniguchi, Y., and M. Kimura, 2021, "$^{12}C + {}^{12}C$ fusion S^*-factor from a full-microscopic nuclear model," Phys. Lett. B **823**, 136790.

Taniguchi, Y., and M. Kimura, 2024, "Impact of the molecular resonances on the $^{12}C + {}^{12}C$ fusion reaction rate," Phys. Lett. B **849**, 138434.

Tanihata, I., H. Savajols, and R. Kanungo, 2013, "Recent experimental progress in nuclear halo structure studies," Prog. Part. Nucl. Phys. **68**, 215–313.

Taylor, N. A., Åsa Nykvist, N. Powers, and J. N. Caldwell, 2019, "Thermoeffector threshold plasticity: The impact of thermal preconditioning on sudomotor, cutaneous vasomotor and thermogenic thresholds," J. Therm. Biol. **83**, 37–46.

Terasawa, M., K. Sumiyoshi, T. Kajino, G. J. Mathews, and I. Tanihata, 2001, "New nuclear reaction flow during *r*-process nucleosynthesis in supernovae: Critical role of light, neutron-rich nuclei," Astrophys. J. **562**, 470–479.

Thielemann, F. K., and W. D. Arnett, 1985, "Hydrostatic nucleosynthesis—Part Two—Core neon to silicon burning and presupernova abundance yields of massive stars," Astrophys. J. **295**, 604.

Thielemann, F. K., M. Arnould, and J. W. Truran, 1986, "Thermonuclear reaction rates from statistical model calculations," in *Advances in Nuclear Astrophysics*, edited by E. Vangioni-Flam, J. Audouze, M. Casse, J.-P. Chieze, and J. Tran Thanh Van (Editions Frontières,Gif-sur-Yvette, France), pp. 525–540.

Thoennessen, M., 2004, "Reaching the limits of nuclear stability," Rep. Prog. Phys. **67**, 1187–1232.

Thomas, R. G., 1951a, "On the determination of reduced widths from the one-level dispersion formula," Phys. Rev. **81**, 148–149.

Thomas, R. G., 1951b, "Radiative capture of thermal neutrons by Li^7," Phys. Rev. **84**, 1061–1062.

Thomas, R. G., 1952, "An analysis of the energy levels of the mirror nuclei, C^{13} and N^{13}," Phys. Rev. **88**, 1109–1125.

Thompson, I. J., and F. M. Nunes, 2009, *Nuclear Reactions for Astrophysics: Principles, Calculation and Applications of Low-Energy Reactions* (Cambridge University Press, Cambridge, England).

Thomson, N., L. Moschini, and A. Diaz-Torres, 2024, "Laser-assisted deuterium-tritium fusion: A quantum dynamical model," Phys. Rev. C **110**, 034614.

Timmes, F. X., S. E. Woosley, and T. A. Weaver, 1996, "The neutron star and black hole initial mass function," Astrophys. J. **457**, 834.

Timofeyuk, N. K., and P. Descouvemont, 2005, "Relation between widths of proton resonances and neutron asymptotic normalization coefficients in mirror states of light nuclei in a microscopic cluster model," Phys. Rev. C **72**, 064324.

Timofeyuk, N. K., R. C. Johnson, and A. M. Mukhamedzhanov, 2006, "Erratum: Relation between Proton and Neutron Asymptotic Normalization Coefficients for Light Mirror Nuclei and Its Relevance to Nuclear Astrophysics [Phys. Rev. Lett. **91**, 232501 (2003)]," Phys. Rev. Lett. **97**, 069904.

Tischhauser, P., *et al.*, 2002, "Elastic α-^{12}C Scattering and the $^{12}C(\alpha,\gamma)^{16}O$ $E2$ S Factor," Phys. Rev. Lett. **88**, 072501.

Toevs, J. W., 1971, "Total yield measurements in $^{16}O(\alpha,\gamma)^{20}Ne$ and $^{28}Si(\alpha,\gamma)^{32}S$," Nucl. Phys. **A172**, 589–602.

Tohsaki, A., H. Horiuchi, P. Schuck, and G. Röpke, 2001, "Alpha Cluster Condensation in ^{12}C and ^{16}O," Phys. Rev. Lett. **87**, 192501.

Tombrello, T. A., 1965, "The capture of protons by Be^7," Nucl. Phys. **71**, 459–464.

Tombrello, T. A., and P. D. Parker, 1963, "Direct-capture model for the $He^3(\alpha,\gamma)Be^7$ and $t(\alpha,\gamma)Li^7$ reactions," Phys. Rev. **131**, 2582–2589.

Tóth, Á., T. Szücs, T. N. Szegedi, G. Gyürky, Z. Halász, G. G. Kiss, and Z. Fülöp, 2023, "Experimental determination of the $^3He(\alpha,\gamma)^7Be$ reaction cross section above the ^{7}Be proton separation threshold," Phys. Rev. C **108**, 025802.

Trentalange, S., S. C. Wu, J. L. Osborne, and C. A. Barnes, 1988, "Elastic scattering and fusion cross sections of $^{13}C + {}^{13}C$," Nucl. Phys. **A483**, 406–428.

Tribble, R. E., C. A. Bertulani, M. La Cognata, A. M. Mukhamedzhanov, and C. Spitaleri, 2014, "Indirect techniques in nuclear astrophysics: A review," Rep. Prog. Phys. **77**, 106901.

Trippella, O., and M. La Cognata, 2017, "Concurrent application of ANC and THM to assess the $^{13}C(\alpha,n)^{16}O$ absolute cross section at astrophysical energies and possible consequences for neutron production in low-mass AGB stars," Astrophys. J. **837**, 41.

Tryti, S., T. Holtebekk, and J. Rekstad, 1973, "Angular distributions of protons near resonance for the reaction $^{12}C(d,p\gamma)^{13}C$ obtained by shape studies of γ-ray lines," Nucl. Phys. **A201**, 135–144.

Tryti, S., T. Holtebekk, and F. Ugletveit, 1975, "Angular distributions of protons from the reaction $^{12}C(d,p\gamma)^{13}C$ obtained by shape studies of γ-ray lines," Nucl. Phys. **A251**, 206–224.

Tsytovich, V. N., 2000, "Suppression of thermonuclear reactions in dense plasmas instead of Salpeter's enhancement," Astron. Astrophys. **356**, L57–L61, https://articles.adsabs.harvard.edu/pdf/2000A%26A...356L..57T.

Tumino, A., C. A. Bertulani, M. La Cognata, L. Lamia, R. G. Pizzone, S. Romano, and S. Typel, 2021, "The Trojan horse method: A nuclear physics tool for astrophysics," Annu. Rev. Nucl. Part. Sci. **71**, 345–376.

Tumino, A., *et al.*, 2014, "New determination of the $^2H(d,p)^3H$ and $^2H(d,n)^3He$ reaction rates at astrophysical energies," Astrophys. J. **785**, 96.

Tumino, A., *et al.*, 2018, "An increase in the $^{12}C + {}^{12}C$ fusion rate from resonances at astrophysical energies," Nature (London) **557**, 687–690.

Tumino, A., *et al.*, 2023, "Coulomb-free $^1S_0$ p-p scattering length from the quasi-free $p + d \to p + p + n$ reaction and its relation to universality," Commun. Phys. **6**, 106.

Tur, C., A. Heger, and S. M. Austin, 2007, "On the sensitivity of massive star nucleosynthesis and evolution to solar abundances and to uncertainties in helium-burning reaction rates," Astrophys. J. **671**, 821–827.

Tur, C., A. Heger, and S. M. Austin, 2009, "Dependence of *s*-process nucleosynthesis in massive stars on triple-alpha and $^{12}C(\alpha,\gamma)^{16}O$ reaction rate uncertainties," Astrophys. J. **702**, 1068–1077.

Tursunov, E. M., S. A. Turakulov, and A. S. Kadyrov, 2021, "Analysis of the $^3He(\alpha,\gamma)^7Be$ and $^3H(\alpha,\gamma)^7Li$ astrophysical direct capture reactions in a modified potential-model approach," Nucl. Phys. **A1006**, 122108.

Typel, S., and G. Baur, 2003, "Theory of the Trojan-Horse method," Ann. Phys. (Amsterdam) **305**, 228–265.

Typel, S., G. Bläge, and K. Langanke, 1991, "The low-energy $d(\alpha,\gamma)^6Li$ and $^6Li + {}^{208}Pb \to d + \alpha + {}^{208}Pb$ cross sections," Z. Phys. A **339**, 335–339.

Umar, A. S., K. Godbey, and C. Simenel, 2023, "Cluster model of ^{12}C in the density functional theory framework," Phys. Rev. C **107**, 064605.

Van Der Leun, C., D. M. Sheppard, and P. J. M. Smulders, 1965, "Levels of ^{20}Ne from radiative alpha-capture in ^{16}O," Phys. Lett. **18**, 134–135.

van Kolck, U., 1999, "Effective field theory of short-range forces," Nucl. Phys. **A645**, 273–302.

Varga, K., Y. Suzuki, and R. G. Lovas, 2002, "Microscopic multicluster model of ^{9,10,11}Li," Phys. Rev. C **66**, 041302(R).

Vogt, E., 1962, "Theory of low energy nuclear reactions," Rev. Mod. Phys. **34**, 723–746.

Volk, H., H. Kräwinkel, R. Santo, and L. Wallek, 1983, "Activation measurement of the ^{3}He(^{4}He, γ)^{7}Be reaction," Z. Phys. A **310**, 91–94.

Volya, A., and V. Zelevinsky, 2006, "Continuum shell model," Phys. Rev. C **74**, 064314.

Volya, A., and V. Zelevinsky, 2024, "Puzzles of exotic decay processes," Few-Body Syst. **65**, 43.

von Oertzen, W., M. Freer, and Y. Kanada-En'yo, 2006, "Nuclear clusters and nuclear molecules," Phys. Rep. **432**, 43–113.

von Oertzen, W., and M. Milin, 2014, "Covalent binding on the femtometer scale: Nuclear molecules," in *Clusters in Nuclei*, Vol. 3, Lecture Notes in Physics Vol. 875, edited by C. Beck (Springer-Verlag, Berlin), pp. 147–182, 10.1007/978-3-319-01077-9_5.

von Oertzen, W., *et al.*, 2004, "Search for cluster structure of excited states in ^{14}C," Eur. Phys. J. A **21**, 193–215.

Vorabbi, M., P. Navrátil, S. Quaglioni, and G. Hupin, 2019, "^{7}Be and ^{7}Li nuclei within the no-core shell model with continuum," Phys. Rev. C **100**, 024304.

Wachter, B., T. Mertelmeier, and H. M. Hofmann, 1988, "Differences in the mirror reactions ^{3}H$(p,\gamma)^4$He and ^{3}He$(n,\gamma)^4$He from an isospin conserving nuclear force," Phys. Rev. C **38**, 1139–1144.

Wagner, L., *et al.*, 2018, "Astrophysical *S* factor of the ^{14}N$(p,\gamma)^{15}$O reaction at 0.4–1.3 MeV," Phys. Rev. C **97**, 015801.

Wallner, A., *et al.*, 2016, "Accelerator mass spectrometry measurements of the ^{13}C$(n,\gamma)^{14}$C and ^{14}N$(n,p)^{14}$C cross sections," Phys. Rev. C **93**, 045803.

Walton, R. B., J. D. Clement, and F. Boreli, 1957, "Interaction of neutrons with oxygen and a study of the C$^{13}(\alpha,n)$O^{16} reaction," Phys. Rev. **107**, 1065–1075.

Wan, N., C. Xu, and Z. Ren, 2015, "Effects of electron screening on α-decay half-lives in different external environments," Phys. Rev. C **92**, 024301.

Wan, N., C. Xu, and Z. Ren, 2016, "α-decay half-life screened by electrons," Nucl. Sci. Technol. **27**, 149.

Wang, B., C. A. Bertulani, and A. B. Balantekin, 2011, "Electron screening and its effects on big-bang nucleosynthesis," Phys. Rev. C **83**, 018801.

Wang, J., S.-I. Chu, and C. Laughlin, 1994, "Multiphoton detachment of H$^-$. II. Intensity-dependent photodetachment rates and threshold behavior-complex-scaling generalized pseudospectral method," Phys. Rev. A **50**, 3208–3215.

Wang, S. M., W. Nazarewicz, R. J. Charity, and L. G. Sobotka, 2019, "Structure and decay of the extremely proton-rich nuclei ^{11,12}O," Phys. Rev. C **99**, 054302.

Wang, S. M., W. Nazarewicz, A. Volya, and Y. G. Ma, 2023, "Probing the nonexponential decay regime in open quantum systems," Phys. Rev. Res. **5**, 023183.

Washington-Allen, R. A., and L. F. Salo, 2007, "Catastrophic thresholds: Perspectives, definitions, and applications," Bull. Ecol. Soc. Am. **88**, 219–225.

Weaver, T. A., and S. E. Woosley, 1993, "Nucleosynthesis in massive stars and the ^{12}C$(\alpha,\gamma)^{16}$O reaction rate," Phys. Rep. **227**, 65–96.

Weinberg, S., 1990, "Nuclear forces from chiral Lagrangians," Phys. Lett. B **251**, 288–292.

Weinberg, S., 1991, "Effective chiral Lagrangians for nucleon-pion interactions and nuclear forces," Nucl. Phys. **B363**, 3–18.

Weinberg, S., 1992, "Three-body interactions among nucleons and pions," Phys. Lett. B **295**, 114–121.

Weiss, A., M. Flaskamp, and V. N. Tsytovich, 2001, "Solar models and electron screening," Astron. Astrophys. **371**, 1123–1127.

Weizsäcker, C.-F., 1937, "Über die Elementumwandlungen im Inneren der Sterne I," Phys. Z. **38**, 176–191.

Wells, J. T., A. B. Tucker, and W. E. Meyerhof, 1963, "Threshold effects in neutron elastic scattering," Phys. Rev. **131**, 1644–1660.

Wen, Q.-G., *et al.*, 2008, "Trojan horse method applied to ^{9}Be$(p,\alpha)^6$Li at astrophysical energies," Phys. Rev. C **78**, 035805.

Wiescher, M., and T. Ahn, 2017, "Clusters in astrophysics," in *Nuclear Particle Correlations and Cluster Physics*, edited by W.-U. Schröder (World Scientific, Singapore), p. 203.

Wiescher, M., H. W. Becker, J. Görres, K. U. Kettner, H. P. Trautvetter, W. E. Kieser, C. Rolfs, R. E. Azuma, K. P. Jackson, and J. W. Hammer, 1980, "Nuclear and astrophysical aspects of ^{18}O$(p,\gamma)^{19}$F," Nucl. Phys. **A349**, 165–216.

Wiescher, M., O. Clarkson, R. J. deBoer, and P. Denisenkov, 2021, "Nuclear clusters as the first stepping stones for the chemical evolution of the Universe," Eur. Phys. J. A **57**, 24.

Wiescher, M., R. J. deBoer, and J. Görres, 2022, "Threshold effects in the ^{10}B$(p,\alpha)^7$Be, ^{12}C$(p,\gamma)^{13}$N and ^{14}N$(p,\gamma)^{15}$O reactions," Front. Phys. **10**, 1009489.

Wiescher, M., R. J. deBoer, and J. Görres, 2023, "The resonances in the ^{22}Ne + α fusion reactions," Eur. Phys. J. A **59**, 11.

Wiescher, M., R. J. deBoer, J. Görres, and R. E. Azuma, 2017, "Low energy measurements of the ^{10}B$(p,\alpha)^7$Be reaction," Phys. Rev. C **95**, 044617.

Wiescher, M., J. Gorres, S. Graff, L. Buchmann, and F. K. Thielemann, 1989, "The hot proton-proton chains in low-metallicity objects," Astrophys. J. **343**, 352.

Wiescher, M., J. Görres, and H. Schatz, 1999, "Topical review: Break-out reactions from the CNO cycles," J. Phys. G **25**, R133–R161.

Wiescher, M., J. Görres, E. Uberseder, G. Imbriani, and M. Pignatari, 2010, "The cold and hot CNO cycles," Annu. Rev. Nucl. Part. Sci. **60**, 381–404.

Wiescher, M., and K. U. Kettner, 1982, "Warm CNO nucleosynthesis as a possible enrichment mechanism for oxygen and fluorine isotopes," Astrophys. J. **263**, 891–901.

Wiescher, M., and K. Langanke, 2024, "Manhattan Project astrophysics," Phys. Today **77**, No. 3, 34–41.

Wiescher, M., *et al.*, 1983, "^{11}C level structure via the ^{10}B(p,γ) reaction," Phys. Rev. C **28**, 1431–1442.

Wigner, E., and F. Seitz, 1933, "On the constitution of metallic sodium," Phys. Rev. **43**, 804–810.

Wigner, E. P.1946, "Resonance reactions," Phys. Rev. **70**, 606–618.

Wigner, E. P.1948, "On the behavior of cross sections near thresholds," Phys. Rev. **73**, 1002–1009.

Wigner, E. P., 1995, "On the development of the compound nucleus model," in *Philosophical Reflections and Syntheses*, edited by J. Mehra (Springer, Berlin), pp. 459–475.

Wigner, E. P., and L. Eisenbud, 1947, "Higher angular momenta and long range interaction in resonance reactions," Phys. Rev. **72**, 29–41.

Witała, H., W. Glöckle, J. Golak, A. Nogga, H. Kamada, R. Skibiński, and J. Kuroś-Żołnierczuk, 2001, "Nd elastic scattering as a tool to probe properties of 3N forces," Phys. Rev. C **63**, 024007.

Wolke, K., H. W. Becker, C. Rolfs, U. Schröder, H. P. Trautvetter, V. Harms, K. L. Kratz, J. W. Hammer, M. Wiescher, and A. Wöhr, 1989, "Helium burning of ^{22}Ne," Z. Phys. A **334**, 491–510.

Wong, C. Y., 1973, "Interaction Barrier in Charged-Particle Nuclear Reactions," Phys. Rev. Lett. **31**, 766–769.

Woosley, S. E., and A. Heger, 2021, "The pair-instability mass gap for black holes," Astrophys. J. Lett. **912**, L31.

Woosley, S. E., A. Heger, A. Cumming, R. D. Hoffman, J. Pruet, T. Rauscher, J. L. Fisker, H. Schatz, B. A. Brown, and M. Wiescher, 2004, "Models for type I x-ray bursts with improved nuclear physics," Astrophys. J. Suppl. Ser. **151**, 75–102.

Woosley, S. E., and R. E. Taam, 1976, "γ-ray bursts from thermonuclear explosions on neutron stars," Nature (London) **263**, 101–103.

Wuosmaa, A. H., *et al.*, 2005, "Neutron Spectroscopic Factors in ^{9}Li from ^{2}H(^{8}Li, p)^{9}Li," Phys. Rev. Lett. **94**, 082502.

Wylie, J., J. Okołowicz, W. Nazarewicz, M. Płoszajczak, S. M. Wang, X. Mao, and N. Michel, 2021, "Spectroscopic factors in dripline nuclei," Phys. Rev. C **104**, L061301.

Wyly, L. D., and A. Zucker, 1953, "Activities in light nuclei from nitrogen ion bombardment," Phys. Rev. **89**, 524–525.

Xu, Y., K. Takahashi, S. Goriely, M. Arnould, M. Ohta, and H. Utsunomiya, 2013, "NACRE II: An update of the NACRE compilation of charged-particle-induced thermonuclear reaction rates for nuclei with mass number $A < 16$," Nucl. Phys. **A918**, 61–169.

Yakovlev, D. G., M. Beard, L. R. Gasques, and M. Wiescher, 2010, "Simple analytic model for astrophysical S factors," Phys. Rev. C **82**, 044609.

Yakovlev, D. G., L. R. Gasques, A. V. Afanasjev, M. Beard, and M. Wiescher, 2006, "Fusion reactions in multicomponent dense matter," Phys. Rev. C **74**, 035803.

Yuan, C.-X., 2017, "Impact of off-diagonal cross-shell interaction on ^{14}C," Chin. Phys. C **41**, 104102.

Zahnow, D., C. Rolfs, S. Schmidt, and H. P. Trautvetter, 1997, "Low-energy $S(E)$ factor of ^{9}Be$(p,\alpha)^6$Li and ^{9}Be$(p,d)^8$Be," Z. Phys. A **359**, 211–218.

Zecher, P. D., *et al.*, 1998, "Measurement of the ^{8}Li$(n,\gamma)^9$Li cross section at astrophysical energies by reverse kinematics," Phys. Rev. C **57**, 959–966.

Zha, S., S.-C. Leung, T. Suzuki, and K. Nomoto, 2019, "Evolution of ONeMg core in super-AGB stars toward electron-capture supernovae: Effects of updated electron-capture rate," Astrophys. J. **886**, 22.

Zhang, L., *et al.*, 2022, "Measurement of ^{19}F$(p,\gamma)^{20}$Ne reaction suggests CNO breakout in first stars," Nature (London) **610**, 656–660.

Zhang, X., K. M. Nollett, and D. R. Phillips, 2015, "Halo effective field theory constrains the solar $^7\mathrm{Be} + p \to {}^8\mathrm{B} + \gamma$ rate," Phys. Lett. B **751**, 535–540.

Zhang, X., K. M. Nollett, and D. R. Phillips, 2018, "Models, measurements, and effective field theory: Proton capture on ^{7}Be at next-to-leading order," Phys. Rev. C **98**, 034616.

Zhang, X., K. M. Nollett, and D. R. Phillips, 2020, "S-factor and scattering-parameter extractions from $^3\mathrm{He} + {}^4\mathrm{He} \to {}^7\mathrm{Be} + \gamma$," J. Phys. G **47**, 054002.

Zickefoose, J., *et al.*, 2018, "Measurement of the ^{12}C$(^{12}$C$, p)^{23}$Na cross section near the Gamow energy," Phys. Rev. C **97**, 065806.

Ziegler, J. F., M. D. Ziegler, and J. P. Biersack, 2010, "SRIM—The stopping and range of ions in matter (2010)," Nucl. Instrum. Methods Phys. Res., Sect. B **268**, 1818–1823.

Zinner, N. T., 2007, "Alpha decay rate enhancement in metals: An unlikely scenario," Nucl. Phys. **A781**, 81–87.

Zylstra, A. B., *et al.*, 2016, "Using Inertial Fusion Implosions to Measure the $t + {}^3$He Fusion Cross Section at Nucleosynthesis-Relevant Energies," Phys. Rev. Lett. **117**, 035002.

Zylstra, A. B., *et al.*, 2017, "Proton Spectra from $^3\mathrm{He} + t$ and $^3\mathrm{He} + {}^3$He Fusion at Low Center-of-Mass Energy, with Potential Implications for Solar Fusion Cross Sections," Phys. Rev. Lett. **119**, 222701.

Zylstra, A. B., *et al.*, 2022, "Burning plasma achieved in inertial fusion," Nature (London) **601**, 542–548.